Chapter 6

RIGID BODY DYNAMICS

6.1 Introduction

The dynamics of rigid bodies and fluid motions are governed by the combined actions of different external forces and moments as well as by the inertia of the bodies themselves. In fluid dynamics these forces and moments can no longer be considered as acting at a single point or at discrete points of the system. Instead, they must be regarded as distributed in a relatively smooth or a continuous manner throughout the mass of the fluid particles. The force and moment distributions and the kinematic description of the fluid motions are in fact continuous, assuming that the collection of discrete fluid molecules can be analyzed as a continuum.
Typically, one can anticipate force mechanisms associated with the fluid inertia, its weight, viscous stresses and secondary effects such as surface tension. In general three principal force mechanisms (inertia, gravity and viscous) exist, which can be of comparable importance. With very few exceptions, it is not possible to analyze such complicated situations exactly - either theoretically or experimentally. It is often impossible to include all force mechanisms simultaneously in a (mathematical) model. They can be treated in pairs as has been done when defining dimensionless numbers - see chapter 4 and appendix B. In order to determine which pair of forces dominate, it is useful first to estimate the orders of magnitude of the inertia, the gravity and the viscous forces and moments, separately. Depending on the problem, viscous effects can often be ignored; this simplifies the problem considerably.
This chapter discusses the hydromechanics of a simple rigid body; mainly the attention focuses on the motions of a simple floating vertical cylinder. The purpose of this chapter is to present much of the theory of ship motions while avoiding many of the purely hydrodynamic complications; these are left for later chapters.

6.2 Ship Definitions

When on board a ship looking toward the **bow** (front end) one is looking **forward**. The **stern** is **aft** at the other end of the ship. As one looks forward, the **starboard** side is one's right and the **port** side is to one's left.

[0] J.M.J. Journée and W.W. Massie, *"OFFSHORE HYDROMECHANICS"*, First Edition, January 2001, Delft University of Technology. For updates see web site: http://www.shipmotions.nl.

6.2.1 Axis Conventions

The motions of a ship, just as for any other rigid body, can be split into three mutually perpendicular translations of the center of gravity, G, and three rotations around G. In many cases these motion components will have small amplitudes.

Three right-handed orthogonal coordinate systems are used to define the ship motions:

- An **earth-bound** coordinate system $S(x_0, y_0, z_0)$.
  The (x_0, y_0)-plane lies in the still water surface, the positive x_0-axis is in the direction of the wave propagation; it can be rotated at a horizontal angle μ relative to the translating axis system $O(x, y, z)$ as shown in figure 6.1. The positive z_0-axis is directed upwards.

- A **body–bound** coordinate system $G(x_b, y_b, z_b)$.
  This system is connected to the ship with its origin at the ship's center of gravity, G. The directions of the positive axes are: x_b in the longitudinal forward direction, y_b in the lateral port side direction and z_b upwards. If the ship is floating upright in still water, the (x_b, y_b)-plane is parallel to the still water surface.

- A **steadily translating** coordinate system $O(x, y, z)$.
  This system is moving forward with a constant ship speed V. If the ship is stationary, the directions of the $O(x, y, z)$ axes are the same as those of the $G(x_b, y_b, z_b)$ axes. The (x, y)-plane lies in the still water surface with the origin O at, above or under the time-averaged position of the center of gravity G. The ship is supposed to carry out oscillations around this steadily translating $O(x, y, z)$ coordinate system.

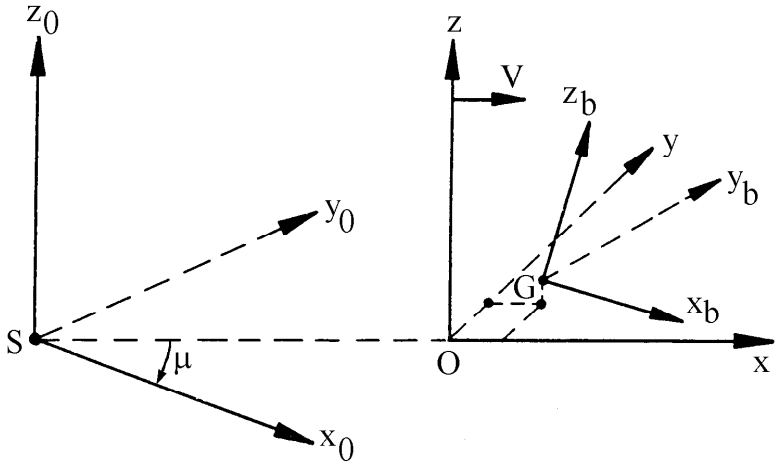

Figure 6.1: Coordinate Systems

The harmonic elevation of the wave surface ζ is defined in the earth-bound coordinate system by:

$$\zeta = \zeta_a \cos(\omega t - k x_0) \tag{6.1}$$

in which:

ζ_a	=	wave amplitude (m)
$k = 2\pi/\lambda$	=	wave number (rad/m)
λ	=	wave length (m)
ω	=	circular wave frequency (rad/s)
t	=	time (s)

6.2.2 Frequency of Encounter

The wave speed c, defined in a direction with an angle μ (wave direction) relative to the ship's speed vector V, follows from:

$$\boxed{c = \frac{\omega}{k} = \frac{\lambda}{T}} \qquad \text{(see chapter 5)} \tag{6.2}$$

The steadily translating coordinate system $O(x, y, z)$ is moving forward at the ship's speed V, which yields:

$$\boxed{x_0 = Vt\cos\mu + x\cos\mu + y\sin\mu} \tag{6.3}$$

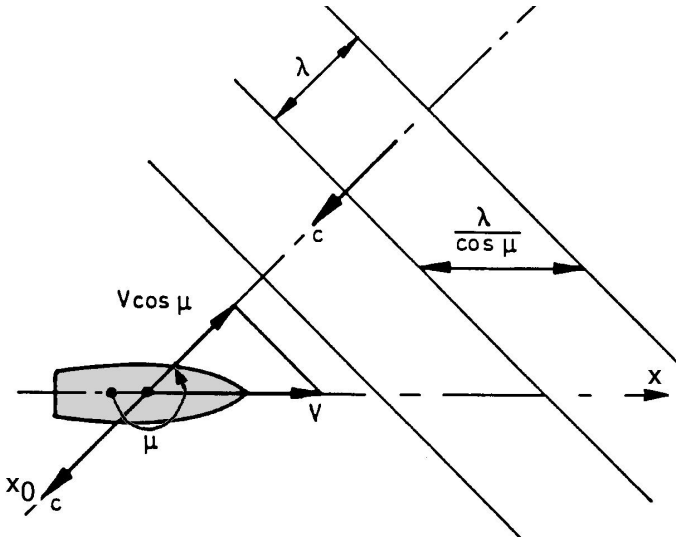

Figure 6.2: Frequency of Encounter

When a ship moves with a forward speed, the frequency at which it encounters the waves, ω_e, becomes important. Then the period of encounter, T_e, see figure 6.2, is:

$$T_e = \frac{\lambda}{c + V\cos(\mu - \pi)} = \frac{\lambda}{c - V\cos\mu} \tag{6.4}$$

and the circular frequency of encounter, ω_e, becomes:

$$\omega_e = \frac{2\pi}{T_e} = \frac{2\pi\,(c - V\cos\mu)}{\lambda} = k\,(c - V\,\cos\mu) \tag{6.5}$$

Note that $\mu = 0$ for following waves.
Using $k \cdot c = \omega$ from equation 6.2, the relation between the frequency of encounter and the wave frequency becomes:

$$\boxed{\omega_e = \omega - kV\cos\mu} \tag{6.6}$$

Note that at zero forward speed ($V = 0$) or in beam waves ($\mu = 90°$ or $\mu = 270°$) the frequencies ω_e and ω are identical.
In deep water, with the dispersion relation $k = \omega^2/g$, this frequency relation becomes:

$$\omega_e = \omega - \frac{\omega^2}{g} V \cos\mu \qquad \text{(deep water)} \tag{6.7}$$

Using the frequency relation in equation 6.6 and equations 6.1 and 6.3, it follows that the wave elevation can be given by:

$$\underline{\overline{|\zeta = \zeta_a \cos(\omega_e t - kx\cos\mu - ky\sin\mu)|}} \tag{6.8}$$

6.2.3 Motions of and about CoG

The resulting six ship motions in the steadily translating $O(x, y, z)$ system are defined by three translations of the ship's center of gravity (**CoG**) in the direction of the x-, y- and z-axes and three rotations about them as given in the introduction:

$$\begin{aligned}
\text{Surge} &: \quad x = x_a \cos(\omega_e t + \varepsilon_{x\zeta}) \\
\text{Sway} &: \quad y = y_a \cos(\omega_e t + \varepsilon_{y\zeta}) \\
\text{Heave} &: \quad z = z_a \cos(\omega_e t + \varepsilon_{z\zeta}) \\
\text{Roll} &: \quad \phi = \phi_a \cos(\omega_e t + \varepsilon_{\phi\zeta}) \\
\text{Pitch} &: \quad \theta = \theta_a \cos(\omega_e t + \varepsilon_{\theta\zeta}) \\
\text{Yaw} &: \quad \psi = \psi_a \cos(\omega_e t + \varepsilon_{\psi\zeta})
\end{aligned} \tag{6.9}$$

in which each of the ε values is a different phase angle.
The phase shifts of these motions are related to the harmonic wave elevation at the origin of the steadily translating $O(x, y, z)$ system. This origin is located at the average position of the ship's center of gravity - even though no wave can be measured there:

$$\text{Wave elevation at } O \text{ or } G: \qquad \underline{\overline{|\zeta = \zeta_a \cos(\omega_e t)|}} \tag{6.10}$$

6.2.4 Displacement, Velocity and Acceleration

The harmonic velocities and accelerations in the steadily translating $O(x, y, z)$ coordinate system are found by taking the derivatives of the displacements. This will be illustrated here for roll:

$$\begin{aligned}
\text{Displacement} &: \quad \underline{\overline{|\phi = \phi_a \cos(\omega_e t + \varepsilon_{\phi\zeta})|}} \qquad \text{(see figure 6.3)} \\
\text{Velocity} &: \quad \underline{\overline{\left|\dot{\phi} = -\omega_e \phi_a \sin(\omega_e t + \varepsilon_{\phi\zeta})\right|}} = \omega_e \phi_a \cos(\omega_e t + \varepsilon_{\phi\zeta} + \pi/2) \\
\text{Acceleration} &: \quad \underline{\overline{\left|\ddot{\phi} = -\omega_e^2 \phi_a \cos(\omega_e t + \varepsilon_{\phi\zeta})\right|}} = \omega_e^2 \phi_a \cos(\omega_e t + \varepsilon_{\phi\zeta} + \pi)
\end{aligned} \tag{6.11}$$

The phase shift of the roll motion with respect to the wave elevation in figure 6.3, $\varepsilon_{\phi\zeta}$, is positive because when the wave elevation passes zero at a certain instant, the roll motion already has passed zero. Thus, if the roll motion, ϕ, comes before the wave elevation, ζ, then the phase shift, $\varepsilon_{\phi\zeta}$, is defined as positive. This convention will hold for all other responses as well of course.
Figure 6.4 shows a sketch of the time histories of the harmonic angular displacements, velocities and accelerations of roll. Note the mutual phase shifts of $\pi/2$ and π.

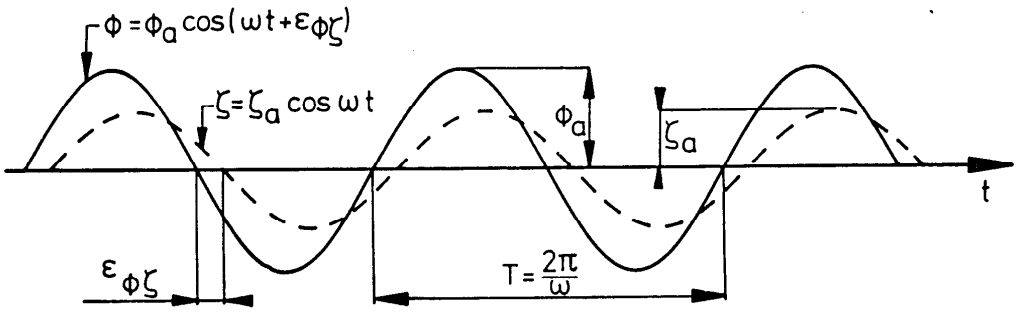

Figure 6.3: Harmonic Wave and Roll Signal

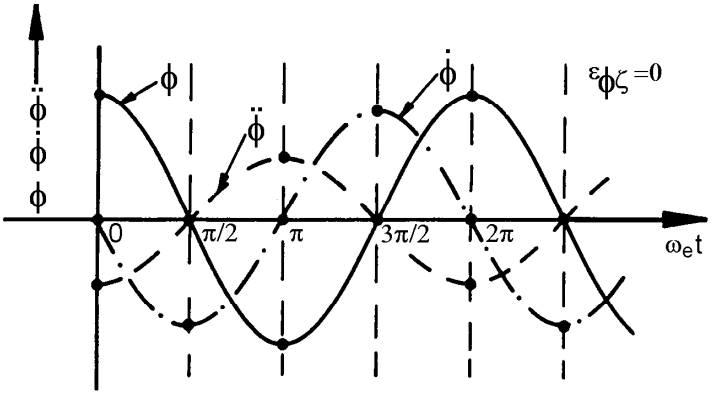

Figure 6.4: Displacement, Acceleration and Velocity

6.2.5 Motions Superposition

Knowing the motions of and about the center of gravity, G, one can calculate the motions in any point on the structure using superposition.

Absolute Motions

Absolute motions are the motions of the ship in the steadily translating coordinate system $O(x, y, z)$. The angles of rotation ϕ, θ and ψ are assumed to be small (for instance < 0.1 rad.), which is a necessity for linearizations. They must be expressed in radians, because in the linearization it is assumed that:

$$\overline{|\sin\phi \approx \phi|} \qquad \text{and} \qquad \overline{|\cos\phi \approx 1.0|} \tag{6.12}$$

For small angles, the transformation matrix from the body-bound coordinate system to the steadily translating coordinate system is very simple:

$$\begin{pmatrix} x \\ y \\ z \end{pmatrix} = \begin{pmatrix} 1 & -\psi & \theta \\ \psi & 1 & -\phi \\ -\theta & \phi & 1 \end{pmatrix} \cdot \begin{pmatrix} x_b \\ y_b \\ z_b \end{pmatrix} \tag{6.13}$$

Using this matrix, the components of the **absolute harmonic motions** of a certain point

$P(x_b, y_b, z_b)$ on the structure are given by:

$$\boxed{\begin{array}{l} |x_P = x - y_b\psi + z_b\theta| \\ \hline |y_P = y + x_b\psi - z_b\phi| \\ \hline |z_P = z - x_b\theta + y_b\phi\,| \end{array}} \tag{6.14}$$

in which x, y, z, ϕ, θ and ψ are the motions of and about the center of gravity, G, of the structure.
As can be seen in equation 6.14, the vertical motion, z_P, in a point $P(x_b, y_b, z_b)$ on the floating structure is made up of heave, roll and pitch contributions. When looking more detailed to this motion, it is called here now h, for convenient writing:

$$\begin{aligned} h\,(\omega_e, t) &= z - x_b\theta + y_b\phi \\ &= z_a\cos(\omega_e t + \varepsilon_{z\zeta}) - x_b\theta_a\cos(\omega_e t + \varepsilon_{\theta\zeta}) + y_b\phi_a\cos(\omega_e t + \varepsilon_{\phi\zeta}) \\ &= \quad \{+z_a\cos\varepsilon_{z\zeta} - x_b\theta_a\cos\varepsilon_{\theta\zeta} + y_b\phi_a\cos\varepsilon_{\phi\zeta}\}\cdot cos(\omega_e t) \\ &\quad -\{+z_a\sin\varepsilon_{z\zeta} - x_b\theta_a\sin\varepsilon_{\theta\zeta} + y_b\phi_a\sin\varepsilon_{\phi\zeta}\}\cdot sin(\omega_e t) \end{aligned} \tag{6.15}$$

As this motion h has been obtained by a linear superposition of three harmonic motions, this (resultant) motion must be harmonic as well:

$$\begin{aligned} h\,(\omega_e, t) &= h_a\cos(\omega_e t + \varepsilon_{h\zeta}) \\ &= \{h_a\cos\varepsilon_{h\zeta}\}\cdot\cos(\omega_e t) - \{h_a\sin\varepsilon_{h\zeta}\}\cdot\sin(\omega_e t) \end{aligned} \tag{6.16}$$

in which h_a is the motion amplitude and $\varepsilon_{h\zeta}$ is the phase lag of the motion with respect to the wave elevation at G.
By equating the terms with $\cos(\omega_e t)$ in equations 6.15 and 6.16 ($\omega_e t = 0$, so the $\sin(\omega_e t)$-terms are zero) one finds the in-phase term $h_a\cos\varepsilon_{h\zeta}$; equating the terms with $\sin(\omega_e t)$ in equations 6.15 and 6.16 ($\omega_e t = \pi/2$, so the $\cos(\omega_e t)$-terms are zero) provides the out-of-phase term $h_a\sin\varepsilon_{h\zeta}$ of the vertical displacement in P:

$$\begin{aligned} h_a\cos\varepsilon_{h\zeta} &= +z_a\cos\varepsilon_{z\zeta} - x_b\theta_a\cos\varepsilon_{\theta\zeta} + y_b\phi_a\cos\varepsilon_{\phi\zeta} \\ h_a\sin\varepsilon_{h\zeta} &= +z_a\sin\varepsilon_{z\zeta} - x_b\theta_a\sin\varepsilon_{\theta\zeta} + y_b\phi_a\sin\varepsilon_{\phi\zeta} \end{aligned} \tag{6.17}$$

Since the right hand sides of equations 6.17 are known, the amplitude h_a and phase shift $\varepsilon_{h\zeta}$ become:

$$\boxed{\begin{array}{l} \left|h_a = \sqrt{(h_a\sin\varepsilon_{h\zeta})^2 + (h_a\cos\varepsilon_{h\zeta})^2}\right| \\ \hline \left|\varepsilon_{h\zeta} = \arctan\left\{\dfrac{h_a\sin\varepsilon_{h\zeta}}{h_a\cos\varepsilon_{h\zeta}}\right\} \quad \text{with: } 0 \le \varepsilon_{h\zeta} \le 2\pi\right| \end{array}} \tag{6.18}$$

The phase angle $\varepsilon_{h\zeta}$ has to be determined in the correct quadrant between 0 and 2π. This depends on the signs of both the numerator and the denominator in the expression for the arctangent. If the phase shift $\varepsilon_{h\zeta}$ has been determined between $-\pi/2$ and $+\pi/2$ and $h_a\cos\varepsilon_{h\zeta}$ is negative, then π should be added or subtracted from this $\varepsilon_{h\zeta}$ to obtain the correct phase shift.

For ship motions, the relations between displacement or rotation, velocity and acceleration are very important. The vertical velocity and acceleration of point P on the structure follow simply from the first and second derivative with respect to the time of the displacement in equation 6.15:

$$\begin{aligned} \dot{h} &= -\omega_e h_a \sin(\omega_e t + \varepsilon_{h\zeta}) = \{\omega_e h_a\} \cdot \cos(\omega_e t + \{\varepsilon_{h\zeta} + \pi/2\}) \\ \ddot{h} &= -\omega_e^2 h_a \cos(\omega_e t + \varepsilon_{h\zeta}) = \{\omega_e^2 h_a\} \cdot \cos(\omega_e t + \{\varepsilon_{h\zeta} + \pi\}) \end{aligned} \tag{6.19}$$

The amplitudes of the motions and the phase shifts with respect to the wave elevation at G are given between braces $\{...\}$ here.

Vertical Relative Motions

The vertical relative motion of the structure with respect to the undisturbed wave surface is the motion that one sees when looking overboard from a moving ship, downwards toward the waves. This relative motion is of importance for shipping water on deck and slamming (see chapter 11). The **vertical relative motion** s at $P(x_b, y_b)$ is defined by:

$$\underline{\overline{|s = \zeta_P - h|}} = \zeta_P - z + x_b\theta - y_b\phi \tag{6.20}$$

with for the local wave elevation:

$$\zeta_P = \zeta_a \cos(\omega_e t - kx_b \cos\mu - ky_b \sin\mu) \tag{6.21}$$

where $-kx_b \cos\mu - ky_b \sin\mu$ is the phase shift of the local wave elevation relative to the wave elevation in the center of gravity.
The amplitude and phase shift of this relative motion of the structure can be determined in a way analogous to that used for the absolute motion.

6.3 Single Linear Mass-Spring System

Consider a seaway with irregular waves of which the energy distribution over the wave frequencies (the wave spectrum) is known. These waves are input to a system that possesses linear characteristics. These frequency characteristics are known, for instance via model experiments or computations. The output of the system is the motion of the floating structure. This motion has an irregular behavior, just as the seaway that causes the motion. The block diagram of this principle is given in figure 6.5.
The first harmonics of the motion components of a floating structure are often of interest, because in many cases a very realistic mathematical model of the motions in a seaway can be obtained by making use of a superposition of these components at a range of frequencies; motions in the so-called **frequency domain** will be considered here.
In many cases the ship motions mainly have a linear behavior. This means that, at each frequency, the different ratios between the motion amplitudes and the wave amplitudes and also the phase shifts between the motions and the waves are constant. Doubling the input (wave) amplitude results in a doubled output amplitude, while the phase shifts between output and input does not change.
As a consequence of linear theory, the resulting motions in irregular waves can be obtained by adding together results from regular waves of different amplitudes, frequencies and possibly propagation directions. With known wave energy spectra and the calculated frequency characteristics of the responses of the ship, the response spectra and the statistics of these responses can be found.

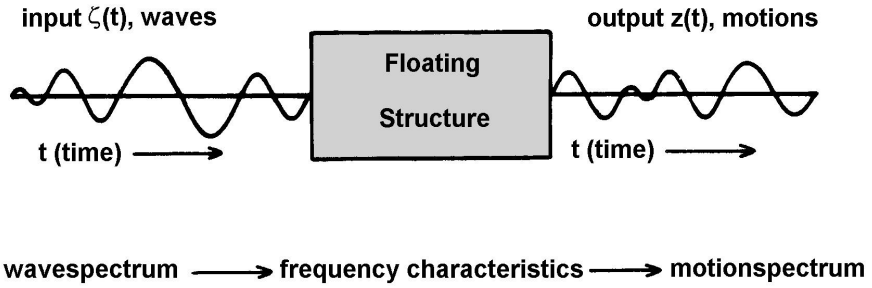

Figure 6.5: Relation between Motions and Waves

6.3.1 Kinetics

A rigid body's equation of motions with respect to an earth-bound coordinate system follow from Newton's second law. The vector equations for the translations of and the rotations about the center of gravity are respectively given by:

$$\boxed{\vec{F} = \frac{d}{dt}\left(m\vec{U}\right)} \quad \text{and} \quad \boxed{\vec{M} = \frac{d}{dt}\left(\vec{H}\right)} \tag{6.22}$$

in which:

$\vec{F}$	=	resulting external force acting in the center of gravity (N)
m	=	mass of the rigid body (kg)
$\vec{U}$	=	instantaneous velocity of the center of gravity (m/s)
$\vec{M}$	=	resulting external moment acting about the center of gravity (Nm)
$\vec{H}$	=	instantaneous angular momentum about the center of gravity (Nms)
t	=	time (s)

The total mass as well as its distribution over the body is considered to be constant during a time which is long relative to the oscillation period of the motions.

Loads Superposition

Since the system is linear, the resulting motion in waves can be seen as a superposition of the motion of the body in still water and the forces on the restrained body in waves. Thus, two important assumptions are made here for the loads on the right hand side of the picture equation in figure 6.6:

a. The so-called **hydromechanical forces and moments** are induced by the harmonic oscillations of the rigid body, moving in the undisturbed surface of the fluid.

b. The so-called **wave exciting forces and moments** are produced by waves coming in on the restrained body.

The vertical motion of the body (a buoy in this case) follows from Newton's second law:

$$\boxed{\frac{d}{dt}\left(\rho\nabla\cdot\dot{z}\right) = \rho\nabla\cdot\ddot{z} = F_h + F_w} \tag{6.23}$$

in which:

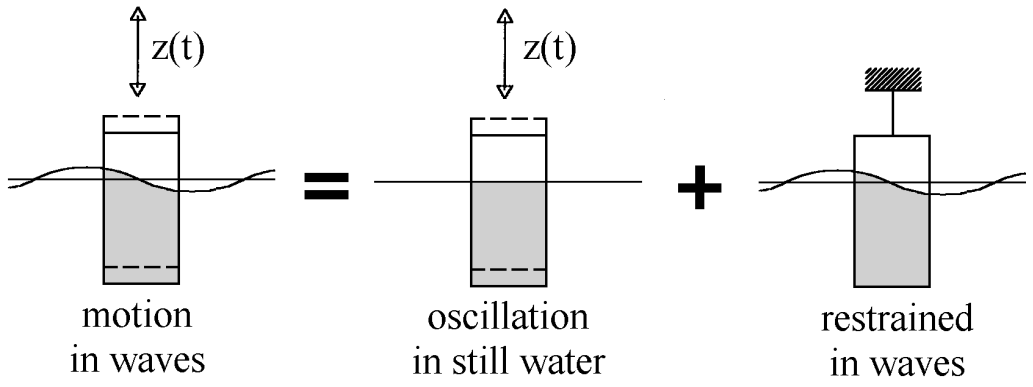

Figure 6.6: Superposition of Hydromechanical and Wave Loads

ρ	=	density of water (kg/m^3)
∇	=	volume of displacement of the body (m^3)
F_h	=	hydromechanical force in the z-direction (N)
F_w	=	exciting wave force in the z-direction (N)

This superposition will be explained in more detail for a circular cylinder, floating in still water with its center line in the vertical direction, as shown in figure 6.7.

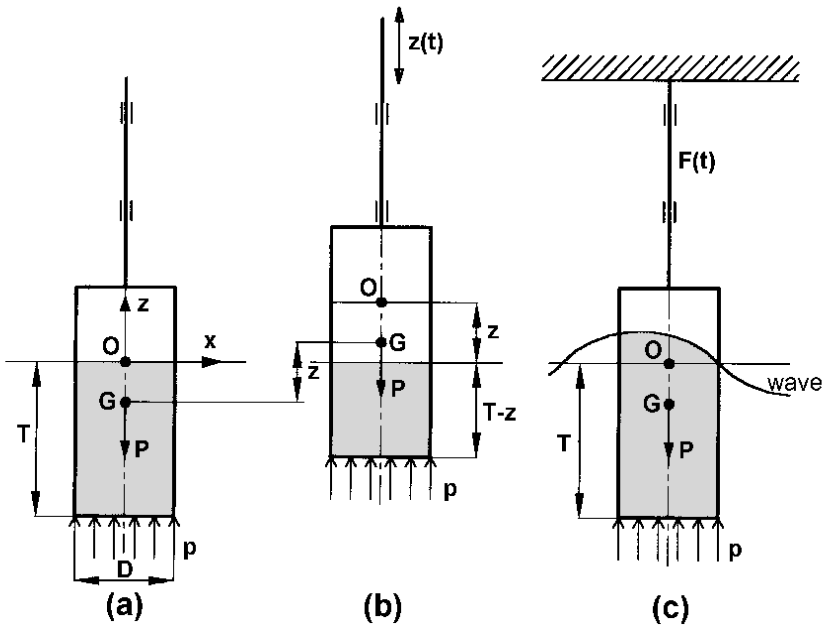

Figure 6.7: Heaving Circular Cylinder

6.3.2 Hydromechanical Loads

First, a **free decay test** in still water will be considered. After a vertical displacement upwards (see 6.7-b), the cylinder will be released and the motions can die out freely. The

vertical motions of the cylinder are determined by the solid mass m of the cylinder and the hydromechanical loads on the cylinder.
Applying Newton's second law for the heaving cylinder:

$$\begin{aligned} m\ddot{z} &= \text{sum of all forces on the cylinder} \\ &= -P + pA_w - b\dot{z} - a\ddot{z} \\ &= -P + \rho g\,(T - z)\,A_w - b\dot{z} - a\ddot{z} \end{aligned} \tag{6.24}$$

With Archimedes' law $P = \rho g T A_w$, the linear equation of the heave motion becomes:

$$\boxed{(m + a)\,\ddot{z} + b\dot{z} + cz = 0} \tag{6.25}$$

in which:

z	=	vertical displacement (m)
$P = mg$	=	mass force downwards (N)
$m = \rho A_w T$	=	solid mass of cylinder (kg)
a	=	hydrodynamic mass coefficient ($\mathrm{Ns^2/m = kg}$)
b	=	hydrodynamic damping coefficient ($\mathrm{Ns/m = kg/s}$)
$c = \rho g A_w$	=	restoring spring coefficient ($\mathrm{N/m = kg/s^2}$)
$A_w = \frac{\pi}{4} D^2$	=	water plane area ($\mathrm{m^2}$)
D	=	diameter of cylinder (m)
T	=	draft of cylinder at rest (s)

The terms $a\ddot{z}$ and $b\dot{z}$ are caused by the hydrodynamic reaction as a result of the movement of the cylinder with respect to the water. The water is assumed to be ideal and thus to behave as in a potential flow.

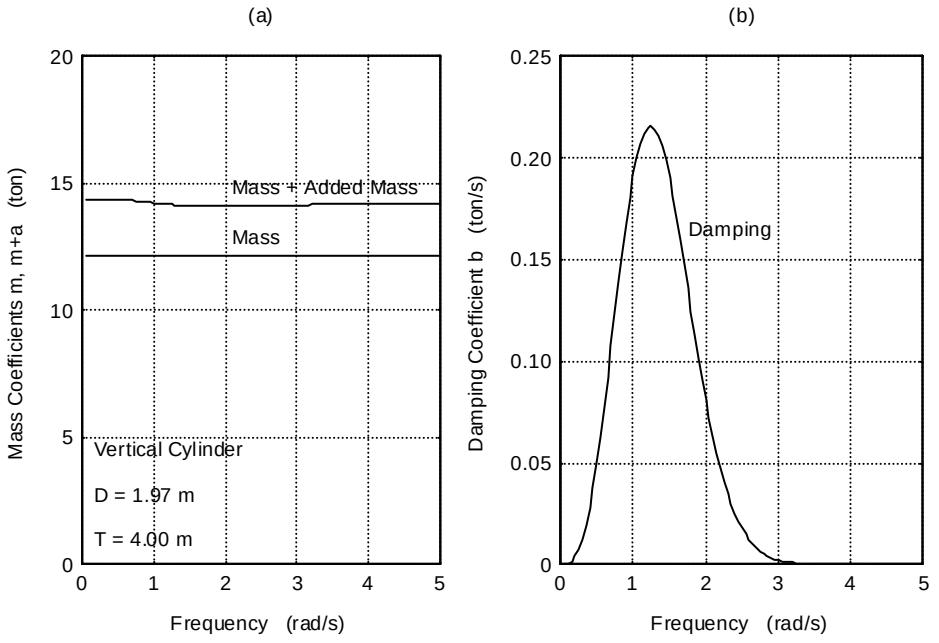

Figure 6.8: Mass and Damping of a Heaving Vertical Cylinder

The vertical oscillations of the cylinder will generate waves which propagate radially from it. Since these waves transport energy, they withdraw energy from the (free) buoy's oscillations; its motion will die out. This so-called wave damping is proportional to the velocity of the cylinder $\dot{z}$ in a linear system. The coefficient b has the dimension of a mass per unit of time and is called the **(wave or potential) damping** coefficient. Figure 6.8-b shows the hydrodynamic damping coefficient b of a vertical cylinder as a function of the frequency of oscillation.
In an actual viscous fluid, friction also causes damping, vortices and separation phenomena quite similar to that discussed in chapter 4. Generally, these viscous contributions to the damping are non-linear, but they are usually small for most large floating structures; they are neglected here for now.

The other part of the hydromechanical reaction force $a\ddot{z}$ is proportional to the vertical acceleration of the cylinder in a linear system. This force is caused by accelerations that are given to the water particles near to the cylinder. This part of the force does not dissipate energy and manifests itself as a standing wave system near the cylinder. The coefficient a has the dimension of a mass and is called the **hydrodynamic mass** or **added mass**. Figure 6.8-a shows the hydrodynamic mass a of a vertical cylinder as a function of the frequency of oscillation.

In his book, [Newman, 1977] provides added mass coefficients for deeply submerged 2-D and 3-D bodies.
Graphs of the three added mass coefficients for 2-D bodies are shown in figure 6.9. The added mass m_{11} corresponds to longitudinal acceleration, m_{22} to lateral acceleration in equatorial plane and m_{66} denotes the rotational added moment of inertia. These potential coefficients have been calculated by using conformal mapping techniques as will be explained in chapter 7.

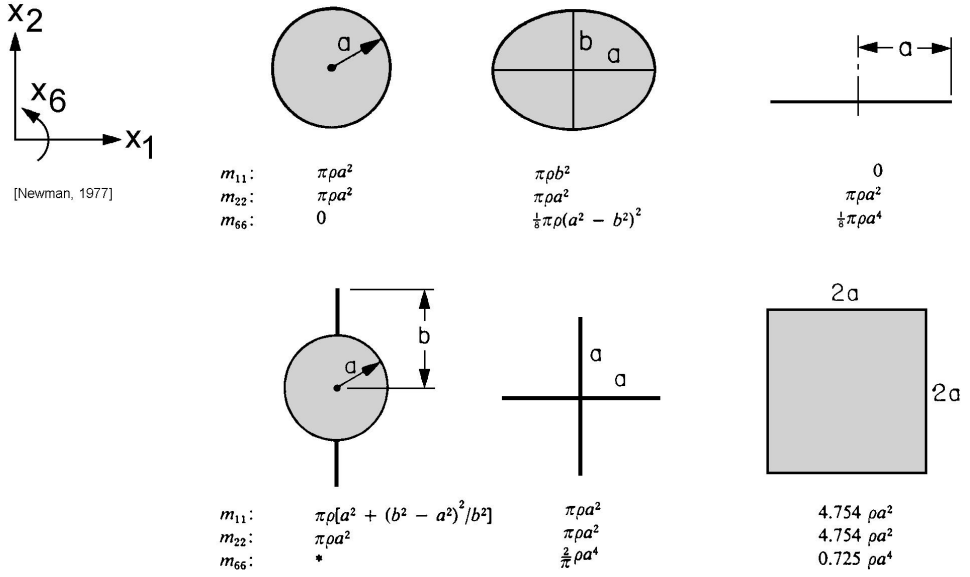

Figure 6.9: Added Mass Coefficients of 2-D Bodies

Graphs of the three added mass coefficients of 3-D spheroids, with a length $2a$ and a maximum diameter $2b$, are shown in figure 6.10. In this figure, the coefficients have been

made dimensionless using the mass and moment of inertia of the displaced volume of the fluid by the body. The added mass m_{11} corresponds to longitudinal acceleration, m_{22} to lateral acceleration in equatorial plane and m_{55} denotes the added moment of inertia for rotation about an axis in the equatorial plane.

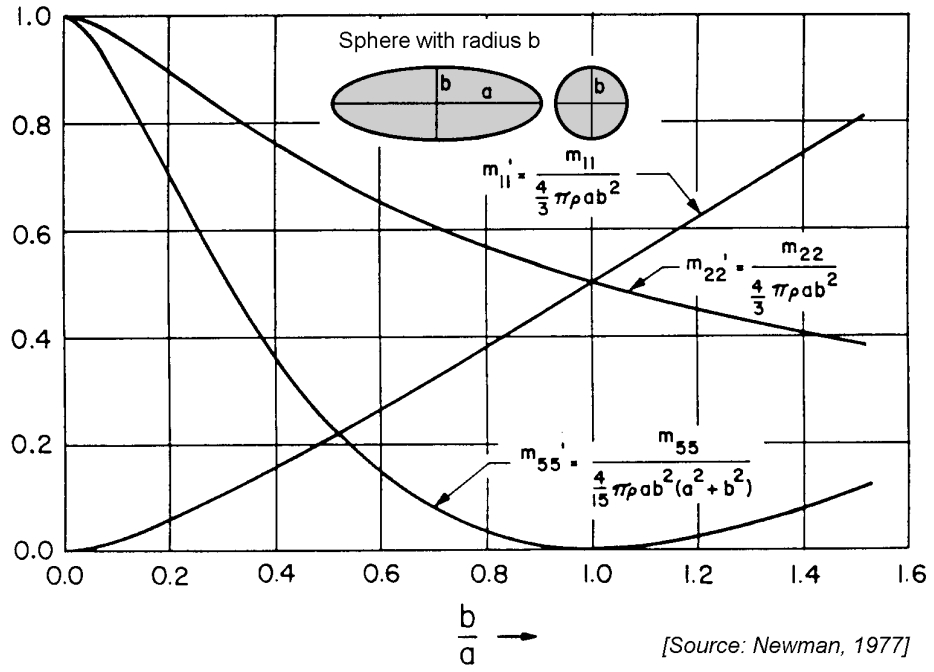

Figure 6.10: Added Mass Coefficients of Ellipsoids

Note that the potential damping of all these deeply submerged bodies is zero since they no longer generate waves on the water surface.
Since the bottom of the cylinder used in figure 6.8 is deep enough under the water surface, it follows from figure 6.10 that the added mass a can be approximated by the mass of a hemisphere of fluid with a diameter D. The damping coefficient, b, will approach to zero, because a vertical oscillation of this cylinder will hardly produce waves. The actual ratio between the added mass and the mass of the hemisphere, as obtained from 3-D calculations, varies for a cylinder as given in figure 6.8-a between 0.95 and 1.05.

It appears from experiments that in many cases both the acceleration and the velocity terms have a sufficiently linear behavior at small amplitudes; they are linear for practical purposes. The **hydromechanical forces** are the total reaction forces of the fluid on the oscillating cylinder, caused by this motion in initially still water:

$$m\ddot{z} = F_h \qquad \text{with:} \quad F_h = -a\ddot{z} - b\dot{z} - cz \tag{6.26}$$

and the equation of motion for the cylinder with a decaying motion in still water becomes:

$$(m + a) \cdot \ddot{z} + b \cdot \dot{z} + c \cdot z = 0 \tag{6.27}$$

A similar approach can be followed for the other motions. In case of angular motions, for instance roll motions, the uncoupled equation of motion (now with moment terms) of the cylinder in still water becomes:

$$(m+a)\cdot\ddot{\phi}+b\cdot\dot{\phi}+c\cdot\phi=0 \tag{6.28}$$

and the coefficients in the acceleration term, a and m, are (added) mass moment of inertia terms. Coupling between motions will be discussed in chapter 8.

Energy Relations

Suppose the cylinder is carrying out a vertical harmonic oscillation:

$$z=z_a\sin\omega t$$

in initially still water of which the linear equation of motion is given by equation 6.27.
The separate work done by the mass, damping and spring force components in this equation (force component times distance) per unit of time during one period of oscillation, T, are:

$$\begin{aligned}
\frac{1}{T}\int_0^T\{(m+a)\cdot\ddot{z}\}\cdot\{\dot{z}\cdot dt\} &= \frac{-{z_a}^2(m+a)\,\omega^3}{T}\int_0^T\sin\omega t\cdot\cos\omega t\cdot dt=0\\
\frac{1}{T}\int_0^T\{b\cdot\dot{z}\}\cdot\{\dot{z}\cdot dt\} &= \frac{{z_a}^2 b\omega^2}{T}\int_0^T\cos^2\omega t\cdot dt=\frac{1}{2}b\,\omega^2{z_a}^2\\
\frac{1}{T}\int_0^T\{c\cdot z\}\cdot\{\dot{z}\cdot dt\} &= \frac{{z_a}^2 c\omega}{T}\int_0^T\sin\omega t\cdot\cos\omega t\cdot dt=0
\end{aligned} \tag{6.29}$$

with:

$$\begin{aligned}
T=2\pi/\omega &= \text{oscillation period (s)}\\
\dot{z}\cdot dt=dz &= \text{distance covered in } dt \text{ seconds (m)}
\end{aligned}$$

It is obvious from these equations that only the damping force $\{b\cdot\dot{z}\}$ dissipates energy; damping is the reason why the heave motion, z, dies out.
Observe now a floating horizontal cylinder as given in figure 6.11, carrying out a vertical harmonic oscillation in initially still water: $z=z_a\sin\omega t$, which causes radiated waves defined by: $\zeta=\zeta_a\sin(\omega t+\varepsilon)$. A frequency-dependent relation between the damping coefficient, b, and the amplitude ratio of radiated waves and the vertical oscillation, ζ_a/z_a, can be found; see also [Newman, 1962].
The energy E (the work done per unit of time) provided by the hydrodynamic damping force is the over one period (T) integrated damping force ($b\cdot\dot{z}$) times covered distance ($\dot{z}\cdot dt$) divided by the time (T):

$$\begin{aligned}
E &= \frac{1}{T}\int_0^T\{b\cdot\dot{z}\}\cdot\{\dot{z}\cdot dt\}\\
&= \frac{1}{2}b\,\omega^2{z_a}^2
\end{aligned} \tag{6.30}$$

This energy provided by the above mentioned hydrodynamic damping force is equal to the energy dissipated by the radiated waves. This is 2 (radiation of waves to two sides) times

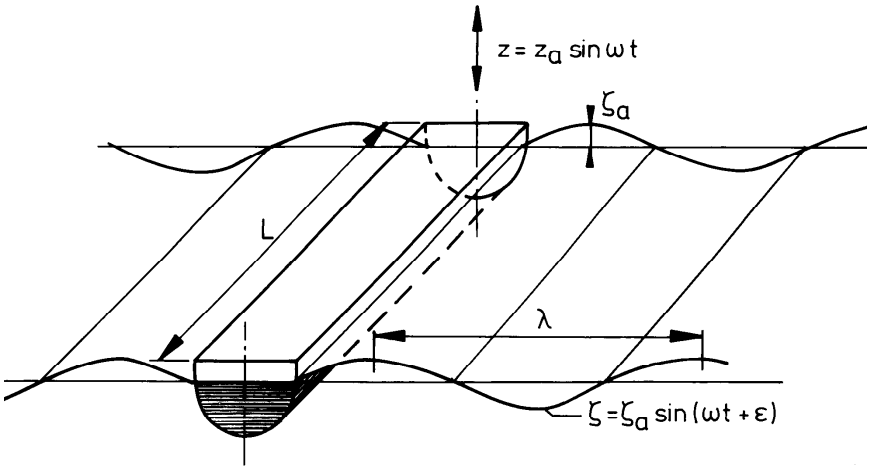

Figure 6.11: Oscillating Horizontal Cylinder

the energy of the waves per unit area ($\frac{1}{2}\rho g {\zeta_a}^2$) times the covered distance by the radiated wave energy ($c_g \cdot T$) in one period (T) times the length of the cylinder (L), divided by the time (T):

$$\begin{aligned} E &= \frac{1}{T} \cdot 2 \cdot \left\{ \frac{1}{2} \rho g {\zeta_a}^2 \right\} \cdot \{ c_g \cdot T \cdot L \} \\ &= \frac{\rho g^2 {\zeta_a}^2 L}{2\omega} \end{aligned} \tag{6.31}$$

To obtain the right hand side of this equation, use has been made of the definition of the group velocity of the waves in deep water: $c_g = c/2 = g/(2\omega)$; see chapter 5.
Thus, the potential damping coefficient per unit of length is defined by:

$$\frac{1}{2} b \, \omega^2 {z_a}^2 = \frac{\rho g^2 {\zeta_a}^2 L}{2\omega} \tag{6.32}$$

or:

$$\boxed{b' = \frac{b}{L} = \frac{\rho g^2}{\omega^3} \left(\frac{\zeta_a}{z_a} \right)^2} \tag{6.33}$$

Similar approaches can be applied for sway and roll oscillations.

The motions are defined here by $z = z_a \sin \omega t$. It is obvious that a definition of the body oscillation by $z = z_a \cos \omega t$ will provide the same results, because this means only an introduction of a constant phase shift of $-\pi/2$ in the body motion as well as in the generated waves.

Linearisation of Nonlinear damping

In some cases (especially roll motions) viscous effects do influence the damping and can result in nonlinear damping coefficients. Suppose a strongly non-linear roll damping moment, M, which can be described by:

$$M = b^{(1)} \cdot \dot{\phi} + b^{(2)} \cdot \left| \dot{\phi} \right| \cdot \dot{\phi} + b^{(3)} \cdot \dot{\phi}^3 \tag{6.34}$$

The modulus of the roll velocity in the second term is required to give the proper sign to its contribution. This damping moment can be linearised by stipulating that an identical amount of energy be dissipated by a linear term with an **equivalent linear damping coefficient** $b^{(eq)}$:

$$\frac{1}{T}\int_0^T \left\{b^{(eq)}\cdot\dot{\phi}\right\}\cdot\left\{\dot{\phi}\cdot dt\right\} = \frac{1}{T}\int_0^T \left\{b^{(1)}\cdot\dot{\phi} + b^{(2)}\cdot\left|\dot{\phi}\right|\cdot\dot{\phi} + b^{(3)}\cdot\dot{\phi}^3\right\}\cdot\left\{\dot{\phi}\cdot dt\right\} \qquad (6.35)$$

Define the roll motion by $\phi = \phi_a\cos(\omega t+\varepsilon_{\phi\zeta})$, as given in equation 6.9. Then a substitution of $\dot{\phi} = -\phi_a\omega\sin(\omega t+\varepsilon_{\phi\zeta})$ in equation 6.35 and the use of some mathematics yields:

$$\boxed{M = b^{(eq)}\cdot\dot{\phi}} \qquad \text{with:} \qquad \boxed{b^{(eq)} = b^{(1)} + \frac{8}{3\pi}\cdot\omega\cdot\phi_a\cdot b^{(2)} + \frac{3}{4}\cdot\omega^2\cdot\phi_a^2\cdot b^{(3)}} \qquad (6.36)$$

Note that this equivalent linear damping coefficient depends on both the frequency and the amplitude of oscillation.

Restoring Spring Terms

For free floating bodies, restoring 'spring' terms are present for the heave, roll and pitch motions only. The restoring spring term for heave has been given already; for the angular motions they follow from the linearized static stability phenomena as given in chapter 2:

$$\begin{aligned} \text{heave} &: \quad c_{zz} = \rho g A_{WL} \\ \text{roll} &: \quad c_{\phi\phi} = \rho g \nabla\cdot\overline{GM} \\ \text{pitch} &: \quad c_{\theta\theta} = \rho g \nabla\cdot\overline{GM}_L \end{aligned}$$

in which $\overline{GM}$ and $\overline{GM}_L$ are the transverse and longitudinal initial metacentric heights.

Free Decay Tests

In case of a pure free heaving cylinder in still water, the linear equation of the heave motion of the center of gravity, G, of the cylinder is given by equation 6.27:

$$\boxed{|(m+a)\cdot\ddot{z} + b\cdot\dot{z} + c\cdot z = 0|}$$

This equation can be rewritten as:

$$\boxed{|\ddot{z} + 2\nu\cdot\dot{z} + {\omega_0}^2\cdot z = 0|} \qquad (6.37)$$

in which the damping coefficient and the undamped natural frequency are defined by:

$$\boxed{\left|2\nu = \frac{b}{m+a}\right|}\ \text{(a)} \qquad \text{and} \qquad \boxed{\left|{\omega_0}^2 = \frac{c}{m+a}\right|}\ \text{(b)} \qquad (6.38)$$

A non-dimensional damping coefficient, κ, is written as:

$$\kappa = \frac{\nu}{\omega_0} = \frac{b}{2\sqrt{(m+a)\cdot c}} \qquad (6.39)$$

This damping coefficient is written as a fraction between the actual damping coefficient, b, and the **critical damping** coefficient, $b_{cr} = 2\sqrt{(m+a)\cdot c}$; so for critical damping: $\kappa_{cr} = 1$. Herewith, the equation of motion 6.37 can be re-written as:

$$\boxed{|\ddot{z} + 2\kappa\omega_0 \cdot \dot{z} + {\omega_0}^2 \cdot z = 0|} \tag{6.40}$$

The buoy is deflected to an initial vertical displacement, z_a, in still water and then released. The solution of the equation 6.37 of this decay motion becomes after some mathematics:

$$z = z_a e^{-\nu t}\left(\cos\omega_z t + \frac{\nu}{\omega_z}\sin\omega_z t\right) \tag{6.41}$$

where $z_a e^{-\nu t}$ is the decrease of the "crest" after one period.
Then the **logarithmic decrement** of the motion is:

$$\nu T_z = \kappa\omega_0 T_z = \ln\left\{\frac{z(t)}{z(t+T_z)}\right\} \tag{6.42}$$

Because ${\omega_z}^2 = {\omega_0}^2 - \nu^2$ for the natural frequency oscillation and the damping is small ($\nu < 0.20$) so that $\nu^2 \ll {\omega_0}^2$, one can neglect ν^2 here and use $\omega_z \approx \omega_0$; this leads to:

$$\omega_0 T_z \approx \omega_z T_z = 2\pi \tag{6.43}$$

The non-dimensional damping is given now by:

$$\boxed{\left|\kappa = \frac{1}{2\pi}\ln\left\{\frac{z(t)}{z(t+T_z)}\right\}\right| = b\cdot\frac{\omega_0}{2c}} \tag{6.44}$$

These κ-values can easily be found when results of decay tests with a model in still water are available. These are usually in a form such as is shown in figure 6.12.

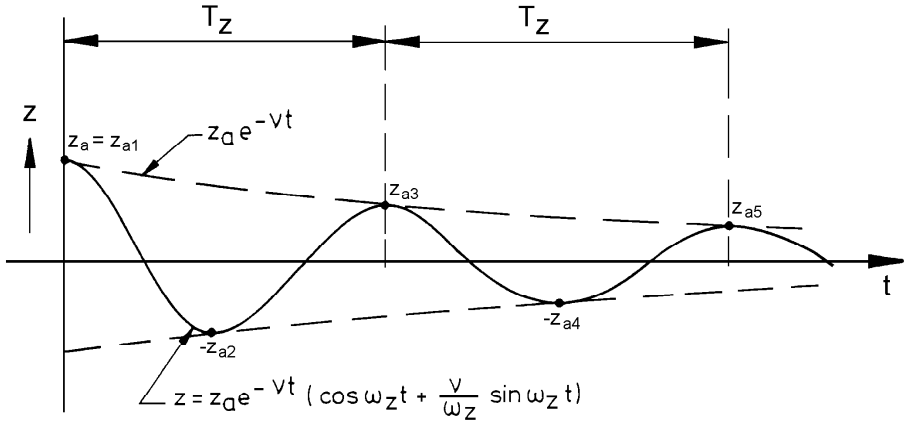

Figure 6.12: Determination of Logarithmic Decrement

Be aware that this damping coefficient is determined by assuming an uncoupled heave motion (no other motions involved). Strictly, this damping coefficient is not valid for the actual coupled motions of a free floating cylinder which will be moving in all directions simultaneously.

The results of free decay tests are presented by plotting the non-dimensional damping coefficient (obtained from two successive positive or negative maximum displacements z_{a_i} and $z_{a_{i+2}}$ by:

$$\boxed{\left|\kappa = \frac{1}{2\pi} \cdot \ln\left\{\frac{z_{a_i}}{z_{a_{i+2}}}\right\}\right|} \quad \text{versus} \quad \overline{z_a} = \left|\frac{z_{a_i} + z_{a_{i+2}}}{2}\right| \tag{6.45}$$

To avoid spreading in the successively determined κ-values, caused by a possible zero-shift of the measuring signal, double amplitudes can be used instead:

$$\boxed{\left|\kappa = \frac{1}{2\pi} \cdot \ln\left\{\frac{z_{a_i} - z_{a_{i+1}}}{z_{a_{i+2}} - z_{a_{i+3}}}\right\}\right|} \quad \text{versus} \quad \overline{z_a} = \left|\frac{z_{a_i} - z_{a_{i+1}} + z_{a_{i+2}} - z_{a_{i+3}}}{4}\right| \tag{6.46}$$

It is obvious that this latter method has preference in case of a record with small amplitudes. The decay coefficient κ can therefore be estimated from the decaying oscillation by determining the ratio between any pair of successive (double) amplitudes. When the damping is very small and the oscillation decays very slowly, several estimates of the decay can be obtained from a single record. The method is not really practical when ν is much greater than about 0.2 and is in any case strictly valid for small values of ν only. Luckily, this is generally the case.
The potential mass and damping at the natural frequency can be obtained from all of this. From equation 6.38-b follows:

$$\boxed{\left|a = \frac{c}{{\omega_0}^2} - m\right|} \tag{6.47}$$

in which the natural frequency, ω_0, follows from the measured oscillation period and the solid mass, m, and the spring coefficient, c, are known from the geometry of the body.
From equation 6.38-a, 6.38-b and equation 6.39 follows:

$$\boxed{\left|b = \frac{2\kappa c}{\omega_0}\right|} \tag{6.48}$$

in which κ follows from the measured record by using equation 6.45 or 6.46 while c and ω_0 have to be determined as done for the added mass a.
It is obvious that for a linear system a constant κ-value should be found in relation to $\overline{z_a}$. Note also that these decay tests provide no information about the relation between the potential coefficients and the frequency of oscillation. Indeed, this is impossible since decay tests are carried out at one frequency only; the natural frequency.

Forced Oscillation Tests

The relation between the potential coefficients and the frequency of oscillation can be found using forced oscillation tests. A schematic of the experimental set-up for the forced heave oscillation of a vertical cylinder is given in figure 6.13. The crank at the top of the figure rotates with a constant and chosen frequency, ω, causing a vertical motion with amplitude given by the radial distance from the crank axis to the pin in the slot. Vertical forces are measured in the rod connecting the exciter to the buoy.
During the forced heave oscillation, the vertical motion of the model is defined by:

$$z(t) = z_a \sin \omega t \tag{6.49}$$

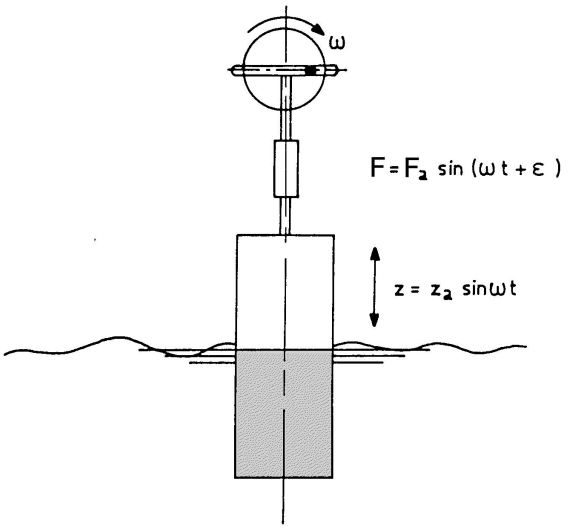

Figure 6.13: Forced Oscillation Test

and the heave forces, measured by the transducer, are:

$$F_z(t) = F_a \sin(\omega t + \varepsilon_{Fz}) \tag{6.50}$$

The (linear) equation of motion is given by:

$$\boxed{(m+a)\,\ddot{z} + b\dot{z} + cz = F_a \sin(\omega t + \varepsilon_{Fz})} \tag{6.51}$$

The component of the exciting force in phase with the heave motion is associated with inertia and stiffness, while the out-of-phase component is associated with damping.
With:

$$\begin{aligned} z &= z_a \sin\omega t \\ \dot{z} &= z_a \omega \cos\omega t \\ \ddot{z} &= -z_a \omega^2 \sin\omega t \end{aligned} \tag{6.52}$$

one obtains:

$$z_a \left\{ -(m+a)\,\omega^2 + c \right\} \sin\omega t + z_a b\omega \cos\omega t = F_a \cos\varepsilon_{Fz} \sin\omega t + F_a \sin\varepsilon_{Fz} \cos\omega t \tag{6.53}$$

which provides:

$$\begin{aligned} \text{from } \omega t = \frac{\pi}{2}\text{:} \quad & \boxed{a = \frac{c - \frac{F_a}{z_a}\cos\varepsilon_{Fz}}{\omega^2} - m} \\ \text{from } \omega t = 0\text{:} \quad & \boxed{b = \frac{\frac{F_a}{z_a}\sin\varepsilon_{Fz}}{\omega}} \\ \text{from geometry:} \quad & \boxed{c = \rho g A_w} \end{aligned} \tag{6.54}$$

To obtain the 'spring' stiffness, c, use has to be made of A_w (area of the waterline), which can be obtained from the geometry of the model. It is possible to obtain the stiffness coefficient from static experiments as well. In such a case equation 6.51 degenerates:

$$\ddot{z} = 0 \quad \text{and} \quad \dot{z} = 0 \qquad \text{yielding:} \qquad c = \frac{F_z}{z}$$

in which z is a constant vertical displacement of the body and F_z is a constant force (Archimedes' law).
The in-phase and out-of-phase parts of the exciting force during an oscillation can be found easily from an integration over a whole number (N) periods (T) of the measured signal $F(t)$ multiplied with $\cos\omega t$ and $\sin\omega t$, respectively:

$$\begin{aligned} F_a \sin\varepsilon_{Fz} &= \frac{2}{NT}\int_0^{NT} F(t)\cdot\cos\omega t\cdot dt \\ F_a \cos\varepsilon_{Fz} &= \frac{2}{NT}\int_0^{NnT} F(t)\cdot\sin\omega t\cdot dt \end{aligned} \tag{6.55}$$

These are nothing more than the first order (and averaged) Fourier series components of $F(t)$; see appendix C.

6.3.3 Wave Loads

Waves are now generated in the test basin for a new series of tests. The object is restrained so that one now measures (in this vertical cylinder example) the vertical wave load on the fixed cylinder. This is shown schematically in figure 6.7-c.
The classic theory of deep water waves (see chapter 5) yields:

$$\text{wave potential} \quad : \quad \Phi = \frac{-\zeta_a g}{\omega} e^{kz}\sin(\omega t - kx) \tag{6.56}$$

$$\text{wave elevation} \quad : \quad \zeta = \zeta_a \cos(\omega t - kx) \tag{6.57}$$

so that the pressure, p, on the **bottom** of the cylinder ($z = -T$) follows from the linearized Bernoulli equation:

$$\begin{aligned} p &= -\rho\frac{\partial\Phi}{\partial t} - \rho g z \\ &= \rho g\zeta_a e^{kz}\cos(\omega t - kx) - \rho g z \\ &= \rho g\zeta_a e^{-kT}\cos(\omega t - kx) + \rho g T \end{aligned} \tag{6.58}$$

Assuming that the diameter of the cylinder is small relative to the wave length ($kD \approx 0$), so that the pressure distribution on the bottom of the cylinder is essentially uniform, then the pressure becomes:

$$p = \rho g\zeta_a e^{-kT}\cos(\omega t) + \rho g T \tag{6.59}$$

Then the vertical force on the bottom of the cylinder is:

$$F = \left\{\rho g\zeta_a e^{-kT}\cos(\omega t) + \rho g T\right\}\cdot\frac{\pi}{4}D^2 \tag{6.60}$$

where D is the cylinder diameter and T is the draft.
The harmonic part of this force is the regular harmonic **wave force**, which will be considered here. More or less in the same way as with the hydromechanical loads (on the oscillating body in still water), this wave force can also be expressed as a spring coefficient c times a **reduced or effective** wave elevation ζ^*:

$$\boxed{|F_{FK} = c \cdot \zeta^*|} \quad \text{with:} \quad \begin{aligned} c &= \rho g \frac{\pi}{4} D^2 \qquad \text{(spring coeff.)} \\ \zeta^* &= e^{-kT} \cdot \zeta_a \cos(\omega t) \qquad \text{(deep water)} \end{aligned} \tag{6.61}$$

This wave force is called the **Froude-Krilov force**, which follows from an integration of the pressures on the body in the **undisturbed** wave.
Actually however, a part of the waves will be diffracted, requiring a correction of this Froude-Krilov force. Using the relative motion principle described earlier in this chapter, one finds additional force components: one proportional to the vertical acceleration of the water particles and one proportional to the vertical velocity of the water particles.
The total **wave force** can be written as:

$$\boxed{\left| F_w = a\ddot{\zeta}^* + b\dot{\zeta}^* + c\zeta^* \right|} \tag{6.62}$$

in which the terms $a\ddot{\zeta}^*$ and $b\dot{\zeta}^*$ are considered to be corrections on the Froude-Krilov force due to diffraction of the waves by the presence of the cylinder in the fluid.
The "reduced" wave elevation is given by:

$$\begin{aligned} \zeta^* &= \zeta_a e^{-kT} \cos(\omega t) \\ \dot{\zeta}^* &= -\zeta_a e^{-kT} \omega \sin(\omega t) \\ \ddot{\zeta}^* &= -\zeta_a e^{-kT} \omega^2 \cos(\omega t) \end{aligned} \tag{6.63}$$

A substitution of equations 6.63 in equation 6.62 yields:

$$F_w = \zeta_a e^{-kT} \left\{ c - a\omega^2 \right\} \cos(\omega t) - \zeta_a e^{-kT} \left\{ b\omega \right\} \sin(\omega t) \tag{6.64}$$

Also, this wave force can be written independently in terms of in-phase and out-of-phase terms:

$$\begin{aligned} F_w &= F_a \cos(\omega t + \varepsilon_{F\zeta}) \\ &= F_a \cos(\varepsilon_{F\zeta}) \cos(\omega t) - F_a \sin(\varepsilon_{F\zeta}) \sin(\omega t) \end{aligned} \tag{6.65}$$

Equating the two in-phase terms and the two out-of-phase terms in equations 6.64 and 6.65 result in two equations with two unknowns:

$$\begin{aligned} F_a \cos(\varepsilon_{F\zeta}) &= \zeta_a e^{-kT} \left\{ c - a\omega^2 \right\} \\ F_a \sin(\varepsilon_{F\zeta}) &= \zeta_a e^{-kT} \left\{ b\omega \right\} \end{aligned} \tag{6.66}$$

Adding the squares of these two equations results in the wave force amplitude:

$$\boxed{\left| \frac{F_a}{\zeta_a} = e^{-kT} \sqrt{\left\{ c - a\omega^2 \right\}^2 + \left\{ b\omega \right\}^2} \right|} \tag{6.67}$$

and a division of the in-phase and the out-of-phase term in equation 6.66, results in the phase shift:

$$\boxed{\varepsilon_{F\zeta} = \arctan\left\{\frac{b\omega}{c - a\omega^2}\right\} \quad \text{with: } 0 \leq \varepsilon_{z\zeta} \leq 2\pi} \tag{6.68}$$

The phase angle, $\varepsilon_{F\zeta}$, has to be determined in the correct quadrant between 0 and 2π. This depends on the signs of both the numerator and the denominator in the expression for the arctangent.
The wave force amplitude, F_a, is proportional to the wave amplitude, ζ_a, and the phase shift $\varepsilon_{F\zeta}$ is independent of the wave amplitude, ζ_a; the system is linear.

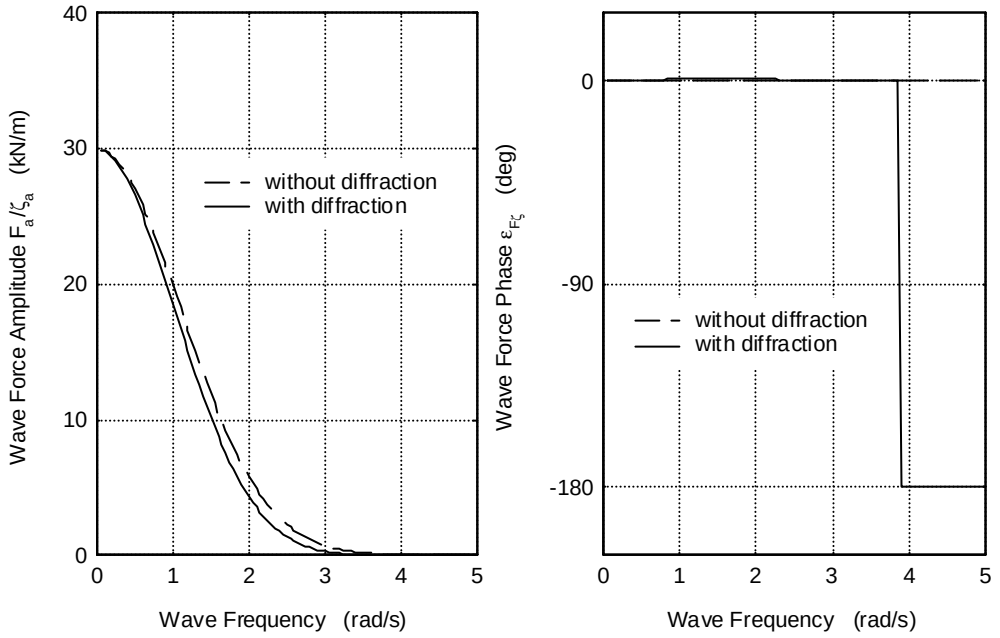

Figure 6.14: Vertical Wave Force on a Vertical Cylinder

Figure 6.14 shows the wave force amplitude and phase shift as a function of the wave frequency. For low frequencies (long waves), the diffraction part is very small and the wave force tends to the Froude-Krilov force, $c\zeta^*$. At higher frequencies there is an influence of diffraction on the wave force on this vertical cylinder. There, the wave force amplitude remains almost equal to the Froude-Krilov force.
Diffraction becomes relatively important for this particular cylinder as the Froude-Krylov force has become small; a phase shift of $-\pi$ occurs then quite suddenly. Generally, this happens the first time as the in-phase term, $F_a \cos(\varepsilon_{F\zeta})$, changes sign (goes through zero); a with ω decreasing positive Froude-Krylov contribution and a with ω increasing negative diffraction contribution (hydrodynamic mass times fluid acceleration), while the out-of-phase diffraction term (hydrodynamic damping times fluid velocity), $F_a \sin(\varepsilon_{F\zeta})$, maintains its sign.

6.3.4 Equation of Motion

Equation 6.23: $m\ddot{z} = F_h + F_w$ can be written as: $m\ddot{z} - F_h = F_w$. Then, the solid mass term and the hydromechanic loads in the left hand side (given in equation 6.25) and the

exciting wave loads in the right hand side (given in equation 6.62) provides the equation of motion for this heaving cylinder in waves:

$$\boxed{(m+a)\,\ddot{z} + b\dot{z} + cz = a\ddot{\zeta}^* + b\dot{\zeta}^* + c\zeta^*} \tag{6.69}$$

Using the relative motion principle, this equation can also be found directly from Newton's second law and the total relative motions of the water particles ($\ddot{\zeta}^*$, $\dot{\zeta}^*$and ζ^*) of the heaving cylinder in waves:

$$m\ddot{z} = a\left(\ddot{\zeta}^* - \ddot{z}\right) + b\left(\dot{\zeta}^* - \dot{z}\right) + c\left(\zeta^* - z\right) \tag{6.70}$$

In fact, this is also a combination of the equations 6.25 and 6.62.

6.3.5 Response in Regular Waves

The heave response to the regular wave excitation is given by:

$$\begin{aligned} z &= z_a \cos(\omega t + \varepsilon_{z\zeta}) \\ \dot{z} &= -z_a\omega \sin(\omega t + \varepsilon_{z\zeta}) \\ \ddot{z} &= -z_a\omega^2 \cos(\omega t + \varepsilon_{z\zeta}) \end{aligned} \tag{6.71}$$

A substitution of 6.71 and 6.63 in the equation of motion 6.69 yields:

$$\begin{aligned} & z_a\left\{c - (m+a)\,\omega^2\right\}\cos(\omega t + \varepsilon_{z\zeta}) - z_a\left\{b\omega\right\}\sin(\omega t + \varepsilon_{z\zeta}) = \\ = \;& \zeta_a e^{-kT}\left\{c - a\omega^2\right\}\cos(\omega t) - \zeta_a e^{-kT}\left\{b\omega\right\}\sin(\omega t) \end{aligned} \tag{6.72}$$

or after splitting the angle $(\omega t + \varepsilon_{z\zeta})$ and writing the out-of-phase term and the in-phase term separately:

$$\begin{aligned} z_a\left\{\left\{c - (m+a)\,\omega^2\right\}\cos(\varepsilon_{z\zeta}) - \left\{b\omega\right\}\sin(\varepsilon_{z\zeta})\right\} \quad & \cos(\omega t) \\ -z_a\left\{\left\{c - (m+a)\,\omega^2\right\}\sin(\varepsilon_{z\zeta}) + \left\{b\omega\right\}\cos(\varepsilon_{z\zeta})\right\} \quad & \sin(\omega t) = \\ = \zeta_a e^{-kT}\left\{c - a\omega^2\right\} \quad & \cos(\omega t) \\ -\zeta_a e^{-kT}\left\{b\omega\right\} \quad & \sin(\omega t) \end{aligned} \tag{6.73}$$

By equating the two out-of-phase terms and the two in-phase terms, one obtains two equations with two unknowns:

$$\begin{aligned} z_a\left\{\left\{c - (m+a)\,\omega^2\right\}\cos(\varepsilon_{z\zeta}) - \left\{b\omega\right\}\sin(\varepsilon_{z\zeta})\right\} &= \zeta_a e^{-kT}\left\{c - a\omega^2\right\} \\ z_a\left\{\left\{c - (m+a)\,\omega^2\right\}\sin(\varepsilon_{z\zeta}) + \left\{b\omega\right\}\cos(\varepsilon_{z\zeta})\right\} &= \zeta_a e^{-kT}\left\{b\omega\right\} \end{aligned} \tag{6.74}$$

Adding the squares of these two equations results in the heave amplitude:

$$\boxed{\frac{z_a}{\zeta_a} = e^{-kT}\sqrt{\frac{\left\{c - a\omega^2\right\}^2 + \left\{b\omega\right\}^2}{\left\{c - (m+a)\,\omega^2\right\}^2 + \left\{b\omega\right\}^2}}} \tag{6.75}$$

and elimination of $z_a/\zeta_a e^{-kT}$ in the two equations in 6.74 results in the phase shift:

$$\boxed{\varepsilon_{z\zeta} = \arctan\left\{\frac{-mb\omega^3}{\left(c - a\omega^2\right)\left\{c - (m+a)\,\omega^2\right\} + \left\{b\omega\right\}^2}\right\} \quad with: 0 \le \varepsilon_{z\zeta} \le 2\pi} \tag{6.76}$$

The phase angle $\varepsilon_{z\zeta}$ has to be determined in the correct quadrant between 0 and 2π. This depends on the signs of both the numerator and the denominator in the expression for the arctangent.
The requirements of linearity is fulfilled: the heave amplitude z_a is proportional to the wave amplitude ζ_a and the phase shift $\varepsilon_{z\zeta}$ is not dependent on the wave amplitude ζ_a.

Generally, these amplitudes and phase shifts are called:

$$\left.\begin{array}{rcl} \frac{F_a}{\zeta_a}(\omega) \text{ and } \frac{z_a}{\zeta_a}(\omega) & = & \text{amplitude characteristics} \\ \varepsilon_{F\zeta}(\omega) \text{ and } \varepsilon_{z\zeta}(\omega) & = & \text{phase characteristics} \end{array}\right\} \textbf{frequency characteristics}$$

The response amplitude characteristics $\frac{z_a}{\zeta_a}(\omega)$ are also referred to as **Response Amplitude Operator** (RAO).

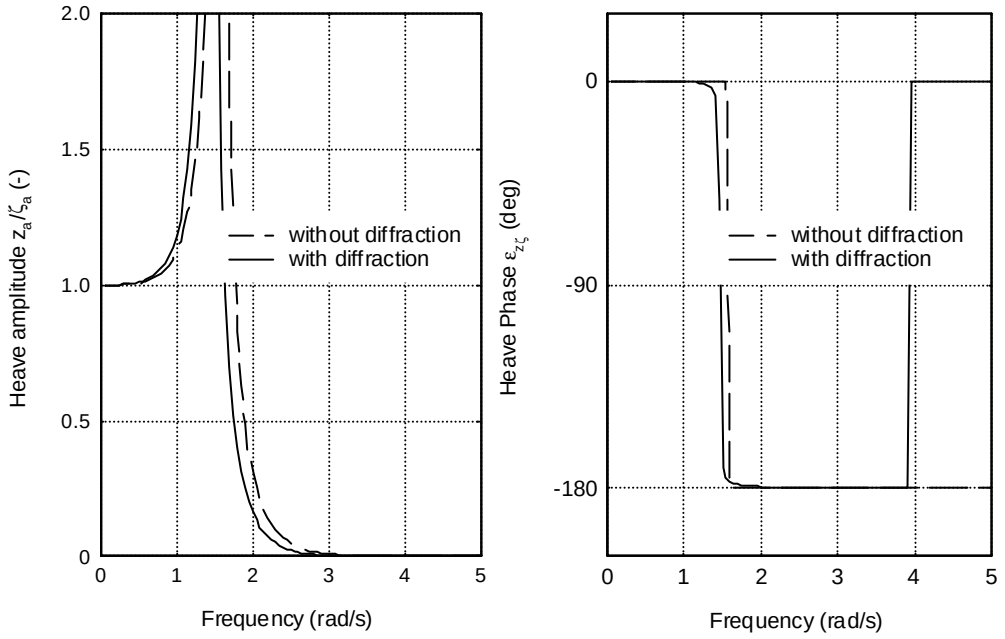

Figure 6.15: Heave Motions of a Vertical Cylinder

Figure 6.15 shows the frequency characteristics for heave together with the influence of diffraction of the waves. The annotation "without diffraction" in these figures means that the wave load consists of the Froude-Krilov force, $c\zeta^*$, only.

Equation 6.75 and figure 6.16 show that with respect to the motional behavior of this cylinder three frequency areas can be distinguished:

1. The low frequency area, $\omega^2 \ll c/(m+a)$, with vertical motions dominated by the restoring spring term.
   This yields that the cylinder tends to "follow" the waves as the frequency decreases; the RAO tends to 1.0 and the phase lag tends to zero. At very low frequencies, the wave length is large when compared with the horizontal length (diameter) of the cylinder and it will "follow" the waves; the cylinder behaves like a ping-pong ball in waves.

2. The natural frequency area, $\omega^2 \approx c/(m+a)$, with vertical motions dominated by the damping term.
   This yields that a high resonance can be expected in case of a small damping. A phase shift of $-\pi$ occurs at about the natural frequency, $\omega^2 \approx c/(m+a)$; see the denominator in equation 6.76. This phase shift is very abrupt here, because of the small damping b of this cylinder.

3. The high frequency area, $\omega^2 \gg c/(m+a)$, with vertical motions dominated by the mass term.
   This yields that the waves are "losing" their influence on the behavior of the cylinder; there are several crests and troughs within the horizontal length (diameter) of the cylinder. A second phase shift appears at a higher frequency, $\omega^2 \approx c/a$; see the denominator in equation 6.76. This is caused by a phase shift in the wave load.

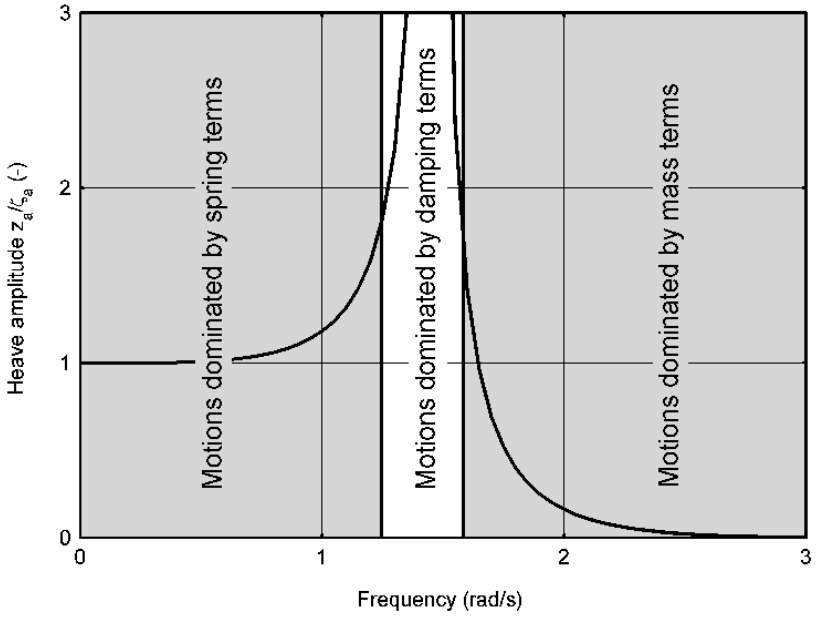

Figure 6.16: Frequency Areas with Respect to Motional Behavior

Note: From equations 6.67 and 6.75 follow also the heave motion - wave force amplitude ratio and the phase shift between the heave motion and the wave force:

$$\boxed{\left|\frac{z_a}{F_a} = \frac{1}{\sqrt{\{c-(m+a)\omega^2\}^2 + \{b\omega\}^2}}\right|}$$

$$\boxed{|\varepsilon_{zF} \;=\; \varepsilon_{z\zeta} + \varepsilon_{\zeta F} \;=\; \varepsilon_{z\zeta} - \varepsilon_{F\zeta}|} \tag{6.77}$$

6.3.6 Response in Irregular Waves

The wave energy spectrum was defined in chapter 5 by:

$$\boxed{\left|S_\zeta(\omega)\cdot d\omega \;=\; \frac{1}{2}\,\zeta_a^2(\omega)\right|} \tag{6.78}$$

Analogous to this, the energy spectrum of the heave response $z(\omega, t)$ can be defined by:

$$\begin{aligned} S_z(\omega) \cdot d\omega &= \frac{1}{2} z_a^2(\omega) \\ &= \left| \frac{z_a}{\zeta_a}(\omega) \right|^2 \cdot \frac{1}{2} \zeta_a^2(\omega) \\ &= \left| \frac{z_a}{\zeta_a}(\omega) \right|^2 \cdot S_\zeta(\omega) \cdot d\omega \end{aligned} \tag{6.79}$$

Thus, the heave response spectrum of a motion can be found by using the t**ransfer function** of the motion and the wave spectrum by:

$$\boxed{S_z(\omega) = \left| \frac{z_a}{\zeta_a}(\omega) \right|^2 \cdot S_\zeta(\omega)} \tag{6.80}$$

The principle of this transformation of wave energy to response energy is shown in figure 6.17 for the heave motions being considered here.
The irregular wave history, $\zeta(t)$ - below in the left hand side of the figure - is the sum of a large number of regular wave components, each with its own frequency, amplitude and a random phase shift. The value $\frac{1}{2}\zeta_a^2(\omega)/\Delta\omega$ - associated with each wave component on the ω-axis - is plotted vertically on the left; this is the wave energy spectrum, $S_\zeta(\omega)$. This part of the figure can be found in chapter 5 as well, by the way.
Each regular wave component can be transferred to a regular heave component by a multiplication with the transfer function $z_a/\zeta_a(\omega)$. The result is given in the right hand side of this figure. The irregular heave history, $z(t)$, is obtained by adding up the regular heave components, just as was done for the waves on the left. Plotting the value $\frac{1}{2}z_a^2(\omega)/\Delta\omega$ of each heave component on the ω-axis on the right yields the heave response spectrum, $S_z(\omega)$.
The **moments** of the heave response spectrum are given by:

$$\boxed{m_{nz} = \int_0^\infty S_z(\omega) \cdot \omega^n \cdot d\omega} \qquad \text{with: } n = 0, 1, 2, ... \tag{6.81}$$

where $n = 0$ provides the area, $n = 1$ the first moment and $n = 2$ the moment of inertia of the spectral curve.
The significant heave amplitude can be calculated from the spectral density function of the heave motions, just as was done for waves. This **significant heave amplitude**, defined as the mean value of the highest one-third part of the amplitudes, is:

$$\boxed{\bar{z}_{a_{1/3}} = 2 \cdot RMS = 2\sqrt{m_{0z}}} \tag{6.82}$$

in which RMS $(=\sqrt{m_{0z}})$ is the **Root Mean Square** value.
A **mean period** can be found from the centroid of the spectrum:

$$\boxed{T_{1z} = 2\pi \cdot \frac{m_{0z}}{m_{1z}}} \tag{6.83}$$

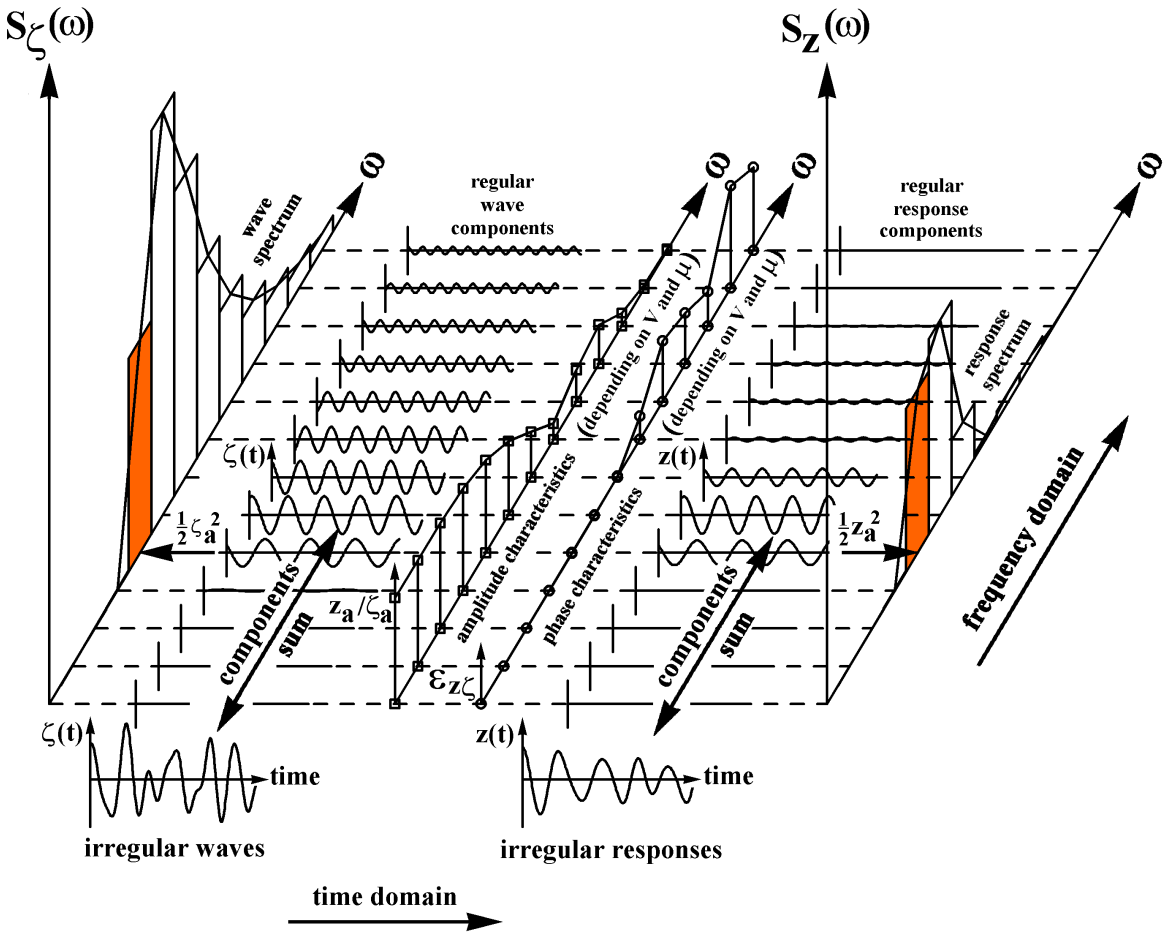

Figure 6.17: Principle of Transfer of Waves into Responses

Another definition, which is equivalent to the **average zero-crossing period**, is found from the spectral radius of gyration:

$$\boxed{T_{2z} = 2\pi \cdot \sqrt{\frac{m_{0z}}{m_{2z}}}} \tag{6.84}$$

6.3.7 Spectrum Axis Transformation

When wave spectra are given as a function of frequencies in Herz ($f = 1/T$) and one needs this on an ω-basis (in radians/sec), they have to be transformed just as was done for waves in chapter 5. The heave spectrum on this ω-basis becomes:

$$\begin{aligned} S_z(\omega) &= \frac{S_z(f)}{2\pi} \\ &= \left|\frac{z_a}{\zeta_a}(f \text{ or } \omega)\right|^2 \cdot \frac{S_\zeta(f)}{2\pi} \end{aligned} \tag{6.85}$$

6.4 Second Order Wave Drift Forces

Now that the first order behavior of linear (both mechanical as well as hydromechanical) systems has been handled, attention in the rest of this chapter shifts to nonlinear systems. Obviously hydrodynamics will get the most emphasis in this section, too.
The effects of second order wave forces are most apparent in the behavior of anchored or moored floating structures. In contrast to what has been handled above, these are horizontally restrained by some form of mooring system. Analyses of the horizontal motions of moored or anchored floating structures in a seaway show that the responses of the structure on the irregular waves include three important components:

1. A mean displacement of the structure, resulting from a constant load component. Obvious sources of these loads are current and wind. In addition to these, there is also a so-called **mean wave drift force**. This drift force is caused by non-linear (second order) wave potential effects. Together with the mooring system, these loads determine the new equilibrium position - possibly both a translation and (influenced by the mooring system) a yaw angle - of the structure in the earth-bound coordinate system. This yaw is of importance for the determination of the wave attack angle.

2. An oscillating displacement of the structure at frequencies corresponding to those of the waves; the wave-frequency region.
   These are linear motions with a harmonic character, caused by the **first order wave loads**. The principle of this has been presented above for the vertically oscillating cylinder. The time-averaged value of this wave load and the resulting motion component are zero.

3. An oscillating displacement of the structure at frequencies which are much lower than those of the irregular waves; the low-frequency region.
   These motions are caused by non-linear elements in the wave loads, the **low-frequency wave drift forces**, in combination with spring characteristics of the mooring system. Generally, a moored ship has a low natural frequency in its horizontal modes of motion as well as very little damping at such frequencies. Very large motion amplitudes can then result at resonance so that a major part of the ship's dynamic displacement (and resulting loads in the mooring system) can be caused by these low-frequency excitations.

Item 2 of this list has been discussed in earlier parts of this chapter; the discussion of item 1 starts below; item 3 is picked up later in this chapter and along with item 1 again in chapter 9.

6.4.1 Mean Wave Loads on a Wall

Mean wave loads in regular waves on a wall can be calculated simply from the pressure in the fluid, now using the more complete (not-linearized!) Bernoulli equation. The superposition principle can still be used to determine these loads in irregular waves. When the waves are not too long, this procedure can be used, too, to estimate the mean wave drift forces on a ship in beam waves (waves approaching from the side of the ship).

Regular Waves

A regular wave (in deep water) hits a vertical wall with an infinite depth as shown in figure 6.18. This wave will be reflected fully, so that a standing wave (as described in chapter 5) results at the wall.

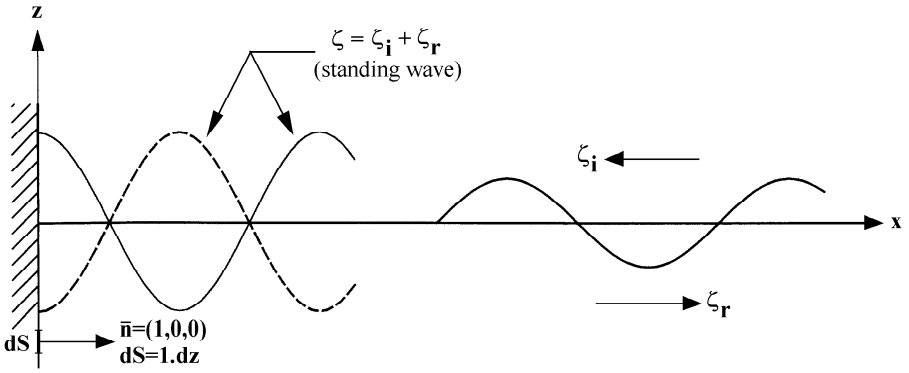

Figure 6.18: Regular Wave at a Wall

The incident undisturbed wave is defined by:

$$\boxed{\Phi_i = -\frac{\zeta_a g}{\omega} \cdot e^{kz} \cdot \sin(+kx + \omega t)} \quad \text{and} \quad \underline{\boxed{\zeta_i = \zeta_a \cdot \cos(+kx + \omega t)}} \tag{6.86}$$

and the reflected wave by:

$$\boxed{\Phi_r = -\frac{\zeta_a g}{\omega} \cdot e^{kz} \cdot \sin(-kx + \omega t)} \quad \text{and} \quad \underline{\boxed{\zeta_r = \zeta_a \cdot \cos(-kx + \omega t)}} \tag{6.87}$$

Then the total wave system can be determined by a superposition of these two waves; this results in a standing wave system:

$$\begin{aligned} \Phi &= \Phi_i + \Phi_r = -2 \cdot \frac{\zeta_a g}{\omega} \cdot e^{kz} \cdot \cos(kx) \cdot \sin(\omega t) \\ \zeta &= \zeta_i + \zeta_r = 2 \cdot \zeta_a \cdot \cos(kx) \cdot \cos(\omega t) \end{aligned} \tag{6.88}$$

The pressure in the fluid follows from the complete Bernoulli equation:

$$\begin{aligned} p &= -\rho g \cdot z - \rho \cdot \frac{\partial \Phi}{\partial t} - \frac{1}{2}\rho \cdot (\nabla \Phi)^2 \\ &= -\rho g \cdot z - \rho \cdot \frac{\partial \Phi}{\partial t} - \frac{1}{2}\rho \cdot \left\{ \left(\frac{\partial \Phi}{\partial x}\right)^2 + \left(\frac{\partial \Phi}{\partial z}\right)^2 \right\} \end{aligned} \tag{6.89}$$

The derivatives of the potential $\Phi(x, z, t)$ with respect to t, x and z are given by:

$$\begin{aligned} \frac{\partial \Phi}{\partial t} &= -2 \cdot \zeta_a \cdot g \cdot e^{kz} \cdot \cos(kx) \cdot \cos(\omega t) \\ u = \frac{\partial \Phi}{\partial x} &= +2 \cdot \zeta_a \cdot \omega \cdot e^{kz} \cdot \sin(kx) \cdot \sin(\omega t) \\ w = \frac{\partial \Phi}{\partial z} &= -2 \cdot \zeta_a \cdot \omega \cdot e^{kz} \cdot \cos(kx) \cdot \sin(\omega t) \end{aligned} \tag{6.90}$$

At the wall ($x = 0$), the wave elevation and the derivatives of the potential are:

$$\begin{aligned} \zeta &= 2 \cdot \zeta_a \cdot \cos(\omega t) \\ \frac{\partial \Phi}{\partial t} &= -2 \cdot \zeta_a \cdot g \cdot e^{kz} \cdot \cos(\omega t) \\ u = \frac{\partial \Phi}{\partial x} &= 0 \\ w = \frac{\partial \Phi}{\partial z} &= -2 \cdot \zeta_a \cdot \omega \cdot e^{kz} \cdot \sin(\omega t) \end{aligned} \tag{6.91}$$

and the pressure on the wall is:

$$\begin{aligned} p &= -\rho g \cdot z - \rho \cdot \frac{\partial \Phi}{\partial t} - \frac{1}{2}\rho \cdot \left\{ \left(\frac{\partial \Phi}{\partial x} \right)^2 + \left(\frac{\partial \Phi}{\partial z} \right)^2 \right\} \\ &= -\rho g \cdot z + 2\rho g \cdot \zeta_a \cdot e^{kz} \cdot \cos(\omega t) - \frac{1}{2}\rho \cdot \left(4{\zeta_a}^2 \cdot \omega^2 \cdot e^{2kz} \sin^2(\omega t) \right) \\ &= -\rho g \cdot z + 2\rho g \cdot \zeta_a \cdot e^{kz} \cdot \cos(\omega t) - \rho \cdot {\zeta_a}^2 \cdot \omega^2 \cdot e^{2kz} \cdot (1 - \cos(2\omega t)) \end{aligned} \tag{6.92}$$

This time-varying pressure on the wall can also be written as:

$$p = \bar{p}^{(0)} + \tilde{p}^{(1)} + \bar{p}^{(2)} + \tilde{p}^{(2)} \tag{6.93}$$

where:

$$\begin{aligned} \bar{p}^{(0)} &= -\rho g \cdot z \\ \tilde{p}^{(1)} &= +2\rho g \cdot \zeta_a \cdot e^{kz} \cdot \cos(\omega t) \\ \bar{p}^{(2)} &= -\rho \cdot {\zeta_a}^2 \cdot \omega^2 \cdot e^{2kz} \\ \tilde{p}^{(2)} &= +\rho \cdot {\zeta_a}^2 \cdot \omega^2 \cdot e^{2kz} \cdot \cos(2\omega t) \end{aligned} \tag{6.94}$$

The general expression for the mean force on the wall follows from:

$$\overline{F} = -\overline{\int_{-\infty}^{\zeta} (\bar{p} \cdot \bar{n}) \cdot dS} \tag{6.95}$$

where the superscript bar over the entire integral indicates a (long) time average.
Because $\bar{n} = (1, 0, 0)$ and $dS = 1 \cdot dz$, this mean force becomes:

$$\bar{F} = -\overline{\int_{-\infty}^{\zeta(t)} p(z,t) \cdot dz} \tag{6.96}$$

which is split into two parts over the vertical axis; one above and one below the still water level:

$$\bar{F} = -\overline{\int_{-\infty}^{0} p(z,t) \cdot dz} - \overline{\int_{0}^{\zeta(t)} p(z,t) \cdot dz} \tag{6.97}$$

$$= \overline{F_1} + \overline{F_2} \tag{6.98}$$

where:

$$p(z,t) = \bar{p}^{(0)} + \tilde{p}^{(1)} + \bar{p}^{(2)} + \tilde{p}^{(2)} \qquad \text{and} \qquad \zeta(t) = \tilde{\zeta}^{(1)}(t) \tag{6.99}$$

The first part $\overline{F_1}$ comes from the integration from $-\infty$ to 0; it contributes to the integration of $\bar{p}^{(0)}$ and $\bar{p}^{(2)}$ only:

$$\begin{aligned}
\overline{F_1} &= -\overline{\int_{-\infty}^{0} p(z,t) \cdot dz} \\
&= -\int_{-\infty}^{0} \left(-\rho g z - \rho \cdot {\zeta_a}^2 \cdot \omega^2 \cdot e^{2kz}\right) \cdot dz \\
&= \rho \cdot \omega^2 \cdot {\zeta_a}^2 \int_{-\infty}^{0} e^{2kz} \cdot dz \\
&= +\frac{1}{2} \rho g \cdot {\zeta_a}^2
\end{aligned} \tag{6.100}$$

This force is directed away from the wall. The static first term $(-\rho g z)$ has been left out of consideration, while the dispersion relation for deep water $(\omega^2 = kg)$ has been utilized in the second term.
The second part, $\overline{F_2}$, comes from the integration from 0 to $\zeta(t)$; it contributes to the integration of $\bar{p}^{(0)}$ and $\tilde{p}^{(1)}$ only, so that the time-dependent force $F_2(t)$ becomes:

$$\begin{aligned}
F_2(t) &= -\int_{0}^{\zeta(t)} p(z,t) \cdot dz \\
&= -\int_{0}^{\zeta(t)} \left(-\rho g \cdot z + \rho g \cdot \zeta(t)\right) \cdot dz \\
&= +\rho g \int_{0}^{\zeta(t)} z \cdot dz \; - \rho g \int_{0}^{\zeta(t)} \zeta(t) \cdot dz \\
&= +\frac{1}{2} \rho g \cdot \{\zeta(t)\}^2 \; - \rho g \cdot \{\zeta(t)\}^2 \\
&= -\frac{1}{2} \rho g \cdot \{\zeta(t)\}^2
\end{aligned} \tag{6.101}$$

Because

$$\zeta(t) = 2 \cdot \zeta_a \cdot \cos(\omega t) \qquad \text{and} \qquad \cos^2(\omega t) = \frac{1}{2} \cdot (1 + \cos(2\omega t)) \tag{6.102}$$

this part of the force becomes:

$$\begin{aligned}
F_2(t) &= -\frac{1}{2} \rho g \cdot 4 \cdot {\zeta_a}^2 \cdot \cos^2(\omega t) \\
&= -\rho g \cdot {\zeta_a}^2 \cdot (1 + \cos(2\omega t))
\end{aligned} \tag{6.103}$$

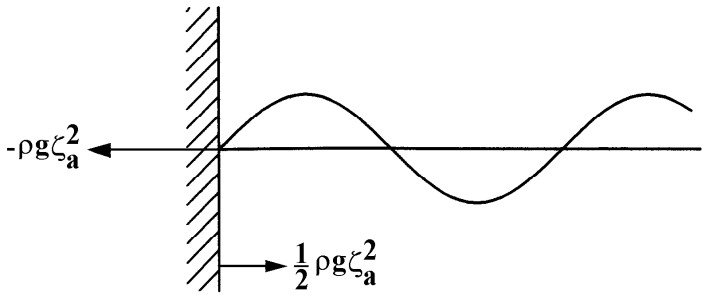

Figure 6.19: Mean Wave Loads on a Wall

The desired time-averaged value becomes:

$$\overline{F_2} = -\rho g \cdot {\zeta_a}^2 \tag{6.104}$$

where ζ_a is the amplitude of the incoming wave. This force is directed toward the wall. Finally, see figure 6.19, the total time-averaged force $\bar{F}$ per meter length of the wall becomes:

$$\begin{aligned} \bar{F} &= \overline{F_1} + \overline{F_2} \\ &= +\frac{1}{2}\rho g \cdot {\zeta_a}^2 - \rho g \cdot {\zeta_a}^2 \end{aligned} \tag{6.105}$$

Thus:

$$\boxed{\bar{F} = -\frac{1}{2}\rho g \cdot {\zeta_a}^2} \tag{6.106}$$

in which it is assumed that the incident wave is fully reflected. This total force has a magnitude proportional to the square of the incoming wave amplitude and it is directed toward the wall.
Note that this force is also directly related to the energy per unit area of the incoming waves as found in chapter 5:

$$E = \frac{1}{2}\rho g \cdot \zeta_a^2 \tag{6.107}$$

Comparison of equations 6.106 and 6.107 reveals that the mean wave drift force is numerically equal to the energy per unit area of the incoming waves.

Irregular Waves

The discovery just made above will be utilized to determine the mean wave drift force from irregular waves as well. This is done via the wave spectrum, defined by:

$$S_\zeta(\omega) \cdot d\omega = \frac{1}{2}{\zeta_a}^2(\omega) \quad \text{with a zero order moment: } m_0 = \int_0^\infty S_\zeta(\omega) \cdot d\omega \tag{6.108}$$

Then the total force on the wall can be written as:

$$\bar{F} = -\sum \frac{1}{2}\rho g \cdot {\zeta_a}^2(\omega)$$

$$= -\rho g \int_0^\infty S_\zeta(\omega) \cdot d\omega$$
$$= -\rho g \cdot m_{0\zeta} \tag{6.109}$$

Because:

$$H_{1/3} = 4\sqrt{m_{0\zeta}} \quad \text{or} \quad m_{0\zeta} = \frac{1}{16} \cdot {H_{1/3}}^2 \tag{6.110}$$

it follows that the mean wave drift force can be expressed as:

$$\boxed{\bar{F} = \frac{-1}{16} \cdot \rho g \cdot {H_{1/3}}^2} \quad \text{per metre length of the wall} \tag{6.111}$$

Approximation for Ships

It has been assumed so far that the incident wave is fully reflected. When the waves are not too long, so that the water motion is more or less concentrated near the sea surface (over the draft of the ship), full reflection can be assumed for large ships too. Then, equation 6.111 can be used for a first estimation of the mean wave drift forces on a ship in beam waves.
The mean wave drift force on an example ship with a length L of 300 meters in beam waves with a significant wave height $H_{1/3}$ of 4.0 meters can be approximated easily. **Assuming that all waves will be reflected**, the mean wave drift force is:

$$\bar{F} = \frac{1}{16} \cdot \rho g \cdot {H_{1/3}}^2 \cdot L$$
$$= \frac{1}{16} \cdot 1.025 \cdot 9.806 \cdot 4.0^2 \cdot 300 \approx 3000 \text{ kN} \tag{6.112}$$

6.4.2 Mean Wave Drift Forces

[Maruo, 1960] showed for the two-dimensional case of an infinitely long cylinder floating in regular waves with its axis perpendicular to the wave direction that the mean wave drift force per unit length satisfies:

$$\boxed{\bar{F}' = \frac{1}{2}\rho g \cdot {\zeta_{ar}}^2} \tag{6.113}$$

in which ζ_{ar} is the amplitude of the wave reflected and scattered by the body in a direction opposite to the incident wave.
Generally only a part of the incident regular wave will be reflected; the rest will be transmitted underneath the floating body. Besides the reflected wave, additional waves are generated by the heave, pitch and roll motions of the vessel. The reflected and scattered waves have the same frequency as the incoming wave, so that the sum of these components still has the same frequency as the incoming wave. Their amplitudes will depend on the amplitudes and relative phases of the reflected and scattered wave components. The amplitudes of these components and their phase differences depend on the frequency of the incident wave, while the amplitudes can be assumed to be linearly proportional to the amplitude of the incident wave. This is because it is the incident wave amplitude which causes the body to move in the first place. In equation form:

$$\zeta_{ar} = R(\omega) \cdot \zeta_a \tag{6.114}$$

in which $R(\omega)$ is a reflection coefficient.
This means that the mean wave drift force in regular waves per meter length of the cylinder can be written as:

$$\boxed{F_d' = \frac{1}{2}\rho g \cdot \{R(\omega) \cdot \zeta_a\}^2} \tag{6.115}$$

This expression indicates that the mean wave drift force is proportional to the incident wave amplitude squared. Note that in case of the previously discussed wall: $R(\omega) = 1.0$.

6.4.3 Low-Frequency Wave Drift Forces

[Hsu and Blenkarn, 1970] and [Remery and Hermans, 1971] studied the phenomenon of the mean and slowly varying wave drift forces in a random sea from the results of model tests with a rectangular barge with breadth B. It was moored in irregular head waves to a fixed point by means of a bow hawser. The wave amplitudes provide information about the slowly varying **wave envelope** of an irregular wave train. The wave envelope is an imaginary curve joining successive wave crests (or troughs); the entire water surface motion takes place with the area enclosed by these two curves.
It seems logical in the light of the earlier results to expect that the square of the envelope amplitude will provide information about the drift forces in irregular waves. To do this, one would (in principle) make a spectral analysis of the square of this wave envelope. In other words, the spectral density of the square of the wave amplitude provides information about the mean period and the magnitude of the slowly varying wave drift force.
In practice it is very difficult to obtain an accurate wave envelope spectrum due to the long wave record required. Assuming that about 200-250 oscillations are required for an accurate spectral analysis and that the mean period of the wave envelope record is about 100 seconds, the total time that the wave elevation has to be recorded can be up to 7 hours.

Another very simple method is based on individual waves in an irregular wave train. Assume that the irregular wave train is made up of a sequence of single waves of which the wave amplitude is characterized by the height of a wave crest or the depth of a wave trough, ζ_{ai}, while the period, T_i, (or really half its value) is determined by the two adjacent zero crossings (see figure 6.20).

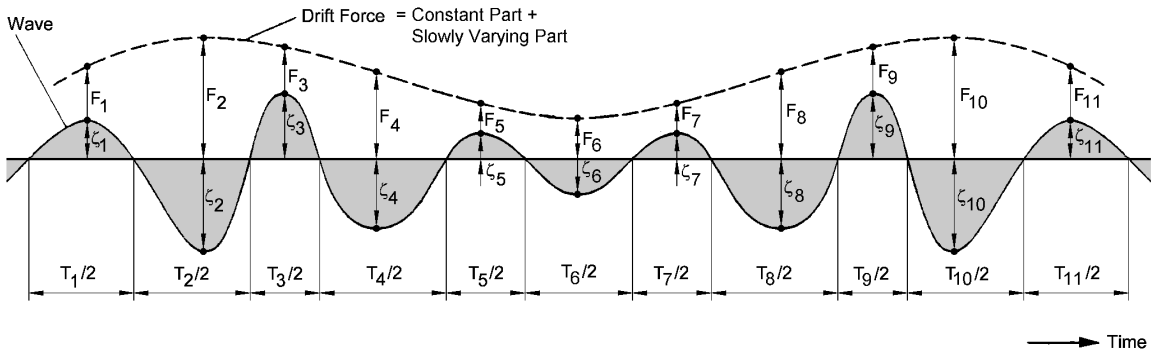

Figure 6.20: Wave Drift Forces Obtained from a Wave Record

Each of the so obtained single waves (one for every crest or trough) is considered to be one out of a regular wave train, which exerts (in this case) a surge drift force on the barge:

$$F_i = \frac{1}{2}\rho g \cdot \{R(\omega_i) \cdot \zeta_{ai}\}^2 \cdot B \qquad \text{with:} \quad \omega_i = \frac{2\pi}{T_i} \tag{6.116}$$

When this is done for all wave crests and troughs in a wave train, points on a curve representing a slowly varying wave drift force, $F(t)$, will be obtained. This drift force consists of a slowly varying force (the low-frequency wave drift force) around a mean value (the mean wave drift force); see figure 6.20.

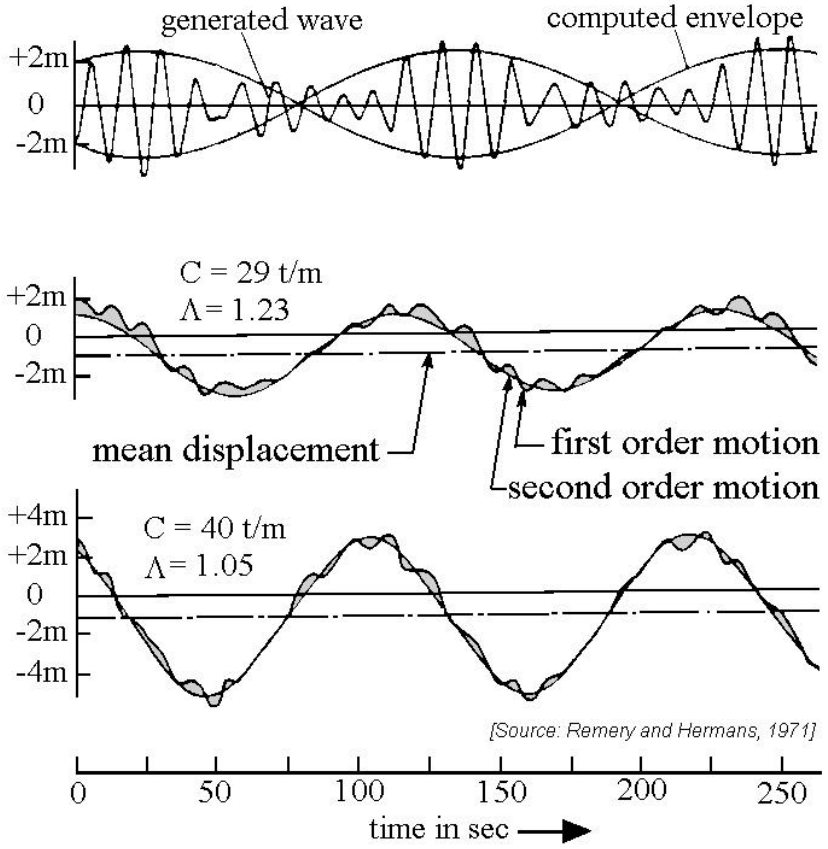

Figure 6.21: Low-Frequency Surge Motions of a Barge

These low-frequency wave drift forces on the barge will induce low-frequency surge motions with periods of for instance over 100 seconds. An example is given in figure 6.21 for two different spring constants, C. The period ratio, Λ, in this figure is the ratio between the natural surge period of the system (ship plus mooring) and the wave envelope period. (Another term for the wave envelope period is **wave group period**.) As can be seen in this figure the first order (wave-frequency) surge motions are relatively small, when compared with the second order (low-frequency) motions. This becomes especially true near resonance (when $\Lambda \rightarrow 1.0$).

Resonance may occur when wave groups are present with a period in the vicinity of the natural period of the mooring system. Due to the low natural frequency for surge of the bow hawser - barge system and the low damping at this frequency, large surge motions can

result. According to [Remery and Hermans, 1971], severe horizontal motions can be built up within a time duration of only a few consecutive wave groups. Obviously, information about the occurrence of wave groups will be needed to predict this response. This is a matter for oceanographers.

6.4.4 Additional Responses

The table below summarizes possible responses of a system (such as a moored vessel) to regular and irregular waves. Both linear and nonlinear mooring systems are included here; mooring systems can be designed to have nearly linear characteristics, but most are at least a bit nonlinear.
The right hand side of the table below gives the motions which are possible via each of the 'paths' from left to right. There will always be first order response to first order excitations; these have been discussed already as has the response of a linear or non-linear system to higher order excitations.

Wave	Excitation	System	Response
Regular	First order	Linear	First order (single frequency)
Regular	First order	Nonlinear	Subharmonic (single low frequency)
Regular	Higher order	Linear	Time-independent drift
Regular	Higher order	Nonlinear	Time-independent drift
Irregular	First order	Linear	First order (wave frequencies)
Irregular	First order	Nonlinear	Subharmonic (uncertain)
Irregular	Higher order	Linear	Time-dependent drift
Irregular	Higher order	Nonlinear	Time-dependent drift

Subharmonic Response

One path in the table above has not been discussed yet. This involves a subharmonic response of a nonlinear system to a first order excitation from either regular or irregular waves. The response, itself, looks much like the response to slow drift forces; these two are difficult indeed to distinguish. Luckily perhaps, a significant time is needed to build up

subharmonic resonant motions of high amplitude. This implies that the excitation must remain very nicely behaved over quite some time in order for this to happen. Waves at sea are very often too irregular; this subharmonic motion breaks down before large amplitudes are generated.

6.5 Time Domain Approach

If (as has been assumed so far in most of this chapter) the system is linear, such that its behavior is linearly related to its displacement, velocity and acceleration, then the behavior of the system can be studied in the frequency domain.
However, in a lot of cases there are several complications which violate this linear assumption, for instance nonlinear viscous damping, forces and moments due to currents, wind, anchoring and not to mention second order wave loads. If the system is nonlinear, then superposition principle - the foundation of the frequency domain approach - is no longer valid. Instead, one is forced to revert to the direct solution of the equations of motion as functions of time. These equations of motion result directly from Newton's second law. Approaches to their solution are presented in this section.

6.5.1 Impulse Response Functions

The hydromechanical reaction forces and moments, due to time varying ship motions, can be described using the classic formulation given by [Cummins, 1962]. Complex potential problems, can be handled via frequency-dependent potential coefficients as done by [Ogilvie, 1964]. The principle of this approach will be demonstrated here for a motion with one degree of freedom. Insight about the possibilities of this method is more important in this section than the details of the derivations involved; the result is more important than the exact route leading to it.

Cummins Equation

The floating object is assumed to be a linear system with a translational (or rotational) velocity as input and the reaction force (or moment) of the surrounding water as output. The object is assumed to be at rest at time $t = t_0$.
During a short time interval, Δt, the body experiences an impulsive displacement, Δx, with a constant velocity, V, so that:

$$\Delta x = V \cdot \Delta t \tag{6.117}$$

During this impulsive displacement, the water particles will start to move. Since potential flow is assumed, a velocity potential, Φ, proportional to the velocity, V, can be defined:

$$\Phi(x, y, z, t) = \Psi(x, y, z) \cdot V(t) \qquad \text{for: } t_0 < t < t_0 + \Delta t \tag{6.118}$$

in which Ψ is the normalized velocity potential.
Note: This Ψ is not a stream function as used in chapter 3; this notation is used here to remain consistent with other literature.

The water particles are still moving after this impulsive displacement, Δx. Because the system is assumed to be linear, the motions of the fluid, described by the velocity potential, Φ, are proportional to the impulsive displacement, Δx. So:

$$\Phi(x,y,z,t) = \chi(x,y,z,t) \cdot \Delta x \qquad \text{for: } t > t_0 + \Delta t \tag{6.119}$$

in which χ is another normalized velocity potential.
A general conclusion can be that the impulsive displacement, Δx, during the time interval $(t_0, t_0 + \Delta t)$ influences the motions of the fluid during this interval as well as during all later time intervals. Similarly, the motions during the interval $(t_0, t_0 + \Delta t)$ are influenced by the motions before this interval; the system has a form of **"memory"**.
When the object performs an arbitrarily time-dependent varying motion, this motion can be considered to be a succession of small impulsive displacements, so that then the resulting total velocity potential, $\Phi(t)$, during the interval $(t_m, t_m + \Delta t)$ becomes:

$$\Phi(t) = V_m \cdot \Psi + \sum_{k=1}^{m} \{\chi(t_{m-k}, t_{m-k} + \Delta t) \cdot V_k \cdot \Delta t\} \tag{6.120}$$

with:

m	=	number of time steps (-)
t_m	=	$t_0 + m \cdot \Delta t$ (s)
t_{m-k}	=	$t_0 + (m-k) \cdot \Delta t$ (s)
V_m	=	velocity component during time interval $(t_m, t_m + \Delta t)$ (m/s)
V_k	=	velocity component during time interval $(t_{m-k}, t_{m-k} + \Delta t)$ (m/s)
Ψ	=	normalized velocity potential caused by a displacement during time interval $(t_m, t_m + \Delta t)$
χ	=	normalized velocity potential caused by a displacement during time interval $(t_{m-k}, t_{m-k} + \Delta t)$

Letting Δt go to zero, yields:

$$\Phi(t) = \dot{x}(t) \cdot \Psi + \int_{-\infty}^{t} \chi(t-\tau) \cdot \dot{x}(\tau) \cdot d\tau \tag{6.121}$$

in which $\dot{x}(\tau)$ is the velocity component of the body at time τ.
The pressure in the fluid follows from the linearized Bernoulli equation:

$$p = -\rho \cdot \frac{\partial \Phi}{\partial t} \tag{6.122}$$

An integration of these pressures over the wetted surface, S, of the floating object yields the expression for the hydrodynamic reaction force (or moment), F.
With n is the generalized directional cosine in a vector notation, F becomes:

$$\begin{aligned} F &= -\int_S \int p \cdot n \cdot dS \\ &= \left\{ \rho \int_S \int \Psi \cdot n \cdot dS \right\} \cdot \ddot{x}(t) \\ &\quad + \int_{-\infty}^{t} \left\{ \rho \int_S \int \frac{\partial \chi(t-\tau)}{\partial t} \cdot n \cdot dS \right\} \cdot \dot{x}(\tau) \cdot d\tau \end{aligned} \tag{6.123}$$

By defining:

$$\begin{aligned} A &= \rho \int_S \int \Psi \cdot n \cdot dS \\ B(t) &= \rho \int_S \int \frac{\partial \chi(t-\tau)}{\partial t} \cdot n \cdot dS \end{aligned} \tag{6.124}$$

the hydrodynamic force (or moment) becomes:

$$F = A \cdot \ddot{x}(t) + \int_{-\infty}^{t} B(t-\tau) \cdot \dot{x}(\tau) \cdot d\tau \tag{6.125}$$

Together with a linear restoring spring term $C \cdot x$ and a linear external load, $X(t)$, Newton's second law yields the linear equation of motion in the time domain:

$$(M + A) \cdot \ddot{x}(t) + \int_{-\infty}^{t} B(t-\tau) \cdot \dot{x}(\tau) \cdot d\tau + C \cdot x(t) = X(t) \tag{6.126}$$

in which:

$\ddot{x}(t)$	=	translational (or rotational) acceleration at time t (m/s^2)
$\dot{x}(t)$	=	translational (or rotational) velocity in at time t (m/s)
$x(t)$	=	translational (or rotational) displacement at time t (m)
M	=	solid mass or mass moment of inertia (kg)
A	=	hydrodynamic (or added) mass coefficient (kg)
$B(t)$, $B(\tau)$	=	retardation functions (Ns/m)
C	=	spring coefficient from ship geometry (N/m)
$X(t)$	=	external load in at time t (N)
t, τ	=	time (s)

By replacing "τ" by "$t - \tau$" in the damping part and changing the integration boundaries, this part can be written in a more convenient form:

$$\boxed{(M + A) \cdot \ddot{x}(t) + \int_{0}^{\infty} B(\tau) \cdot \dot{x}(t-\tau) \cdot d\tau + C \cdot x(t) = X(t)} \tag{6.127}$$

This type of equation is often referred to as a "Cummins Equation" in honor of his work; see [Cummins, 1962].

Coefficient Determination

If present, the linear restoring (hydrostatic) spring coefficient, C, can be determined easily from the underwater geometry and - when rotations are involved - the center of gravity of the floating object.
The velocity potentials, Ψ and χ, have to be found to determine the coefficients, A and B. A direct approach is rather complex. An easier method to determine A and B has

been found by [Ogilvie, 1964]. He made use of the hydrodynamic mass and damping data determined using existing frequency domain computer programs based on potential theory. This allowed him to express the needed coefficients A and B relatively simply in terms of the calculated hydrodynamic mass and damping data. His approach is developed here. The floating object is assumed to carry out an harmonic oscillation with a unit amplitude:

$$x = 1.0 \cdot \cos(\omega t) \tag{6.128}$$

Substitution of this in the Cummins equation 6.127 yields:

$$-\omega^2 \cdot (M + A) \cdot \cos(\omega t) - \omega \cdot \int_0^\infty B(\tau) \cdot \sin(\omega t - \omega\tau) \cdot d\tau + C \cdot cos(\omega t) = X(t) \tag{6.129}$$

which can be worked out to yield:

$$\begin{aligned} -\omega^2 \cdot \quad & \left\{ M + A - \frac{1}{\omega} \cdot \int_0^\infty B(\tau) \sin(\omega\tau) d\tau \right\} \cdot \cos(\omega t) \\ -\omega \cdot \quad & \left\{ \int_0^\infty B(\tau) \cdot \cos(\omega\tau) \cdot d\tau \right\} \sin(\omega t) + \{C\} \cdot cos(\omega t) = X(t) \end{aligned} \tag{6.130}$$

Alternatively, the classical frequency domain description of this motion is given by:

$$\begin{aligned} -\omega^2 \cdot \quad & \{M + a(\omega)\} \cdot \cos(\omega t) \\ -\omega \cdot \quad & \{b(\omega)\} \cdot \sin(\omega t) + \{c\} \cdot cos(\omega t) = X(t) \end{aligned} \tag{6.131}$$

with:

$a(\omega)$	=	frequency-dependent hydrodynamic mass coefficient ($Ns^2/m = kg$)
$b(\omega)$	=	frequency-dependent hydrodynamic damping coefficient (Ns/m)
c	=	restoring spring term coefficient (N/m)
$X(t)$	=	external force (N)

[Ogilvie, 1964] compared the time domain and frequency domain equations 6.130 and 6.131 and found:

$$\begin{aligned} a(\omega) &= A - \frac{1}{\omega} \cdot \int_0^\infty B(\tau) \sin(\omega\tau) d\tau \\ b(\omega) &= \int_0^\infty B(\tau) \cdot \cos(\omega\tau) \cdot d\tau \\ c &= C \end{aligned} \tag{6.132}$$

The first two of these equations look very similar to those for determining the first order coefficients in a Fourier series; see appendix C. An inverse Fourier Transform can be used to isolate the desired function, $B(\tau)$; the coefficient, A, can be evaluated directly with a bit of algebra.

This yields the so-called **retardation function**:

$$\boxed{B(\tau) = \frac{2}{\pi} \cdot \int_0^\infty b(\omega) \cdot \cos(\omega\tau) \cdot d\omega} \tag{6.133}$$

The mass term is simply:

$$A = a(\omega) + \frac{1}{\omega} \cdot \int_0^\infty B(\tau) \cdot \sin(\omega\tau) \cdot d\tau \tag{6.134}$$

This expression is valid for any value of ω, and thus also for $\omega = \infty$; this provides:

$$\boxed{A = a(\omega) \quad \text{evaluated at } \omega = \infty} \tag{6.135}$$

The numerical computational problems that have to be solved, because the integrations have to be carried out from 0 to ∞, are not discussed here.
Figure 6.22, is an example of the retardation function for roll of a ship.

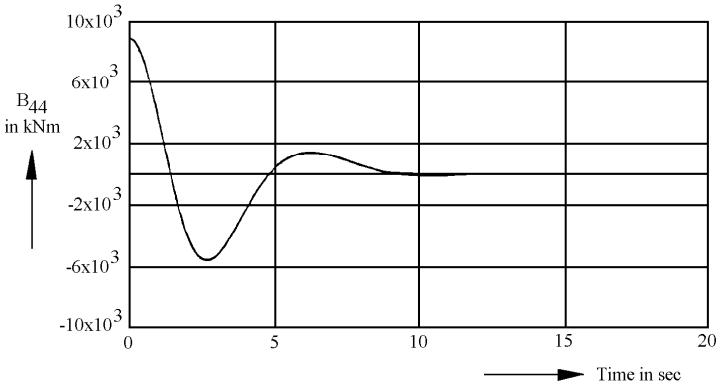

Figure 6.22: Retardation Function for Roll

Addition of (External) Loads

So far, discussion has concentrated on the left hand side of equation 6.127. Notice that this part of the equation is still linear!
Attention shifts now to the right hand side, the external force $X(t)$. Since it can be convenient to keep the left hand side of the equation of motion linear, one often moves all the nonlinear effects - even a nonlinear damping or spring force - to the opposite side, where they are all considered to be part of the external force $X(t)$.
Obviously one will have to know (or at least be able to evaluate) $X(t)$ in order to obtain a solution to the equation of motion.
Since the first order wave force is a linear phenomenon, time histories of the first order wave loads in a certain sea state can be obtained from frequency domain calculations by using the frequency characteristics of the first order wave loads and the wave spectrum by using the superposition principle:

$$\zeta(t) = \sum_{n=1}^{N} \zeta_{a_n} \cos(\omega_n t + \varepsilon_n)$$

with randomly chosen phase shifts, ε_n, between 0 and 2π and:

$$\zeta_{a_n} = \sqrt{2 \cdot S_\zeta(\omega_n) \cdot \Delta\omega} \quad \text{which follows from:} \quad \frac{1}{2}\zeta_{a_n}^2 = S_\zeta(\omega_n) \cdot \Delta\omega$$

see chapter 5.
With this, the time history of the first order wave load then becomes:

$$\boxed{X_w(t) = \sum_{n=1}^{N} \left(\frac{X_{wa_n}}{\zeta_{a_n}}\right) \cdot \zeta_{a_n} \cos(\omega_n t + \varepsilon_n + \varepsilon_{X_w\zeta_n})} \tag{6.136}$$

in which:

$X_w(t)$	=	wave load (N)
N	=	number of frequencies (-)
ω_n	=	wave frequency rad/s)
$\frac{X_{wa_n}}{\zeta_{a_n}}$	=	transfer function of wave load (N/m)
$\varepsilon_{X_w\zeta_n}$	=	phase shift of wave load (rad)
ε_n	=	phase shift of wave (rad)

Note that with a constant frequency interval , $\Delta\omega$, this time history repeats itself after $2\pi/\Delta\omega$ seconds.
With known coefficients and the right hand side of this equation of motion, equation 6.127 can be integrated a numerically. Comparisons of calculated and transformed linear motions in the frequency domain with time domain results show a perfect agreement.

Validation Tests

A series of simple model experiments have been carried out to validate the time domain calculation routines with non-linear terms. Towing tank number 2 of the Delft Ship Hydromechanics Laboratory with a 1:40 model of the Oil Skimming Vessel m.v. Smal Agt (51.00 x 9.05 x 3.25 meter) was used for this. Horizontal impulse forces in the longitudinal and lateral direction have been introduced in a tow line between a torque-motor and the model in still water. The measured motions of the ship model have been compared with the data calculated in the time domain, using the measured time-series of the impulse forces and assumed points of application as an input. An example of the comparison is presented in figure 6.23 for the sway velocities due to a lateral impulse force amidships.
The figure shows a good agreement between the calculated and the measured sway motions. Comparable agreements have been found for the other tests.
A few years ago, the Centre for Applied Research in The Netherlands (TNO) carried out a series of full scale collision tests with two inland waterway tankers in still water, see figure 6.24. The contact forces between the two ships and the motions of the rammed ship (80.00 x 8.15 x 2.20 meter) were measured. Computer simulations of the motion behavior of the rammed ship during the collision have been carried out, using the measured contact forces on the rammed ship as an input.
Figure 6.25 shows some comparative results for a test with a collision of the rammed ship at about 0.40 L_{pp} from the bow on the port side. The ramming ship had a speed of about 15 km/hr. The measured and calculated motions of the rammed ship are presented. Sway, roll and yaw velocities are predicted here very well.

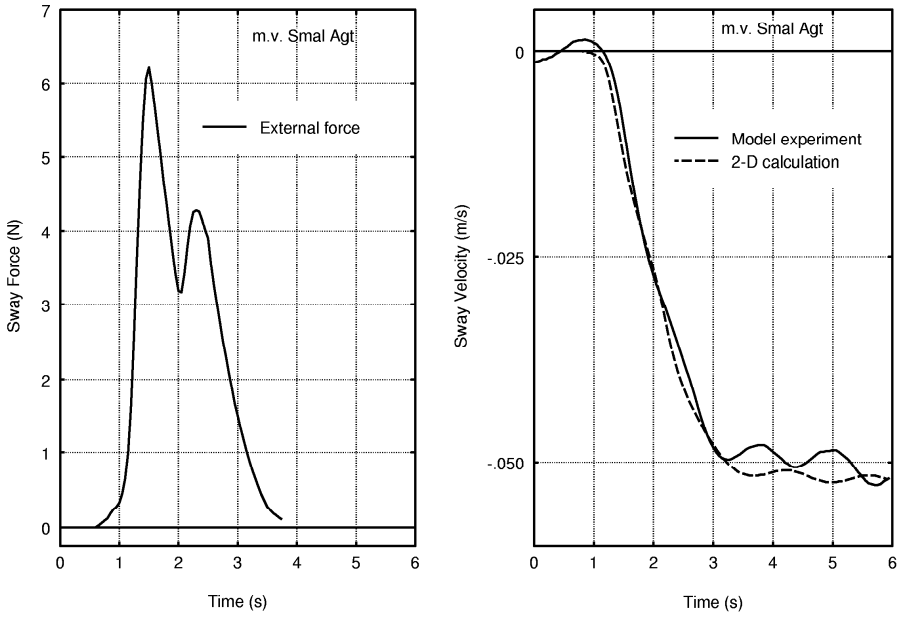

Figure 6.23: External Impulse and Resulting Motions

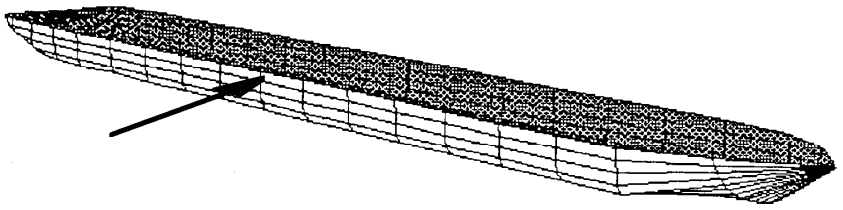

Figure 6.24: Underwater Portion of Rammed Ship

6.5.2 Direct Time Domain Simulation

Retardation functions as described above can be used to solve the equations of motion for cases in which the nonlinearities can be included in the time-dependent excitation on the right hand side of the equation. While it is possible to "move" some nonlinearities to the excitation side of the equation of motion more or less artificially, there are still many relevant physical systems which do not lend themselves to such a treatment.

One example of such a system will come up at the end of chapter 12 when the hydrodynamic drag on a moving cylinder in waves will be discussed. A perhaps more spectacular example involves the launching of an offshore tower structure from a barge. It should be obvious that the hydrodynamic mass and damping of such a structure - and of the barge from which it is launched - will change quite rapidly as the tower enters the water and load is transferred from the barge. Notice, now, that the hydromechanical coefficients - for both the tower and barge - can best be expressed as (nonlinear) *functions of the position* of the respective structures rather than of time. These functions can easily be accommodated in a time domain calculation in which all conditions can be re-evaluated at the start of each time step.

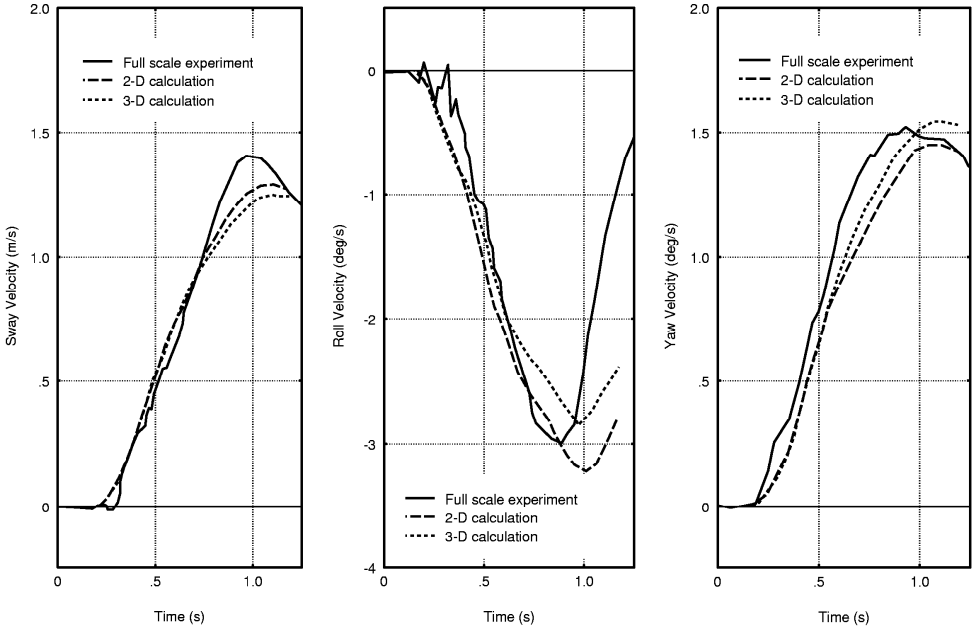

Figure 6.25: Measured and Calculated Velocities During a Ship Collision

Indeed, any system can be solved by direct integration of the equations of motion in the time domain. This approach is direct and certainly straightforward in theory, but it is often so cumbersome to carry out that it becomes impractical in practice. Admittedly, modern computers continue to shift the limits of practicality, but these limits are still very present for many offshore engineering applications.

Basic Approach

The approach is simple enough: the differential equations of motion resulting from the application of Newton's law are simply integrated - using an appropriate numerical method - in the time domain. This means that all of the input (such as a wave record) must be known as a function of time, and that a time record of the output (such as a time history of hydrodynamic force on a vibrating cable) will be generated.

Difficulties

A first and obvious difficulty with time domain simulation is that a time record of the input - such as the waves - must be provided, while generally, one only has information about the wave spectrum available. Wave records will have to be re-generated using methods as given in chapter 5.
As indicated there, by choosing different series of random phases one can generate a seemingly endless series of time records, all with identical statistical properties. There is no-one who can say which - if any - particular time record is correct. What difference does it make? The difference lies in the fact that the largest wave - very important for an extreme response, for example - may occur early in the record, or later or even not at all (during a finite record). This can have a significant influence on the interpretation of the results, of course - especially when extreme values are needed.

The interpretation of time domain simulation results forms a second difficulty in practice. A designer often needs a "design response" (an extreme dynamic internal load or displacement) with an associated (small) probability that it will be exceeded as "output" from a dynamic analysis. This interpretation difficulty is brought into focus by reviewing the process for a linear system, first.
One will generally analyze a linear system in the frequency domain; spectra of the desired response are generated directly. Since the response spectra will be of essentially the same form as the input spectra, the output can be transformed to convenient statistical data for distributions interpretation - just as is done for waves. Once this theoretical distribution has been fitted, it is a simple matter to extrapolate this to get the value associated with the chosen design probability.
When time domain simulation is used instead, one must first convert the generated time record of the output to some form of spectrum. If the system being analyzed is nonlinear, then the spectrum of the output need not look much like that of the input at all: it can contain energy at entirely different frequencies for example, so that its best representation in a mathematical form is not known. This means that one must numerically fit several theoretical forms in order to find the best one. Once this has been done, one will need to extrapolate - just as above - to a desired (low) probability of exceedance. Since the quality of this extrapolation is no better than the quality of equation fit, and the (few) computed extreme values in the generated time record disproportional influence the 'tail' of the probability distribution, one needs either very long or very many time records of the output in order to determine these extremes with sufficient accuracy. This implies that hours or even days of dynamic response will need to be simulated. Since such simulations often still run at less than real time on even fast computers, the computational effort becomes prohibitively expensive.

Constrained Time Domain Simulation

Quite some research has been invested to come to more efficient ways of carrying out a time domain simulation. Tromans has been one of the leaders in this. Since these newer methods are not yet (as of this writing) widely accepted (and the details of their mathematics would make this work significantly thicker), they will not be treated here.

Chapter 7

POTENTIAL COEFFICIENTS

7.1 Introduction

Consider a rigid body, oscillating in or below the free surface of a fluid. The fluid is assumed to be incompressible, inviscid and irrotational and without surface tension. The body is forced to carry out simple harmonic motions with a prescribed frequency of oscillation, ω. It is assumed that steady state conditions have been attained. The motion amplitudes and velocities are small enough so that all but the linear terms of the free surface condition, the kinematic boundary condition on the body and the Bernoulli equation may be neglected. The hydrodynamic pressures on the surface of the body can be obtained from the linearized Bernoulli equation, using the known velocity potentials. Integration of these pressures in the required direction provides the hydrodynamic force or moment. This force or moment can also be expressed in terms of potential mass and damping. Comparisons of the in-phase and out-of-phase parts of the two expressions provide the potential mass and damping coefficients.
This chapter details the steps needed to carry out such a computation.

7.2 Principles

Consider a rigid body floating in an ideal fluid with harmonic waves. The water depth is assumed to be finite. The time-averaged speed of the body is zero in all directions. For the sake of simple notation, it is assumed here that the $O(x, y, z)$ system is identical to the $S(x_0, y_0, z_0)$ system described in chapter 6. The x-axis is coincident with the undisturbed still water free surface and the z-axis and z_0-axis are positive upwards.
The potential theory used here will be developed (and extended) from the relations presented in chapter 5. There are a few differences, however. The velocity components (u, v, w) in chapter 5 are replaced here by (v_x, v_y, v_z) in this chapter; this is the more common notation found in the relevant literature. The wave velocity potential Φ_w in chapter 5 has been replaced here by a more general velocity potential, Φ.

The linear fluid velocity potential can be split into three parts:

$$\underline{|\Phi(x, y, z; t) = \Phi_r + \Phi_w + \Phi_d|} \tag{7.1}$$

[0] J.M.J. Journée and W.W. Massie, *"OFFSHORE HYDROMECHANICS"*, First Edition, January 2001, Delft University of Technology. For updates see web site: http://www.shipmotions.nl.

in which:

- Φ_r = **radiation potential** from the oscillatory motion of the body in still water.
- Φ_w = incident undisturbed **wave potential.**
- Φ_d = **diffraction potential** of the waves about the restrained body.

7.2.1 Requirements

Just as in chapter 5, each of these velocity potentials has to fulfill a number of requirements and boundary conditions in the fluid. Of these, the first four are identical to those in chapter 5; only their results are presented here. Additional boundary conditions are associated with the floating body which is now present. These will be discussed in detail.

1. **Continuity Condition or Laplace Equation**

$$\boxed{\nabla^2\Phi = \frac{\partial^2\Phi}{\partial x^2} + \frac{\partial^2\Phi}{\partial y^2} + \frac{\partial^2\Phi}{\partial z^2} = 0} \qquad \text{(see chapter 5)} \tag{7.2}$$

2. **Sea Bed Boundary Condition**

$$\boxed{\frac{\partial\Phi}{\partial z} = 0 \qquad \text{for: } z = -h} \qquad \text{(see chapter 5)} \tag{7.3}$$

3. **Boundary Condition at the Free Surface**
   For the free surface dynamic boundary condition was found:

$$\frac{\partial\Phi}{\partial t} + g\zeta = 0 \quad \text{or} \quad \frac{\partial^2\Phi}{\partial t^2} + g\frac{\partial\zeta}{\partial t} = 0 \qquad \text{for: } z = 0 \qquad \text{(see chapter 5)} \tag{7.4}$$

   and the vertical velocity of the water particle at $z = 0$ follows from free surface kinematic boundary condition:

$$\frac{\partial\Phi}{\partial z} = \frac{\partial\zeta}{\partial t} \qquad \text{for: } z = 0 \qquad \text{(see chapter 5)} \tag{7.5}$$

   Combining equations 7.4 and 7.5 yields:

$$\boxed{\frac{\partial^2\Phi}{\partial t^2} + g\frac{\partial\Phi}{\partial z} = 0 \qquad for: z = 0} \tag{7.6}$$

   This equation is has been found already in chapter 5, when determining the Cauchy-Poisson condition in short waves (deep water). However, equation 7.6 is also valid for finite water depths.

4. **Kinematic Boundary Condition on the Oscillating Body Surface**
   The boundary condition at the surface of the rigid body, S, plays a very important role. The velocity of a water particle at a point at the surface of the body is equal to the velocity of this (watertight) body point itself. The outward normal velocity,

v_n, at a point $P(x, y, z)$ at the surface of the body (positive in the direction of the fluid) is given by:

$$\frac{\partial \Phi}{\partial n} = v_n(x, y, z; t) \tag{7.7}$$

Because the solution of the potential will be linearized, this can be written as:

$$\boxed{\left| \frac{\partial \Phi}{\partial n} = v_n(x, y, z; t) = \sum_{j=1}^{6} v_j \cdot f_j(x, y, z) \right|} \tag{7.8}$$

in terms of oscillatory velocities and generalized direction cosines on the surface of the body, S, given by:

$$\begin{aligned}
\text{surge}: &\quad f_1 = \cos(n, x) \\
\text{sway}: &\quad f_2 = \cos(n, y) \\
\text{heave}: &\quad f_3 = \cos(n, z) \\
\text{roll}: &\quad f_4 = y\cos(n, z) - z\cos(n, y) = yf_3 - zf_2 \\
\text{pitch}: &\quad f_5 = z\cos(n, x) - x\cos(n, z) = zf_1 - xf_3 \\
\text{yaw}: &\quad f_6 = x\cos(n, y) - y\cos(n, x) = xf_2 - yf_1
\end{aligned} \tag{7.9}$$

The direction cosines are called generalized, because f_1, f_2 and f_3 have been normalized (the sum of their squares is equal to 1) and used to obtain f_4, f_5 and f_6.
Note: The subscripts $1, 2, ...6$ are used here to indicate the mode of the motion. Also displacements are often indicated in literature in the same way: $x_1, x_2, ...x_6$.

5. **Radiation Condition**
The radiation condition states that as the distance, R, from the oscillating body becomes large, the potential value tends to zero:

$$\boxed{\left| \lim_{R \to \infty} \Phi = 0 \right|} \tag{7.10}$$

6. **Symmetric or Anti-symmetric Condition**
Since ships and many other floating bodies are symmetric with respect to its middle line plane, one can make use of this to simplify the potential equations:

$$\begin{aligned}
&\boxed{|\Phi_2(-x, y) = -\Phi_2(+x, y)|} && \text{for sway} \\
&\boxed{|\Phi_3(-x, y) = +\Phi_3(+x, y)|} && \text{for heave} \\
&\boxed{|\Phi_4(-x, y) = -\Phi_4(+x, y)|} && \text{for roll}
\end{aligned} \tag{7.11}$$

in which Φ_i is the velocity potential for the given direction i.
This indicates that for sway and roll oscillations, the horizontal velocities of the water particles, thus the derivative $\partial\Phi/\partial x$, at any time on both sides of the body must have the same direction; these motions are anti-symmetric. For heave oscillations these velocities must be of opposite sign; this is a symmetric motion. However, for all three modes of oscillations the vertical velocities, thus the derivative $\partial\Phi/\partial y$, on both sides must have the same directions at any time.

7.2.2 Forces and Moments

The forces $\vec{F}$ and moments $\vec{M}$ follow from an integration of the pressure, p, over the submerged surface, S, of the body:

$$\begin{aligned} \vec{F} &= -\iint_S (p \cdot \vec{n}) \cdot dS \\ \vec{M} &= -\iint_S p \cdot (\vec{r} \times \vec{n}) \cdot dS \end{aligned} \tag{7.12}$$

in which $\vec{n}$ is the outward normal vector on surface dS and $\vec{r}$ is the position vector of surface dS in the $O(x, y, z)$ coordinate system.
The pressure p - via the linearized Bernoulli equation - is determined from the velocity potentials by:

$$\begin{aligned} p &= -\rho \frac{\partial \Phi}{\partial t} - \rho g z \\ &= -\rho \left(\frac{\partial \Phi_r}{\partial t} + \frac{\partial \Phi_w}{\partial t} + \frac{\partial \Phi_d}{\partial t} \right) - \rho g z \end{aligned} \tag{7.13}$$

which can obviously be split into four separate parts, so that the hydromechanical forces $\vec{F}$ and moments $\vec{M}$ can be split into four parts too:

$$\boxed{\vec{F} = \rho \iint_S \left(\frac{\partial \Phi_r}{\partial t} + \frac{\partial \Phi_w}{\partial t} + \frac{\partial \Phi_d}{\partial t} + g z \right) \vec{n} \cdot dS} \tag{7.14}$$

$$\boxed{\vec{M} = \rho \iint_S \left(\frac{\partial \Phi_r}{\partial t} + \frac{\partial \Phi_w}{\partial t} + \frac{\partial \Phi_d}{\partial t} + g z \right) (\vec{r} \times \vec{n}) \cdot dS} \tag{7.15}$$

or:

$$\begin{aligned} \vec{F} &= \vec{F}_r + \vec{F}_w + \vec{F}_d + \vec{F}_s \\ \vec{M} &= \vec{M}_r + \vec{M}_w + \vec{M}_d + \vec{M}_s \end{aligned} \tag{7.16}$$

Summarizing:

Source	**Terms**
Waves radiated from the oscillating body in still water	$\vec{F}_r$, $\vec{M}_r$
Approaching waves on the fixed body	$\vec{F}_w$, $\vec{M}_w$
Diffracted waves of the fixed body	$\vec{F}_d$, $\vec{M}_d$
Hydrostatic buoyancy in still water	$\vec{F}_s$, $\vec{M}_s$

These will each be discussed separately below.

7.2.3 Hydrodynamic Loads

The hydrodynamic loads are the dynamic forces and moments caused by the fluid on an oscillating body in still water; waves are radiated from the body. The **radiation potential**, Φ_r, which is associated with this oscillation in still water, can be written in terms, Φ_j, for 6 degrees of freedom as:

$$\begin{aligned} \Phi_r(x,y,z,t) &= \sum_{j=1}^{6} \Phi_j(x,y,z,t) \\ &= \sum_{j=1}^{6} \phi_j(x,y,z) \cdot v_j(t) \end{aligned} \tag{7.17}$$

in which the space and time dependent potential term, $\Phi_j(x,y,z,t)$ in direction j, is now written in terms of a separate space dependent potential, $\phi_j(x,y,z)$ in direction j, multiplied by an oscillatory velocity, $v_j(t)$ in direction j.
This allows the normal velocity on the surface of the body to be written as:

$$\begin{aligned} \frac{\partial \Phi_r}{\partial n} &= \frac{\partial}{\partial n} \sum_{j=1}^{6} \Phi_j \\ &= \sum_{j=1}^{6} \left\{ \frac{\partial \phi_j}{\partial n} \cdot v_j \right\} \end{aligned} \tag{7.18}$$

and the generalized direction cosines, as given in equation 7.9, are given by:

$$f_j = \frac{\partial \phi_j}{\partial n} \tag{7.19}$$

With this, the radiation term in the hydrodynamic force of equation 7.14 becomes:

$$\begin{aligned} \vec{F}_r &= \rho \iint_S \left(\frac{\partial \Phi_r}{\partial t} \right) \vec{n} \cdot dS \\ &= \rho \iint_S \left(\frac{\partial}{\partial t} \sum_{j=1}^{6} \phi_j v_j \right) \vec{n} \cdot dS \end{aligned} \tag{7.20}$$

and the moment term of equation 7.15 becomes:

$$\begin{aligned} \vec{M}_r &= \rho \iint_S \left(\frac{\partial \Phi_r}{\partial t} \right) (\vec{r} \times \vec{n}) \cdot dS \\ &= \rho \iint_S \left(\frac{\partial}{\partial t} \sum_{j=1}^{6} \phi_j v_j \right) (\vec{r} \times \vec{n}) \cdot dS \end{aligned} \tag{7.21}$$

The components of these radiation forces and moments are defined by:

$$\vec{F}_r = (X_{r_1}, X_{r_2}, X_{r_3}) \qquad \text{and} \qquad \vec{M}_r = (X_{r_4}, X_{r_5}, X_{r_6}) \tag{7.22}$$

with (see 7.19):

$$\begin{aligned} \vec{X}_{r_k} &= \rho \iint_S \left(\frac{\partial}{\partial t} \sum_{j=1}^{6} \phi_j v_j \right) f_k \cdot dS \\ &= \rho \iint_S \left(\frac{\partial}{\partial t} \sum_{j=1}^{6} \phi_j v_j \right) \frac{\partial \phi_k}{\partial n} \cdot dS \qquad \text{for: } k = 1, ...6 \end{aligned} \tag{7.23}$$

Since ϕ_j and ϕ_k are not time-dependent in this expression, it reduces to:

$$\boxed{X_{r_k} = \sum_{j=1}^{6} X_{r_{kj}}} \qquad \text{for: } k = 1, ...6 \tag{7.24}$$

with:

$$\boxed{X_{r_{kj}} = \frac{dv_j}{dt} \rho \int_S \int \phi_j \frac{\partial \phi_k}{\partial n} \cdot dS} \tag{7.25}$$

This radiation force or moment $X_{r_{kj}}$ in the direction k is caused by a forced harmonic oscillation of the body in the direction j. This is generally true for all j and k in the range from 1 to 6. When $j = k$, the force or moment is caused by a motion in that same direction. When $j \neq k$, the force in one direction results from the motion in another direction. This introduces what is called **coupling** between the forces and moments (or motions).
The above equation expresses the force and moment components, $X_{r_{kj}}$ in terms of still unknown potentials, ϕ_j; not everything is solved yet! A solution for this will be found later in this chapter.

Oscillatory Motion

Now an oscillatory motion is defined; suppose a motion (in a complex notation) given by:

$$\boxed{s_j = s_{a_j} e^{-i\omega t}} \tag{7.26}$$

Then the velocity and acceleration of this oscillation are:

$$\begin{aligned} \dot{s}_j &= v_j = -i\omega s_{a_j} e^{-i\omega t} \\ \ddot{s}_j &= \frac{dv_j}{dt} = -\omega^2 s_{a_j} e^{-i\omega t} \end{aligned} \tag{7.27}$$

The hydrodynamic forces and moments can be split into a load in-phase with the acceleration and a load in-phase with the velocity:

$$\begin{aligned} X_{r_{kj}} &= -M_{kj} \ddot{s}_j - N_{kj} \dot{s}_j \\ &= \left(s_{a_j} \omega^2 M_{kj} + i s_{a_j} \omega N_{kj} \right) e^{-i\omega t} \\ &= \left(-s_{a_j} \omega^2 \rho \iint_S \phi_j \frac{\partial \phi_k}{\partial n} \cdot dS \right) e^{-i\omega t} \end{aligned} \tag{7.28}$$

in which the last part is similar to the right hand side of equation 7.25.

So in case of an oscillation of the body in the direction j with a velocity potential ϕ_j, the hydrodynamic mass and damping (coupling)coefficients are defined by:

$$\boxed{M_{kj} = -\Re e\left\{\rho \iint\limits_S \phi_j \frac{\partial \phi_k}{\partial n} \cdot dS\right\} \qquad \text{and} \qquad N_{kj} = -\Im m\left\{\rho\omega \iint\limits_S \phi_j \frac{\partial \phi_k}{\partial n} \cdot dS\right\}} \tag{7.29}$$

In case of an oscillation of the body in the direction k with a velocity potential ϕ_k, the hydrodynamic mass and damping (coupling) coefficients are defined by:

$$\boxed{M_{jk} = -\Re e\left\{\rho \iint\limits_S \phi_k \frac{\partial \phi_j}{\partial n} \cdot dS\right\} \qquad \text{and} \qquad N_{jk} = -\Im m\left\{\rho\omega \iint\limits_S \phi_k \frac{\partial \phi_j}{\partial n} \cdot dS\right\}} \tag{7.30}$$

Green's Second Theorem

Green's second theorem transforms a large volume-integral into a much easier to handle surface-integral. Its mathematical background is beyond the scope of this text. It is valid for any potential function, regardless the fact if it fulfills the Laplace condition or not.
Consider two separate velocity potentials ϕ_j and ϕ_k. Green's second theorem, applied to these potentials, is then:

$$\boxed{\iiint\limits_{V^*} \left(\phi_j \cdot \nabla^2\phi_k - \phi_k \cdot \nabla^2\phi_j\right) \cdot dV^* = \iint\limits_{S^*} \left(\phi_j \frac{\partial \phi_k}{\partial n} - \phi_k \frac{\partial \phi_j}{\partial n}\right) \cdot dS^*} \tag{7.31}$$

This theorem is generally valid for all kinds of potentials; it is not necessary that they fullfil the Laplace equation.
In Green's theorem, S^* is a closed surface with a volume V^*. This volume is bounded by the wall of an imaginary vertical circular cylinder with a very large radius R, the sea bottom at $z = -h$, the water surface at $z = \zeta$ and the wetted surface of the floating body, S; see figure 7.1.

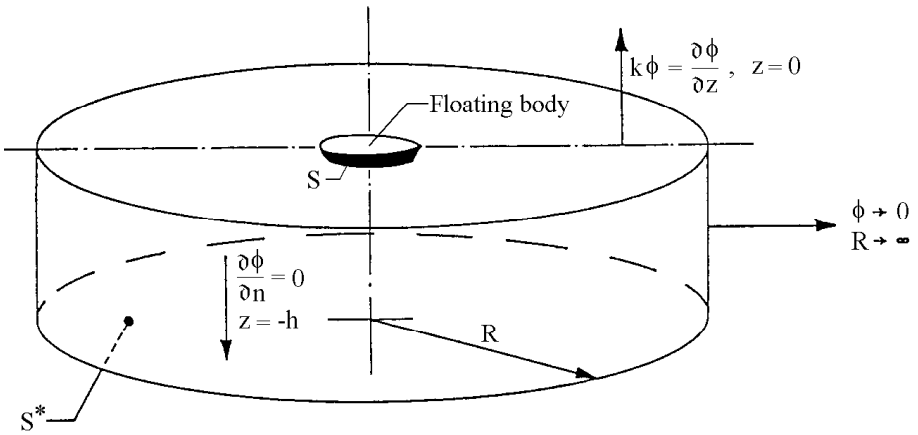

Figure 7.1: Boundary Conditions

Both of the above radiation potentials ϕ_j and ϕ_k must fulfill the Laplace equation 7.2:

$$\nabla^2\phi_j = \nabla^2\phi_k = 0 \tag{7.32}$$

So the left hand side of equation 7.31 becomes zero, which yields for the right hand side of equation 7.31:

$$\iint\limits_{S^*} \phi_j \frac{\partial\phi_k}{\partial n}\cdot dS^* = \iint\limits_{S^*} \phi_k \frac{\partial\phi_j}{\partial n}\cdot dS^* \tag{7.33}$$

The boundary condition at the free surface, equation 7.6, becomes for $\Phi = \phi \cdot e^{-i\omega t}$:

$$-\omega^2\phi + g\frac{\partial\phi}{\partial z} = 0 \qquad \text{for: } z = 0 \tag{7.34}$$

or with the dispersion relation, $\omega^2/g = k\tanh kh$:

$$k\tanh kh\phi = \frac{\partial\phi}{\partial z} \qquad \text{for: } z = 0 \tag{7.35}$$

This implies that at the free surface of the fluid one can write:

$$\left.\begin{aligned} k\tanh kh\cdot\phi_k = \tfrac{\partial\phi_k}{\partial z} = \tfrac{\partial\phi_k}{\partial n} \longrightarrow \phi_k = \tfrac{1}{k\tanh kh}\cdot\tfrac{\partial\phi_k}{\partial n} \\ k\tanh kh\cdot\phi_j = \tfrac{\partial\phi_j}{\partial z} = \tfrac{\partial\phi_j}{\partial n} \longrightarrow \phi_j = \tfrac{1}{k\tanh kh}\cdot\tfrac{\partial\phi_j}{\partial n} \end{aligned}\right\} \text{ at the free surface} \tag{7.36}$$

When taking also the boundary condition at the sea bed (equation 7.3) and the radiation condition on the wall of the cylinder in figure 7.1 (equation 7.10):

$$\frac{\partial\phi}{\partial n} = 0 \text{ (for: } z = -h) \quad \text{and} \quad \lim_{R\to\infty}\phi = 0$$

into account, the integral equation 7.33 over the surface S^* reduces to:

$$\boxed{\iint\limits_{S} \phi_j \frac{\partial\phi_k}{\partial n}\cdot dS = \iint\limits_{S} \phi_k \frac{\partial\phi_j}{\partial n}\cdot dS} \tag{7.37}$$

in which S is the wetted surface of the body only.
Note that in the light of the restriction introduced above, this is now (at least formally) only valid for deep water. The reader is also reminded that the ϕ_j and ϕ_k still have to be evaluated as well; this comes up again later in this chapter.

Potential Coefficients

A substitution of equation 7.37 in equations 7.29 and 7.30 provides symmetry - for the zero forward ship speed case - in the coefficients matrices with respect to their diagonals so that:

$$M_{jk} = M_{kj} \qquad \text{and} \qquad N_{jk} = N_{kj} \tag{7.38}$$

Because of the symmetry of a ship some coefficients are zero and the two matrices with hydrodynamic coefficients for ship become:

$$\text{Hydrodynamic mass matrix:} \quad \begin{pmatrix} M_{11} & 0 & M_{13} & 0 & M_{15} & 0 \\ 0 & M_{22} & 0 & M_{24} & 0 & M_{26} \\ M_{31} & 0 & M_{33} & 0 & M_{35} & 0 \\ 0 & M_{42} & 0 & M_{44} & 0 & M_{46} \\ M_{51} & 0 & M_{53} & 0 & M_{55} & 0 \\ 0 & M_{62} & 0 & M_{64} & 0 & M_{66} \end{pmatrix} \tag{7.39}$$

$$\text{Hydrodynamic damping matrix:} \quad \begin{pmatrix} N_{11} & 0 & N_{13} & 0 & N_{15} & 0 \\ 0 & N_{22} & 0 & N_{24} & 0 & N_{26} \\ N_{31} & 0 & N_{33} & 0 & N_{35} & 0 \\ 0 & N_{42} & 0 & N_{44} & 0 & N_{46} \\ N_{51} & 0 & N_{53} & 0 & N_{55} & 0 \\ 0 & N_{62} & 0 & N_{64} & 0 & N_{66} \end{pmatrix} \tag{7.40}$$

For clarity, the symmetry of terms about the diagonal in these matrices (for example that $M_{13} = M_{31}$ for zero forward speed) has not been included here. The terms on the diagonals (such as M_{nn} for example) are the primary coefficients relating properties such as hydrodynamic mass in one direction to the inertia forces in that same direction. Off-diagonal terms (such as M_{13}) represent hydrodynamic mass only which is associated with an inertia dependent force in one direction caused by a motion component in another.

Forward speed has an effect on the velocity potentials, but is not discussed here. This effect is quite completely explained by [Timman and Newman, 1962]. Another good reference is [Vugts, 1970].

7.2.4 Wave and Diffraction Loads

The second and third term in 7.16 can be treated together. The wave and diffraction terms in the hydrodynamic force and moment are:

$$\vec{F}_w + \vec{F}_d = \rho \iint_S \left(\frac{\partial \Phi_w}{\partial t} + \frac{\partial \Phi_d}{\partial t} \right) \vec{n} \cdot dS \tag{7.41}$$

and:

$$\vec{M}_w + \vec{M}_d = \rho \iint_S \left(\frac{\partial \Phi_w}{\partial t} + \frac{\partial \Phi_d}{\partial t} \right) (\vec{r} \times \vec{n}) \cdot dS \tag{7.42}$$

The principles of linear superposition allow the determination of these forces on a restrained body with zero forward speed; $\partial\Phi/\partial n = 0$. This simplifies the kinematic boundary condition on the surface of the body to:

$$\frac{\partial \Phi}{\partial n} = \frac{\partial \Phi_w}{\partial n} + \frac{\partial \Phi_d}{\partial n} = 0 \tag{7.43}$$

The space and time dependent potentials, $\Phi_w(x, y, z, t)$ and $\Phi_d(x, y, z, t)$, are written now in terms of isolated space dependent potentials, $\phi_w(x, y, z)$ and $\phi_d(x, y, z)$, multiplied by a normalized oscillatory velocity, $v(t) = 1 \cdot e^{-i\omega t}$:

$$\begin{aligned} \Phi_w(x, y, z, t) &= \phi_w(x, y, z) \cdot e^{-i\omega t} \\ \Phi_d(x, y, z, t) &= \phi_d(x, y, z) \cdot e^{-i\omega t} \end{aligned} \tag{7.44}$$

Then from equation 7.43 follows:

$$\frac{\partial \phi_w}{\partial n} = -\frac{\partial \phi_d}{\partial n} \tag{7.45}$$

With this equation and equation 7.19 for the generalized direction cosines, one then finds the wave forces and moments on the restrained body in waves:

$$\begin{aligned} X_{w_k} &= -i\rho e^{-i\omega t} \iint_S (\phi_w + \phi_d)\, f_k \cdot dS \\ &= -i\rho e^{-i\omega t} \iint_S (\phi_w + \phi_d) \frac{\partial \phi_k}{\partial n} \cdot dS \qquad \text{for: } k = 1, ...6 \end{aligned} \tag{7.46}$$

in which ϕ_k is the radiation potential in direction k.
The potential of the incident waves, ϕ_w, is known (see chapter 5), but the diffraction potential, ϕ_d, has to be determined. Green's second theorem from equation 7.37 provides a relation between this diffraction potential, ϕ_d, and a radiation potential, ϕ_k:

$$\iint_S \phi_d \frac{\partial \phi_k}{\partial n} \cdot dS = \iint_S \phi_k \frac{\partial \phi_d}{\partial n} \cdot dS \tag{7.47}$$

and with equation 7.45 one finds:

$$\iint_S \phi_d \frac{\partial \phi_k}{\partial n} \cdot dS = -\iint_S \phi_k \frac{\partial \phi_w}{\partial n} \cdot dS \tag{7.48}$$

This elimination of the diffraction potential results into the so-called **Haskind relations**:

$$\boxed{X_{w_k} = -i\rho e^{-i\omega t} \iint_S \left(\phi_w \frac{\partial \phi_k}{\partial n} + \phi_k \frac{\partial \phi_w}{\partial n} \right) \cdot dS} \qquad \text{for: } k = 1, ...6 \tag{7.49}$$

This limits the problem of the diffraction potential because the expression for X_{w_k} depends only on the wave potential ϕ_w and the radiation potential ϕ_k.

Note: These relations, found by [Haskind, 1957], are very important; they underlie the relative motion (displacement - velocity - acceleration) hypothesis, as used in chapter 6 and in strip theory in chapter 8. These relations are valid only for a floating body with a zero time-averaged speed in all directions. [Newman, 1962] however, has generalized the Haskind relations for a body with a constant forward speed. He derived equations which differ only slightly from those found by Haskind. According to Newman's approach the wave potential has to be defined in the moving $O(x, y, z)$ system. The radiation potential has to be determined for the constant forward speed case, taking an opposite sign into account.

The corresponding wave potential for deep water, as given in chapter 5, now becomes:

$$\begin{aligned} \Phi_w &= \frac{\zeta_a g}{\omega} \cdot e^{kz} \cdot \sin(\omega t - kx\cos\mu - ky\sin\mu) \\ &= \frac{i\zeta_a g}{\omega} \cdot e^{kz} \cdot e^{-ik(x\cos\mu + y\sin\mu)} e^{-i\omega t} \end{aligned} \tag{7.50}$$

so that the isolated space dependent term is given by:

$$\phi_w = \frac{i\zeta_a g}{\omega} \cdot e^{kz} \cdot e^{-ik(x\cos\mu + y\sin\mu)} \tag{7.51}$$

In these equations, μ is the wave direction.
The velocity of the water particles in the direction of the outward normal n on the surface of the body is:

$$\begin{aligned}
\frac{\partial \phi_w}{\partial n} &= \frac{i\zeta_a g}{\omega} \cdot k \left\{ \frac{\partial z}{\partial n} - i\left(\frac{\partial x}{\partial n}\cos\mu + \frac{\partial y}{\partial n}\sin\mu \right) \right\} \cdot e^{kz} \cdot e^{-ik(x\cos\mu + y\sin\mu)} \\
&= \phi_w \cdot k \cdot \left\{ \frac{\partial z}{\partial n} - i\left(\frac{\partial x}{\partial n}\cos\mu + \frac{\partial y}{\partial n}\sin\mu \right) \right\} \\
&= \phi_w \cdot k \cdot \{ f_3 - i\,(f_1\cos\mu + f_2\sin\mu) \}
\end{aligned} \tag{7.52}$$

With this, the wave loads are given by:

$$\begin{aligned}
X_{w_k} &= -i\rho\omega e^{-i\omega t} \iint_S \phi_w f_k \cdot dS \\
&\quad + i\rho\omega e^{-i\omega t} k \iint_S \phi_w \phi_k \{ f_3 - i\,(f_1\cos\mu + f_2\sin\mu) \} \cdot dS \\
&\qquad\qquad \text{for: } k = 1, \ldots 6
\end{aligned} \tag{7.53}$$

The first term in this expression for the wave loads is the so-called **Froude-Krilov** force or moment, which is the wave load caused by the undisturbed incident wave. The second term is caused by the wave disturbance due to the presence of the (fixed) body, the so-called **diffraction force**.

7.2.5 Hydrostatic Loads

These buoyancy forces and moments are determined using the methods explained in chapter 2. In the notation used here:

$$\vec{F}_s = \rho g \iint_S z\vec{n} \cdot dS \quad \text{and} \quad \vec{M}_s = \rho g \iint_S z\,(\vec{r}\ \text{x}\ \vec{n}) \cdot dS$$

or more generally:

$$\boxed{X_{s_k} = \rho g \iint_S z f_k \cdot dS} \qquad \text{for: } k = 1, \ldots 6 \tag{7.54}$$

in which the X_{s_k} are the components of these hydrostatic forces and moments.

7.3 2-D Potential Theory

This section describes the 2-D potential theory as for instance has been applied in the computer code SEAWAY, developed at the Delft University of Technology, see [Journée, 1999]. This program computes the potential coefficients and the wave-frequency hydrodynamic loads on and motions of ships and other free-floating bodies with $L/B \geqslant 3$, with and without forward speed.
So far, the wave potential, $\phi_w(x, y, z)$ is known from chapter 5, but the body-shape-dependent radiation potentials, $\phi_j(x, y, z)$, have still to be determined. Several 2-D approaches for solving this problem will be shown. For this 2-D approach, each cross section of the body is considered to be part of a horizontal cylinder with constant cross section and infinite length; see figure 7.2.

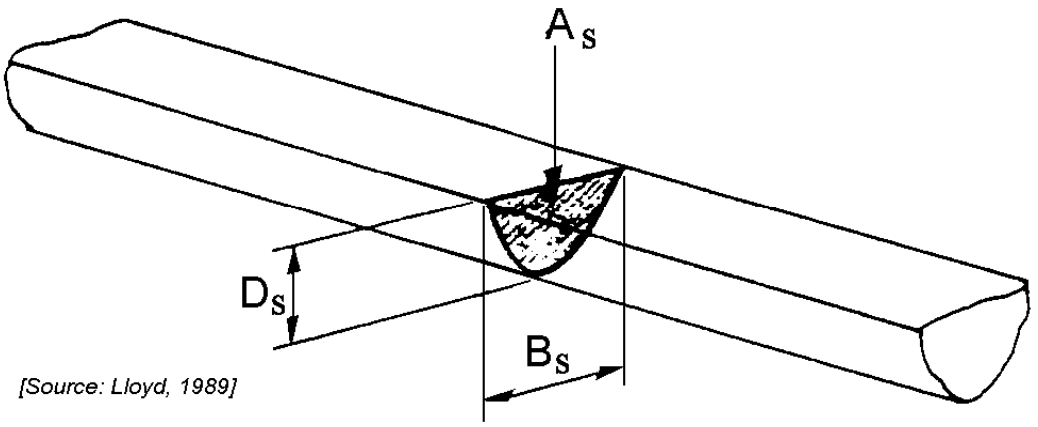

Figure 7.2: 2-D Configuration

The three-dimensional coefficients for the ship at zero mean forward speed are simply found by an integration of the 2-D values over the ship length. This so-called "strip theory method" allows also a relatively simple inclusion of the effect of ship speed.
Three basic 2-D methods are discussed here:

- **Ursell**'s analytical solution of the potential theory for a circular cross section.
- **Conformal mapping** of a ship-like cross section to the unit circle and **Tasai**'s extension of Ursell's theory to conformal mapped cross sections.
- **Frank**'s pulsating source theory, directly applied to a ship-like cross section.

These methods have been developed sequentially in time; each extends the applicability of an earlier form. Each method is discussed separately and is presented using more or less the notation of the relevant literature; this makes it easier for readers to investigate these further. Since all of the methods share the same general boundary conditions, some presentations seem very similar, but they often differ in detail.

7.3.1 Theory of Ursell

[Ursell, 1949] made the first step towards solving the general problem of calculating the two-dimensional flow around a cylinder of arbitrary shape floating in a free surface of infinitely deep water. He derived an analytical solution for an infinitely long oscillating circular cylinder, semi-immersed in a fluid, as shown for heave in figure 7.3-a. The forced oscillation of this cylinder causes a surface disturbance of the fluid. Because the cylinder is assumed to be infinitely long, the generated waves will be two-dimensional. After initial transients have died away, the oscillating cylinder generates a train of regular waves which radiate away to infinity on either side of the cylinder; these waves dissipate energy from the system.

Consider an infinitely long circular cylinder, oscillating in the surface of a fluid; its cross section is the heavy circle in figure 7.3-b. Note that a different coordinate system is used here; the x-axis is in the still water level and the y-axis is positive downwards. θ is now defined from the y-axis instead of the x-axis, too.

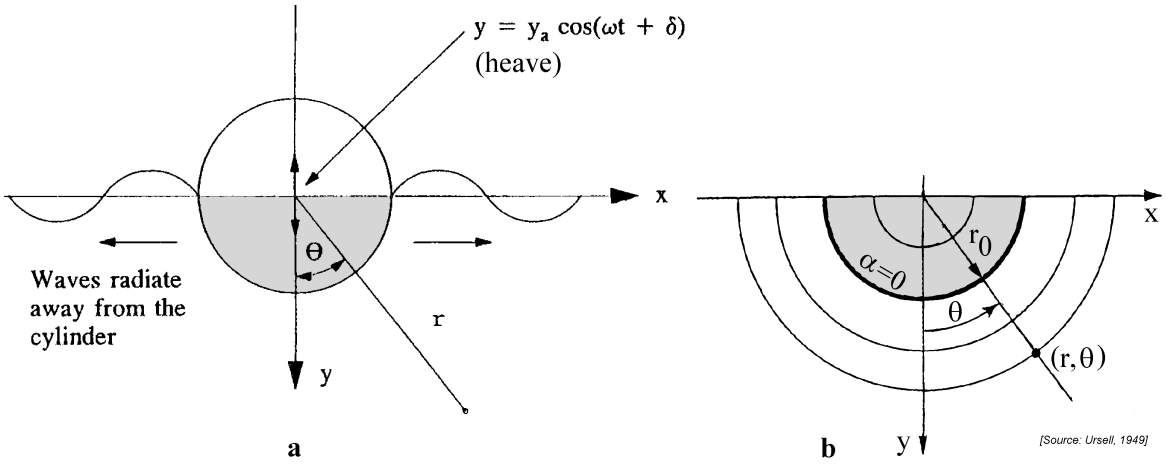

Figure 7.3: Axis System as Used by Ursell

Any point in the fluid can be described by x and y or by $r = r_0 \cdot e^{\alpha}$ and θ, in which e^{α} is the scale. The relations between the (x, y) and the (r, θ) coordinate systems are given by:

$$x = r \cdot \sin\theta = r_0 \cdot e^{\alpha} \cdot \sin\theta \qquad \text{and} \qquad y = r \cdot \cos\theta = r_0 \cdot e^{\alpha} \cdot \cos\theta \tag{7.55}$$

The contour of the cross section of the circular cylinder follows from substituting $\alpha = 0$ in equation 7.55:

$$x_0 = r_0 \cdot \sin\theta \qquad \text{and} \qquad y_0 = r_0 \cdot \cos\theta \tag{7.56}$$

The cylinder is forced to carry out a simple harmonic sway, heave or roll motion with a frequency of oscillation ω and a small amplitude of displacement x_a, y_a or β_a, respectively:

$$\begin{aligned} \text{for sway} \quad &: \quad x = x_a \cos(\omega t + \varepsilon) \\ \text{for heave} \quad &: \quad y = y_a \cos(\omega t + \delta) \\ \text{for roll} \quad &: \quad \beta = \beta_a \cos(\omega t + \gamma) \end{aligned} \tag{7.57}$$

in which ε, δ and γ are phase angles with respect to the velocity potentials.

The sway, heave and roll velocity and acceleration components of the cylinder are now:

$$\begin{array}{lllll} \text{for sway:} & \dot{x} = -\omega x_a \sin(\omega t + \varepsilon) & \text{and} & \ddot{x} = -\omega^2 x_a \cos(\omega t + \varepsilon) \\ \text{for heave:} & \dot{y} = -\omega y_a \sin(\omega t + \delta) & \text{and} & \ddot{y} = -\omega^2 y_a \cos(\omega t + \delta) \\ \text{for roll:} & \dot{\beta} = -\omega \beta_a \sin(\omega t + \gamma) & \text{and} & \ddot{\beta} = -\omega^2 \beta_a \cos(\omega t + \gamma) \end{array} \quad (7.58)$$

These forced oscillations of the cylinder cause a surface disturbance of the fluid. Because the cylinder is assumed to be infinitely long, the generated waves will be two-dimensional. These waves travel away from the cylinder and a stationary state is rapidly attained; they dissipate the energy that the forced oscillation adds.

The fluid is assumed to be incompressible, inviscid and irrotational, without any effects of surface tension. The motion amplitudes and velocities are small enough, so that all but the linear terms of the free surface condition, the kinematic boundary condition on the cylinder and the Bernoulli equation may be neglected.

Boundary Conditions

For these oscillations, the two-dimensional velocity potentials of the fluid have to fulfill the six requirements as discussed in the first section of this chapter:

1. **Laplace equation**

$$\nabla^2 \Phi = \frac{\partial^2 \Phi}{\partial x^2} + \frac{\partial^2 \Phi}{\partial y^2} = 0 \quad (7.59)$$

2. **Sea bed boundary condition**
   The boundary condition on the bottom in **deep water** is expressed by:

$$\frac{\partial \Phi}{\partial y} \rightarrow 0 \qquad \text{for:} \quad y \rightarrow \infty \quad (7.60)$$

3. **Free surface boundary condition**
   The linearized free surface condition in **deep water** is expressed as follows:

$$\frac{\partial^2 \Phi}{\partial t^2} - g \cdot \frac{\partial \Phi}{\partial y} = 0 \quad \text{or} \quad k\Phi + \frac{\partial \Phi}{\partial y} = 0$$
$$\text{for:} \quad |x| \geq r_0 \quad \text{and} \quad y = 0 \qquad \text{with:} \quad k = \frac{\omega^2}{g} \quad (7.61)$$

   In the polar coordinate system, this becomes:

$$-\xi_r \cdot e^{\alpha} \cdot \Phi \pm \frac{\partial \Phi}{\partial \theta} = 0 \quad \text{for:} \quad \alpha \geq 0 \quad \text{and} \quad \theta = \pm\frac{\pi}{2} \quad (7.62)$$

   in which ξ_r is the non-dimensional frequency squared:

$$\xi_r = \frac{\omega^2}{g} \cdot r_0 \quad (7.63)$$

4. **Kinematic boundary condition on the oscillating body surface**
The boundary conditions for sway, heave and roll follow from the definition of the velocity potential on the surface S of the oscillating cylinder (thus for $\alpha = 0$):

$$\begin{aligned} \text{sway}: \quad & \frac{\partial \Phi_0(\theta)}{\partial n} = \dot{x} \cdot \frac{\partial x_0}{\partial n} \\ \text{heave}: \quad & \frac{\partial \Phi_0(\theta)}{\partial n} = \dot{y} \cdot \frac{\partial y_0}{\partial n} \\ \text{roll}: \quad & \frac{\partial \Phi_0(\theta)}{\partial n} = r_0 \dot{\beta} \cdot \frac{\partial r_0}{\partial s} \end{aligned} \tag{7.64}$$

in which n is the outward normal of the cylinder surface S. Using the stream functions Ψ, these boundary conditions are:

$$\begin{aligned} \text{sway}: \quad & \frac{\partial \Psi_0(\theta)}{\partial \theta} = -\dot{x} \cdot \frac{\partial x_0}{\partial \alpha} \\ \text{heave}: \quad & \frac{\partial \Psi_0(\theta)}{\partial \theta} = -\dot{y} \cdot \frac{\partial y_0}{\partial \alpha} \\ \text{roll}: \quad & \frac{\partial \Psi_0(\theta)}{\partial s} = -\dot{\beta} \cdot \frac{\partial}{\partial s}\left(\frac{r_0^2}{2}\right) \end{aligned} \tag{7.65}$$

Integration results into the following requirements for the stream functions on the surface of the cylinder:

$$\begin{aligned} \text{sway}: \quad & \Psi_0(\theta) = -\dot{x} r_0 \cos\theta + C(t) \\ \text{heave}: \quad & \Psi_0(\theta) = -\dot{y} r_0 \sin\theta + C(t) \\ \text{roll}: \quad & \Psi_0(\theta) = -\dot{\beta}\frac{r_0^2}{2} + C(t) \end{aligned} \tag{7.66}$$

in which $C(t)$ is a function of the time only.

5. **Radiation condition**
At a large distance from the cylinder the disturbed surface of the fluid has to take the form of a regular progressive outgoing gravity wave. This means that all other (possibly present) wave systems have to tend to zero as α tends to infinity.

6. **Symmetric or anti-symmetric condition**
If, for instance for ships, both the sway and the roll motion of the fluid are anti-symmetric and the heave motion is symmetrical, these velocity potentials have the following relation:

$$\begin{aligned} \text{sway}: \Phi^{(2)}(-x,y) &= -\Phi^{(2)}(+x,y) \quad \text{or} \quad \Phi^{(2)}(r,-\theta) = -\Phi^{(2)}(r,+\theta) \\ \text{heave}: \Phi^{(3)}(-x,y) &= +\Phi^{(3)}(+x,y) \quad \text{or} \quad \Phi^{(3)}(r,-\theta) = +\Phi^{(3)}(r,+\theta) \\ \text{roll}: \Phi^{(4)}(-x,y) &= -\Phi^{(4)}(+x,y) \quad \text{or} \quad \Phi^{(4)}(r,-\theta) = -\Phi^{(4)}(r,+\theta) \end{aligned} \tag{7.67}$$

The superscript number $^{(i)}$ denotes the mode of the motions (direction) as explained at the beginning of this chapter.

Velocity Potentials and Stream Functions

Ursell assumed two types of waves were produced by the oscillating cylinder in still water:

A: Standing Wave
This wave system can be described by an infinite number of **pulsating multipoles** (pulsating source-sink combinations) along the y-axis, with velocity potentials and stream functions denoted here by Φ_A and Ψ_A. The amplitudes of these waves decrease rapidly with the increasing distance from the cylinder. These waves do not dissipate energy.

B: Regular Progressive Wave
This wave system can be described by a **pulsating horizontal doublet** at the origin for the anti-symmetric sway and roll motions and a **pulsating source** at the origin for the symmetric heave motion, with velocity potentials and stream functions denoted here by Φ_B and Ψ_B. These waves dissipate energy. At a distance of a few wave lengths from the cylinder, the waves on each side can be described by a single regular wave train. The wave amplitude at infinity, η_a, is proportional to the amplitude of oscillation of the cylinder x_a, y_a or β_a, provided that these amplitudes are sufficiently small compared with the radius of the cylinder and the wave length is not much smaller than the diameter of the cylinder.

Then, the total velocity potentials and stream functions to describe the waves generated by the oscillating cylinder are:

$$\boxed{\boxed{|\Phi = \Phi_A + \Phi_B|}\\ \boxed{|\Psi = \Psi_A + \Psi_B|}} \tag{7.68}$$

[Ursell, 1949] found these potentials and worked this out further as outlined below.

The remainder of this section is intended primarily as a reference. The resulting pressure on the cross section - and the path leading to it - is more important than the derivation details.

The following **set of velocity potentials** fulfill the previous requirements for swaying, heaving and rolling circular cross sections:

$$\begin{aligned}
\Phi_A &= \frac{g\eta_a}{\pi\omega}\left(\sum_{m=1}^{\infty}\left\{P_{2m}\phi_{A_{2m}}(\alpha,\theta)\cos(\omega t)\right\} + \sum_{m=1}^{\infty}\left\{Q_{2m}\phi_{A_{2m}}(\alpha,\theta)\sin(\omega t)\right\}\right)\\
\Phi_B &= \frac{g\eta_a}{\pi\omega}\left(\phi_{B_c}(\alpha,\theta)\cos(\omega t) + \phi_{B_s}(\alpha,\theta)\sin(\omega t)\right)\\
&= \frac{g\eta_a}{\pi\omega}\left(\phi_{B_c}(x,y)\cos(\omega t) + \phi_{B_s}(x,y)\sin(\omega t)\right)
\end{aligned} \tag{7.69}$$

in which for sway and roll:

$$\begin{aligned}
\phi_{A_{2m}}(\alpha,\theta) &= +e^{-(2m+1)\alpha}\sin\left((2m+1)\,\theta\right) + \xi_r\frac{e^{-2m\alpha}\sin(2m\theta)}{2m}\\
\phi_{B_c}(x,y) &= -\pi e^{-ky}\sin(kx)
\end{aligned}$$

$$\begin{aligned}\phi_{B_s}(x,y) &= +\frac{|x|}{x}\pi e^{-ky}\cos(kx) \\ &\quad -\int_0^\infty \frac{|x|}{x}\frac{k\cos(\nu y)+\nu\sin(\nu y)}{\nu^2+k^2}e^{-\nu|x|}d\nu + \frac{x}{k(x^2+y^2)}\end{aligned} \tag{7.70}$$

and for heave:

$$\begin{aligned}\phi_{A_{2m}}(\alpha,\theta) &= +e^{-2m\alpha}\cos(2m\theta) + \xi_r\frac{e^{-(2m-1)\alpha}\cos\left((2m-1)\,\theta\right)}{2m-1} \\ \phi_{B_c}(x,y) &= +\pi e^{-ky}\cos(kx) \\ \phi_{B_s}(x,y) &= +\pi e^{-ky}\sin(k|x|) + \int_0^\infty \frac{k\sin(\nu y)-\nu\cos(\nu y)}{\nu^2+k^2}e^{-\nu|x|}d\nu\end{aligned} \tag{7.71}$$

The **set of conjugate stream functions** is expressed as:

$$\begin{aligned}\Psi_A &= \frac{g\eta_a}{\pi\omega}\left(\sum_{m=1}^{\infty}\left\{P_{2m}\psi_{A_{2m}}(\alpha,\theta)\cos(\omega t)\right\} + \sum_{m=1}^{\infty}\left\{Q_{2m}\psi_{A_{2m}}(\alpha,\theta)\sin(\omega t)\right\}\right) \\ \Psi_B &= \frac{g\eta_a}{\pi\omega}\left(\psi_{B_c}(\alpha,\theta)\cos(\omega t) + \psi_{B_s}(\alpha,\theta)\sin(\omega t)\right) \\ &= \frac{g\eta_a}{\pi\omega}\left(\psi_{B_c}(x,y)\cos(\omega t) + \psi_{B_s}(x,y)\sin(\omega t)\right)\end{aligned} \tag{7.72}$$

in which for sway and roll:

$$\begin{aligned}\psi_{A_{2m}}(\alpha,\theta) &= -e^{-(2m+1)\alpha}\cos\left((2m+1)\,\theta\right) - \xi_r\frac{e^{-2m\alpha}\cos(2m\theta)}{2m} \\ \psi_{B_c}(x,y) &= +\pi e^{-ky}\cos(kx) \\ \psi_{B_s}(x,y) &= +\pi e^{-ky}\sin(k|x|) \\ &\quad +\int_0^\infty \frac{k\sin(\nu y)-\nu\cos(\nu y)}{\nu^2+k^2}e^{-\nu|x|}d\nu - \frac{y}{k(x^2+y^2)}\end{aligned} \tag{7.73}$$

and for heave:

$$\begin{aligned}\psi_{A_{2m}}(\alpha,\theta) &= +e^{-2m\alpha}\sin(2m\theta) + \xi_r\frac{e^{-(2m-1)\alpha}\sin\left((2m-1)\,\theta\right)}{2m-1} \\ \psi_{B_c} &= +\pi e^{-ky}\sin(kx) \\ \psi_{B_s} &= -\pi e^{-ky}\frac{|x|}{x}\cos(kx) + \int_0^\infty \frac{k\cos(\nu y)+\nu\sin(\nu y)}{\nu^2+k^2}e^{-\nu|x|}d\nu\end{aligned} \tag{7.74}$$

The standing wave (A) is defined in a polar coordinate system, while the regular progressive wave (B) is defined in the (x,y) coordinate system. The wave number, k, in the latter one is related to the frequency of oscillation, ω, by the dispersion relation in deep water:

$k = \omega^2/g$. The variable ν has the dimension of the wave number k; it is not the kinematic viscosity here.
Notice the symmetric and anti-symmetric relations in the set of velocity potentials and stream functions.
The unknowns P_{2m} and Q_{2m} in these equations have to be found; they follow from the boundary conditions in the fluid.

Solution

The **stream functions for sway, heave and roll** on the surface of the cylinder ($\alpha = 0$) reduce to:

$$\begin{aligned}\Psi_0(\theta) = \frac{g\eta_a}{\pi\omega} \quad & \left\{ \left(\psi_{B0_c}(\theta) + \sum_{m=1}^{\infty} \left\{ P_{2m} \psi_{A0_{2m}}(\theta) \right\} \right) \cos(\omega t) \right. \\ + \quad & \left. \left(\psi_{B0_s}(\theta) + \sum_{m=1}^{\infty} \left\{ Q_{2m} \psi_{A0_{2m}}(\theta) \right\} \right) \sin(\omega t) \right\} \end{aligned} \tag{7.75}$$

in which:

$$\begin{aligned} \text{for sway and roll} \quad : \quad & \psi_{A0_{2m}}(\theta) = \cos\left((2m+1)\theta\right) + \xi_r \frac{\cos(2m\theta)}{2m} \\ \text{for heave} \quad : \quad & \psi_{A0_{2m}}(\theta) = \sin(2m\theta) + \xi_r \frac{\sin\left((2m-1)\theta\right)}{2m-1} \end{aligned} \tag{7.76}$$

where $\psi_{B0_c}(\theta)$ and $\psi_{B0_s}(\theta)$ are the values of $\psi_{B_c}(\alpha, \theta)$ and $\psi_{B_s}(\alpha, \theta)$ at the surface of the cylinder and ξ_r is the non-dimensional frequency of oscillation squared.
These expressions for the stream functions should be equal to the stream functions that satisfy the kinematic boundary conditions on the surface of the oscillating cylinder, given in equations 7.66. Doing this makes it possible to determine the values for the P_{2m} and Q_{2m} series of values as well as the amplitude ratios x_a/η_a, y_a/η_a and $\beta_a/k\eta_a$ and the phase shifts ε, δ and γ.

Once the P_{2m} and Q_{2m} series of values have been found, the **velocity potentials for sway, heave and roll** can be determined, too:

$$\begin{aligned}\Phi_0(\theta) = \frac{g\eta_a}{\pi\omega} \quad & \left\{ \left(\phi_{B0_c}(\theta) + \sum_{m=1}^{\infty} \left\{ P_{2m} \phi_{A0_{2m}}(\theta) \right\} \right) \cos(\omega t) \right. \\ & \left. + \left(\phi_{B0_s}(\theta) + \sum_{m=1}^{\infty} \left\{ Q_{2m} \phi_{A0_{2m}}(\theta) \right\} \right) \sin(\omega t) \right\} \end{aligned} \tag{7.77}$$

in which:

$$\begin{aligned} \text{for sway and roll} \quad : \quad & \phi_{A0_{2m}}(\theta) = \sin\left((2m+1)\theta\right) + \xi_r \frac{\sin(2m\theta)}{2m} \\ \text{for heave} \quad : \quad & \phi_{A0_{2m}}(\theta) = \cos(2m\theta) + \xi_r \frac{\cos\left((2m-1)\theta\right)}{2m-1} \end{aligned} \tag{7.78}$$

Hydrodynamic Pressure

With known velocity potentials, the hydrodynamic pressure on the surface of the cylinder can be obtained from the linearized Bernoulli equation 7.13:

$$\begin{aligned} p(\theta) &= -\rho\frac{\partial\Phi_0(\theta)}{\partial t} \\ &= \frac{-\rho g\eta_a}{\pi}\left\{\left(\phi_{B0_s}(\theta)+\sum_{m=1}^{\infty}\left\{Q_{2m}\phi_{A0_{2m}}(\theta)\right\}\right)\cos(\omega t)\right. \\ &\quad \left.-\left(\phi_{B0_c}(\theta)+\sum_{m=1}^{\infty}\left\{P_{2m}\phi_{A0_{2m}}(\theta)\right\}\right)\sin(\omega t)\right\} \end{aligned} \tag{7.79}$$

where $\phi_{B0_c}(\theta)$ and $\phi_{B0_s}(\theta)$ are the values of $\phi_{B_c}(\alpha,\theta)$ and $\phi_{B_s}(\alpha,\theta)$ at the surface of the cylinder.
It is obvious that the pressures for sway and roll are skew-symmetric in θ, thus $p(-\theta) = -p(+\theta)$, and symmetric in θ for heave, thus: $p(-\theta) = p(+\theta)$.

Hydrodynamic Loads

The two-dimensional hydrodynamic sway and heave force and roll moment can be obtained from integrations of these pressures over the contour, C_0 at $r = r_0$, of the circular cross section. When switching to polar coordinates, derivatives with respect to θ have to be used:

$$\frac{dx_0}{d\theta} = +r_0\cos\theta \quad \text{and} \quad \frac{dy_0}{d\theta} = -r_0\sin\theta \tag{7.80}$$

With these, the loads can be expressed in terms of potential mass and damping, as equations 7.81, 7.82 and 7.83 show. A comparison of the in-phase terms ($\cos(\omega t)$) in each of these equations provides the potential mass coefficients, while a comparison of the out-of-phase terms ($\sin(\omega t)$) the potential damping coefficients provides.

$$\begin{aligned} F_x' &= \int_{C_0} p(\theta)dy_0 = 2\int_0^{\frac{1}{2}\pi} p(\theta)\frac{dy_0}{d\theta}d\theta \\ &\quad \left\{= -2r_0\int_0^{\frac{1}{2}\pi} p(\theta)\sin\theta\, d\theta \quad \text{(for this circular cylinder)}\right\} \\ &= -M_{22}'\cdot\ddot{x} - N_{22}'\cdot\dot{x} \qquad \text{(for a swaying cylinder)} \\ &= -M_{24}'\cdot\ddot{\beta} - N_{24}'\cdot\dot{\beta} \qquad \text{(for a rolling cylinder)} \end{aligned} \tag{7.81}$$

$$\begin{aligned} F_y' &= -\int_{C_0} p(\theta)dx_0 = -2\int_0^{\frac{1}{2}\pi} p(\theta)\frac{dx_0}{d\theta}d\theta \\ &\quad \left\{= -2r_0\int_0^{\frac{1}{2}\pi} p(\theta)\cos\theta\, d\theta \quad \text{(for this circular cylinder)}\right\} \end{aligned}$$

$$= -M_{33}' \cdot \ddot{y} - N_{33}' \cdot \dot{y} \qquad \text{(for a heaving cylinder)} \tag{7.82}$$

$$\begin{aligned} M_R' &= -\int_{C_0} p(\theta) x_0 dx_0 - \int_{C_0} p(\theta) y_0 dy_0 \\ &= -2 \int_0^{\frac{1}{2}\pi} p(\theta) \left(x_0 \frac{dx_0}{d\theta} + y_0 \frac{dy_0}{d\theta} \right) d\theta \\ &\left\{ = -2{r_0}^2 \int_0^{\frac{1}{2}\pi} p(\theta)(\sin\theta\cos\theta - \sin\theta\cos\theta)\, d\theta \quad = 0 \quad \text{(for this circular cylinder)} \right\} \\ &= -M_{42}' \cdot \ddot{x} - N_{42}' \cdot \dot{x} \qquad \text{(for a swaying cylinder)} \\ &= -M_{44}' \cdot \ddot{\beta} - N_{44}' \cdot \dot{\beta} \qquad \text{(for a rolling cylinder)} \end{aligned} \tag{7.83}$$

with:

M_{22}'	=	2-D hydrodynamic mass coefficient of sway
N_{22}'	=	2-D hydrodynamic damping coefficient of sway
M_{42}'	=	2-D hydrodynamic mass coupling coefficient of sway into roll
N_{42}'	=	2-D hydrodynamic damping coupling coefficient of sway into roll
M_{33}'	=	2-D hydrodynamic mass coefficient of heave
N_{33}'	=	2-D hydrodynamic damping coefficient of heave
M_{24}'	=	2-D hydrodynamic mass coupling coefficient of roll into sway
N_{24}'	=	2-D hydrodynamic damping coupling coefficient of roll into sway
M_{44}'	=	2-D hydrodynamic mass moment of inertia coefficient of roll
N_{44}'	=	2-D hydrodynamic damping coefficient of roll

7.3.2 Conformal Mapping

Ursell's derivation is valid only for a circular cross section. Since few ships have this shape, a method is needed to transform realistic shapes so that "it looks like" a circular cylinder in Ursell's method.

More or less arbitrary, but still symmetrical, cross sections can be mapped conformal to a unit circle. The general transformation formula to do this is given by:

$$\boxed{z = M_s \sum_{n=0}^{N} \left\{ a_{2n-1} \zeta^{-(2n-1)} \right\}} \tag{7.84}$$

with:

$z = x + iy$	=	specifies the ship's cross section shape (figure 7.4-b)
$\zeta = ie^{\alpha}e^{-i\theta}$	=	specifies the circular cross section shape (figure 7.4-a)
M_s	=	scale factor
a_{-1}	=	$+1$
a_{2n-1}	=	conformal mapping coefficients ($n = 1, ..., N$)
N	=	number of parameters used

Equation 7.84 is valid only for cross sections which pass through the still water level. It will not work for fully submerged cross sections, like those of a bulbous bow or a submarine. Those sections have to be treated by other methods.

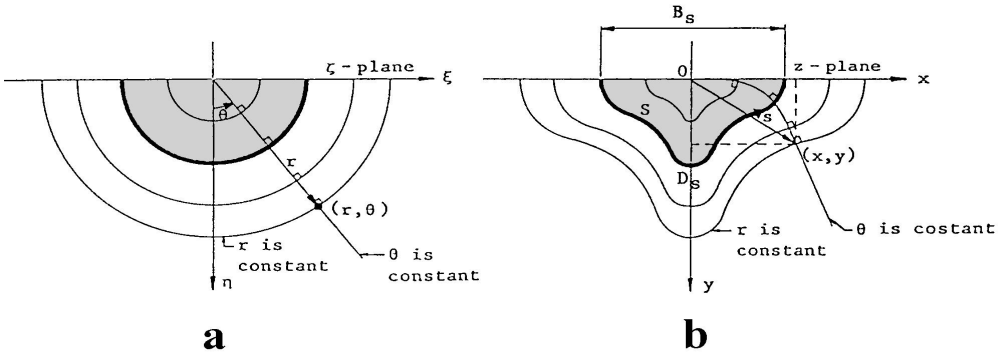

Figure 7.4: Mapping Relation between Two Planes

Equation 7.84 yields the relation between the coordinates in the z-plane (of the ship's cross section) and the variables in the ζ-plane (of the circular cross section):

$$\boxed{x = -M_s \sum_{n=0}^{N} \{(-1)^n a_{2n-1} e^{-(2n-1)\alpha} \sin((2n-1)\theta)\}}$$

$$\boxed{y = +M_s \sum_{n=0}^{N} \{(-1)^n a_{2n-1} e^{-(2n-1)\alpha} \cos((2n-1)\theta)\}} \tag{7.85}$$

$\alpha = 0$ in Ursell's solution corresponds to the contour of his circular cross section. Similarly, the contour of the ship's cross section follows from putting $\alpha = 0$ in the above equation, yielding:

$$\begin{aligned} x_0 &= -M_s \sum_{n=0}^{N} \{(-1)^n a_{2n-1} \sin((2n-1)\theta)\} \\ y_0 &= +M_s \sum_{n=0}^{N} \{(-1)^n a_{2n-1} \cos((2n-1)\theta)\} \end{aligned} \tag{7.86}$$

The breadth on the waterline and the draft of the conformal mapped approximation of the actual cross section are given by:

$$\begin{aligned} b_0 = 2M_s\lambda_b &= B_s \qquad \text{with:} \qquad \lambda_b = \sum_{n=0}^{N} a_{2n-1} \\ \text{so that :} \quad M_s &= \frac{B_s}{2\lambda_b} \\ d_0 = M_s\lambda_d &= D_s \qquad \text{with:} \qquad \lambda_d = \sum_{n=0}^{N} \{(-1)^n a_{2n-1}\} \\ \text{so that :} \quad M_s &= \frac{D_s}{\lambda_d} \end{aligned} \tag{7.87}$$

Lewis Conformal Mapping

A very simple and in a lot of cases also a more or less realistic transformation of the cross section can be obtained with $N = 2$ in the transformation formula (7.84). This yields the well known **Lewis transformation** (see [Lewis, 1929]).
The contour of this so-called **Lewis form** is expressed by:

$$\begin{aligned} x_0 &= M_s \cdot ((1 + a_1)\sin\theta - a_3 \sin 3\theta) \\ y_0 &= M_s \cdot ((1 - a_1)\cos\theta + a_3 \cos 3\theta) \end{aligned} \tag{7.88}$$

with the scale factor:

$$M_s = \frac{B_s/2}{1 + a_1 + a_3} \qquad \text{or:} \qquad M_s = \frac{D_s}{1 - a_1 + a_3} \tag{7.89}$$

and:

$$\begin{aligned} b_0 = B_s &= \text{sectional breadth on the water line} \\ d_0 = D_s &= \text{sectional draft} \end{aligned}$$

Now the coefficients a_1 and a_3 and the scale factor M_s can be determined in such a way that the sectional breadth, draft and area of the approximate cross section and of the actual ship cross section are identical.
The half breadth to draft ratio H_0 is given by:

$$H_0 = \frac{B_s/2}{D_s} = \frac{1 + a_1 + a_3}{1 - a_1 + a_3} \tag{7.90}$$

An integration of the Lewis form delivers the sectional area coefficient σ_s:

$$\sigma_s = \frac{A_s}{B_s D_s} = \frac{\pi}{4} \cdot \frac{1 - {a_1}^2 - 3{a_3}^2}{(1 + a_3)^2 - {a_1}^2} \tag{7.91}$$

in which A_s is the area of the cross section.
Putting a_1, derived from the expression for H_0, into the expression for σ_s yields a quadratic equation in a_3:

$$c_1 {a_3}^2 + c_2 a_3 + c_3 = 0 \tag{7.92}$$

in which:

$$\begin{aligned} c_1 &= 3 + \frac{4\sigma_s}{\pi} + \left(1 - \frac{4\sigma_s}{\pi}\right) \cdot \left(\frac{H_0 - 1}{H_0 + 1}\right)^2 \\ c_2 &= 2c_1 - 6 \\ c_3 &= c_1 - 4 \end{aligned} \tag{7.93}$$

The (valid) solutions for a_3 and a_1 become:

$$\begin{aligned} a_3 &= \frac{-c_1 + 3 + \sqrt{9 - 2c_1}}{c_1} \\ a_1 &= \frac{H_0 - 1}{H_0 + 1} \cdot (a_3 + 1) \end{aligned} \tag{7.94}$$

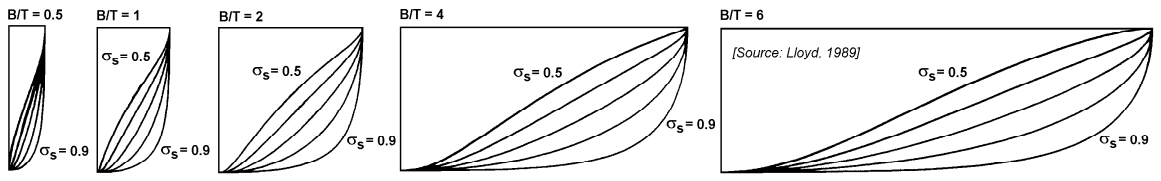

Figure 7.5: Typical Lewis Forms

Lewis forms with the solution $a_3 = \left(-c_1 + 3 - \sqrt{9 - 2c_1}\right)/c_1$ - with a minus sign before the square root - are looped; they intersect themselves somewhere in the fourth quadrant. Since ship shapes are "better behaved", these solutions are not considered here.
It is obvious that a transformation of a half immersed circle with radius R will result in $M_s = R$, $a_1 = 0$ and $a_3 = 0$.
Some typical and realistic Lewis forms are presented in figure 7.5.
In some cases the Lewis transformation can give more or less ridiculous results. The ranges of the half breadth to draft ratio H_0 and the area coefficient σ_s for the different typical Lewis forms are shown in figure 7.6.
The re-entrant and the asymmetric forms are not acceptable; conventional, bulbous and tunneled forms are considered to be valid here. Then, the area coefficient σ_s is bounded by a lower limit to omit re-entrant Lewis forms and by an upper limit to omit non-symmetric Lewis forms:

$$\begin{aligned} \text{for} \quad H_0 \leq 1.0: \qquad & \frac{3\pi}{32}(2 - H_0) < \quad \sigma_s < \frac{\pi}{32}\left(10 + H_0 + \frac{1}{H_0}\right) \\ \text{for} \quad H_0 \geq 1.0: \qquad & \frac{3\pi}{32}\left(2 - \frac{1}{H_0}\right) < \quad \sigma_s < \frac{\pi}{32}\left(10 + H_0 + \frac{1}{H_0}\right) \end{aligned} \tag{7.95}$$

If a value of σ_s is outside this range, it has to be set to the value at the nearest border of this range, in order to calculate the (best possible) Lewis coefficients.
Numerical problems with bulbous or shallow cross sections can be avoided by the requirement: $0.01 < H_0 < 100.0$.

Close-Fit Conformal Mapping

A more accurate transformation of the cross section can be obtained by using a greater number of parameters N. The scale factor M_s and the conformal mapping coefficients a_{2n-1}, with a maximum value of n varying from N=2 until N=10, can be determined successfully from the offsets of a cross section in such a manner that the mean squares of the deviations of the actual cross section from the approximate cross section is minimized.
A very simple and direct iterative least squares method to determine the Close-Fit conformal mapping coefficients is given by [Journée, 1992]. The procedure starts with initial values for $[M_s \cdot a_{2n-1}]$. The initial values of M_s, a_1 and a_3 are obtained with the Lewis method, while the initial values of a_5 until a_{2N-1} are set to zero. With these $[M_s \cdot a_{2n-1}]$ values, a θ_i-value is determined for each offset in such a manner that the actual offset (x_i, y_i) lies on the normal to the approximate contour of the cross section in (x_{0i}, y_{0i}). Now θ_i has to be determined. Therefore a function $F(\theta_i)$ will be defined by the distance from the offset (x_i, y_i) to the normal of the contour to the actual cross section through (x_{0i}, y_{0i}), see figure 7.7.

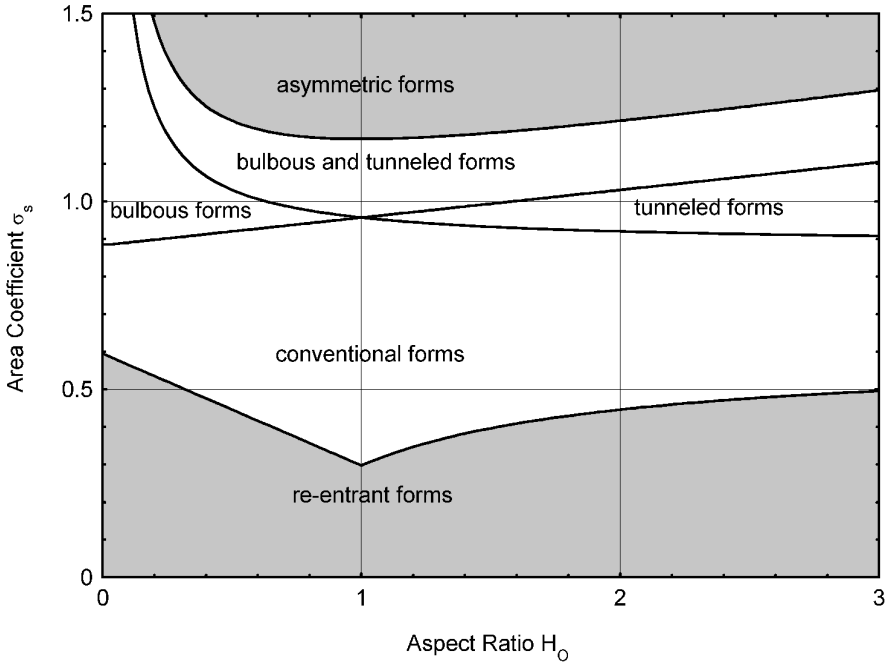

Figure 7.6: Ranges of Lewis Parameters

These offsets have to be selected at approximately equal mutual circumferential lengths, eventually with somewhat more dense offsets near sharp corners. Then α_i is defined by:

$$\begin{aligned} \cos\alpha_i &= \frac{+x_{i+1} - x_{i-1}}{\sqrt{(x_{i+1} - x_{i-1})^2 + (y_{i+1} - y_{i-1})^2}} \\ \sin\alpha_i &= \frac{-y_{i+1} + y_{i-1}}{\sqrt{(x_{i+1} - x_{i-1})^2 + (y_{i+1} - y_{i-1})^2}} \end{aligned} \tag{7.96}$$

With this θ_i-value, the numerical value of the square of the deviation of (x_i, y_i) from (x_{0i}, y_{0i}) is calculated:

$$\boxed{|e_i = (x_i - x_{0i})^2 + (y_i - y_{0i})^2|} \tag{7.97}$$

After doing this for all I+1 offsets, the numerical value of he sum of the squares of the deviations is known:

$$\boxed{\left|E = \sum_{i=0}^{I} \{e_i\}\right|} \tag{7.98}$$

The sum of the squares of these deviations can also be expressed as:

$$\begin{aligned} E &= \sum_{i=0}^{I} \left(x_i + \sum_{n=0}^{N} (-1)^n [M_s \cdot a_{2n-1}] \sin\left((2n-1)\theta_i\right) \right)^2 \\ &\quad + \sum_{i=0}^{I} \left(y_i - \sum_{n=0}^{N} (-1)^n [M_s \cdot a_{2n-1}] \cos\left((2n-1)\theta_i\right) \right)^2 \end{aligned} \tag{7.99}$$

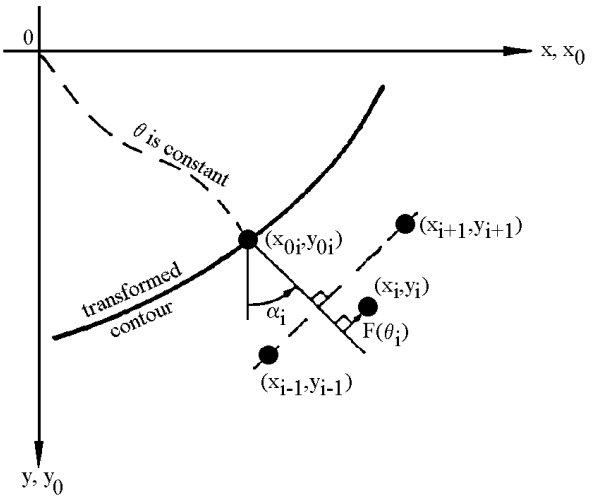

Figure 7.7: Close-Fit Conformal Mapping Definitions

Then new values of $[M_s \cdot a_{2n-1}]$ have to be obtained in such a manner that E is minimized. This means that each of the derivatives of this equation with respect to each coefficient $[M_s \cdot a_{2n-1}]$ is zero, so:

$$\boxed{\frac{\partial E}{\partial\{M_s a_{2j-1}\}} = 0} \qquad \text{for: } j = 0, ...N \tag{7.100}$$

This yields $N+1$ equations:

$$\begin{aligned} &\sum_{n=0}^{N} \left\{ (-1)^n [M_s \cdot a_{2n-1}] \sum_{i=0}^{I} \cos\left((2j-2n)\theta_i\right) \right\} \\ = &\sum_{i=0}^{I} \left\{ -x_i \sin\left((2j-1)\theta_i\right) + y_i \cos\left((2j-1)\theta_i\right) \right\} \\ &\qquad\qquad \text{for: } j = 0, ...N \end{aligned} \tag{7.101}$$

To obtain the exact breadth and draft, the last two equations are replaced by the equations for the breadth at the waterline and the draft:

$$\begin{aligned} &\sum_{n=0}^{N} \left\{ (-1)^n [M_s \cdot a_{2n-1}] \sum_{i=0}^{I} \cos\left((2j-2n)\theta_i\right) \right\} \\ = &\sum_{i=0}^{I} \left\{ -x_i \sin\left((2j-1)\theta_i\right) + y_i \cos\left((2j-1)\theta_i\right) \right\} \\ &\qquad\qquad \text{for: } j = 0, ...N-2 \\ &\sum_{n=0}^{N} \{ \qquad [M_s \cdot a_{2n-1}] \} = B_s/2 \qquad j = N-1 \\ &\sum_{n=0}^{N} \{ (-1)^n [M_s \cdot a_{2n-1}] \} = D_s \qquad j = N \end{aligned} \tag{7.102}$$

These N+1 equations can be solved numerically so that new values for $[M_s \cdot a_{2n-1}]$ will be obtained. These new values are used instead of the initial values to obtain new θ_i-values of the I+1 offsets again, etc. This procedure is repeated several times and stops when the difference between the numerical E-values of two subsequent calculations becomes less than a certain threshold value, depending on the dimensions of the cross section. Because $a_{-1} = +1$ the scale factor M_s is equal to the final solution of the first coefficient (n=0). The N other coefficients a_{2n-1} can be found by dividing the final solutions of $[M_s \cdot a_{2n-1}]$ by this M_s-value.
Attention has to be paid to divergence in the calculation routines and re-entrant forms. In these cases the number N will be increased until the divergence or re-entrance vanish. In the worst case a "maximum" value of N will be attained without success. One can then switch to Lewis coefficients with an area coefficient of the cross section set to the nearest border of the valid Lewis coefficient area.

Comparison

An example of conformal mapping results is given here for the amidships cross section of a container vessel, with a breadth of 25.40 meter and a draft of 9.00 meter. For the least squares method in the conformal mapping method, 33 new offsets at equidistant length intervals on the contour of this cross section can be determined by a second degree interpolation routine. The calculated data of the two-parameter Lewis and the N-parameter Close-Fit conformal mapping of this amidships cross section are given in the table below. The last line lists the RMS-values for the deviations of the 33 equidistant points on the approximate contour of this cross section.

		Lewis Conformal Mapping	N-Parameter Close Fit Conformal Mapping								
N	(−)	2	2	3	4	5	6	7	8	9	10
$2N$-1	(−)	3	3	5	7	9	11	13	15	17	19
M_s	(m)	12.2400	12.2457	12.2841	12.3193	12.3186	12.3183	12.3191	12.3190	12.3195	12.3194
a_{-1}	(−)	+1.0000	+1.0000	+1.0000	+1.0000	+1.0000	+1.0000	+1.0000	+1.0000	+1.0000	+1.0000
a_1	(−)	+0.1511	+0.1511	+0.1640	+0.1634	+0.1631	+0.1633	+0.1633	+0.1632	+0.1632	+0.1632
a_3	(−)	-0.1136	-0.1140	-0.1167	-0.1245	-0.1246	-0.1243	-0.1244	-0.1245	-0.1245	-0.1245
a_5	(−)			-0.0134	-0.0133	-0.0105	-0.0108	-0.0108	-0.0108	-0.0107	-0.0107
a_7	(−)				+0.0053	+0.0054	+0.0031	+0.0030	+0.0032	+0.0031	+0.0030
a_9	(−)					-0.0024	-0.0023	-0.0024	-0.0026	-0.0029	-0.0029
a_{11}	(−)						+0.0021	+0.0022	+0.0012	+0.0014	+0.0015
a_{13}	(−)							+0.0002	+0.0002	+0.0021	+0.0020
a_{15}	(−)								+0.0009	+0.0007	+0.0000
a_{17}	(−)									-0.0016	-0.0015
a_{19}	(−)										+0.0006
RMS	(m)	0.181	0.180	0.076	0.039	0.027	0.019	0.018	0.017	0.009	0.008

Figure 7.8 shows the differences between a Lewis transformation and a 10-parameter close-fit conformal mapping of a rectangular cross section with a breadth of 20.00 meters and a draft of 10.00 meters.

7.3.3 Theory of Tasai

The approach of [Ursell, 1949] is valid for circular cross sections. [Tasai, 1959] (but others too) used Ursell's approach and a conformal mapping method to obtain 2-D potential

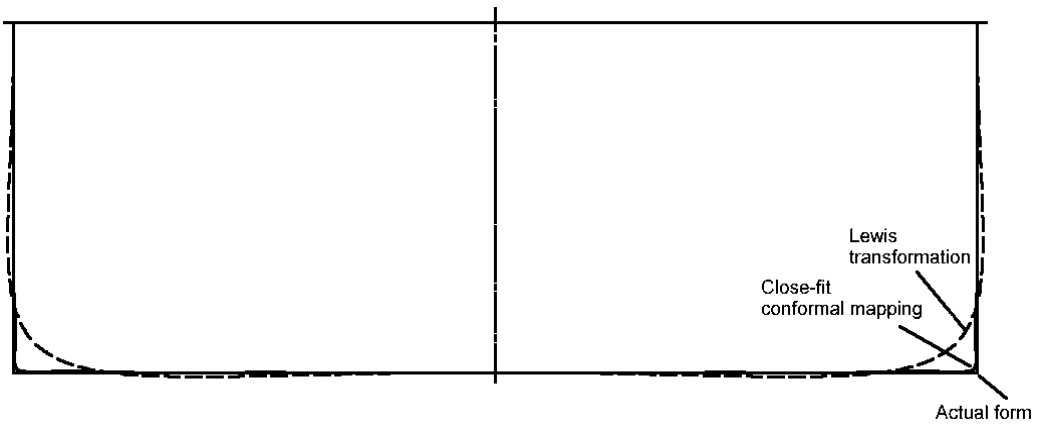

Figure 7.8: Lewis and Close-Fit Conformal Mapping of a Rectangle

coefficients for an infinitely long cylinder with ship-like cross sections, swaying, heaving and rolling in the surface of a fluid. Its cross sections are given in figure 7.9.

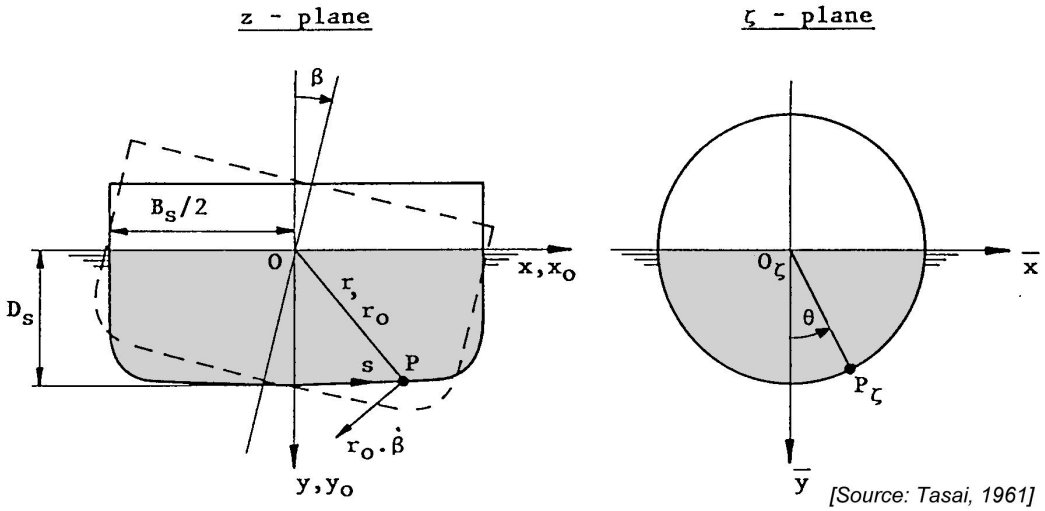

Figure 7.9: Axis System and Form used by Tasai

This represents an attempt to bring a more realistic ship form into an Ursell-like computation. The development followed here is very much like that used by Ursell.

Again, the fluid is assumed to be incompressible, inviscid and irrotational, without any effects of surface tension. The motion amplitudes and velocities are small enough, so that all but the linear terms of the free surface condition, the kinematic boundary condition on the cylinder and the Bernoulli equation may be neglected.

Boundary Conditions

Conformal mapping requires that two boundary conditions of Ursell be rewritten:

- **Free surface boundary condition**
  The free surface condition becomes:

$$\frac{\xi_b}{\lambda_b}\Phi\sum_{n=0}^{N}\left\{(2n-1)a_{2n-1}e^{-(2n-1)\alpha}\right\}\pm\frac{\partial\Phi}{\partial\theta}=0$$
$$\text{for}: \quad \alpha\geq 0 \quad \text{and} \quad \theta=\pm\frac{\pi}{2} \tag{7.103}$$

  in which:

$$\frac{\xi_b}{\lambda_b}=\frac{\omega^2}{g}M_s \quad \text{or:} \quad \xi_b=\frac{\omega^2 b_0}{2g}\ \text{(non-dimensional frequency squared)} \tag{7.104}$$

- **Kinematic boundary condition on the oscillating body surface**
  Conformal mapping results in the following requirements for the stream function on the surface of the cylinder:

$$\begin{aligned}
\text{for sway}: \quad & \Psi_0(\theta)=\dot{x}M_s\sum_{n=0}^{N}\left\{(-1)^n a_{2n-1}\cos\left((2n-1)\theta\right)\right\}+C(t)\\
\text{for heave}: \quad & \Psi_0(\theta)=\dot{y}M_s\sum_{n=0}^{N}\left\{(-1)^n a_{2n-1}\sin\left((2n-1)\theta\right)\right\}+C(t)\\
\text{for roll}: \quad & \Psi_0(\theta)=-\dot{\beta}\frac{b_0^2}{8\lambda_b}\left\{+\sum_{n=0}^{N}(-1)^n a_{2n-1}\sin\left((2n-1)\theta\right)\right\}^2\\
& -\dot{\beta}\frac{b_0^2}{8\lambda_b}\left\{-\sum_{n=0}^{N}(-1)^n a_{2n-1}\cos\left((2n-1)\theta\right)\right\}^2+C(t)
\end{aligned} \tag{7.105}$$

  in which $C(t)$ is a function of the time only.

Velocity Potentials and Stream Functions

The **velocity potentials and stream functions** in the fluid for sway and roll become:

$$\begin{aligned}
\phi_{A_{2m}}(\alpha,\theta) &= +e^{-(2m+1)\alpha}\sin\left((2m+1)\theta\right)\\
&\quad -\frac{\xi_b}{\lambda_b}\sum_{n=0}^{N}(-1)^n\frac{2n-1}{2m+2n}a_{2n-1}e^{-(2m+2n)\alpha}\sin\left((2m+2n)\theta\right)\\
\psi_{A_{2m}}(\alpha,\theta) &= -e^{-(2m+1)\alpha}\cos\left((2m+1)\theta\right)\\
&\quad +\frac{\xi_b}{\lambda_b}\sum_{n=0}^{N}(-1)^n\frac{2n-1}{2m+2n}a_{2n-1}e^{-(2m+2n)\alpha}\cos\left((2m+2n)\theta\right)
\end{aligned} \tag{7.106}$$

and for heave:

$$\begin{aligned}
\phi_{A_{2m}}(\alpha,\theta) &= +e^{-2m\alpha}\cos(2m\theta)\\
&\quad -\frac{\xi_b}{\lambda_b}\sum_{n=0}^{N}(-1)^n\frac{2n-1}{2m+2n-1}a_{2n-1}e^{-(2m+2n-1)\alpha}\cos\left((2m+2n-1)\theta\right)\\
\psi_{A_{2m}}(\alpha,\theta) &= +e^{-2m\alpha}\sin(2m\theta)\\
&\quad -\frac{\xi_b}{\lambda_b}\sum_{n=0}^{N}(-1)^n\frac{2n-1}{2m+2n-1}a_{2n-1}e^{-(2m+2n-1)\alpha}\sin\left((2m+2n-1)\theta\right)
\end{aligned} \tag{7.107}$$

Solution

The velocity potentials and stream functions for sway and roll on the surface of the cylinder, $\alpha = 0$, reduce to:

$$\begin{aligned}
\phi_{A0_{2m}}(\theta) &= \sin((2m+1)\theta) \\
&\quad -\frac{\xi_b}{\lambda_b}\sum_{n=0}^{N}(-1)^n\frac{2n-1}{2m+2n}a_{2n-1}\sin((2m+2n)\theta) \\
\psi_{A0_{2m}}(\theta) &= \cos((2m+1)\theta) \\
&\quad -\frac{\xi_b}{\lambda_b}\sum_{n=0}^{N}(-1)^n\frac{2n-1}{2m+2n}a_{2n-1}\cos((2m+2n)\theta)
\end{aligned} \tag{7.108}$$

and for heave to:

$$\begin{aligned}
\phi_{A0_{2m}}(\theta) &= \cos(2m\theta) \\
&\quad -\frac{\xi_b}{\lambda_b}\sum_{n=0}^{N}(-1)^n\frac{2n-1}{2m+2n-1}a_{2n-1}\cos((2m+2n-1)\theta) \\
\psi_{A0_{2m}}(\theta) &= \sin(2m\theta) \\
&\quad -\frac{\xi_b}{\lambda_b}\sum_{n=0}^{N}(-1)^n\frac{2n-1}{2m+2n-1}a_{2n-1}\sin((2m+2n-1)\theta)
\end{aligned} \tag{7.109}$$

Again, the resulting pressure on the cross section - and the path leading to it - is more important than the derivation details.

Hydrodynamic Pressure

With known velocity potentials, the hydrodynamic pressure on the surface of the cylinder can be obtained from the linearized Bernoulli equation:

$$\begin{aligned}
p(\theta) &= -\rho\frac{\partial\Phi_0(\theta)}{\partial t} \\
&= \frac{-\rho g\eta_a}{\pi}\left(\phi_{B0_s}(\theta)+\sum_{m=1}^{\infty}Q_{2m}\phi_{A0_{2m}}(\theta)\right)\cos(\omega t) \\
&\quad \frac{-\rho g\eta_a}{\pi}\left(\phi_{B0_c}(\theta)+\sum_{m=1}^{\infty}P_{2m}\phi_{A0_{2m}}(\theta)\right)\sin(\omega t)
\end{aligned} \tag{7.110}$$

The pressures for sway and roll are still skew-symmetric in θ and for heave still symmetric in θ.

Hydrodynamic Loads

The two-dimensional hydrodynamic sway and heave force and roll moment can be obtained from integrations of these pressures over the contour, $r = r_0$, of the circular cross section. When switching to polar coordinates, derivatives with respect to θ has to be used:

$$\frac{dx_0}{d\theta} = -M_s\sum_{n=0}^{N}(-1)^n(2n-1)a_{2n-1}\cos((2n-1)\theta)$$

$$\frac{dy_0}{d\theta} = -M_s \sum_{n=0}^{N} (-1)^n (2n-1) a_{2n-1} \sin\left((2n-1)\theta\right) \tag{7.111}$$

With these, the loads can be expressed in terms of potential mass and damping terms and a comparison of the in-phase and out-of-phase terms delivers the potential coefficients.

$$\begin{aligned} F_x{}' &= \int_{C_0} p(\theta) dy_0 = 2 \int_0^{\frac{1}{2}\pi} p(\theta) \frac{dy_0}{d\theta} d\theta \\ &= -M_{22}{}' \cdot \ddot{x} - N_{22}{}' \cdot \dot{x} \qquad \text{(for a swaying cylinder)} \\ &= -M_{24}{}' \cdot \ddot{\beta} - N_{24}{}' \cdot \dot{\beta} \qquad \text{(for a rolling cylinder)} \end{aligned}$$

$$\begin{aligned} F_y{}' &= -\int_{C_0} p(\theta) dx_0 = -2 \int_0^{\frac{1}{2}\pi} p(\theta) \frac{dx_0}{d\theta} d\theta \\ &= -M_{33}{}' \cdot \ddot{y} - N_{33}{}' \cdot \dot{y} \qquad \text{(for a heaving cylinder)} \end{aligned}$$

$$\begin{aligned} M_R{}' &= -\int_{C_0} p(\theta) x_0 dx_0 - \int_{C_0} p(\theta) y_0 dy_0 = -2 \int_0^{\frac{1}{2}\pi} p(\theta) \left(x_0 \frac{dx_0}{d\theta} + y_0 \frac{dy_0}{d\theta} \right) d\theta \\ &= -M_{42}{}' \cdot \ddot{x} - N_{42}{}' \cdot \dot{x} \qquad \text{(for a swaying cylinder)} \\ &= -M_{44}{}' \cdot \ddot{\beta} - N_{44}{}' \cdot \dot{\beta} \qquad \text{(for a rolling cylinder)} \end{aligned} \tag{7.112}$$

Thus, comparisons of the in-phase and out-of-phase parts of these expressions for sway, heave and roll deliver the 2-D potential coefficients of this approximate cross section. Notice that, in contradiction with the case of Ursell's rolling circular cross section, the roll moment $M_R{}'$ is not zero here.

7.3.4 Theory of Frank

As a consequence of conformal mapping to the unit circle, the cross sections need to have a certain breadth at the water surface; $x = r_0 \cdot e^{\alpha}$. Fully submersed cross sections, such as at the bulbous bow, cannot be mapped. Mapping problems can also appear for cross sections outside the area coefficients range $0.5 < \sigma_s < 1.0$. These cases require another approach, which is discussed here.

[Frank, 1967] considered an actual cross section of a ship. He used a non-circular cylinder, whose cross section is a simply connected region, which is fully or partly immersed horizontally in a previously undisturbed fluid of infinite depth; see figure 7.10.

The x-axis coincides with the undisturbed free surface and the y-axis is positive upwards. The cross sectional contour C_0 of the submerged portion of the cylinder lies in the lower half plane and the y-axis is the axis of symmetry of C_0.

The cylinder is forced to carry out a simple harmonic motion $A^{(m)} \cdot \cos(\omega t)$ with a prescribed frequency of oscillation ω. The superscript $^{(m)}$ (as used by Frank and maintained here) may take on the values 2, 3 and 4, denoting swaying, heaving and rolling motions, respectively, as explained earlier. It is assumed that steady state conditions have been attained.

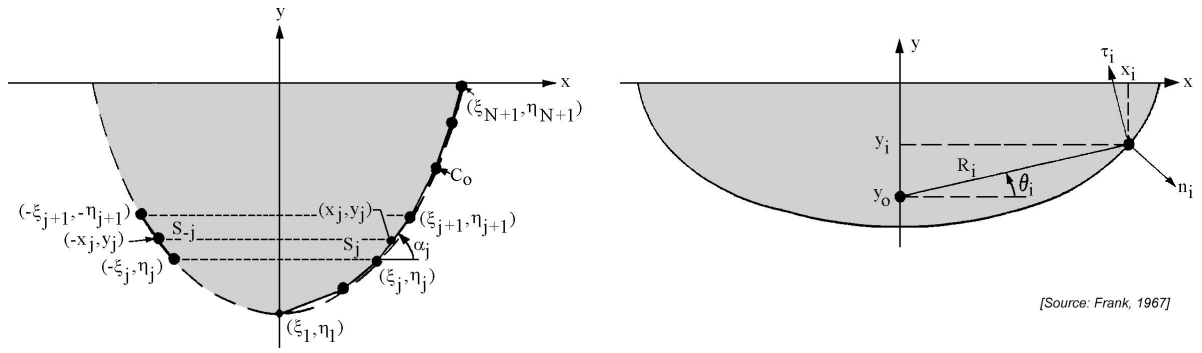

Figure 7.10: Axes System and Notation, as Used by Frank

Again, the fluid is assumed to be incompressible, inviscid and irrotational, without any effects of surface tension. The motion amplitudes and velocities are small enough, so that all but the linear terms of the free surface condition, the kinematic boundary condition on the cylinder and the Bernoulli equation may be neglected.

Boundary Conditions

A velocity potential has to be found:

$$\boxed{\Phi^{(m)}(x,y,t) = \Re e\left\{\phi^{(m)}(x,y)\cdot e^{-i\omega t}\right\}} \tag{7.113}$$

satisfying the six conditions as discussed in the first section of this chapter:

1. **Laplace equation**
   The equation of Laplace is now:

$$\nabla^2\Phi^{(m)} = \frac{\partial^2\Phi^{(m)}}{\partial x^2} + \frac{\partial^2\Phi^{(m)}}{\partial y^2} = 0 \tag{7.114}$$

2. **Sea bed boundary condition**
   For deep water, the boundary condition on the bottom is expressed by:

$$\frac{\partial\Phi^{(m)}}{\partial y} \rightarrow 0 \qquad \text{for:} \quad y \rightarrow -\infty \tag{7.115}$$

3. **Free surface boundary condition**
   The linearized free surface condition outside the cylinder in deep water is expressed as follows:

$$\frac{\partial^2\Phi^{(m)}}{\partial t^2} + g\frac{\partial\Phi^{(m)}}{\partial y} = 0 \qquad \text{for:} \quad y = 0 \tag{7.116}$$

   in which g is the acceleration of gravity.

4. **Kinematic boundary condition on the oscillating body surface**
   The normal velocity component of the fluid at the surface of the oscillating cylinder is equal to the normal component of the forced velocity of the cylinder. If v_n is the

component of the forced velocity of the cylinder in the direction of the outgoing unit normal vector $\mathbf{n}$, then the kinematic boundary condition has to be satisfied at the mean position of the cylindrical surface:

$$\vec{n} \cdot \vec{\nabla}\Phi^{(m)} = v_n \tag{7.117}$$

5. **Radiation condition**
   At a large distance from the cylinder the disturbed surface of the fluid has to take the form of a regular progressive outgoing gravity wave.

6. **Symmetric or anti-symmetric condition**
   Because both the sway and the roll motion are anti-symmetric and the heave motion is symmetrical, these velocity potentials have the following relation:

$$\begin{aligned} \text{sway}: &\quad \Phi^{(2)}(-x,y) = -\Phi^{(2)}(+x,y) \\ \text{heave}: &\quad \Phi^{(3)}(-x,y) = +\Phi^{(3)}(+x,y) \\ \text{roll}: &\quad \Phi^{(4)}(-x,y) = -\Phi^{(4)}(+x,y) \end{aligned} \tag{7.118}$$

Velocity Potentials

A potential function, based on pulsating point-sources and satisfying these six conditions, has been given by [Frank, 1967]. Based on earlier work of [Wehausen and Laitone, 1960], the complex potential at z of a pulsating point-source of unit strength at the point ζ in the lower half plane, as shown in figure 7.10, was given by Frank as:

$$\begin{aligned} G^*(z,\zeta;t) = \frac{1}{2\pi} \Bigg\{ \ln(z-\zeta) - \ln(z-\widehat{\zeta}) + 2PV \int_0^\infty \frac{e^{-ik(z-\widehat{\zeta})}}{\nu - k} dk \Bigg\} \cdot &\quad \cos\omega t \\ - \left\{ e^{-i\nu(z-\widehat{\zeta})} \right\} \cdot &\quad \sin\omega t \end{aligned} \tag{7.119}$$

where:

$$z = x + iy \qquad \zeta = \xi + i\eta \qquad \widehat{\zeta} = \xi - i\eta \tag{7.120}$$

In here, ζ is defined in the lower half plane and $\widehat{\zeta}$ in the upper half plane (mirrored), while $\nu = \omega^2/g$ is the wave number in deep water and $PV \int_0^\infty \frac{e^{-ik(z-\widehat{\zeta})}}{\nu-k} dk$ is a principle value integral with a variable k. These somewhat unconventional notations come from Frank's report and are maintained here.
With this, the real part of the point-source potential is defined by:

$$H(x,y,\xi,\eta;t) \;=\; \Re e \left\{ G^*(z,\zeta;t) \right\} \tag{7.121}$$

The space and time dependent source potential term, $G^*(z,\zeta;t)$, is now written in terms of a separate space dependent potential, $G(z,\zeta)$, multiplied by an oscillatory motion, $e^{-i\omega t}$:

$$G^*(z,\zeta;t) = G(z,\zeta) \cdot e^{-i\omega t} \tag{7.122}$$

With this space dependent potential:

$$G(z,\zeta) = \frac{1}{2\pi}\cdot \quad \Re e\left\{\ln(z-\zeta) - \ln(z-\widehat{\zeta}) + 2\int_0^\infty \frac{e^{-ik(z-\widehat{\zeta})}}{\nu - k}dk\right\}$$
$$-i\cdot \quad \Re e\left\{e^{-i\nu(z-\widehat{\zeta})}\right\} \tag{7.123}$$

two expressions for the point-source potential, satisfying all six boundary conditions, are found:

$$\begin{aligned} H(x,y,\xi,\eta;t \quad\;\;) &= \Re e\left\{\;\; G(z,\zeta)\cdot e^{-i\omega t}\right\} \\ H(x,y,\xi,\eta;t-\frac{\pi}{2\omega}) &= \Re e\left\{i\cdot G(z,\zeta)\cdot e^{-i\omega t}\right\} \end{aligned} \tag{7.124}$$

Since the problem is linear, a superposition of these two valid expressions for the point-source potential H results in the velocity potential:

$$\boxed{\Phi^{(m)}(x,y;t) = \Re e\left\{\int_{C_0} Q(s)\cdot G(z,\zeta)\cdot e^{-i\omega t}\cdot ds\right\}} \tag{7.125}$$

where C_0 is the submerged contour of the cylindrical cross section at its mean or rest position and $Q(s)$ represents the complex source density as a function of the position along C_0.
Application of the kinematic boundary condition on the oscillating cylinder at z yields:

$$\begin{aligned} \Re e\left\{(\vec{n}\cdot\vec{\nabla})\int_{C_0} Q(s)\cdot G(z,\zeta)\cdot ds\right\} &= 0 \\ \Im m\left\{(\vec{n}\cdot\vec{\nabla})\int_{C_0} Q(s)\cdot G(z,\zeta)\cdot ds\right\} &= A^{(m)}\cdot\omega\cdot n^{(m)} \end{aligned} \tag{7.126}$$

where $A^{(m)}$ denotes the amplitude of oscillation and $n^{(m)}$ the direction cosine of the normal velocity at z on the cylinder. Both $A^{(m)}$ and $n^{(m)}$ depend on the mode of motion of the cylinder, as will be shown below.
The fact that $Q(s)$ is complex implies that the last two equations represent a set of coupled integral equations for the real functions $\Re e\{Q(s)\}$ and $\Im m\{Q(s)\}$. Frank describes the evaluation of the integrals in his report; special attention is focussed there on the singularity for $z=\zeta$ and $k=\nu$.

Solution

Select $N+1$ points (ξ_i,η_i) which lie on C_0 in the fourth quadrant. Connect these $N+1$ points by successive straight lines. N straight line segments are obtained which, together with their reflected images in the third quadrant, yield an approximation to the given contour as shown in figure 7.10. The coordinates, length and angle associated with the j-th segment are identified by the subscript j, whereas the corresponding quantities for the

reflected image in the third quadrant are denoted by the subscript $-j$, so that by symmetry $\xi_{-j} = -\xi_j$ and $\eta_{-j} = -\eta_j$ for $1 \leq j \leq N+1$.
Potentials and pressures are to be evaluated at the midpoint of each segment and for $1 \leq i \leq N$ the coordinates of the midpoint of the i-th segment are:

$$x_i = \frac{\xi_i + \xi_{i+1}}{2} \qquad \text{and} \qquad y_i = \frac{\eta_i + \eta_{i+1}}{2} \tag{7.127}$$

The length of the i-th segment and the angle between by this segment and the positive x axis are:

$$|s_i| = \sqrt{\left(\xi_{i+1} - \xi_i\right)^2 + \left(\eta_{i+1} - \eta_i\right)^2} \qquad \alpha_i = \arctan\left\{\frac{\eta_{i+1} - \eta_i}{\xi_{i+1} - \xi_i}\right\} \tag{7.128}$$

The outgoing unit vector normal to the cross section at the i-th midpoint (x_i, y_i) is:

$$\vec{n}_i = \vec{i}\sin\alpha_i - \vec{j}\cos\alpha_i \tag{7.129}$$

where $\vec{i}$ and $\vec{j}$ are unit vectors in the x- and y-directions, respectively.

The cylinder is forced into a simple harmonic motion with radian frequency ω, according to the displacement equation:

$$S^{(m)} = A^{(m)} \cdot \cos\omega t \tag{7.130}$$

for $m = 2$, 3 or 4, corresponding to sway, heave or roll, respectively. The rolling motions are about an axis through a point $(0, y_0)$ in the symmetry plane of the cylinder.
In the translational modes, any point on the cylinder moves with the velocity:

$$\begin{aligned} \text{sway:} \qquad \vec{v}^{(2)} &= -\vec{i}\, A^{(2)}\omega\sin\omega t \\ \text{heave:} \qquad \vec{v}^{(3)} &= -\vec{j}\, A^{(3)}\omega\sin\omega t \end{aligned} \tag{7.131}$$

The rolling motion is illustrated in figure 7.10. Considering a point (x_i, y_i) on C_0, an inspection of this figure yields:

$$R_i = \sqrt{{x_i}^2 + \left(y_i - y_0\right)^2} \qquad \text{and} \qquad \begin{aligned} \theta_i &= \arctan\left\{\frac{y_i - y_0}{x_i}\right\} \\ &= \arcsin\left\{\frac{y_i - y_0}{R_i}\right\} \\ &= \arccos\left\{\frac{x_i}{R_i}\right\} \end{aligned} \tag{7.132}$$

Therefore, by elementary two-dimensional kinematics, the unit vector in the direction θ is:

$$\begin{aligned} \vec{\tau}_i &= -\vec{i}\sin\theta_i + \vec{j}\cos\theta_i \\ &= -\frac{y_i - y_0}{R_i}\vec{i} + \frac{x_i}{R_i}\vec{j} \end{aligned} \tag{7.133}$$

so that:

$$\begin{aligned} \text{roll:} \qquad \vec{v}^{(4)} &= R_i S^{(4)}\vec{\tau}_i \\ &= \omega A^{(4)}\left\{\left(y_i - y_0\right)\vec{i} - x_i\vec{j}\right\}\sin\omega t \end{aligned} \tag{7.134}$$

The normal components of the velocity ${v_i}^{(m)} = \vec{n}_i \cdot \vec{v}^{(m)}$ at the midpoint of the i-th segment (x_i, y_i) are:

$$\begin{aligned} \text{sway:} \quad & {v_i}^{(2)} = -\omega A^{(2)} \sin\alpha_i \sin\omega t \\ \text{heave:} \quad & {v_i}^{(3)} = +\omega A^{(3)} \cos\alpha_i \sin\omega t \\ \text{roll:} \quad & {v_i}^{(4)} = +\omega A^{(4)} \{(y_i - y_0)\sin\alpha_i + x_i \cos\alpha_i\} \sin\omega t \end{aligned} \tag{7.135}$$

Defining:

$${n_i}^{(m)} = \frac{{v_i}^{(m)}}{A^{(m)}\omega \sin\omega t} \tag{7.136}$$

then, consistent with the previously mentioned notation, the direction cosines for the three modes of motion are:

$$\begin{aligned} \text{sway:} \quad & {n_i}^{(2)} = +\sin\alpha_i \\ \text{heave:} \quad & {n_i}^{(3)} = -\cos\alpha_i \\ \text{roll:} \quad & {n_i}^{(4)} = +(y_i - y_0)\sin\alpha_i + x_i\cos\alpha_i \end{aligned} \tag{7.137}$$

These equations illustrate that heaving is symmetrical: ${n_{-i}}^{(3)} = {n_i}^{(3)}$. Swaying and rolling, however are antisymmetric modes: ${n_{-i}}^{(2)} = -{n_i}^{(2)}$ and ${n_{-i}}^{(4)} = -{n_i}^{(4)}$.
The set of two coupled integral equations for the real functions $\Re e\{Q(s)\}$ and $\Im m\{Q(s)\}$, given before, are applied at the midpoints of each of the N segments. It is assumed that over an individual segment the complex source strength $Q(s)$ remains constant, although it varies from segment to segment. With these stipulations, the set of coupled integral equations becomes a set of $2N$ linear algebraic equations in the unknowns:

$$\begin{aligned} \Re e\left\{Q^{(m)} \cdot (s_j)\right\} &= {Q_j}^{(m)} \\ \Im m\left\{Q^{(m)} \cdot (s_j)\right\} &= {Q_{N+j}}^{(m)} \end{aligned} \tag{7.138}$$

Thus, for $i = 1, 2, ..., N$:

$$\begin{aligned} +\sum_{j=1}^{N}\left\{{Q_j}^{(m)} \cdot {I_{ij}}^{(m)}\right\} + \sum_{j=1}^{N}\left\{{Q_{N+j}}^{(m)} \cdot {J_{ij}}^{(m)}\right\} &= 0 \\ -\sum_{j=1}^{N}\left\{{Q_j}^{(m)} \cdot {J_{ij}}^{(m)}\right\} + \sum_{j=1}^{N}\left\{{Q_{N+j}}^{(m)} \cdot {I_{ij}}^{(m)}\right\} &= \omega \cdot A^{(m)} \cdot {n_i}^{(m)} \end{aligned} \tag{7.139}$$

where the superscript $^{(m)}$ in these $2N^2$ equations denotes the mode of motion.
The influence coefficients ${I_{ij}}^{(m)}$ and ${J_{ij}}^{(m)}$ and the potential $\Phi^{(m)}(x_i, y_i; t)$ have been evaluated by [Frank, 1967]. The resulting velocity potential consists of a term in-phase with the displacement and a term in-phase with the velocity.
The hydrodynamic pressure at (x_i, y_i) along the cylinder is obtained from the velocity potential by means of the linearized Bernoulli equation:

$$p^{(m)}(x_i, y_i, \omega; t) = -\rho \cdot \frac{\partial \Phi^{(m)}}{\partial t}(x_i, y_i, \omega; t) \tag{7.140}$$

Since:

$$\begin{aligned} p^{(m)}(x_i, y_i, \omega; t) = {} & {p_a}^{(m)}(x_i, y_i; \omega) \cdot \cos\omega t \\ & + {p_v}^{(m)}(x_i, y_i; \omega) \cdot \sin\omega t \end{aligned} \tag{7.141}$$

where ${p_a}^{(m)}$ and ${p_v}^{(m)}$ are the hydrodynamic pressures in-phase with the displacement and in-phase with the velocity, respectively.
As indicated by the previous expressions, the potential as well as the pressure is a function of the oscillation frequency ω. The hydrodynamic force or moment per unit length of the cylinder, necessary to sustain the oscillations, is the integral of $p^{(m)} \cdot n^{(m)}$ over the submerged contour of the cross section C_0. It is assumed that the pressure at the i-th midpoint is the mean pressure for the i-th segment, so that the integration reduces to a summation, so that:

$$\boxed{M^{(m)}(\omega) = 2\sum_{i=1}^{N} {p_a}^{(m)}(x_i, y_i; \omega) \cdot {n_i}^{(m)} \cdot |s_i|}$$

$$\boxed{N^{(m)}(\omega) = 2\sum_{i=1}^{N} {p_v}^{(m)}(x_i, y_i; \omega) \cdot {n_i}^{(m)} \cdot |s_i|} \tag{7.142}$$

for the potential inertia and damping forces or moments, respectively.

7.3.5 Comparative Results

Figure 7.11 compares the calculated coefficients for an amidships cross section of a container vessel with the three previous methods:

- Ursell-Tasai's method with 2-parameter Lewis conformal mapping.

- Ursell-Tasai's method with 10-parameter close-fit conformal mapping.

- Frank's pulsating source method.

With the exception of the roll motions, the three results are very close. The roll motion deviation, predicted with the Lewis conformal mapping method, is caused by the description of the "bilge" by the simple Lewis transformation, as can be seen in figure 7.8.
A disadvantage of Frank's method can be the large computing time, when compared with Ursell-Tasai's method. Generally, it is advised to use Ursell-Tasai's method with 10 parameter close-fit conformal mapping. For submerged sections, bulbous sections and sections with an area coefficient, σ_s, less than 0.5, Frank's pulsating source method should be used.

7.4 3-D Potential Theory

The previous main section of this chapter has discussed the potential theory for two-dimensional (plane) shapes. Floating bodies are obviously three-dimensional and it can be appropriate therefore to attempt to determine their potential theory coefficients directly in three dimensions, similar to what Frank did in the two-dimensional case. Just as earlier in this chapter, the presentation here is intended to provide only a bit of insight into the derivation path being followed. The path and the result is more important than the derivation details.
Three-dimensional methods to evaluate the hydrodynamic loads and motions of fixed or (with zero mean forward speed) floating structures in waves have been developed based

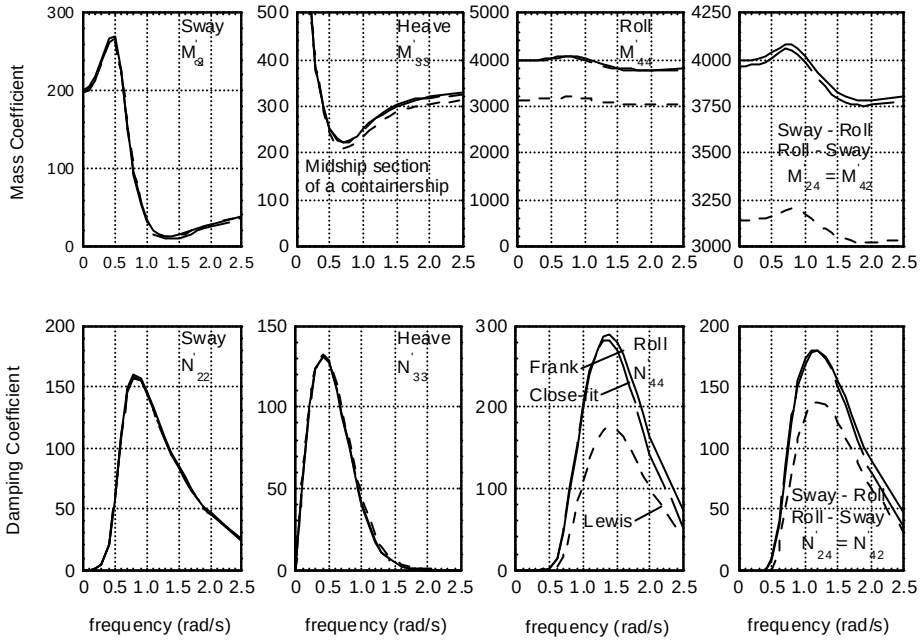

Figure 7.11: Comparison of Calculated Coefficients

on linear three-dimensional potential theory, see for instance [Oortmerssen, 1976a]. Experimental verification of results of computations has been carried out for bodies with a large variety of shapes, see [Oortmerssen, 1976a] and [Pinkster, 1980]. Such comparisons show that 3-D diffraction methods generally can be applied to most body shapes and are therefore a good tool to investigate such effects at zero mean forward speed.
This section gives a brief description of the 3-D diffraction theory as used in the computer program DELFRAC developed at the Delft University of Technology. It computes the wave-frequency hydrodynamic loads on free-floating or fixed bodies as well as the wave-frequency motions of floating bodies. Second order wave drift forces can be computed as well; these are discussed in chapter 9.
The method is restricted to arbitrarily shaped bodies with **zero mean forward speed**. This is an acceptable simplification for the majority of the fixed or floating structures in use today in the offshore industry. It should be mentioned however, that attention is shifting to the development of methods taking into account low forward speed or (alternatively) current effects; see [Huijsmans, 1996]. The treatment of such methods is beyond the scope of this text, however.

7.4.1 Diffraction Theory

The diffraction theory used in this approach is given here for an arbitrarily shaped, fixed or free-floating body. Use is made of a right-handed, earth-bound $S(x_0, y_0, z_0)$ system of axes with origin at the mean water level and the z_0-axis vertically upwards. The body axis $G(x_b, y_b, z_b)$ has its origin in the center of gravity G of the body; the x_b-axis is towards the bow and y_b to port. The positive z_b-axis is upwards. This coordinate system coincides with another earth-bound system of fixed axes $O(x, y, z)$ in the mean position of the structure. This is the same system as was used in chapter 6.

The wave elevation and all potentials are referenced to the fixed $O(x, y, z)$ system of axes. Phase shifts of body motions are referenced to the undisturbed wave elevation at the center of gravity ($G = O$) of the body; even though no wave can be measured there.
According to linear potential theory, the potential of a floating body is a superposition of the potentials due to the undisturbed incoming wave Φ_w, the potential due to the diffraction of the undisturbed incoming wave on the fixed body Φ_d and the radiation potentials due to the six body motions Φ_j:

$$\boxed{\Phi = \sum_{j=1}^{6} \Phi_j + \Phi_w + \Phi_d} \tag{7.143}$$

Again, the fluid is assumed to be incompressible, inviscid and irrotational, without any effects of surface tension. The motion amplitudes and velocities are small enough, so that all but the linear terms of the free surface condition, the kinematic boundary condition on the body and the Bernoulli equation may be neglected.

The potentials have to satisfy the same boundary conditions, as discussed before:

1. **Laplace equation**
   The continuity condition or Laplace equation:

   $$\frac{\partial^2 \Phi}{\partial x^2} + \frac{\partial^2 \Phi}{\partial y^2} + \frac{\partial^2 \Phi}{\partial z^2} = 0 \tag{7.144}$$

   holds in the fluid domain.

2. **Sea bed boundary condition**
   At the sea bed:

   $$\frac{\partial \Phi}{\partial z} = 0 \quad \text{with:} \quad z = -h_o \tag{7.145}$$

   in which h_o is the distance from the origin of the earth-bound coordinate system, $O(x, y, z)$, to the sea bed. Note that, in contrast to the earlier theory, this treatment is for water with a finite depth.

3. **Free surface boundary condition**
   At the mean free surface:

   $$g\frac{\partial \Phi}{\partial z} + \frac{\partial^2 \Phi}{\partial t^2} = 0 \tag{7.146}$$

4. **Kinematic boundary condition on the oscillating body surface**
   On the wetted part of the oscillating hull of the structure (in its mean position):

   $$\frac{\partial \Phi}{\partial n} = \vec{v}.\vec{n} \tag{7.147}$$

   in which $\vec{v}$ is the velocity of a point on the hull of the body and $\vec{n}$ is the normal vector of the hull, positive into the fluid.

5. **Radiation condition**
   The body motion and diffraction potentials have to satisfy a radiation condition which states that at great distance from the body these potentials disappear. This condition imposes a uniqueness which would not otherwise be present, see [Oortmerssen, 1976a].

6. **Symmetric or anti-symmetric condition**
   If, for instance for ships, both the sway and the roll motion of the fluid are anti-symmetric and the heave motion is symmetrical, the velocity potentials have the following relation:

$$\begin{aligned} \Phi^{(2)}(-x,y) &= -\Phi^{(2)}(+x,y) \qquad \text{for sway} \\ \Phi^{(3)}(-x,y) &= +\Phi^{(3)}(+x,y) \qquad \text{for heave} \\ \Phi^{(4)}(-x,y) &= -\Phi^{(4)}(+x,y) \qquad \text{for roll} \end{aligned} \tag{7.148}$$

   However, this symmetry condition has not to be used in DELFRAC necessarily, because this program is suitable for any hull form..

The free-surface condition follows from the assumptions that the pressure at the surface is constant and that water particles do not pass through the free surface. The condition on the wetted surface of the body assures the no-leak condition of the (oscillating) hull. The condition at the sea bed is also a no-leak condition.
Up to now no specific wave conditions have been applied. The boundary conditions are general and apply to all possible realizations of wave conditions. The theory is developed here for a unidirectional regular wave. Just as in chapter 5, superposition can then be used to study all sorts of irregular wave conditions - even those with directional spreading.
In regular waves a linear potential Φ, which is a function of the earth-fixed coordinates and of time t, can be written as a product of a space-dependent term and a harmonic time-dependent term as follows:

$$\boxed{\Phi(x,y,z;t) = \phi(x,y,z) \cdot e^{-i\omega t}} \tag{7.149}$$

The boundary conditions for the potential, Φ, result in similar conditions for the space dependent term, ϕ.

Note: Following [Tuck, 1970] a convenient formulation can be obtained by writing:

$$\phi = -i\omega \sum_{j=0}^{7} \phi_j \zeta_j \tag{7.150}$$

in which $j = 0$ represents the undisturbed incoming wave, $j = 1, ...6$ are associated with each of the motion modes of the body and $j = 7$ represents the diffracted wave.

The **space-dependent part** of the velocity potential ϕ_0 - associated with an undisturbed long-crested regular wave in water of constant depth h - is given by:

$$\phi_0 = \frac{\zeta_0 g}{\omega} \cdot \frac{\cosh k(h_o + z)}{\cosh kh} \cdot e^{ik(x\cos\mu + y\sin\mu)} \tag{7.151}$$

in which:

ζ_0	=	amplitude of undisturbed wave (m)
$k = 2\pi/\lambda$	=	wave number at shallow water (rad/m)
λ	=	wave length (m)
μ	=	wave direction (rad); zero for a wave travelling in the positive x-direction
ω	=	wave frequency (rad/s)
h_o	=	distance from the origin, O, of the earth-fixed axes to the sea bed (m)
h	=	water depth (m)

The following dispersion relation links the water depth h, the wave frequency ω, and the wave number k:

$$\begin{aligned} \nu \cdot g &= \omega^2 \\ &= kg \cdot \tanh kh \end{aligned} \tag{7.152}$$

in which $\nu = \omega^2/g$ is the wave number in deep water.
In regular long-crested waves the undisturbed wave elevation follows from the free surface dynamic boundary condition:

$$\zeta = -\frac{1}{g} \cdot \frac{\partial \Phi}{\partial t} \qquad \text{(see chapter 5)} \tag{7.153}$$

which results in:

$$\zeta(x, y; t) = \zeta_0 \cdot e^{ik(x\cos\mu + y\sin\mu) - i\omega t} \tag{7.154}$$

The motions of the body in the j-mode relative to its body axes are given by:

$$\zeta_j(t) = \overline{\zeta}_j \cdot e^{-i\omega t} \tag{7.155}$$

in which the overline indicates the complex amplitude of the motion.
Note that this overline (which applies to the complex potentials etc.) is neglected in the remainder of this section.

The complex potential ϕ follows from the superposition of the undisturbed wave potential ϕ_0, the wave diffraction potential ϕ_7 and the potentials ϕ_j associated with the j-modes of motion of the body ($j = 1, ...6$):

$$\phi = -i\omega \left\{ (\phi_0 + \phi_7)\, \zeta_0 + \sum_{j=1}^{6} \phi_j\, \zeta_j \right\} \tag{7.156}$$

The fluid pressure follows from the Bernoulli equation:

$$\begin{aligned} p(x, y, z; t) &= -\rho \frac{\partial \Phi}{\partial t} \\ &= \rho\omega^2 \left\{ (\phi_0 + \phi_7)\, \zeta_0 + \sum_{j=1}^{6} \phi_j\, \zeta_j \right\} \cdot e^{-i\omega t} \end{aligned} \tag{7.157}$$

The first order wave exciting forces ($k = 1, 2, 3$) and moments ($k = 4, 5, 6$) in the k^{th} direction are:

$$\begin{aligned} X_k &= -\iint_{S_0} p\, n_k \cdot dS_0 \\ &= -\rho\omega^2 \zeta_0 e^{-i\omega t} \iint_{S_0} (\phi_0 + \phi_7)\, n_k \cdot dS_0 \end{aligned} \tag{7.158}$$

and the oscillating hydrodynamic forces and moments in the k^{th} direction are:

$$\begin{aligned} F_k &= -\iint_{S_0} p\, n_k \cdot dS_0 \\ &= -\rho\omega^2 \sum_{j=1}^{6} \zeta_j e^{-i\omega t} \iint_{S_0} \phi_j\, n_k \cdot dS_0 \end{aligned} \tag{7.159}$$

in which:

S_0 = mean wetted surface of the body
n_k = direction cosine of surface element dS_0 for the k-mode

The generalized direction cosines on S_0 are defined as follows:

$$\begin{aligned} n_1 &= \cos(n,x) \\ n_2 &= \cos(n,y) \\ n_3 &= \cos(n,z) \\ n_4 &= yn_3 - zn_2 \\ n_5 &= zn_1 - xn_3 \\ n_6 &= xn_2 - yn_1 \end{aligned} \tag{7.160}$$

The added mass and damping (coupling) coefficients are defined as follows:

$$\begin{aligned} a_{kj} &= -\Re e\left[\rho \iint_{S_0} \phi_j \, n_k \cdot dS_0\right] \\ b_{kj} &= -\Im m\left[\rho\omega \iint_{S_0} \phi_j \, n_k \cdot \, dS_0\right] \end{aligned} \tag{7.161}$$

The following symmetry relationships apply to these coefficients :

$$\begin{aligned} a_{kj} &= a_{jk} \\ b_{kj} &= b_{jk} \end{aligned} \tag{7.162}$$

so that both matrices are symmetric.

7.4.2 Solving Potentials

The incident wave potential, ϕ_0, is given in equation 7.151

According to [Lamb, 1932], the potential ϕ_j at a point (x,y,z) on the mean wetted body surface S_0 due to a motion in the mode j ($j = 1,...6$) and the diffraction potential ϕ_7 can be represented by a continuous distribution of single sources on the body surface:

$$\boxed{\phi_j(x,y,z) = \frac{1}{4\pi} \iint_{S_0} \sigma_j(\widehat{x},\widehat{y},\widehat{z}) \cdot \, G(x,y,z,\widehat{x},\widehat{y},\widehat{z}) \, \cdot dS_0} \qquad \text{for } j = 1,...7 \tag{7.163}$$

in which:

- $\phi_j(x,y,z)$ is the **potential function** in a point (x,y,z) on the mean wetted body surface, S_0. The cases with $j = 1,...6$ correspond to the potentials due to a motion of the body in the j^{th} mode, while ϕ_7 is the potential of the diffracted waves. The individual potentials satisfy all boundary conditions.
- $\sigma_j(\widehat{x},\widehat{y},\widehat{z})$ is the complex **source strength** in a point $(\widehat{x},\widehat{y},\widehat{z})$ on the mean wetted body surface, S_0, due to a motion of the body in the j-mode.

- $G(x,y,z,\widehat{x},\widehat{y},\widehat{z})$ is the **Green's function** or **influence function** of the pulsating source $\sigma_j(\widehat{x},\widehat{y},\widehat{z})$ in a point located at $(\widehat{x},\widehat{y},\widehat{z})$ on the potential $\phi_j(x,y,z)$ in a point located at (x,y,z), singular for $(\widehat{x},\widehat{y},\widehat{z}) = (x,y,z)$. This Green's function satisfies the Laplace equation, the linearized boundary conditions on the sea bed and on the free surface and the radiation condition at infinity.

Equivalent Green's functions are given by [Wehausen and Laitone, 1960] and [John, 1949]:

$$\overline{|G(x,y,z,\widehat{x},\widehat{y},\widehat{z})|} \text{ according to [Wehausen and Laitone, 1960]} = \tag{7.164}$$
$$\frac{1}{r} + \frac{1}{r_1}$$
$$+PV \int_0^\infty \frac{2(\xi+\nu)e^{-\xi h}\cdot\cosh\xi(h_o+\widehat{z})\cdot\cosh\xi(h_o+z)}{\xi\sinh\xi h - \nu\cosh\xi h}\cdot J_0(\xi R)\cdot d\xi$$
$$+i\cdot\frac{2\pi(k^2-\nu^2)\cdot\cosh k(h_o+\widehat{z})\cdot\cosh k(h_o+z)}{(k^2-\nu^2)h-\nu}\cdot J_0(kR)$$

$$\overline{|G(x,y,z,\widehat{x},\widehat{y},\widehat{z})|} \text{ according to [John, 1949]} = \tag{7.165}$$
$$2\pi\cdot\frac{\nu^2-k^2}{(k^2-\nu^2)\,h+\nu}\cdot\cosh k(h_o+z)\cdot\cosh k(h_o+\widehat{z})\cdot\{Y_0(kr)-iJ_0(kR)\}$$
$$+\sum_{i=1}^{\infty}\frac{4\,(k_i^2+\nu^2)}{(k_i^2+\nu^2)\,h-\nu}\cdot\cos k_i(h_o+z)\cdot\cos k_i(h_o+\widehat{z})\cdot K_0(k_iR)$$

in which:

$$\begin{aligned}
r &= \sqrt{(x-\widehat{x})^2+(y-\widehat{y})^2+(z-\widehat{z})^2}\\
r_1 &= \sqrt{(x-\widehat{x})^2+(y-\widehat{y})^2+(z+2h_o+\widehat{z})^2} \quad (=\text{mirrored})\\
R &= \sqrt{(x-\widehat{x})^2+(y-\widehat{y})^2}\\
\xi &= \text{a variable}\\
J_0,\ K_0 \text{ and } Y_0 &= \text{Bessel functions}\\
k_i &= \text{positive solutions of } \tanh(k_ih)+\nu=0
\end{aligned}$$

Although these two representations are equivalent, one of the two may be preferred for numerical computations depending on the values of the variables. In general, equation 7.165 is the most convenient representation for calculations, but when $R=0$ the value of K_0 becomes infinite, so that equation 7.164 must be used when R is small or zero.
In DELFRAC and many other similar diffraction computer codes, use is made of the FINGREEN subroutine supplied by MIT for the purpose of computing the Green's function and its derivatives. Computation involving both formulations has been speeded up through the use of polynomial expressions, see [Newman, 1985].
The unknown source strengths $\sigma_j(\widehat{x},\widehat{y},\widehat{z})$ are determined based on the normal velocity boundary condition on the body, see equation 7.157 combined with equation 7.163:

$$\begin{aligned}
\frac{\partial\phi_j}{\partial n} &= n_j\\
&= -\frac{1}{2}\sigma_j(x,y,z)+\frac{1}{4\pi}\iint_{S_0}\sigma_j(\widehat{x},\widehat{y},\widehat{z})\cdot\frac{\partial G(x,y,z,\widehat{x},\widehat{y},\widehat{z})}{\partial n}\cdot dS_0
\end{aligned} \tag{7.166}$$

In the above equations, the operator $\partial/\partial n$ signifies the gradient in the direction of the normal to the surface of the body. For the solution of the motion potentials ϕ_j, the right-hand side of the above equation 7.166 is given by the direction cosines defined by equation 7.160.

For the solution of the diffraction potential ϕ_7 (restrained body), the right-hand side is given by:

$$n_7 = \frac{\partial \phi_7}{\partial n} = -\frac{\partial \phi_0}{\partial n} \tag{7.167}$$

Solving the integral equation 7.166 results in the unknown source strengths. Substitution of these in equation 7.162 and in equation 7.159 yields the added mass and damping coefficients and the wave forces respectively.

Finally the motions ζ_j are determined from the solution of the following coupled equations of motion for six degrees of freedom:

$$\boxed{\left| \sum_{j=1}^{6} \{-\omega^2(m_{kj} + a_{kj}) - i\omega b_{kj} + c_{kj}\} \cdot \zeta_j = X_k \right|} \qquad \text{for } k = 1, ...6 \tag{7.168}$$

with:

m_{kj}	=	inertia matrix of the body for inertia coupling in the k-mode for acceleration in the j-mode
a_{kj}	=	added mass matrix for the force on the body in the k-mode due to acceleration of the body in the j-mode
b_{kj}	=	damping matrix for the force on the body in the k-mode due to velocity of the body in the j-mode
c_{kj}	=	spring matrix for the force on the body in the k-mode due to motion of the body in the j-mode
X_k	=	wave force on the body in the k-mode

The b_{kj} and c_{kj} matrices may contain contributions arising from mechanical damping devices and springs or even a mooring system.

7.4.3 Numerical Aspects

By discretizing the mean wetted surface of a body into N panels, on which the source strengths are homogeneously distributed, the following discretized form of equation 7.166 is obtained:

$$-\frac{1}{2}\sigma_{mj} + \frac{1}{4\pi} \sum_{n=1}^{N} \sigma_{nj} \frac{\partial G_{mn}}{\partial n} \triangle S_n = n_{mj} \qquad \text{for } m = 1, ...N \quad n \neq m \tag{7.169}$$

The normal velocity requirement can only be met at one point for each panel into which the mean wetted surface of the hull is divided. It is customary to chose the centroid of the panel. Such points are known as **collocation points**; see appendix D.

Equation 7.169 is transformed into a set of simultaneous linear equations in N unknown complex source strengths:

$$\begin{pmatrix} A_{11} & ... & ... & ... & A_{1N} \\ ... & A_{22} & ... & ... & ... \\ ... & ... & A_{33} & ... & ... \\ ... & ... & ... & ... & ... \\ A_{N1} & ... & ... & ... & A_{NN} \end{pmatrix} . \begin{pmatrix} \sigma_{1,j} \\ ... \\ ... \\ ... \\ \sigma_{N,j} \end{pmatrix} = \begin{pmatrix} n_{1,j} \\ ... \\ ... \\ ... \\ n_{N,j} \end{pmatrix} \tag{7.170}$$

in which:

$$\begin{aligned} A_{nn} &= -\frac{1}{2} \\ A_{nm} &= \frac{1}{4\pi}\frac{\partial G_{mn}}{\partial n} \triangle S_n \\ \sigma_{n,j} &= \text{unknown source strength} \\ n_{nj} &= \text{normal velocity component on the oscillating body} \end{aligned}$$

This set of equations can be solved by direct solution techniques or by iterative solvers. The computational effort involved with iterative solvers is quadratic in the number of unknowns while for direct solvers the effort is a cubic function of the number of unknowns.
It should be noted that in the evaluation of the coefficients A_{nm} due care has to be taken when the field point (center of a target panel) is close to the source point. Inaccuracies will occur due to the $1/r$-behavior of the influence function G_{mn} as seen in equation 7.164. In this case, the $1/r$-contribution is subtracted from the influence function and is analytically integrated over the finite sized source panel under the assumption that the source strength is homogeneously distributed. Use can be made of an algorithm provided by [Fang, 1985]. Similar cases of inaccurate evaluations of the influence functions based directly upon equation 7.164 and equation 7.165 are found when a source panel is very close to the sea bed and when close to the free surface. The solution in both cases is to remove the relevant terms from the above-mentioned equations and to insert equivalent analytical integrations over the source panel.
The above modifications concern simple contributions to the influence function, such as the $1/r$, $1/r_1$ or logarithmic contributions. Where more complicated contributions are concerned such as expressed in the Principle Value integral part of equation 7.164, $(PV \int ..... d\xi)$, a more accurate evaluation of the contribution to the influence function can be made for smaller values of r by the application of Gauss quadrature methods. These simply imply that for smaller values of r the source panel is split into 4 or more parts and the total influence function is the sum of the influences from the parts of the total panel under the assumption that the source strength per unit surface is the same for all parts of the panel. In this way the influence function can be determined more accurately without increasing the number of unknowns to be solved.

A numerical problem associated with the solution of equation 7.170 is the occurrence of so-called **irregular frequencies**. For certain, discrete wave frequencies the determinant of the coefficients A_{mn} will become zero, yielding unrealistic results. "Leakage" of the effects of these irregular frequencies to a band around these frequencies occurs due to the discretization of the body. Irregular frequencies are associated with eigenfrequencies of the internal (non-physical) flow of the body. An effective method to reduce the effects of

irregular frequencies is, among others, to "close" the body by means of discretization of the free surface inside the body (putting a "lid" on the free surface inside the body); see the added mass and damping of a hemisphere in figure 7.12. The solid line in this figure results from including the "lid". Increasing the number of panels does not remove the irregular frequency but tends to restrict the effects to a narrower band around it; see for instance [Huijsmans, 1996]. It should be mentioned that irregular frequencies only occur for free surface piercing bodies; fully submerged bodies do not display these characteristics.

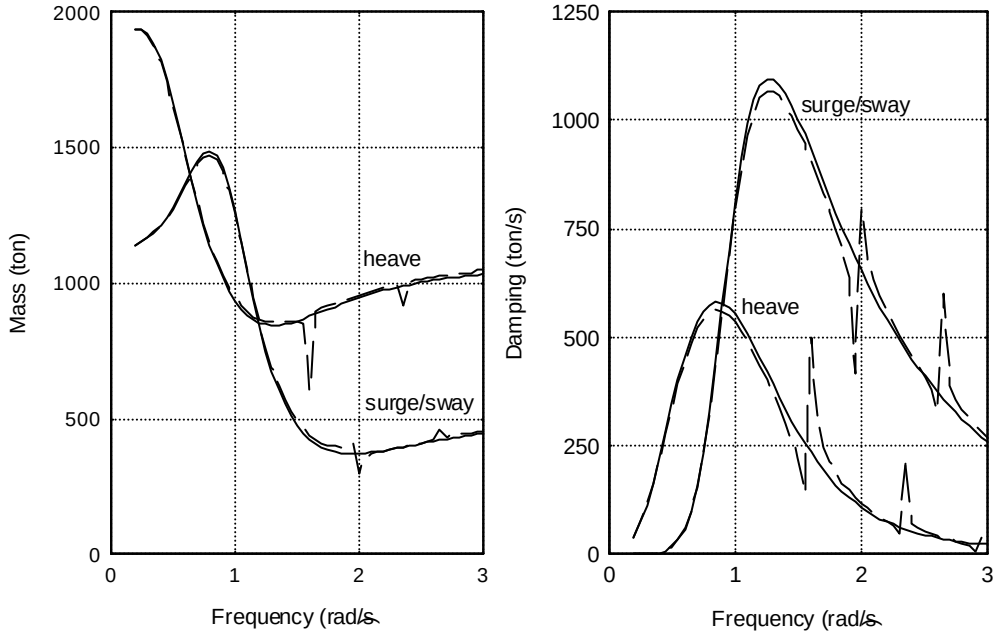

Figure 7.12: Effect of "Lid-Method" on Irregular Frequencies

Solving equation 7.170 using direct solution methods (LU-decomposition) is time consuming if the number of unknowns (N complex quantities σ) is large. The time taken to solve the equations by a direct method is proportional to N^3. Iterative solvers are proportional to N^2. However, due to other program overhead, such as the evaluation of the coefficients A_{mn} for each wave frequency, iterative solvers only become faster if there are more than about 500 panels on a body. Normally a tanker-shaped vessel can be described adequately by 300-600 panels. In day-to-day practice one tends to use the direct method based on LU-decomposition.

A useful method to reduce computation times lies in exploiting any geometrical symmetry a body may have. A ship-shaped vessel will generally have port side - starboard side symmetry while, for instance a simple barge or a semi-submersible will often have both port side - starboard side as well as fore - aft symmetry. In the latter case we need only describe one quadrant of the hull shape. The three remaining quadrants can be obtained by simply copying, but taking into account sign changes in the coordinates.

The reduction in computation time lies in the fact that, for instance for a vessel with port side - starboard side symmetry, the matrix of influence coefficients A_{mn} also shows

symmetry. In such cases the matrix of influence coefficients has the following structure:

$$\begin{pmatrix} A_{11} & ... & ... & A_{1N} \\ ... & A_{22} & ... & ... \\ ... & ... & ... & ... \\ A_{N1} & ... & ... & A_{NN} \end{pmatrix} = \begin{pmatrix} A & B \\ B & A \end{pmatrix} \tag{7.171}$$

The right-hand-side of equation 7.171 expresses the fact that the self-influence of the port side half of the vessel (upper left A) is the same as the self-influence of the starboard half of the vessel (lower right A). The cross-influence of sources on the port side half of the vessel on panels on the starboard half of the vessel is contained in the lower left matrix B. The corresponding cross-influence of sources on the starboard half of the vessel on panels on the port side half are contained in the upper right matrix B.
For vessels which have double symmetry i.e. port side - starboard and fore - aft symmetry, the matrix of influence coefficients has the following structure:

$$\begin{pmatrix} A_{11} & ... & ... & A_{1N} \\ ... & A_{22} & ... & ... \\ ... & ... & ... & ... \\ A_{N1} & ... & ... & A_{NN} \end{pmatrix} = \begin{pmatrix} A & B & C & D \\ B & A & D & C \\ C & D & A & B \\ D & C & B & A \end{pmatrix} \tag{7.172}$$

It is left as an exercise for the reader to deduce the effect that exploitation of such symmetries can have on the computational effort involved in solving equation 7.170.

7.5 Experimental Determination

The hydrodynamic coefficients in the equations of motion can be obtained experimentally by decay tests or by forced oscillation tests with ship models. The principle and limitations of these tests have been explained in chapter 6.
Free decay tests with a ship model in still water can be carried out only for those motions which have a hydromechanical restoring force or moment; heave, pitch and roll motions. External springs can be used for the other ship motions: surge, sway and yaw. The hydrodynamic coefficients can be found for a restricted range of (natural) frequencies, by varying the stiffness of these springs (if possible) in these decay tests.
Forced oscillation tests in still water yield the hydrodynamic mass and damping coefficients at any frequency of oscillation from the measured exciting loads. The coupling coefficients between the motions can be obtained as well. By means of forced oscillation tests with ship models, the relation between the potential coefficients and the frequency of oscillation can be found.

7.5.1 Free Decay Tests

Free decay test methodology has been discussed in chapter 6; only an example of some results for roll of ships is given here.
The successively found values for the dimensionless roll damping coefficient, κ, plotted as a function of the mean roll amplitude, ϕ_a, will often have a non-linear behavior as illustrated in figure 7.13.

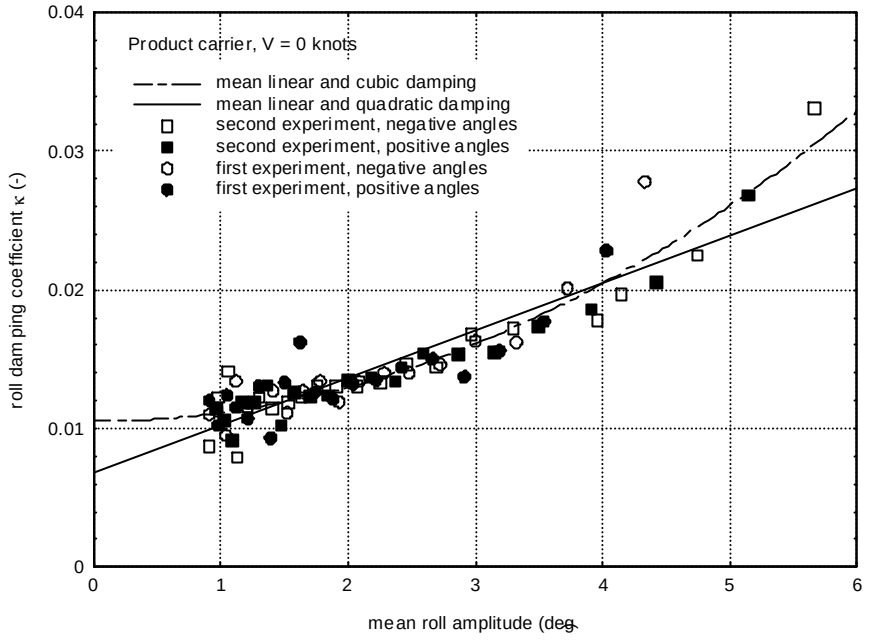

Figure 7.13: Nonlinear Roll Damping

This behavior can be described by:

$$\boxed{\kappa = \kappa_1 + \kappa_2 \phi_a \quad \left(+\kappa_3 \phi_a^2\right)} \tag{7.173}$$

This implies that during frequency domain calculations the damping term depends on the solution for the roll amplitude. With a certain wave amplitude, this problem can be solved in an iterative manner. A less accurate method is to use a fixed ϕ_a. Generally, a linearization will be carried out as described in chapter 6.
Note that a linear damping results in a 'horizontal' line in figure 7.13, $\kappa = \kappa_1$.

[Journée, 1991] published results of a series of free decay experiments with rectangular barge models at an even keel condition and with the center of gravity at the waterline. During these experiments, the models (with B/T values up to 10) were free to carry out heave and roll motions only. He found that the roll damping coefficients of these barges can be approximated by:

$$\begin{aligned} \kappa_1 &= 0.00130 \cdot \left(\frac{B}{T}\right)^2 \qquad \text{(barge with } G \text{ at waterline)} \\ \kappa_2 &= 0.500 \\ \kappa_3 &= 0.000 \end{aligned} \tag{7.174}$$

in which B is the breadth and T is the draft of the barge.
For large breadth-draft ratios of these barges ($B/T > 10$), generally the potential part of the roll damping becomes so important that, at least from a practical point of view, the viscous part of the damping can be ignored.

7.5.2 Forced Oscillation Tests

The model is mounted on two vertical struts along its longitudinal center line, spaced symmetrically with respect to the center of gravity. If the struts are oscillated in unison, so that the strut motions aft and forward are the same, the model executes a sinusoidal heave motion. If the strut motions are opposite (a phase shift of 180 degrees) the model executes a sinusoidal pitch motion. All other motions are restrained and the forces necessary to impose the heave or pitch oscillation are measured by transducers at the ends of the struts and suitably recorded. To avoid internal stresses, the aft transducer is fitted with a swinging link or mounted on a horizontal sled.
A schematic of the experimental set-up for forced heave and pitch oscillations is given in figure 7.14.

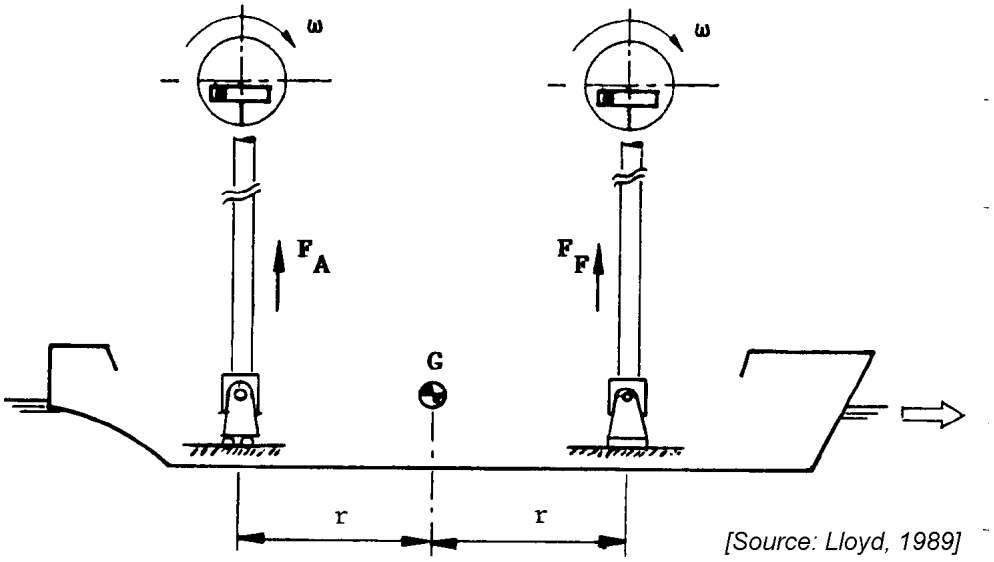

Figure 7.14: Forced Heave Oscillation Experiment

During the forced heave or pitch oscillations the vertical motions of the transducer aft and forward are $z_A(t)$ and $z_F(t)$ respectively, with equal amplitudes z_a.
Then the motions of the model are defined by:

$$\begin{aligned} \text{heave oscillations} \quad &: \quad z(t) = z_A(t) = z_F(t) = z_a \sin \omega t \\ \text{pitch oscillations} \quad &: \quad \theta(t) = \arctan\left\{\frac{z_A(t) - z_F(t)}{2r}\right\} \approx \frac{z_a}{r} \sin \omega t = \theta_a \sin \omega t \end{aligned} \tag{7.175}$$

During both type of oscillations, the heave forces and pitch moments can be obtained from the measured forces in the transducer aft $F_A(t)$ and the transducer forward $F_F(t)$:

$$\begin{aligned} \text{heave force} \quad &: \quad F_z(t) = F_A(t) + F_F(t) \quad = F_a \sin(\omega t + \varepsilon_{Fz}) \\ \text{pitch moment} \quad &: \quad M_\theta(t) = r\left\{F_A(t) - F_F(t)\right\} = M_a \sin(\omega t + \varepsilon_{Mz}) \end{aligned} \tag{7.176}$$

Heave Oscillations

The linear equations of motion during the heave oscillations are given by:

$$a\ddot{z} + b\dot{z} + cz \quad = \quad F_a \sin\left(\omega t + \varepsilon_{Fz}\right)$$

$$d\ddot{z} + e\dot{z} + fz = M_a \sin(\omega t + \varepsilon_{Mz}) \tag{7.177}$$

The components of the force and moment which are in-phase with the heave motion are associated with the inertia and stiffness coefficients, while the out-of-phase components (also called in literature: quadrature components) are associated with damping.
With:

$$z = z_a \sin\omega t \qquad \dot{z} = z_a\omega\cos\omega t \qquad \ddot{z} = -z_a\omega^2 \sin\omega t \tag{7.178}$$

we obtain:

$$\begin{aligned} z_a\left(-a\omega^2 + c\right)\sin\omega t + z_a b\omega\cos\omega t &= F_a\cos\varepsilon_{Fz}\sin\omega t + F_a\sin\varepsilon_{Fz}\cos\omega t \\ z_a\left(-d\omega^2 + f\right)\sin\omega t + z_a e\omega\cos\omega t &= M_a\cos\varepsilon_{Mz}\sin\omega t + M_a\sin\varepsilon_{Mz}\cos\omega t \end{aligned} \tag{7.179}$$

which provides:

$$\begin{aligned} a = \rho\nabla + a_{zz} &= \frac{c - \frac{F_a}{z_a}\cos\varepsilon_{Fz}}{\omega^2} \quad \text{with:} \quad c = c_{zz} = \rho g A_w \\ b = \qquad b_{zz} &= \frac{\frac{F_a}{z_a}\sin\varepsilon_{Fz}}{\omega} \\ d = \qquad a_{\theta z} &= \frac{f - \frac{M_a}{z_a}\cos\varepsilon_{Mz}}{\omega^2} \quad \text{with:} \quad f = c_{\theta z} = \rho g S_w \\ e = \qquad b_{\theta z} &= \frac{\frac{M_a}{z_a}\sin\varepsilon_{Mz}}{\omega} \end{aligned} \tag{7.180}$$

To obtain the stiffness coefficients c and f, use has to be made of A_w (area of the waterline) and S_w (first order moment of the waterline), which can be obtained from the geometry of the ship model.
It is also possible to obtain the stiffness coefficients from static experiments:

$$\ddot{z} = 0 \quad \text{and} \quad \dot{z} = 0 \qquad \text{provides:} \qquad c = \frac{F}{z} \quad \text{and} \quad f = \frac{M}{z}$$

Pitch Oscillations

The linear equations during the pitch oscillations are given by:

$$\begin{aligned} a\ddot{\theta} + b\dot{\theta} + c\theta &= F_a\sin(\omega t + \varepsilon_{F\theta}) \\ d\ddot{\theta} + e\dot{\theta} + f\theta &= M_a\sin(\omega t + \varepsilon_{M\theta}) \end{aligned} \tag{7.181}$$

The components of the force and moment which are in-phase with the pitch motion are associated with the inertia and stiffness coefficients, while the out-of-phase components are associated with damping.
With:

$$\theta = \theta_a \sin\omega t \qquad \dot{\theta} = \theta_a\omega\cos\omega t \qquad \ddot{\theta} = -\theta_a\omega^2\sin\omega t \tag{7.182}$$

we obtain:

$$\begin{aligned} \theta_a\left(-a\omega^2 + c\right)\sin\omega t + \theta_a b\omega\cos\omega t &= F_a\cos\varepsilon_{F\theta}\sin\omega t + F_a\sin\varepsilon_{F\theta}\cos\omega t \\ \theta_a\left(-d\omega^2 + f\right)\sin\omega t + \theta_a e\omega\cos\omega t &= M_a\cos\varepsilon_{M\theta}\sin\omega t + M_a\sin\varepsilon_{M\theta}\cos\omega t \end{aligned} \tag{7.183}$$

which provides:

$$\begin{aligned}
a = \quad a_{z\theta} &= \frac{c - \frac{F_a}{\theta_a}\cos\varepsilon_{F\theta}}{\omega^2} \quad \text{with:} \quad c = c_{z\theta} = \rho g S_w \\
b = \quad b_{z\theta} &= \frac{\frac{F_a}{\theta_a}\sin\varepsilon_{F\theta}}{\omega} \\
d = I_{yy} + a_{\theta\theta} &= \frac{f - \frac{M_a}{\theta_a}\cos\varepsilon_{M\theta}}{\omega^2} \quad \text{with:} \quad f = c_{\theta\theta} = \rho g \nabla \overline{GM_L} \\
e = \quad b_{\theta\theta} &= \frac{\frac{M_a}{\theta_a}\sin\varepsilon_{M\theta}}{\omega}
\end{aligned} \tag{7.184}$$

To obtain the stiffness coefficients c and f, use has been made of S_w (first order moment of the waterline) and $\overline{GM_L}$ (longitudinal metacentric height), which can be obtained from the geometry of the ship model.
It is also possible to obtain the stiffness coefficients from static experiments:

$$\ddot{\theta} = 0 \quad \text{and} \quad \dot{\theta} = 0 \qquad \text{provides:} \qquad c = \frac{F}{\theta} \quad \text{and} \quad f = \frac{M}{\theta} \tag{7.185}$$

Signal Processing

The in-phase and out-of-phase parts of the measured signal can be found easily from an integration over an integer number n of periods T of the measure signals multiplied by $\cos\omega t$ and $\sin\omega t$, respectively. This is in fact a first order Fourier analysis; see appendix C.
For the heave oscillations, this results in:

$$\begin{aligned}
F_a \sin\varepsilon_{Fz} &= \frac{2}{nT}\int_0^{nT} (F_A(t) + F_F(t)) \cdot \cos\omega t \cdot dt \\
F_a \cos\varepsilon_{Fz} &= \frac{2}{nT}\int_0^{nT} (F_A(t) + F_F(t)) \cdot \sin\omega t \cdot dt \\
M_a \sin\varepsilon_{Mz} &= \frac{2r}{nT}\int_0^{nT} (F_A(t) - F_F(t)) \cdot \cos\omega t \cdot dt \\
M_a \cos\varepsilon_{Mz} &= \frac{2r}{nT}\int_0^{nT} (F_A(t) - F_F(t)) \cdot \sin\omega t \cdot dt
\end{aligned} \tag{7.186}$$

Similar expressions can be found for the pitch oscillations.

Equations of Motion

With the measured hydromechanical coefficients, the coupled linear equations of heave and pitch motions in still water are given by:

$$\begin{aligned}
(\rho\nabla + a_{zz})\ddot{z} + b_{zz}\dot{z} + c_{zz}z + a_{z\theta}\ddot{\theta} + b_{z\theta}\dot{\theta} + c_{z\theta}\theta &= 0 \\
(I_{xx} + a_{\theta\theta})\ddot{\theta} + b_{\theta\theta}\dot{\theta} + c_{\theta\theta}\theta + a_{\theta z}\ddot{z} + b_{\theta z}\dot{z} + c_{\theta z}z &= 0
\end{aligned} \tag{7.187}$$

7.6 Viscous Damping

Motion damping is caused by the generated waves which dissipate energy from the moving structure as well as by viscous effects such as skin friction, vortices, etc. In most cases viscous effects are neglected in motion calculations of offshore structures as well as for the sway, heave, pitch and yaw motions of ships. The major part of the damping is caused by the wave (or potential) damping and the viscous damping contribution to these are of minor importance.

7.6.1 Viscous Surge Damping

Generally, the hydromechanical coefficients for surge are small. The hydrodynamic mass is 5-8 % of the ship's mass and the damping is small. In fact, the total damping components for surge of sailing ships have been treated already in chapter 4, because this damping coefficient can be written as:

$$b_{xx} = \frac{dR_t}{dV} = \frac{dR_f}{dV} + \frac{dR_r}{dV}$$

where R_t is the total resistance, R_f is the frictional (viscous) resistance and R_r is the residual (potential) resistance and V is the forward ship speed; the viscous part of the surge damping is dR_f/dV.

7.6.2 Viscous Roll Damping

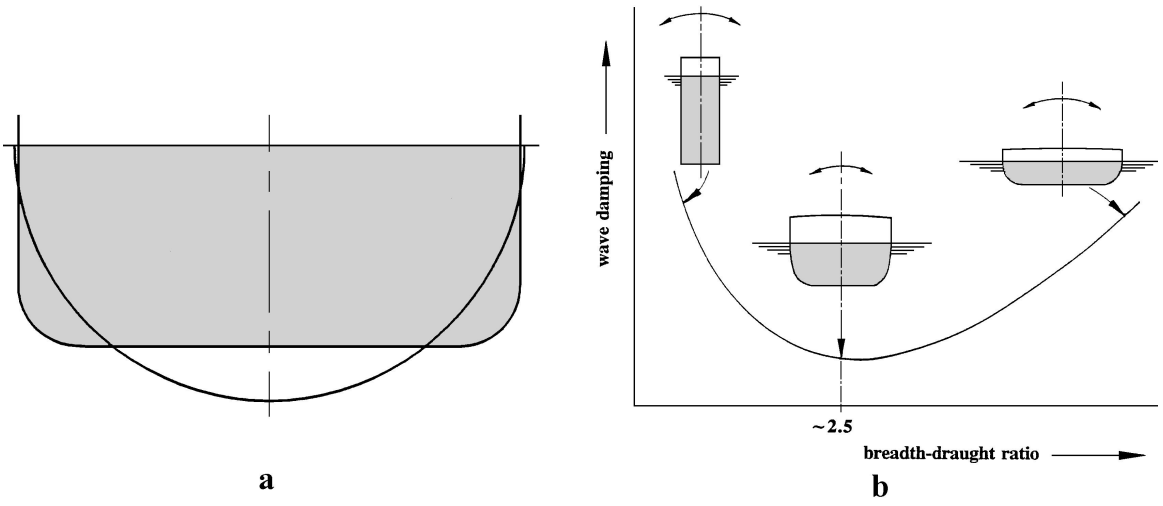

Figure 7.15: Roll Damping as Function of Shape and B/T Ratio

Viscous damping can be significant for rolling ships. This is because the wave potential damping for roll is generally relatively small itself. A circular cylinder, rotating about its center, does not produce waves; its potential roll damping is zero. For a breadth-draft ratio of about 2.5, the major part of the ship has a "more or less" circular cross section, see figure 7.15-a.

Thus, for many ships a small potential roll damping can be expected too. A relatively significant viscous contribution, for instance due to bilge keels, can be expected.
The relation between the roll damping and the breadth-draft ratio of a cross section of a ship is given in figure 7.15-b.
As indicated above, the roll damping is minimum at a breadth-draft ratio of about 2.5. For very low breadth-draft ratios (paddle-type wave maker) and for high breadth-draft ratios (wave damper of a towing carriage in a towing tank) the wave damping component is very high.

For the estimation of the non-potential parts of the roll damping, in many cases use can be made of work published by [Ikeda et al., 1978]. This empirical method is often called the "Ikeda method" and it estimates viscous roll damping contributions due to forward ship speed, skin friction, eddy making, lift and bilge keels, see figure 7.16.

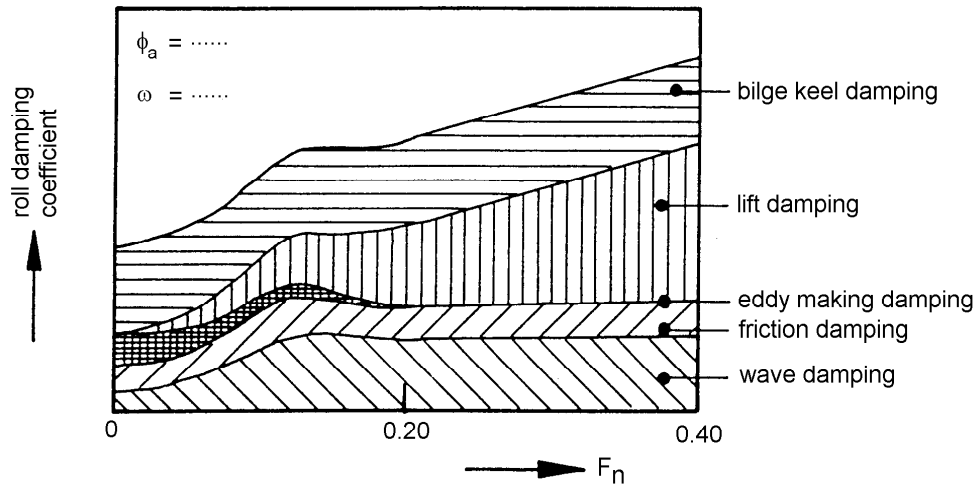

Figure 7.16: Roll Damping Components

Ikeda, Himeno and Tanaka claim fairly good agreements between their prediction method and experimental results. They conclude that the method can be used safely for ordinary ship forms, which conclusion has been confirmed by numerous experiments carried out by other researchers. But for unusual ship forms, very full ship forms and ships with a very large breadth to draft ratio the method is not always accurate sufficiently.

Chapter 8

FLOATING STRUCTURES IN WAVES

8.1 Introduction

The (uncoupled) motions of a simple rigid body at zero forward speed have been discussed in chapter 6. Potential coefficients and their determination for more complex hull forms, such as those of ships and offshore structures, have been described in chapter 7.
This chapter deals with the kinetics, the equations of motion for six degrees of freedom and some motion related phenomena for ships and offshore structures, partly including the forward speed effect.

8.2 Kinetics

The total mass as well as its distribution over the body is considered to be constant with time. For ships and other floating structures, this assumption is normally valid during a time which is large relative to the period of the motions. This holds that small effects, such as for instance a decreasing mass due to fuel consumption, can be ignored.
The solid mass matrix of a floating structure is given below.

$$\text{Solid mass matrix: } m = \begin{pmatrix} \rho\nabla & 0 & 0 & 0 & 0 & 0 \\ 0 & \rho\nabla & 0 & 0 & 0 & 0 \\ 0 & 0 & \rho\nabla & 0 & 0 & 0 \\ 0 & 0 & 0 & I_{xx} & 0 & -I_{xz} \\ 0 & 0 & 0 & 0 & I_{yy} & 0 \\ 0 & 0 & 0 & -I_{zx} & 0 & I_{zz} \end{pmatrix} \tag{8.1}$$

The moments of inertia here are often expressed in terms of the radii of inertia and the solid mass of the structure. Since Archimedes law is valid for a floating structure:

$$\begin{aligned} I_{xx} &= {k_{xx}}^2 \cdot \rho\nabla \\ I_{yy} &= {k_{yy}}^2 \cdot \rho\nabla \\ I_{zz} &= {k_{zz}}^2 \cdot \rho\nabla \end{aligned} \tag{8.2}$$

[0] J.M.J. Journée and W.W. Massie, *"OFFSHORE HYDROMECHANICS"*, First Edition, January 2001, Delft University of Technology. For updates see web site: http://www.shipmotions.nl.

When the distribution of the solid mass of a ship is unknown, the radii of inertia can be approximated by:

$$\text{for ships:} \quad \begin{cases} k_{xx} & \approx & 0.30 \cdot B \text{ to } 0.40 \cdot B \\ k_{yy} & \approx & 0.22 \cdot L \text{ to } 0.28 \cdot L \\ k_{zz} & \approx & 0.22 \cdot L \text{ to } 0.28 \cdot L \end{cases}$$

in which L is the length and B is the breadth of the ship; the (generally small) coupling terms, $I_{xz} = I_{zx}$, are simply neglected.
Bureau Veritas proposes for the gyradius in roll:

$$k_{xx} = 0.289 \cdot B \cdot \left(1.0 + \left(\frac{2 \cdot \overline{KG}}{B} \right)^2 \right) \tag{8.3}$$

in which $\overline{KG}$ is the height of the center of gravity, G, above the keel.
For many ships without cargo on board (ballast condition), the mass is concentrated at the ends (engine room aft and ballast water forward to avoid a large trim), while for ships with cargo on board (full load condition) the - more or less amidships laden - cargo plays an important role. Thus, the radii of inertia, k_{yy} and k_{zz}, are usually smaller in the full load condition than in the ballast condition for normal ships. Note that the longitudinal radius of gyration of a long homogeneous rectangular beam with a length L is equal to about $0.29 \cdot L \left(= \sqrt{1/12} \cdot L \right)$.
As already mentioned in chapter 6, the equations of motions of a rigid body in a space fixed coordinate system follow from Newton's second law. The vector equations for the translations of and the rotations about the center of gravity are given respectively by:

$$\boxed{\vec{F} = \frac{d}{dt}\left(m\vec{U} \right)} \qquad \text{and} \qquad \boxed{\vec{M} = \frac{d}{dt}\left(\vec{H} \right)} \tag{8.4}$$

in which:

$\vec{F}$	=	resulting external force acting in the center of gravity
m	=	mass of the rigid body
$\vec{U}$	=	instantaneous velocity of the center of gravity
$\vec{M}$	=	resulting external moment acting about the center of gravity
$\vec{H}$	=	instantaneous angular momentum about the center of gravity
t	=	time

As mentioned in chapter 6 as well, two important assumptions are made for the loads in the right hand side of these equations:

a. The so-called **hydromechanical forces and moments** are induced by the harmonic oscillations of the rigid body, moving in the undisturbed surface of the fluid.

b. The so-called **wave exciting forces and moments** are produced by waves coming in on the restrained body.

Since the system is linear, these loads are added to obtain the total loads. Thus, after assuming small motions, symmetry of the body and that the x-, y- and z-axes are principal

axes, one can write the following six motion equations for the ship:

$$\begin{array}{rlll}
\text{Surge:} & \frac{d}{dt}\left(\rho\nabla\cdot\dot{x}\right) & = \rho\nabla\cdot\ddot{x} & = X_{h_1}+X_{w_1} \\
\text{Sway:} & \frac{d}{dt}\left(\rho\nabla\cdot\dot{y}\right) & = \rho\nabla\cdot\ddot{y} & = X_{h_2}+X_{w_2} \\
\text{Heave:} & \frac{d}{dt}\left(\rho\nabla\cdot\dot{z}\right) & = \rho\nabla\cdot\ddot{z} & = X_{h_3}+X_{w_3} \\
\text{Roll:} & \frac{d}{dt}\left(I_{xx}\cdot\dot{\phi}-I_{xz}\cdot\dot{\psi}\right) & = I_{xx}\cdot\ddot{\phi}-I_{xz}\cdot\ddot{\psi} & = X_{h_4}+X_{w_4} \\
\text{Pitch:} & \frac{d}{dt}\left(I_{yy}\cdot\dot{\theta}\right) & = I_{xx}\cdot\ddot{\theta} & = X_{h_5}+X_{w_5} \\
\text{Yaw:} & \frac{d}{dt}\left(I_{zz}\cdot\dot{\psi}-I_{zx}\cdot\dot{\phi}\right) & = I_{zz}\cdot\ddot{\psi}-I_{zx}\cdot\ddot{\phi} & = X_{h_6}+X_{w_6}
\end{array} \tag{8.5}$$

in which:

ρ	=	density of water
∇	=	volume of displacement of the ship
I_{ij}	=	solid mass moment of inertia of the ship
X_{h_1}, X_{h_2}, X_{h_3}	=	hydromechanical forces in the x-, y- and z-directions respectively
X_{h_4}, X_{h_5}, X_{h_6}	=	hydromechanical moments about the x-, y- and z-axes respectively
X_{w_1}, X_{w_2}, X_{w_3}	=	exciting wave forces in the x-, y- and z-directions respectively
X_{w_4}, X_{w_5}, X_{w_6}	=	exciting wave moments about the x-, y- and z-axes respectively

Note: in many applications, $I_{xz} = I_{zx}$ is not known or small; hence their terms are often omitted.

8.3 Coupled Equations of Motion

Once the mass of the floating object and its distribution within that object are known, the coupled equations of motion in 6 degrees of freedom in waves can be written.

8.3.1 General Definition

Based on Newton's second law, the general equations of motion are given by:

$$\boxed{\left|\sum_{j=1}^{6} m_{i,j}\cdot\ddot{x}_j = F_i\right|} \qquad \text{for: } i = 1,...6 \tag{8.6}$$

in which:

$m_{i,j}$	=	6x6 matrix of solid mass and inertia of the body
$\ddot{x}_j$	=	acceleration of the body in direction j
F_i	=	sum of forces or moments acting in direction i

When defining a linear system, with simple harmonic wave exciting forces and moments given by:

$$\underline{\underline{|F_{w_i}(\omega_e,t) = F_{wa_i}(\omega_e) \cdot \cos\left(\omega_e t + \varepsilon_{F_i}(\omega_e)\right)|}} \tag{8.7}$$

the resulting simple harmonic motions are:

$$\begin{aligned} x_j(\omega_e,t) &= x_{a_j}(\omega_e) \cdot \cos(\omega_e t) \\ \dot{x}_j(\omega_e,t) &= -\omega_e \cdot x_{a_j}(\omega_e) \cdot \sin(\omega_e t) \\ \ddot{x}_j(\omega_e,t) &= -\omega_e^2 \cdot x_{a_j}(\omega_e) \cdot \cos(\omega_e t) \end{aligned} \tag{8.8}$$

The hydromechanical forces and moments $F_{h_{i,j}}$, acting on an oscillating object in still water, consist of:

- linear hydrodynamic reaction forces and moments expressed in terms with the hydrodynamic mass and damping coefficients:

$$-a_{i,j}(\omega_e) \cdot \ddot{x}_j(\omega_e,t) - b_{i,j}(\omega_e) \cdot \dot{x}_j(\omega_e,t) \tag{8.9}$$

- linear hydrostatic restoring forces and moments expressed in a term with a spring coefficient:

$$-c_{i,j} \cdot x_j(\omega_e,t) \tag{8.10}$$

With these expressions, the 6 equations of motion become:

$$\begin{aligned} \sum_{j=1}^{6} m_{i,j} \cdot \ddot{x}_j &= \sum_{j=1}^{6} \{-a_{i,j}(\omega_e) \cdot \ddot{x}_j(\omega_e,t) - b_{i,j}(\omega_e) \cdot \dot{x}_j(\omega_e,t) - c_{i,j} \cdot x_j(\omega_e,t) \\ &\quad + F_{wa_i}(\omega_e) \cdot \cos\left(\omega_e t + \varepsilon_i(\omega_e)\right)\} \\ &\qquad \text{for: } i = 1,...6 \end{aligned} \tag{8.11}$$

After ordering the terms, the general linear equations of motion for 6 degrees of freedom in the frequency domain are:

$$\begin{aligned} &\sum_{j=1}^{6} \{(m_{i,j} + a_{i,j}(\omega_e)) \cdot \ddot{x}_j(\omega_e,t) + b_{i,j}(\omega_e) \cdot \dot{x}_j(\omega_e,t) + c_{i,j} \cdot x_j(\omega_e,t)\} \\ &\quad = F_{wa_i}(\omega_e) \cdot \cos(\omega_e t + \varepsilon_i(\omega_e)) \\ &\qquad \text{for: } i = 1,...6 \end{aligned} \tag{8.12}$$

The hydrodynamic coefficients, $a_{i,j}(\omega_e)$ and $b_{i,j}(\omega_e)$, and the exciting wave load components, $F_{wa_i}(\omega_e)$ and $\varepsilon_i(\omega_e)$, can be calculated with two- or three-dimensional techniques given in chapter 7.

8.3.2 Motion Symmetry of Ships

Generally, a ship has a vertical-longitudinal plane of symmetry, so that its motions can be split into symmetric and anti-symmetric components. Surge, heave and pitch motions are symmetric motions, that is to say that a point to starboard has the same motion as the mirrored point to port side. It is obvious that the remaining motions sway, roll and yaw are anti-symmetric motions. Symmetric and anti-symmetric motions are not coupled; they

don't have any effect on each other. For instance, a vertical force acting at the center of gravity can cause surge, heave and pitch motions, but will not result in sway, roll or yaw motions.
Because of this symmetry and anti-symmetry, two sets of three coupled equations of motion can be distinguished for ships:

$$\left.\begin{array}{rlll} \text{Surge}: & \rho\nabla\cdot\ddot{x} & -X_{h_1} & = X_{w_1} \\ \text{Heave}: & \rho\nabla\cdot\ddot{z} & -X_{h_3} & = X_{w_3} \\ \text{Pitch}: & I_{xx}\cdot\ddot{\theta} & -X_{h_5} & = X_{w_5} \end{array}\right\} \quad \text{symmetric motions}$$

$$\left.\begin{array}{rlll} \text{Sway}: & \rho\nabla\cdot\ddot{y} & -X_{h_2} & = X_{w_2} \\ \text{Roll}: & I_{xx}\cdot\ddot{\phi} \quad -I_{xz}\cdot\ddot{\psi} & -X_{h_4} & = X_{w_4} \\ \text{Yaw}: & I_{zz}\cdot\ddot{\psi} \quad -I_{zx}\cdot\ddot{\phi} & -X_{h_6} & = X_{w_6} \end{array}\right\} \quad \text{anti-symmetric motions}$$

The coupled surge, heave and pitch equations of motion are:

$$\left.\begin{array}{rrrll} (\rho\nabla + a_{11})\cdot\ddot{x} & +b_{11}\cdot\dot{x} & +c_{11}\cdot x & & \\ +a_{13}\cdot\ddot{z} & +b_{13}\cdot\dot{z} & +c_{13}\cdot z & & \\ +a_{15}\cdot\ddot{\theta} & +b_{15}\cdot\dot{\theta} & +c_{15}\cdot\theta & = X_{w_1} & \text{(surge)} \\ & & & & \\ a_{31}\cdot\ddot{x} & +b_{31}\cdot\dot{x} & +c_{31}\cdot x & & \\ +(\rho\nabla + a_{33})\cdot\ddot{z} & +b_{33}\cdot\dot{z} & +c_{33}\cdot z & & \\ +a_{35}\cdot\ddot{\theta} & +b_{35}\cdot\dot{\theta} & +c_{35}\cdot\theta & = X_{w_3} & \text{(heave)} \\ & & & & \\ a_{51}\cdot\ddot{x} & +b_{51}\cdot\dot{x} & +c_{51}\cdot x & & \\ +a_{53}\cdot\ddot{z} & +b_{53}\cdot\dot{z} & +c_{53}\cdot z & & \\ +(+I_{yy} + a_{55})\cdot\ddot{\theta} & +b_{55}\cdot\dot{\theta} & +c_{55}\cdot\theta & = X_{w_5} & \text{(pitch)} \end{array}\right\} \quad \begin{array}{c}\text{symmetric}\\ \text{motions}\end{array}$$

The coupled sway, roll and yaw equations of motion are:

$$\left.\begin{array}{rrrll} (\rho\nabla + a_{22})\cdot\ddot{y} & +b_{22}\cdot\dot{y} & +c_{22}\cdot y & & \\ +a_{24}\cdot\ddot{\phi} & +b_{24}\cdot\dot{\phi} & +c_{24}\cdot\phi & & \\ +a_{26}\cdot\ddot{\psi} & +b_{26}\cdot\dot{\psi} & +c_{26}\cdot\psi & = X_{w_2} & \text{(sway)} \\ & & & & \\ a_{42}\cdot\ddot{y} & +b_{42}\cdot\dot{y} & +c_{42}\cdot y & & \\ +(+I_{xx} + a_{44})\cdot\ddot{\phi} & +b_{44}\cdot\dot{\phi} & +c_{44}\cdot\phi & & \\ +(-I_{xz} + a_{46})\cdot\ddot{\psi} & +b_{46}\cdot\dot{\psi} & +c_{46}\cdot\psi & = X_{w_4} & \text{(roll)} \\ & & & & \\ a_{62}\cdot\ddot{y} & +b_{62}\cdot\dot{y} & +c_{62}\cdot y & & \\ +(-I_{zx} + a_{64})\cdot\ddot{\phi} & +b_{64}\cdot\dot{\phi} & +c_{64}\cdot\phi & & \\ +(+I_{zz} + a_{66})\cdot\ddot{\psi} & +b_{66}\cdot\dot{\psi} & +c_{66}\cdot\psi & = X_{w_6} & \text{(yaw)} \end{array}\right\} \quad \begin{array}{c}\text{anti-symmetric}\\ \text{motions}\end{array}$$

Note that this distinction between symmetric and anti-symmetric motions disappears when the ship is anchored. Then, for instance, the pitch motions can generate roll motions via the anchor lines.

8.3.3 2-D Strip Theory

Strip theory is a computational method by which the forces on and motions of a three-dimensional floating body can be determined using results from two-dimensional potential

theory. This method has been described in the literature by several of authors; for a clear description reference is given to a doctor's thesis by [Vugts, 1970]. The two-dimensional potential theory has been discussed in chapter 7; its utilization will be discussed in the present chapter. Just as in chapter 7, the result of the theoretical work and the path leading to it, is more important than the derivation details.

Strip theory considers a ship to be made up of a finite number of transverse two-dimensional slices which are rigidly connected to each other. Each of these slices will have a form which closely resembles the segment of the ship which it represents. Each slice is treated hydrodynamically as if it is a segment of an infinitely long floating cylinder; see figure 8.1.

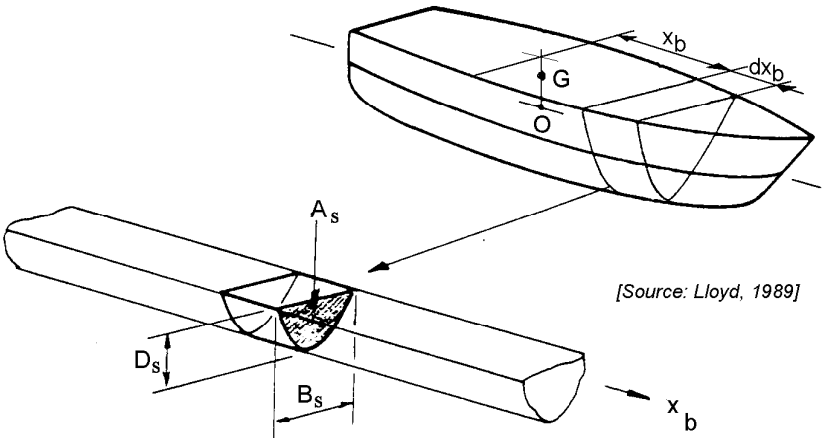

Figure 8.1: Strip Theory Representation by Cross Sections

This means that all waves which are produced by the oscillating ship (hydromechanical loads) and the diffracted waves (wave loads) are assumed to travel perpendicular to the middle line plane (thus parallel to the y-z plane) of the ship. This holds too that the strip theory supposes that the fore and aft side of the body (such as a pontoon) does not produce waves in the x direction. For the zero forward speed case, interactions between the cross sections are ignored as well.

Fundamentally, strip theory is valid for long and slender bodies only. In spite of this restriction, experiments have shown that strip theory can be applied successfully for floating bodies with a length to breadth ratio larger than three, ($L/B \geqq 3$), at least from a practical point of view.

When applying the strip theory, the loads on the body are found by an integration of the 2-D loads:

$$\text{surge:} \qquad X_{h_1} = \int_L X'_{h_1} \cdot dx_b \qquad X_{w_1} = \int_L X'_{w_1} \cdot dx_b$$

$$\text{sway:} \qquad X_{h_2} = \int_L X'_{h_2} \cdot dx_b \qquad X_{w_2} = \int_L X'_{w_2} \cdot dx_b$$

$$\text{heave:} \qquad X_{h_3} = \int_L X'_{h_3} \cdot dx_b \qquad X_{w_3} = \int_L X'_{w_3} \cdot dx_b$$

$$
\begin{array}{lllll}
\text{roll:} & X_{h_4} = \int_L X'_{h_4} \cdot dx_b & & X_{w_4} = \int_L X'_{w_4} \cdot dx_b & \\
\text{pitch:} & X_{h_5} = -\int_L X'_{h_3} \cdot x_b \cdot dx_b & & X_{w_5} = -\int_L X'_{w_3} \cdot x_b \cdot dx_b & \\
\text{yaw:} & X_{h_6} = \int_L X'_{h_2} \cdot x_b \cdot dx_b & & X_{w_6} = \int_L X'_{w_2} \cdot x_b \cdot dx_b & (8.13)
\end{array}
$$

in which:

$$
\begin{array}{lcl}
X'_{h_j} & = & \text{sectional hydromechanical force or moment} \\
 & & \text{in direction } j \text{ per unit ship length} \\
X'_{w_j} & = & \text{sectional exciting wave force or moment} \\
 & & \text{in direction } j \text{ per unit ship length}
\end{array}
$$

The appearance of two-dimensional surge forces seems strange here. It is strange! A more or less empirical method is used in program SEAWAY of [Journée, 1999] for the surge motion, by defining an equivalent longitudinal cross section which is swaying. Then, the 2-D hydrodynamic sway coefficients of this equivalent cross section are translated to 2-D hydrodynamic surge coefficients by an empirical method based on theoretical results from three-dimensional calculations and these coefficients are used to determine 2-D loads. In this way, all sets of six surge loads can be treated in the same numerical way in program SEAWAY for the determination of the 3-D loads. Inaccuracies of the hydromechanical coefficients of (slender) ships are of minor importance, because these coefficients are relatively small.
Note how in the strip theory the pitch and yaw moments are derived from the 2-D heave and sway forces, respectively, while the roll moments are obtained directly.
The equations of motions are defined in the moving axis system with the origin at the average position of the center of gravity, G. All two-dimensional potential coefficients have been defined so far in an axis system with the origin, O, in the water plane; the hydromechanical and exciting wave moments have to be corrected for the distance $\overline{OG}$.

Potential Coefficients

As mentioned before, in strip theory calculations the two-dimensional sway, heave and roll coefficients can be calculated by three methods which are summarized here; full details are given in chapter 7:

1. Ursell-Tasai's Method with Lewis Conformal Mapping
   Ursell derived an analytical solution for solving the problem of calculating the hydrodynamic coefficients of an oscillating circular cylinder in the surface of a fluid. Tasai added the so-called Lewis transformation - which is a very simple and in a lot of cases also more or less realistic method to transform ship-like cross sections to this unit circle - to Ursell's solution . This transformation is carried out by using a scale factor and two mapping coefficients. Only the breadth, the draft and the area of the mapped cross section will be equal to that of the actual cross section.

2. Ursell-Tasai's Method with N-Parameter Conformal Mapping
   A more accurate mapping has been added by Tasai too, by using more than only two mapping coefficients. The accuracy obtained depends on the number of mapping coefficients. Generally, a maximum of 10 coefficients are used for defining the cross section. These coefficients are determined in such a way that the Root Mean Square of the differences between the offsets of the mapped and the actual cross section is minimal.

3. Frank's Pulsating Source Method
   Mapping methods require an intersection of the cross section with the water plane and, as a consequence of this, they are not suitable for submerged cross sections, like at a bulbous bow. Also, conformal mapping can fail for cross sections with very low sectional area coefficients, such as are sometimes present in the aft body of a ship. Frank considered a cylinder of constant cross sections with an arbitrarily symmetrical shape, of which the cross sections are simply a region of connected line elements. This vertical cross section can be fully or partly immersed in a previously undisturbed fluid of infinite depth. He developed an integral equation method utilizing the Green's function which represents a complex potential of a pulsating point source of unit strength at the midpoint of each line element. Wave systems were defined in such a way that all required boundary conditions were fulfilled. The linearized Bernoulli equation provides the pressures after which the potential coefficients were obtained from the in-phase and out-of-phase components of the resultant hydrodynamic loads.

Forward Ship Speed

In case of a forward ship speed V, potential functions defined in the earth bounded coordinate system (x_0, y_0, z_0) have to be transformed to potential functions in the ship's steadily translating coordinate system (x, y, z). This requires an operator which transforms the derivative of a function $F(x_0, y_0, z_0, t)$, in the earth bounded (fixed) coordinate system, to the derivative of a function $F(x, y, z, t)$, in the ship's steadily translating coordinate system:

$$\begin{aligned} x &= x_0 - Vt \qquad y = y_0 \qquad z = z_0 \\ \frac{\partial}{\partial t}F(x_0, y_0, z_0, t) &= \frac{\partial}{\partial t}F(x, y, z, t) + \frac{\partial}{\partial x}F(x, y, z, t) \cdot \frac{dx}{dt} \\ &= \frac{\partial}{\partial t}F(x, y, z, t) - V \cdot \frac{\partial}{\partial x}F(x, y, z, t) \\ &= \left(\frac{\partial}{\partial t} - V \cdot \frac{\partial}{\partial x}\right) F(x, y, z, t) \\ &= \frac{D}{Dt}F(x, y, z, t) \end{aligned} \tag{8.14}$$

Thus, the operator is given by:

$$\boxed{\frac{D}{Dt} = \left(\frac{\partial}{\partial t} - V \cdot \frac{\partial}{\partial x}\right)} \tag{8.15}$$

When assuming small surge motions ($x \approx x_b$), this operator can also be written as:

$$\boxed{\frac{D}{Dt} \approx \left(\frac{\partial}{\partial t} - V \cdot \frac{\partial}{\partial x_b} \right)} \tag{8.16}$$

The effect of this operator can be understood easily when one realizes that in that earth-bound coordinate system the sailing ship penetrates through a "virtual vertical disk". When a ship sails with speed V and a trim angle, θ, through still water, the relative vertical velocity of a water particle with respect to the bottom of the sailing ship becomes $V \cdot \theta$.

Relative to an oscillating ship moving forward with speed V in the undisturbed surface of the fluid, the equivalent displacements, $\zeta^*_{h_j}$, velocities, $\dot{\zeta}^*_{h_j}$, and accelerations, $\ddot{\zeta}^*_{h_j}$, in the arbitrary direction j of a water particle in a cross section are defined by:

$$\zeta^*_{h_j}, \qquad \dot{\zeta}^*_{h_j} = \frac{D}{Dt}\left\{\zeta^*_{h_j}\right\} \qquad \text{and} \qquad \ddot{\zeta}^*_{h_j} = \frac{D}{Dt}\left\{\dot{\zeta}^*_{h_j}\right\} \tag{8.17}$$

Relative to a restrained ship, moving forward with speed V in waves, the equivalent j components of water particle displacements, $\zeta^*_{w_j}$, velocities, $\dot{\zeta}^*_{w_j}$, and accelerations, $\ddot{\zeta}^*_{w_j}$, in a cross section are defined in a similar way by:

$$\zeta^*_{w_j}, \qquad \dot{\zeta}^*_{w_j} = \frac{D}{Dt}\left\{\zeta^*_{w_j}\right\} \qquad \text{and} \qquad \ddot{\zeta}^*_{w_j} = \frac{D}{Dt}\left\{\dot{\zeta}^*_{w_j}\right\} \tag{8.18}$$

Two different types of strip theory methods are discussed here:

1. **Ordinary Strip Theory Method**
   According to this classic method, the uncoupled two-dimensional potential hydromechanical loads and wave loads in an arbitrary direction j are defined by:

$$\boxed{\begin{array}{l} X^*_{h_j} = \dfrac{D}{Dt}\left\{M'_{jj} \cdot \dot{\zeta}^*_{h_j}\right\} + N'_{jj} \cdot \dot{\zeta}^*_{h_j} + X'_{rs_j} \\ \\ X^*_{w_j} = \dfrac{D}{Dt}\left\{M'_{jj} \cdot \dot{\zeta}^*_{w_j}\right\} + N'_{jj} \cdot \dot{\zeta}^*_{w_j} + X'_{fk_j} \end{array}} \tag{8.19}$$

   This is the first formulation of the strip theory that can be found in the literature. It contains a more or less intuitive approach to the forward speed problem, as published in detail by [Korvin-Kroukovsky and Jacobs, 1957] and others.

2. **Modified Strip Theory Method**
   According to this modified method, these loads become:

$$\boxed{\begin{array}{l} X^*_{h_j} = \dfrac{D}{Dt}\left\{\left(M'_{jj} - \dfrac{i}{\omega_e}N'_{jj}\right) \cdot \dot{\zeta}^*_{h_j}\right\} + X'_{rs_j} \\ \\ X^*_{w_j} = \dfrac{D}{Dt}\left\{\left(M'_{jj} - \dfrac{i}{\omega_e}N'_{jj}\right) \cdot \dot{\zeta}^*_{w_j}\right\} + X'_{fk_j} \end{array}} \tag{8.20}$$

   This formulation is a more fundamental approach of the forward speed problem, as published in detail by [Tasai, 1969] and others.

In equations 8.19 and 8.20 M'_{jj} and N'_{jj} are the 2-D potential mass and damping coefficients. X'_{rs_j} is the two-dimensional quasi-static restoring spring term, generally present for heave, roll and pitch only. X'_{fk_j} is the two-dimensional Froude-Krilov force or moment which is calculated by an integration of the directional pressure gradient in the undisturbed wave over the cross sectional area of the hull.
Equivalent directional components of the orbital acceleration and velocity, derived from these Froude-Krilov loads, are used to calculate the diffraction parts of the total wave forces and moments.
From a theoretical point of view, one should prefer the use of the modified method, but it appeared from user's experience that for ships with moderate forward speed ($Fn \leqq 0.30$), the ordinary method provides sometimes a better fit with experimental data.

The hydromechanical and wave loads are explained in the following sections as an example for coupled heave and pitch motions only. A similar approach can be used for the other motions.
Note however, that the potential coefficients will be determined in an axes system with the origin, O, in the waterline and that ship motions will be defined with the origin at the center of gravity, G. This requires, for instance, for roll moments corrections with sway forces times the lever arm $\overline{OG}$. Detailed information about these corrections are given by [Vugts, 1970] or [Journée, 2000].

Hydromechanical Loads

The hydromechanical forces for heave and moments for pitch are found by integrating the two-dimensional heave values over the ship length:

$$\begin{aligned} X_{h_3} &= \int_L X'_{h_3} \cdot dx_b \\ X_{h_5} &= -\int_L X'_{h_3} \cdot x_b \cdot dx_b \end{aligned} \tag{8.21}$$

The vertical motions of the water particles, relative to each cross section of an oscillating ship in still water, are defined by using equations 8.17 and 8.15:

$$\begin{aligned} \zeta^*_{h_3} &= -z + x_b \cdot \theta \\ \dot{\zeta}^*_{h_3} &= -\dot{z} + x_b \cdot \dot{\theta} - V \cdot \theta \\ \ddot{\zeta}^*_{h_3} &= -\ddot{z} + x_b \cdot \ddot{\theta} - 2V \cdot \dot{\theta} \end{aligned} \tag{8.22}$$

The two-dimensional potential hydromechanical force on a heaving cross section in still water, as defined in equations 8.19 and 8.20, becomes:

$$\boxed{X'_{h_3} = \left(M'_{33} \boxed{+\frac{V}{\omega_e^2} \cdot \frac{dN'_{33}}{dx_b}} \right) \cdot \ddot{\zeta}^*_{h_3} + \left(N'_{33} - V \cdot \frac{dM'_{33}}{dx_b} \right) \cdot \dot{\zeta}^*_{h_3} + 2\rho g \cdot y_w \cdot \zeta^*_{h_3}} \tag{8.23}$$

In this and following equations, the additional terms associated with the Modified Strip Theory are enclosed in rectangles. Ignore these terms to get the Ordinary Strip Theory.

This results in the following hydromechanical expressions and coefficients for the coupled heave and pitch equations:

$$\begin{aligned} -X_{h_3} &= a_{33}\cdot\ddot{z} + b_{33}\cdot\dot{z} + c_{33}\cdot z + a_{35}\cdot\ddot{\theta} + b_{35}\cdot\dot{\theta} + c_{35}\cdot\theta \\ -X_{h_5} &= a_{53}\cdot\ddot{z} + b_{53}\cdot\dot{z} + c_{53}\cdot z + a_{55}\cdot\ddot{\theta} + b_{55}\cdot\dot{\theta} + c_{55}\cdot\theta \end{aligned} \tag{8.24}$$

with:

$$\begin{aligned} a_{33} &= +\int_L M'_{33}\cdot dx_b \quad \boxed{+\tfrac{V}{\omega_e^2}\int_L \tfrac{dN'_{33}}{dx_b}\cdot dx_b} \\ b_{33} &= +\int_L \left(N'_{33} - V\cdot\frac{dM'_{33}}{dx_b}\right)\cdot dx_b \\ c_{33} &= +2\rho g\int_L y_w\cdot dx_b \\ a_{35} &= -\int_L M'_{33}\cdot x_b\cdot dx_b - \frac{V}{\omega_e^2}\int_L \left(N'_{33} - V\cdot\frac{dM'_{33}}{dx_b}\right)\cdot dx_b \\ &\quad \boxed{-\tfrac{V}{\omega_e^2}\int_L N'_{33}\cdot dx_b - \tfrac{V}{\omega_e^2}\int_L \tfrac{dN'_{33}}{dx_b}\cdot x_b\cdot dx_b} \\ b_{35} &= -\int_L \left(N'_{33} - V\cdot\frac{dM'_{33}}{dx_b}\right)\cdot x_b\cdot dx_b + 2V\int_L M'_{33}\cdot dx_b \quad \boxed{+\tfrac{V^2}{\omega_e^2}\int_L \tfrac{dN'_{33}}{dx_b}\cdot dx_b} \\ c_{35} &= -2\rho g\int_L y_w\cdot x_b\cdot dx_b \end{aligned} \tag{8.25}$$

$$\begin{aligned} a_{53} &= -\int_L M'_{33}\cdot x_b\cdot dx_b \quad \boxed{-\tfrac{V}{\omega_e^2}\int_L \tfrac{dN'_{33}}{dx_b}\cdot x_b\cdot dx_b} \\ b_{53} &= -\int_L \left(N'_{33} - V\cdot\frac{dM'_{33}}{dx_b}\right)\cdot x_b\cdot dx_b \\ c_{53} &= -2\rho g\int_L y_w\cdot x_b\cdot dx_b \\ a_{55} &= +\int_L M'_{33}\cdot x_b^2\cdot dx_b + \frac{V}{\omega_e^2}\int_L \left(N'_{33} - V\cdot\frac{dM'_{33}}{dx_b}\right)\cdot x_b\cdot dx_b \\ &\quad \boxed{+\tfrac{V}{\omega_e^2}\int_L N'_{33}\cdot x_b\cdot dx_b + \tfrac{V}{\omega_e^2}\int_L \tfrac{dN'_{33}}{dx_b}\cdot x_b^2\cdot dx_b} \\ b_{55} &= +\int_L \left(N'_{33} - V\cdot\frac{dM'_{33}}{dx_b}\right)\cdot x_b^2\cdot dx_b - 2V\int_L M'_{33}\cdot x_b\cdot dx_b \quad \boxed{-\tfrac{V^2}{\omega_e^2}\int_L \tfrac{dN'_{33}}{dx_b}\cdot x_b\cdot dx_b} \\ c_{55} &= +2\rho g\int_L y_w\cdot x_b^2\cdot dx_b \end{aligned} \tag{8.26}$$

The derivatives of M'_{33} and N'_{33} have to be determined numerically over the whole ship length in such a way that the following relation is fulfilled:

$$\begin{aligned}\int_{x_b(0)-\varepsilon}^{x_b(L)+\varepsilon} \frac{df(x_b)}{dx_b}dx_b &= \int_{x_b(0)-\varepsilon}^{x_b(0)} \frac{df(x_b)}{dx_b}dx_b + \int_{x_b(0)}^{x_b(L)} \frac{df(x_b)}{dx_b}dx_b + \int_{x_b(L)}^{x_b(L)+\varepsilon} \frac{df(x_b)}{dx_b}dx_b \\ &= f(0) + \int_{x_b(0)}^{x_b(L)} \frac{df(x_b)}{dx_b}dx_b - f(L) \\ &= 0 \end{aligned} \tag{8.27}$$

with $\varepsilon \ll L$, while $f(x_b)$ is equal to the local values of $M'_{33}(x_b)$ or $N'_{33}(x_b)$; see figure 8.2.

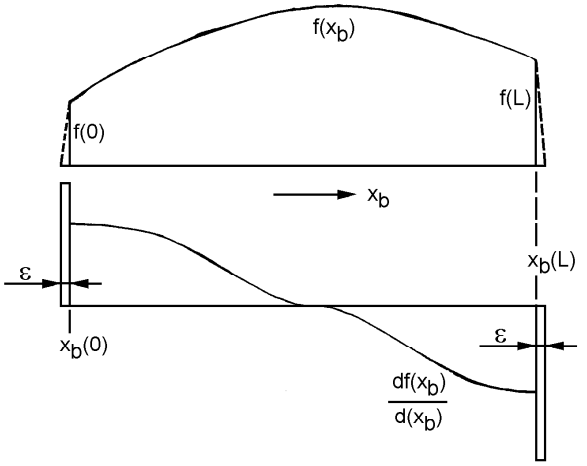

Figure 8.2: Integration of Longitudinal Derivatives

The numerical integrations of the derivatives are carried out in the region $x_b(0) \leq x_b \leq x_b(L)$ only. So, the additional **so-called "end terms"** $f(0)$ and $f(L)$ are defined by:

$$f(0) = \int_{x_b(0)-\varepsilon}^{x_b(0)} \frac{df(x_b)}{dx_b} \cdot dx_b \qquad \text{and} \qquad f(L) = \int_{x_b(L)}^{x_b(L)+\varepsilon} \frac{df(x_b)}{dx_b} \cdot dx_b \tag{8.28}$$

Because the integration of the derivatives has to be carried out in the region $x_b(0) - \varepsilon \leq x_b \leq x_b(L) + \varepsilon$, some algebra provides the integral and the first and second order moments (with respect to G) over the whole ship length:

$$\int_{x_b(0)-\varepsilon}^{x_b(L)+\varepsilon} \frac{df(x_b)}{dx_b} \cdot dx_b = 0$$

$$\int_{x_b(0)-\varepsilon}^{x_b(L)+\varepsilon} \frac{df(x_b)}{dx_b} \cdot x_b \cdot dx_b = -\int_{x_b(0)}^{x_b(L)} f(x_b) \cdot dx_b$$
$$\int_{x_b(0)-\varepsilon}^{x_b(L)+\varepsilon} \frac{df(x_b)}{dx_b} \cdot x_b^2 \cdot dx_b = -2\int_{x_b(0)}^{x_b(L)} f(x_b) \cdot x_b \cdot dx_b \qquad (8.29)$$

Using this, more simple expressions for the total hydromechanical coefficients in the coupled heave and pitch equations can be obtained:

$$\begin{aligned}
a_{33} &= +\int_L M'_{33} \cdot dx_b \\
b_{33} &= +\int_L N'_{33} \cdot dx_b \\
c_{33} &= +2\rho g \int_L y_w \cdot dx_b \\
a_{35} &= -\int_L M'_{33} \cdot x_b \cdot dx_b - \frac{V}{\omega_e^2}\int_L N'_{33} \cdot dx_b \\
b_{35} &= -\int_L N'_{33} \cdot x_b \cdot dx_b + V\int_L M'_{33} \cdot dx_b \\
c_{35} &= -2\rho g \int_L y_w \cdot x_b \cdot dx_b
\end{aligned} \qquad (8.30)$$

$$\begin{aligned}
a_{53} &= -\int_L M'_{33} \cdot x_b \cdot dx_b \boxed{+\tfrac{V}{\omega_e^2}\int_L N'_{33} \cdot dx_b} \\
b_{53} &= -\int_L N'_{33} \cdot x_b \cdot dx_b - V\int_L M'_{33} \cdot dx_b \\
c_{53} &= -2\rho g \int_L y_w \cdot x_b \cdot dx_b \\
a_{55} &= +\int_L M'_{33} \cdot x_b^2 \cdot dx_b + \frac{V}{\omega_e^2}\int_L N'_{33} \cdot x_b \cdot dx_b + \frac{V^2}{\omega_e^2}\int_L M'_{33} \cdot dx_b \\
&\quad \boxed{-\tfrac{V}{\omega_e^2}\int_L N'_{33} \cdot x_b \cdot dx_b} \\
b_{55} &= +\int_L N'_{33} \cdot x_b^2 \cdot dx_b \boxed{+\tfrac{V^2}{\omega_e^2}\int_L N'_{33} \cdot dx_b} \\
c_{55} &= +2\rho g \int_L y_w \cdot x_b^2 \cdot dx_b \approx \rho g \nabla \cdot \overline{GM}_L
\end{aligned} \qquad (8.31)$$

Note that both strip theory methods are identical for the zero forward speed case.

Wave Loads

By assuming that:

$$x \approx x_b \qquad y \approx y_b \qquad z \approx z_b \tag{8.32}$$

which is exactly true for the restrained ship, the expressions for the wave surface and the first order wave potential can be written in the body-bound coordinate system as:

$$\begin{aligned} \zeta &= \zeta_a \cos(\omega_e t - k x_b \cos\mu - k y_b \sin\mu) \\ \Phi_w &= \frac{-\zeta_a g}{\omega} \cdot \frac{\cosh k(h+z_b)}{\cosh(kh)} \cdot \sin(\omega_e t - k x_b \cos\mu - k y_b \sin\mu) \end{aligned} \tag{8.33}$$

in which μ is the wave direction.
The local vertical relative orbital velocity of the water particles follows from the derivative of the wave potential as given in chapter 5. Equations 8.18 and 8.15 provide the vertical relative orbital acceleration:

$$\begin{aligned} \dot{\zeta}'_{w3} &= \frac{\partial \Phi_w}{\partial z_b} \\ &= \frac{-kg}{\omega} \cdot \frac{\sinh k(h+z_b)}{\cosh(kh)} \cdot \zeta_a \sin(\omega_e t - k x_b \cos\mu - k y_b \sin\mu) \\ \ddot{\zeta}'_{w3} &= -kg \cdot \frac{\sinh k(h+z_b)}{\cosh(kh)} \cdot \zeta_a \cos(\omega_e t - k x_b \cos\mu - k y_b \sin\mu) \end{aligned} \tag{8.34}$$

The pressure in the fluid follows from the linearized Bernoulli equation:

$$\begin{aligned} p &= -\rho g z_b + \rho g \cdot \frac{\cosh k(h+z_b)}{\cosh(kh)} \cdot \zeta_a \cos(\omega_e t - k x_b \cos\mu - k y_b \sin\mu) \\ &= p_0 + \frac{\partial p}{\partial x_b} \cdot dx_b + \frac{\partial p}{\partial y_b} \cdot dy_b + \frac{\partial p}{\partial z_b} \cdot dz_b \end{aligned} \tag{8.35}$$

Only the vertical pressure gradient is of importance for the vertical loads on of a cross section:

$$\frac{\partial p}{\partial z_b} = -\rho g + \rho k g \cdot \frac{\sinh k(h+z_b)}{\cosh(kh)} \cdot \zeta_a \cos(\omega_e t - k x_b \cos\mu - k y_b \sin\mu) \tag{8.36}$$

which can be expressed in terms of the vertical orbital acceleration - instead - as:

$$\frac{\partial p}{\partial z_b} = -\rho \cdot (g + \ddot{\zeta}'_{w3}) \tag{8.37}$$

Figure 8.3 shows that the vertical Froude-Krilov force can be written as:

$$\begin{aligned} X'_{fk_3} &= -\int_{-T}^{\zeta}\int_{-y_b}^{+y_b} \frac{\partial p}{\partial z_b} \cdot dy_b \cdot dz_b \\ &= \rho \int_{-T}^{\zeta}\int_{-y_b}^{+y_b} (g + \ddot{\zeta}'_{w_3}) \cdot dy_b \cdot dz_b \end{aligned} \tag{8.38}$$

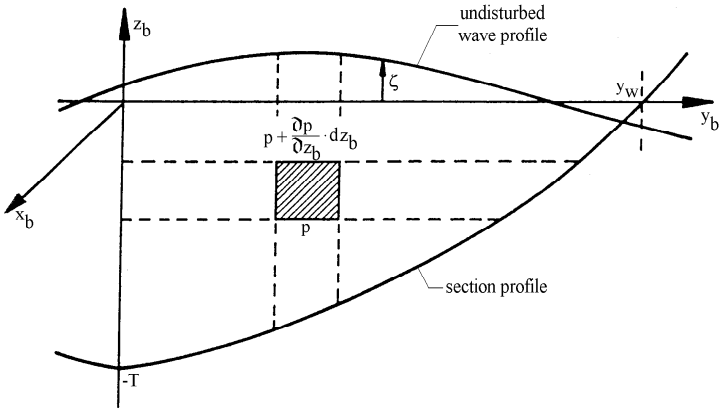

Figure 8.3: Wave Pressure Distribution for Heave

After neglecting the second order terms and some algebra, this Froude-Krilov force can be written as a spring term:

$$X'_{fk_3} = 2\rho g y_w \cdot C_3 \cdot \zeta_a \cos(\omega_e t - k x_b \cos\mu) \tag{8.39}$$

with:

$$C_3 = \frac{\sin(-k y_w \sin\mu)}{-k y_w \sin\mu} - \frac{k}{y_w} \cdot \int_{-T}^{0} \frac{\sin(-k y_b \sin\mu)}{-k y_b \sin\mu} \cdot \frac{\sinh k(h+z_b)}{\cosh(kh)} \cdot y_b \cdot dz_b \tag{8.40}$$

or in deep water with long waves relative to the breadth of the cross section ($k y_w \ll 1$):

$$C_3 = 1 - \frac{k}{y_w} \cdot \int_{-T}^{0} e^{k z_b} \cdot y_b \cdot dz_b \tag{8.41}$$

By expanding the exponent in C_3 from equation 8.41 in a series, one finds:

$$C_3 = 1 \; - k \cdot \frac{A}{2y_w} \; - k^2 \cdot \frac{S_y}{2y_w} \; - k^3 \cdot \frac{I_y}{4y_w} \; - ..... \tag{8.42}$$

with:

$$A = 2\int_{-T}^{0} y_b \cdot dz_b \qquad S_y = 2\int_{-T}^{0} y_b \cdot z_b \cdot dz_b \qquad I_y = 2\int_{-T}^{0} y_b \cdot z_b^2 \cdot dz_b \tag{8.43}$$

For deep water with long waves relative to the breadth and draft of the cross section ($k y_w \ll 1$ and $kT \ll 1$) one can write:

$$C_3 \approx e^{-kT_3^*} \qquad \text{or} \qquad T_3^* \approx \frac{-\ln C_3}{k} \tag{8.44}$$

Now, T_3^* can be considered as the draft at which the pressure is equal to the average pressure on the cross section in the fluid. By defining $\zeta_{a3}^* = C_3 \cdot \zeta_{a3}$, the term $\rho g \cdot \zeta_{a3}^*$ becomes the amplitude of this mean pressure.

The effective vertical components of the orbital accelerations and velocities in undisturbed waves are defined at this draft T_3^* too:

$$\begin{aligned} \ddot{\zeta}^*_{w_3} &= -kg \cdot \zeta^*_{a_3} \cos(\omega_e t - k x_b \cos\mu) \\ \dot{\zeta}^*_{w_3} &= \frac{-kg}{\omega} \cdot \zeta^*_{a_3} \sin(\omega_e t - k x_b \cos\mu) \end{aligned} \tag{8.45}$$

With this, the two-dimensional wave exciting force on a restrained cross section of a ship in waves, as defined in equations 8.19 and 8.20, becomes:

$$X'_{w_3} = \left(M'_{33} \boxed{+\tfrac{V}{\omega_e^2} \cdot \tfrac{dN'_{33}}{dx_b}} \right) \cdot \ddot{\zeta}^*_{w_3} + \left(N'_{33} - V \cdot \frac{dM'_{33}}{dx_b} \right) \cdot \dot{\zeta}^*_{w_3} + X'_{fk_3} \tag{8.46}$$

in which only the modified strip theory includes the outlined term.
These **equivalent accelerations and velocities** in the undisturbed wave are used to determine the additional wave loads due to diffraction of the waves. They are considered as potential mass and damping terms, just as applied for the hydromechanical loads. This is the reason why this approach called the **relative motion principle** in strip theory.
The total wave loads for heave and pitch follows from all this:

$$\begin{aligned} X_{w_3} &= + \int_L M'_{33} \cdot \ddot{\zeta}^*_{w_3} \cdot dx_b \; \boxed{+\tfrac{V}{\omega \cdot \omega_e} \int_L \tfrac{dN'_{33}}{dx_b} \cdot \ddot{\zeta}^*_{w_3} \cdot dx_b} \\ &\quad + \int_L \left(\boxed{\tfrac{\omega}{\omega_e} \cdot} N'_{33} - V \cdot \frac{dM'_{33}}{dx_b} \right) \cdot \dot{\zeta}^*_{w_3} \cdot dx_b \\ &\quad + \int_L X'_{fk_3} \cdot dx_b \end{aligned} \tag{8.47}$$

$$\begin{aligned} X_{w_5} &= - \int_L M'_{33} \cdot x_b \cdot \ddot{\zeta}^*_{w_3} \cdot dx_b \; \boxed{-\tfrac{V}{\omega \cdot \omega_e} \int_L \tfrac{dN'_{33}}{dx_b} \cdot x_b \cdot \ddot{\zeta}^*_{w_3} \cdot dx_b} \\ &\quad - \int_L \left(\boxed{\tfrac{\omega}{\omega_e} \cdot} N'_{33} - V \cdot \frac{dM'_{33}}{dx_b} \right) \cdot x_b \cdot \dot{\zeta}^*_{w_3} \cdot dx_b \\ &\quad - \int_L X'_{fk_3} \cdot x_b \cdot dx_b \end{aligned} \tag{8.48}$$

Note that both strip theory methods are identical here for the zero forward speed case and that the (generally small) influence of the surge wave loads on the pitch wave moment has been ignored here, too.

Heave and Pitch Equations

Putting all this together yields the coupled equations of motion of heave and pitch:

$$\begin{aligned} (\rho\nabla + a_{33}) \cdot \ddot{z} + b_{33} \cdot \dot{z} + c_{33} \cdot z + a_{35} \cdot \ddot{\theta} + b_{35} \cdot \dot{\theta} + c_{35} \cdot \theta &= X_{w_3} \\ a_{53} \cdot \ddot{z} + b_{53} \cdot \dot{z} + c_{53} \cdot z + (I_{xx} + a_{55}) \cdot \ddot{\theta} + b_{55} \cdot \dot{\theta} + c_{55} \cdot \theta &= X_{w_5} \end{aligned} \tag{8.49}$$

which can be solved as described in chapter 6.

8.3.4 3-D Panel Method

This method is restricted to arbitrarily shaped bodies with zero mean forward speed. This is an acceptable simplification for the majority of the fixed or floating structures in use today in the offshore industry.
The panel method is a numerical method to calculate the (potential) flow around a body, based on the principle of Green's integral theorem. According to this theorem it is possible to transform a three-dimensional linear homogeneous differential equation into a two-dimensional integral equation. In that way the three-dimensional Laplace (potential) equation can be transformed to a surface integral equation, known as Green's identity. The integral equation represents a distribution of sources (or sinks) and dipoles on the surface. To solve the integral equation numerically, the surface of the body is divided in a number of panels, as shown for a crude oil carrier in figure 8.4.

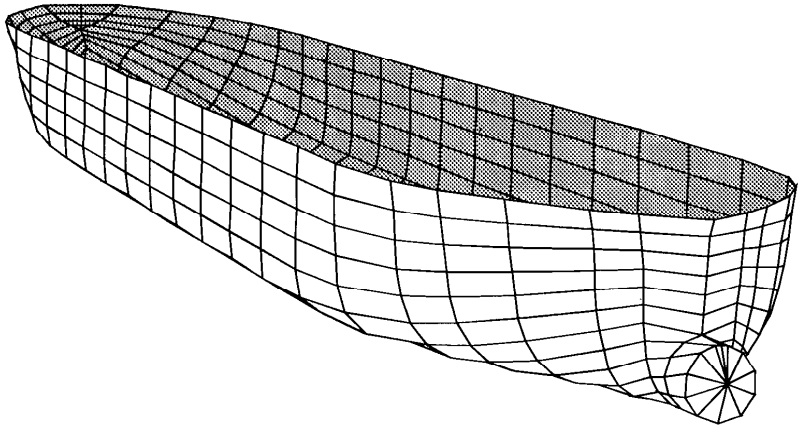

Figure 8.4: 3-D Representation of the Hull Form of a Crude Oil Carrier

The body surface is divided in N panels small enough to assume that the sources and doublets strength and the fluid pressure is constant over each element. Now a set of integral equations is made, from which the velocity potentials can be found. The integral equation can be discretized for each panel by substituting an unknown strength of the source and dipole distribution. By using the boundary condition of tangential flow, the unknown strength of the sources and dipoles can be solved. If the strength of each dipole or source is known the velocities can be determined on the surface.
Note that there are now no restrictions on the form and shape of the body. This method works equally well for a ship, the base of a concrete GBS structure or a semi-submersible. The method will work - in principle - with any size of structure as well.
The advantage of panel methods is that the problem is reduced to a two-dimensional (surface) problem instead of a three-dimensional (volume) problem. The grid generation is also reduced to a two dimensional problem. So the grid has to be generated on the surface of the body only. This is in contrast to the three dimensional grid generation, where a lot of points have to be generated in the space around the body. Another advantage is that N^2 equations, instead of N^3 equations, have to be solved to determine the velocity field.
Panel methods are the most common technique used to analyze the linear steady state response of large-volume structures in regular waves. A wave spectrum is used to describe

a sea state and irregular sea results can be obtained by linear superposition of results from regular incident waves.
It is assumed that oscillation amplitudes of the fluid and the body are small relative to cross-sectional dimensions of the body.
Since the panel is based on potential theory, the effect of flow separation is neglected. As a consequence, the method should not be applied to slender structures, risers or tethers. Methods for such structures are discussed in chapter 12.
The quality of the results depends on the size and the number of panels used to schematic the body. There is no unique way to approximate the body surface by elements. Since it assumed that the source and dipole densities - and consequently the fluid pressure - are constant over each element, one should use smaller elements in areas where the flow changes more rapidly. It should be realized that the numerical solution for velocities never is satisfactory on an element closest to a sharp corner. The reason is that the potential flow solution has a singularity there, and that this is inconsistent with the assumption that the source density and velocity potential are constant over an element. In reality the flow will separate at a sharp corner. This effect is not included in the method.
In the wave zone the element size should be small compared to the wave length. A characteristic length of an element ought to be less than 1/8 of the wave length.
In the case of semi-submersibles and at least a vertical column with circular cross-section there ought to be at least 16 circumferential elements at any height. As a consequence panelling of a semi-submersible platform requires a relatively fine grid mesh. The result of that is that numerical models of diffraction radiation should not be used in the pre-design process of for instance semi-submersibles.
Typical values for the total number of elements for an offshore structure may vary from 500 to 1500. However, figure 8.5 shows an example where 12608 panels where used for the total structure.

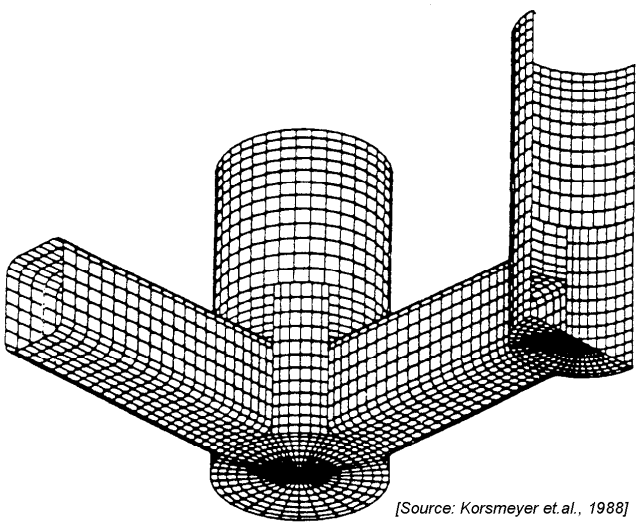

Figure 8.5: Submerged Portion of One Quadrant of a Six Column TLP

Iterative solutions of the system of linear equations for the source densities are required in order to be within practical limits of CPU time on available computer hardware. The best way to find a sufficient number of elements, is to do calculations with increasing numbers

of elements and check the convergence of the results.
Methods to evaluate the hydrodynamic loads and motions of floating or fixed structures in waves have been developed based on linear three-dimensional potential theory, see for instance [Oortmerssen, 1976a]. Both, the wave-frequency hydrodynamic loads on free-floating or fixed bodies and the wave-frequency motions of floating bodies as well as the second order wave drift forces can be computed. Experimental verification of results of computations has been carried out for bodies with a large variety of shapes. Such comparisons have shown that 3-D diffraction methods generally can be applied to most body shapes and are therefore a good tool to investigate such effects.
It may be noted that the 3-D method as described here is suitable for the zero forward speed case only. Generally the potential coefficients are determined in a coordinate system with $G = O$ in the water line, so that a correction for the actual $\overline{OG}$-value is required.

8.4 Motions in Regular Waves

Each equation of motion can be split into an equation with in-phase parts and an equation with out-of-phase components. After dividing the left and right hand terms of these equations by the wave amplitude ζ_a, two sets of six coupled equations of motion are available. The unknown variables in the 6 coupled equations of motions in the **vertical plane** are:

$$\left.\begin{array}{lllll} \text{surge:} & \frac{x_a}{\zeta_a} \cdot \cos\varepsilon_{x\zeta} & \text{and} & \frac{x_a}{\zeta_a} \cdot \sin\varepsilon_{x\zeta} \\ \text{heave:} & \frac{z_a}{\zeta_a} \cdot \cos\varepsilon_{z\zeta} & \text{and} & \frac{z_a}{\zeta_a} \cdot \sin\varepsilon_{z\zeta} \\ \text{pitch:} & \frac{\theta_a}{\zeta_a} \cdot \cos\varepsilon_{\theta\zeta} & \text{and} & \frac{\theta_a}{\zeta_a} \cdot \sin\varepsilon_{\theta\zeta} \end{array}\right\} \tag{8.50}$$

The unknown variables in the 6 coupled equations of motions in the **horizontal plane** are:

$$\left.\begin{array}{lllll} \text{sway:} & \frac{y_a}{\zeta_a} \cdot \cos\varepsilon_{y\zeta} & \text{and} & \frac{y_a}{\zeta_a} \cdot \sin\varepsilon_{y\zeta} \\ \text{roll:} & \frac{\phi_a}{\zeta_a} \cdot \cos\varepsilon_{\phi\zeta} & \text{and} & \frac{\phi_a}{\zeta_a} \cdot \sin\varepsilon_{\phi\zeta} \\ \text{yaw:} & \frac{\psi_a}{\zeta_a} \cdot \cos\varepsilon_{\psi\zeta} & \text{and} & \frac{\psi_a}{\zeta_a} \cdot \sin\varepsilon_{\psi\zeta} \end{array}\right\} \tag{8.51}$$

These 2 sets of equations of motion have to be solved numerically. Their terms are explained below.

8.4.1 Frequency Characteristics

The **transfer functions** (also called **response amplitude operators**) of the motions are the motion amplitude component to wave amplitude ratios. They and the phase shifts of these motions relative to the (virtual) wave elevation at the ship's center of gravity follow from the solution to 8.50 and 8.51:

$$\frac{x_a}{\zeta_a} \quad \frac{y_a}{\zeta_a} \quad \frac{z_a}{\zeta_a} \quad \frac{\theta_a}{\zeta_a} \quad \frac{\phi_a}{\zeta_a} \quad \frac{\psi_a}{\zeta_a}$$

and

$$\varepsilon_{x\zeta} \quad \varepsilon_{y\zeta} \quad \varepsilon_{z\zeta} \quad \varepsilon_{\theta\zeta} \quad \varepsilon_{\phi\zeta} \quad \varepsilon_{\psi\zeta}$$

The transfer functions of the translations are dimensionless. The transfer functions of the rotations can be made non-dimensional by dividing the amplitude of the rotations by the amplitude of the wave slope, $k\zeta_a$, instead of the wave amplitude, ζ_a, yielding:

$$\frac{x_a}{\zeta_a} \quad \frac{y_a}{\zeta_a} \quad \frac{z_a}{\zeta_a} \quad \frac{\theta_a}{k\zeta_a} \quad \frac{\psi_a}{k\zeta_a} \quad \frac{\phi_a}{k\zeta_a}$$

The remainder of this section gives some general properties of these frequency characteristics.

Figures 8.6 and 8.7 show the frequency characteristics of the coupled heave and pitch motions of a crude oil carrier, as computed, using the SEAWAY strip theory program, see [Journée, 1999], for 0 and 16 knots forward ship speed in head and beam deep water waves.

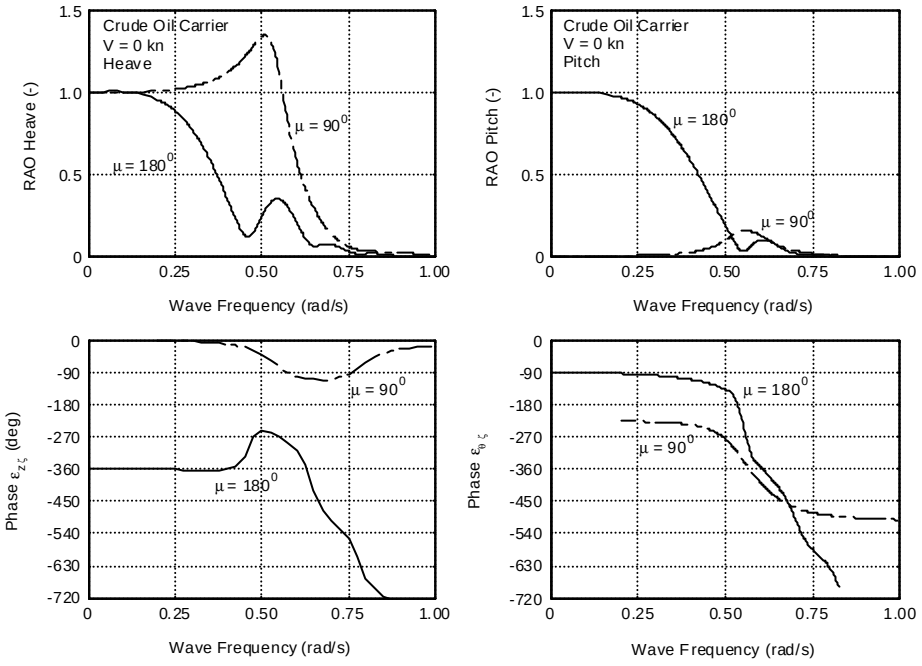

Figure 8.6: Heave and Pitch of a Crude Oil Carrier, V = 0 Knots

Examine first the heave and pitch motions at zero forward speed in head waves at deep water. These are the solid line curves in figure 8.6. In very long waves ($\omega \to 0$), the ship behaves like a sea gull in waves; she follows the wave surface. The heave amplitude, z_a, tends to the wave amplitude, ζ_a, and the pitch amplitude, θ_a, tends to the wave slope amplitude, $k\zeta_a$. Both dimensionless transfer functions tend to 1.0. The ship follows the wave surface, so the phase shift for heave, $\varepsilon_{z\zeta}$, tends to zero or -360°and the phase of the pitch angle relative to the wave elevation, $\varepsilon_{\theta\zeta}$, tends to -90°. Resonance can appear, depending on the magnitude of the damping, somewhere in the neighborhood of the natural frequencies.

Notice that resonance does not always appear at the natural frequency. When determining the natural frequency, the right hand side of the (uncoupled) equation of motion is zero, while when determining the resonant frequency, the right hand side of the (coupled) equation of motion contains the frequency-dependent wave load(s). Both, the natural frequencies and the frequency-dependent wave loads determine the resonant frequencies. Also, coupling effects play a role.

Resonances are usually marked in these diagrams by a local maximum in the response amplitude operator (**RAO**) and a rather abrupt change in response phase. At frequencies somewhat higher than the natural frequencies of heave and pitch, the transfer functions decrease and at still higher frequencies - as wave lengths becomes shorter than the ship length - the transfer functions tend to zero. No general conclusion can be drawn about the behavior of the phase shifts at higher frequencies.
Examining these motions in beam waves ($\mu = 90°$, the dashed lined in figure 8.6), in very long waves ($\omega \rightarrow 0$), the ship behaves like a sea-gull in waves again; it follows the wave surface. The heave amplitude, z_a, tends to the wave amplitude, ζ_a; the non-dimensional transfer function tends to 1.0. The phase shift, $\varepsilon_{z\zeta}$, tends to zero. In beam waves, it is not the wave length to ship length ratio but the wave length to ship breadth ratio that is of importance. When taking this into account, the heave motion behavior in beam waves is more or less similar to this motion in head waves, but the resonance peak can be higher. However, the pitch moments and motions become very small in the whole frequency range. Pitch motions in beam waves can be caused only by the anti-symmetry of the aft and fore body of the vessel with respect to its amidships section.
Comparable considerations can be given for the motions at forward speed, as given in figure 8.7. Notice the start of an "overshoot" in the heave and pitch motions in head waves. RAO's larger than 1.0 at wave lengths of about the ship length are common for high speed vessels.

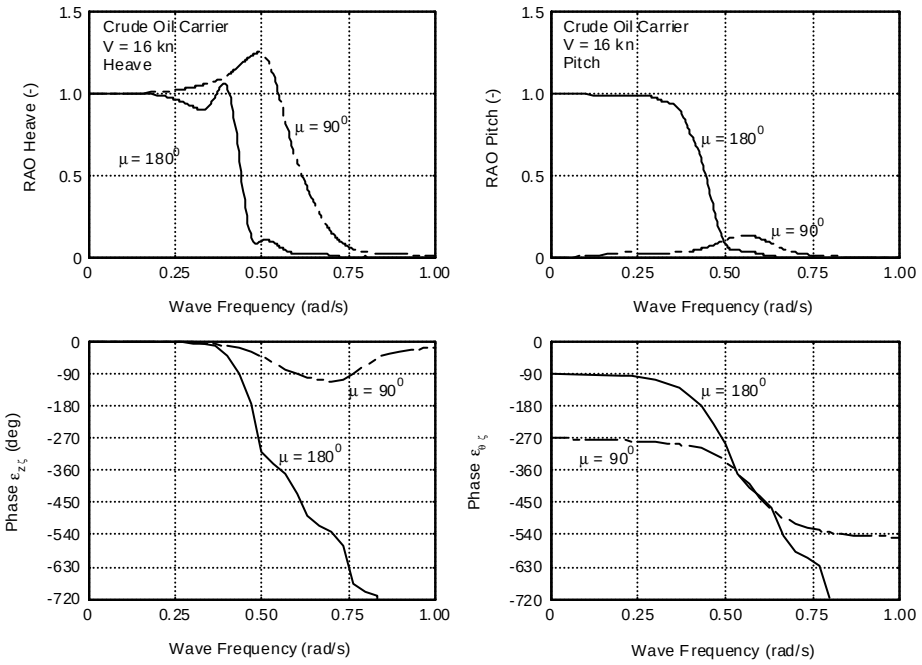

Figure 8.7: Heave and Pitch of a Crude Oil Carrier, V = 16 Knots

An example of predicted and measured transfer functions of the motions in all six degrees of freedom of an aircraft carrier sailing at 25 knots (obtained from Principles of Naval Architecture,1989) is given in figure 8.8. Each column in the figure is for a different wave direction. Notice that the frequency scale has been changed to an equivalent wave length over ship length scale.

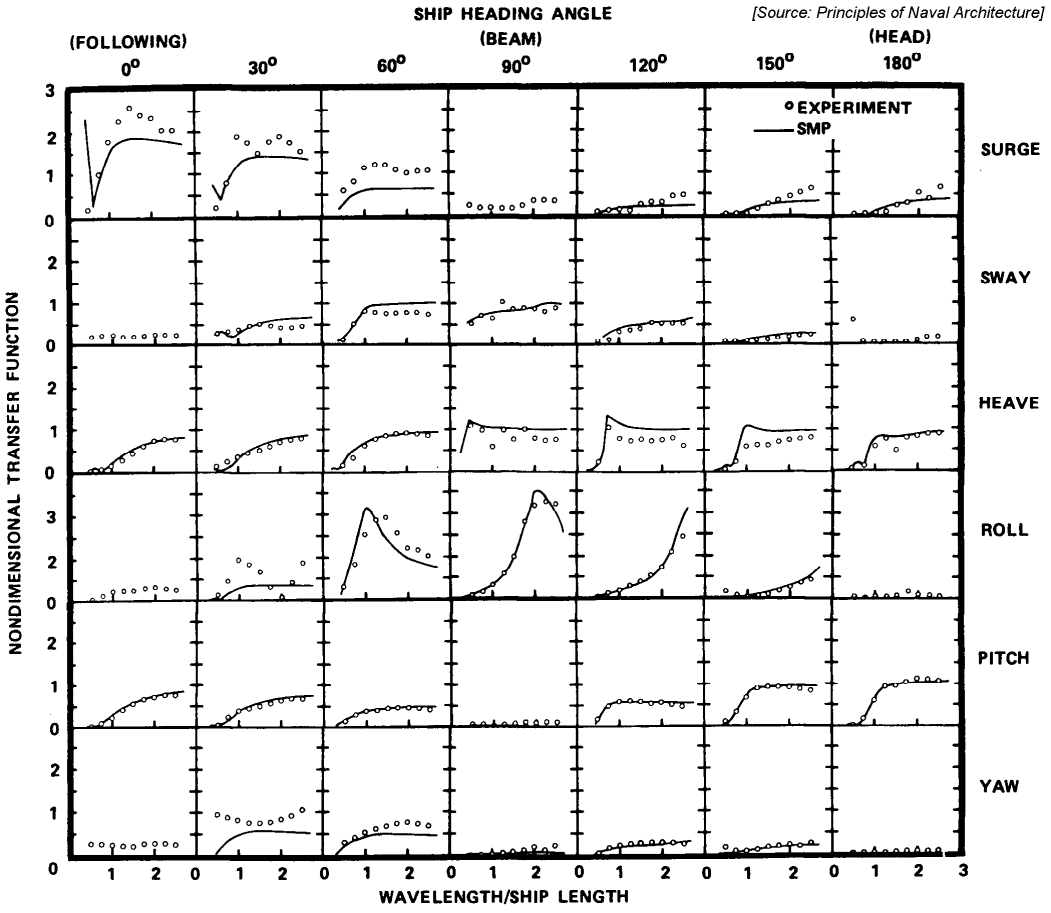

Figure 8.8: Measured and Calculated RAO's of an Aircraft Carrier

Figure 8.9 shows the speed dependent transfer functions of the roll motions in beam waves and the pitch motions in head waves of a container ship. Notice the opposite effect of forward speed on these two angular motions, caused by a with forward speed strongly increasing lift-damping of the roll motions. The flow around the sailing and rolling ship is asymmetric and the ship behaves like an airfoil.

8.4.2 Harmonic Motions

When the translations of, and the rotations about, the center of gravity are known, the motions of any point, $P(x_b, y_b, z_b)$, on the ship can be determined - again by superposition.

Displacements

The harmonic **longitudinal displacement** is given by:

$$\begin{aligned} x_p &= x - y_b \cdot \psi + z_b \cdot \theta \\ &= x_{p_a} \cdot \cos(\omega_e t + \varepsilon_{x_p\zeta}) \end{aligned} \tag{8.52}$$

The harmonic **lateral displacement** is given by:

$$y_p = y + x_b \cdot \psi - z_b \cdot \phi$$

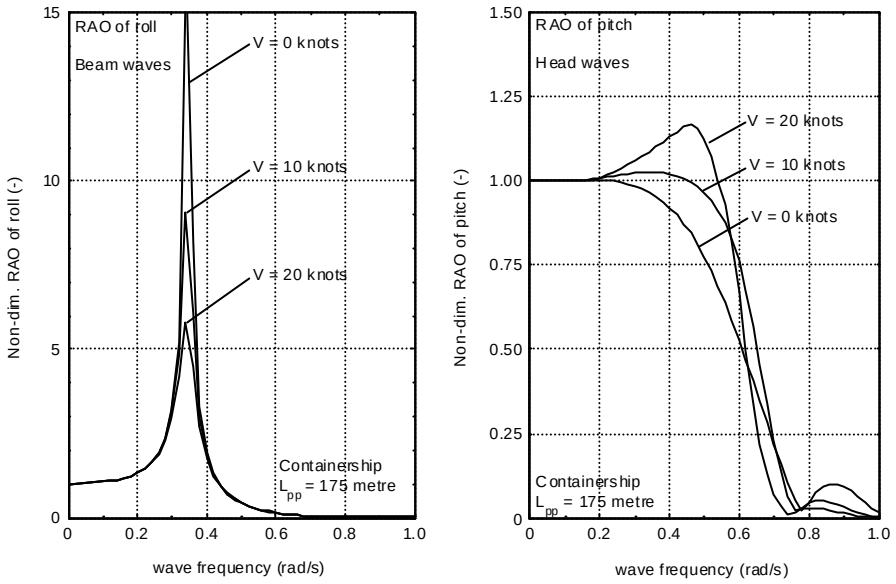

Figure 8.9: RAO's of Roll and Pitch of a Containership

$$= \quad y_{p_a} \cdot \cos(\omega_e t + \varepsilon_{y_p\zeta}) \tag{8.53}$$

The harmonic **vertical displacement** is given by:

$$\begin{aligned} z_p &= z - x_b \cdot \theta - y_b \cdot \phi \\ &= z_{p_a} \cdot \cos(\omega_e t + \varepsilon_{z_p\zeta}) \end{aligned} \tag{8.54}$$

Velocities

The harmonic velocities in the x_b-, y_b- and z_b-direction of point $P(x_b, y_b, z_b)$ on the ship are obtained by taking the derivative of the three harmonic displacements.
The harmonic **longitudinal velocity** is given by:

$$\begin{aligned} \dot{x}_p &= \dot{x} - y_b \cdot \dot{\psi} + z_b \cdot \dot{\theta} \\ &= -\omega_e \cdot x_{p_a} \cdot \sin(\omega_e t + \varepsilon_{x_p\zeta}) \\ &= \dot{x}_{p_a} \cdot \cos(\omega_e t + \varepsilon_{\dot{x}_p\zeta}) \end{aligned} \tag{8.55}$$

The harmonic **lateral velocity** is given by:

$$\begin{aligned} \dot{y}_p &= \dot{y} + x_b \cdot \dot{\psi} - z_b \cdot \dot{\phi} \\ &= -\omega_e \cdot y_{p_a} \cdot \sin(\omega_e t + \varepsilon_{y_p\zeta}) \\ &= \dot{y}_{p_a} \cdot \cos(\omega_e t + \varepsilon_{\dot{y}_p\zeta}) \end{aligned} \tag{8.56}$$

The harmonic **vertical velocity** is given by:

$$\begin{aligned} \dot{z}_p &= \dot{z} - x_b \cdot \dot{\theta} + y_b \cdot \dot{\phi} \\ &= -\omega_e \cdot z_{p_a} \cdot \sin(\omega_e t + \varepsilon_{z_p\zeta}) \\ &= \dot{z}_{p_a} \cdot \cos(\omega_e t + \varepsilon_{\dot{z}_p\zeta}) \end{aligned} \tag{8.57}$$

Accelerations

The harmonic accelerations in the x_b-, y_b- and z_b-direction of point $P(x_b, y_b, z_b)$ on the ship are obtained by taking the second derivative of the three harmonic displacements. However, in a ship-bound axes system, a longitudinal and transverse component of the acceleration of gravity, g, has to be added to the longitudinal and lateral accelerations respectively; this yields the total accelerations that the ship and its structural parts and cargo "feel".
The harmonic **longitudinal acceleration** is given by:

$$\begin{aligned} \ddot{x}_p &= \ddot{x} - y_b \cdot \ddot{\psi} + z_b \cdot \ddot{\theta} - g \cdot \theta \\ &= -\omega_e^2 \cdot x_{p_a} \cdot \cos(\omega_e t + \varepsilon_{x_p\zeta}) - g \cdot \theta_a \cdot \cos(\omega_e t + \varepsilon_{\theta\zeta}) \\ &= \ddot{x}_{p_a} \cdot \cos(\omega_e t + \varepsilon_{\ddot{x}_p\zeta}) \end{aligned} \tag{8.58}$$

The harmonic **lateral acceleration** is given by:

$$\begin{aligned} \ddot{y}_p &= \ddot{y} + x_b \cdot \ddot{\psi} - z_b \cdot \ddot{\phi} + g \cdot \phi \\ &= -\omega_e^2 \cdot y_{p_a} \cdot \cos(\omega_e t + \varepsilon_{y_p\zeta}) + g \cdot \phi_a \cdot \cos(\omega_e t + \varepsilon_{\phi\zeta}) \\ &= \ddot{y}_{p_a} \cdot \cos(\omega_e t + \varepsilon_{\ddot{y}_p\zeta}) \end{aligned} \tag{8.59}$$

The harmonic **vertical acceleration** is given by:

$$\begin{aligned} \ddot{z}_p &= \ddot{z} - x_b \cdot \ddot{\theta} + y_b \cdot \ddot{\phi} \\ &= -\omega_e^2 \cdot z_{p_a} \cdot \cos(\omega_e t + \varepsilon_{z_p\zeta}) \\ &= \ddot{z}_{p_a} \cdot \cos(\omega_e t + \varepsilon_{\ddot{z}_p\zeta}) \end{aligned} \tag{8.60}$$

Vertical Relative Displacements

The harmonic vertical relative displacement with respect to the undisturbed wave surface of point $P(x_b, y_b, z_b)$ connected to the ship can be obtained too:

$$\begin{aligned} s_p &= \zeta_p - z + x_b \cdot \theta - y_b \cdot \phi \\ &= s_{p_a} \cdot \cos(\omega_e t + \varepsilon_{s_p\zeta}) \end{aligned} \tag{8.61}$$

with:

$$\zeta_p = \zeta_a \cos(\omega_e t - k x_b \cos\mu - k y_b \sin\mu) \tag{8.62}$$

This relative motion plays a role in shipping water phenomena, which will be discussed in chapter 11. It may be noted that the sign of the relative motion is chosen here in such a way that a positive relative displacement implies a decrease of the freeboard.
Figure 8.10 shows the speed dependent transfer functions of the absolute and the relative vertical bow motions of a container ship in head waves. Note the opposite characteristics of these two motions in shorter and longer waves.

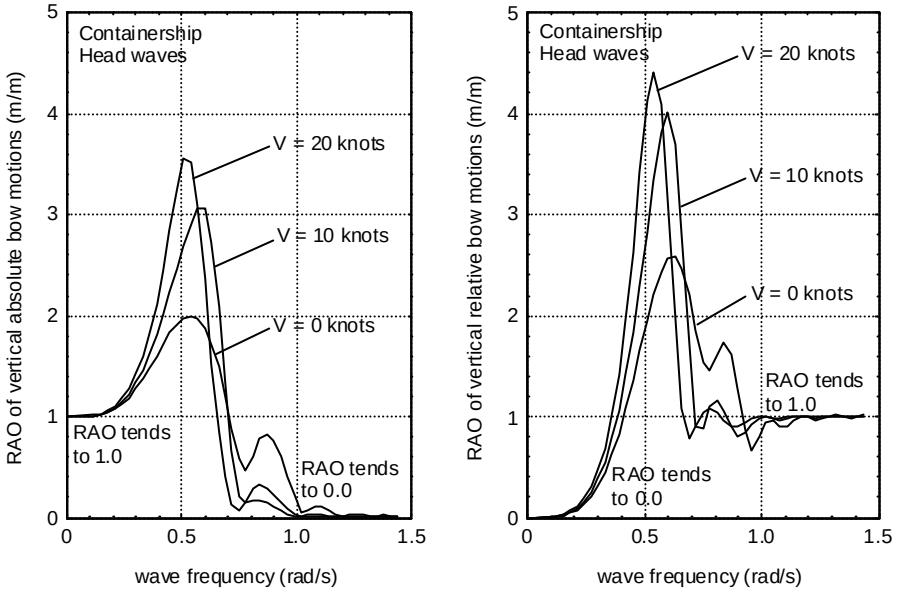

Figure 8.10: Absolute and Relative Vertical Motions at the Bow

Vertical Relative Velocities

The harmonic vertical relative velocity with respect to the undisturbed wave surface of a certain point, $P(x_b, y_b, z_b)$, connected to the ship, can be obtained by:

$$\begin{aligned} \dot{s} &= \frac{D}{Dt}\left\{\zeta_p - z + x_b \cdot \theta - y_b \cdot \phi\right\} \\ &= \dot{\zeta}_p - \dot{z} + x_b \cdot \dot{\theta} - V \cdot \theta - y_b \cdot \dot{\phi} \end{aligned} \tag{8.63}$$

with:

$$\dot{\zeta}_p = -\omega \cdot \zeta_a \sin(\omega_e t - k x_b \cos\mu - k y_b \sin\mu) \tag{8.64}$$

This velocity can play an important role in slamming of the bow of the ship; this will be discussed in chapter 11.

8.4.3 Dynamic Swell-Up

An oscillating ship will produce waves which in turn will influence the vertical relative motion of the ship. A so-called **dynamic swell-up** (which is a typical ship hydromechanical phrase for this phenomenon) should be taken into account.
[Tasaki, 1963] carried out forced oscillation tests with several ship models in still water and obtained an empirical formula for the dynamic swell-up at the forward perpendicular in head waves:

$$\frac{\Delta s_a}{s_a} = \frac{C_B - 0.45}{3} \cdot \sqrt{\frac{\omega_e^2 L}{g}} \tag{8.65}$$

with the restrictions:

block coefficient:	$0.60 < C_B < 0.80$
Froude number:	$0.16 < F_n < 0.29$
frequency of encounter:	$1.60 < \omega_e^2 L_{pp}/g < 2.60$

In this formula, s_a is the amplitude of the relative motion at the forward perpendicular as obtained in head waves, calculated from the heave, the pitch and the wave motions.
Then the actual amplitude of the relative motions becomes:

$$s_a^* = s_a + \Delta s_a \tag{8.66}$$

A simple but much more fundamental method to determine the dynamic swell up forward is given by [Journée and van 't Veer, 1995]; it is explained here.
Let an oscillating body produce damping waves, $\Delta\zeta$, with amplitude $\Delta\zeta_a$. When the vertical relative motions of a point fixed to the vessel with respect to the wave elevation are calculated, the influence of the radiated damping waves must be added to the undisturbed incoming wave. Then the vertical relative motions, s, at a point, $P(x_b, y_b)$, can be calculated using:

$$s(x_b, y_b) = \zeta(x_b, y_b) + \Delta\zeta - z(x_b, y_b) \tag{8.67}$$

where ζ is the incoming wave elevation and $z(x_b, y_b)$ is the vertical motion of the vessel in $P(x_b, y_b)$ and where the radiated wave elevation is given by:

$$\Delta\zeta = \Delta\zeta_a \cdot \cos(\omega t - k|y_b| + \pi) \tag{8.68}$$

For zero forward speed, the amplitude ratio of the local heave motion, $z_a(x_b)$, at a cross section, x_b, of the body and the produced transverse radiated waves, $\Delta\zeta_a(x_b)$, follows from the damping coefficient, $b'_{33}(x_b)$, and the wave speed, $c = g/\omega$:

$$\frac{z_a(x_b)}{\Delta\zeta_a(x_b)} = \frac{1}{\omega} \cdot \sqrt{\frac{\rho g c}{b'_{33}(x_b)}} \tag{8.69}$$

This has already been discussed for an oscillating cylinder in chapter 6.
Using this equation, the ratio of the amplitudes from the radiated waves due to the heaving cross section and the incoming wave becomes:

$$\frac{\Delta\zeta_a(x_b)}{\zeta_a} = \frac{z_a(x_b)}{\zeta_a} \cdot \omega \cdot \sqrt{\frac{b'_{33}(x_b)}{\rho g c}} \tag{8.70}$$

In case of a forward ship speed, V, the cross section is oscillating with the encounter frequency, ω_e, and therefore the wave velocity, c_e, of the radiated waves depends on this frequency:

$$c_e = \frac{g}{\omega_e} \tag{8.71}$$

Due to the forward speed the radiated waves are swept back in the wake. The wave elevation at a certain point, $P(x_p, y_p)$, in the ship-bounded axes system is now a result of the radiated waves from a cross section further ahead. The x_b-position of this cross section can be calculated simply, using:

$$x_b = x_p + |y_p| \cdot \frac{V}{c_e} \tag{8.72}$$

The amplitude of the radiated waves with a non-zero forward speed can now be calculated using the damping coefficient based on the encounter frequency and the previous expression for x_b:

$$\boxed{\frac{\Delta\zeta_a(x_p, y_p)}{\zeta_a} = \frac{z_a(x_b)}{\zeta_a} \cdot \omega_e \cdot \sqrt{\frac{b'_{33}(x_b)}{\rho g c_e}}} \tag{8.73}$$

This calculation method has been verified by using available results of experiments of [Journée, 1976a], carried out with a self propelled 1:50 model of a fast cargo ship in regular head waves; see figure 8.11. In the ballast condition of the model, the vertical relative motions have been measured at four ship speeds at 10 % of the length aft of the forward perpendicular. The curves in these figures marked by "undisturbed wave" refer to not accounting for a dynamic swell-up; the curves marked by "disturbed wave" refer to accounting for a dynamic swell-up as described above. The figures show a strongly improved agreement between the measured and the predicted relative motions taking a dynamic swell-up in to account, especially at frequencies near resonance.

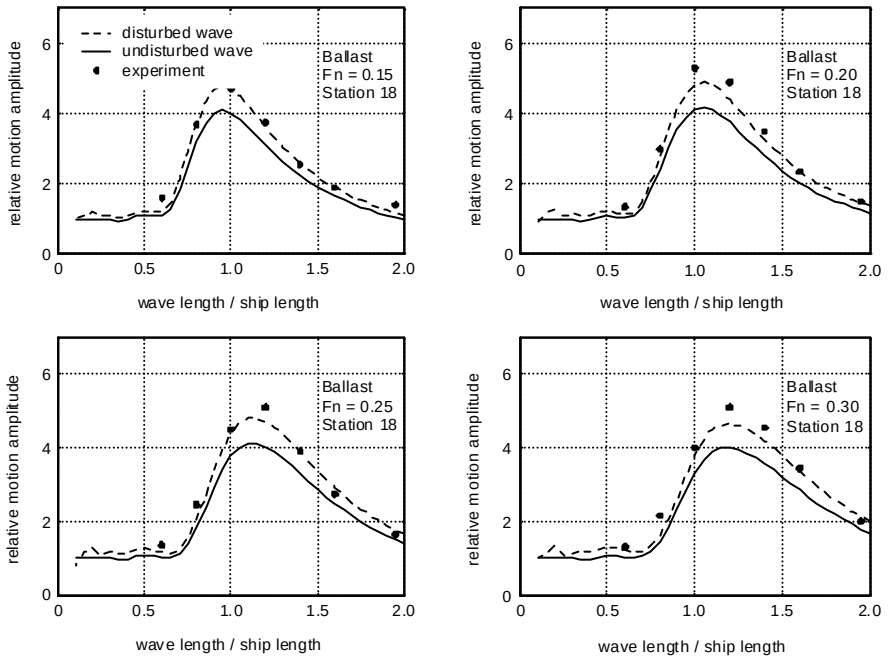

Figure 8.11: Vertical Relative Motions in Head Waves of a Fast Cargo Ship

8.5 Motions in Irregular Waves

Once the transfer functions between wave energy and motion (component) energy are known, one can transform any wave energy spectrum to a corresponding motion energy spectrum. This was explained in chapter 6 for a ship which is not sailing; the average speed was zero.
When a ship is sailing, it will generally encounter or "meet" the waves with a different apparent frequency, the frequency of encounter ω_e, than one would observe from a fixed location; see chapter 6. The first part of this section describes additional necessary wave spectrum axis transformations.

8.5.1 Spectrum Transformations

The spectral value of the waves, $S_\zeta(\omega_e)$, based on ω_e is not equal to the spectral value, $S_\zeta(\omega)$, based on ω. Because there must be an equal amount of energy in the frequency

bands $\Delta\omega$ and $\Delta\omega_e$, it follows that:

$$\boxed{|S_\zeta(\omega_e) \cdot d\omega_e = S_\zeta(\omega) \cdot d\omega|} \tag{8.74}$$

This transformation rule is demonstrated in figure 8.12.

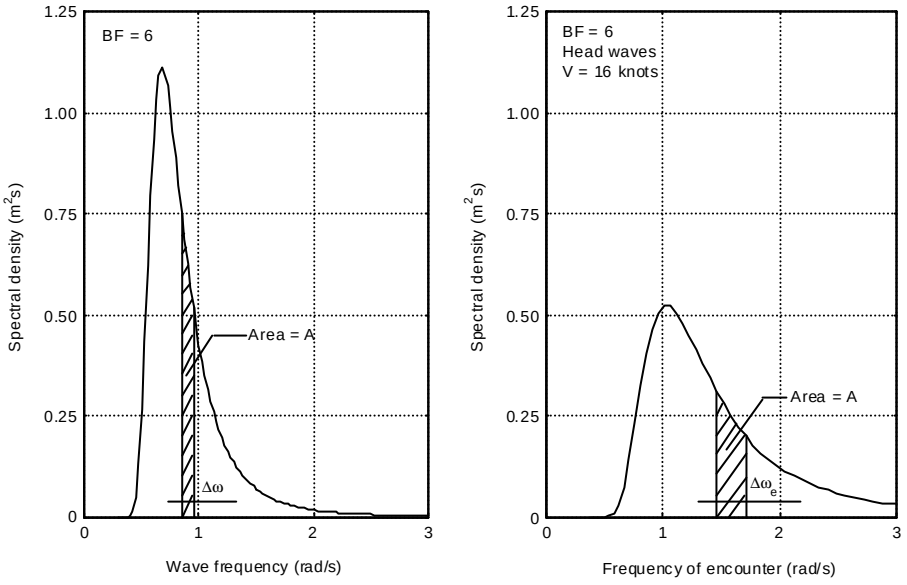

Figure 8.12: Transformation of Wave Spectra

The following relation is found from equation 8.74:

$$\boxed{S_\zeta(\omega_e) = \frac{S_\zeta(\omega)}{\frac{d\omega_e}{d\omega}}} \tag{8.75}$$

The relation between the frequency of encounter and the wave frequency in deep water has been found in chapter 6:

$$\begin{aligned} \omega_e &= \omega - \frac{\omega^2}{g} V \cdot \cos\mu \\ &= \omega \cdot \left(1 - \frac{V}{c} \cdot \cos\mu\right) \qquad \text{(by using: } c = g/\omega) \end{aligned} \tag{8.76}$$

in which:

ω	=	wave frequency in a fixed reference (rad/s)
ω_e	=	frequency of encounter in a moving reference (rad/s)
V	=	forward ship speed (m/s)
c	=	wave speed (m/s)
μ	=	ship heading relative to wave direction (rad)

Thus, for deep water:

$$\frac{d\omega_e}{d\omega} = 1 - \frac{2\omega V \cdot \cos\mu}{g} \tag{8.77}$$

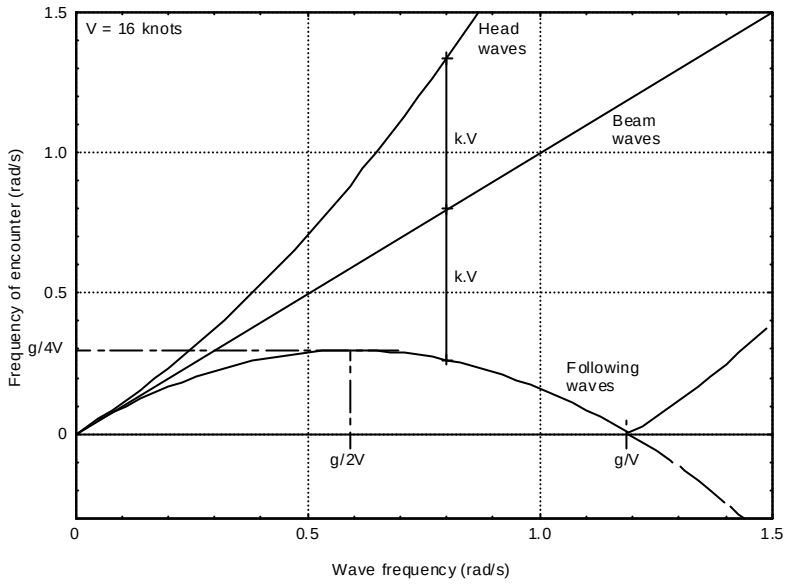

Figure 8.13: Relation between ω_e and ω

Equation 8.76 is plotted in figure 8.13 for a forward speed of 16 knots. The upper curve is for head waves - approaching from the bow; the frequency of encounter becomes higher than the wave frequency ($\omega_e > \omega$).
There is no frequency shift for waves which approach from abeam ($\mu = \pm\pi/2$) so that $\omega_e = \omega$ as is shown in the figure, too.

The situation with following seas requires the most thought:

- When $\omega_e \to 0$, the speed of the waves becomes high and ω_e is only slightly influenced by V (which is smaller than c).
- As ω increases - from small values - the wave speed decreases slowly so that V becomes more and more important. From equation 8.77 follows that ω_e has a maximum value (with waves coming from behind) when $\omega = g/(2V)$. The corresponding ω_e value is $\omega_e = g/(4V)$; this is the highest apparent frequency that will be observed with waves coming from behind. Since $d\omega_e/d\omega$ is here zero, one can expect problems with $S_\zeta(\omega_e)$ at this frequency - see equation 8.75.
- As ω increases beyond $\omega = g/(2V)$, the wave speeds continue to decrease so that ω_e deceases as well.
- At some even higher frequency $\omega = g/V$, the wave speed, c, matches the ship speed, V. The ship can "surf" on this wave!
- Waves with frequencies higher than $\omega = g/V$ are moving more slowly than the ship. The ship intercepts these waves from behind so that these behave as head waves! Because negative frequencies are not "normal" - these values are shown by the dashed line - their absolute value is plotted instead.

Note as well that for any wave frequency, ω, the difference between the encounter frequency in head waves and the absolute wave frequency (equal to the encounter frequency in beam

seas) is the same as the difference between this absolute wave frequency and its encounter frequency in a following sea. This follows from the symmetry in equation 8.76. These two values are labeled "$k \cdot V$" in figure 8.13.

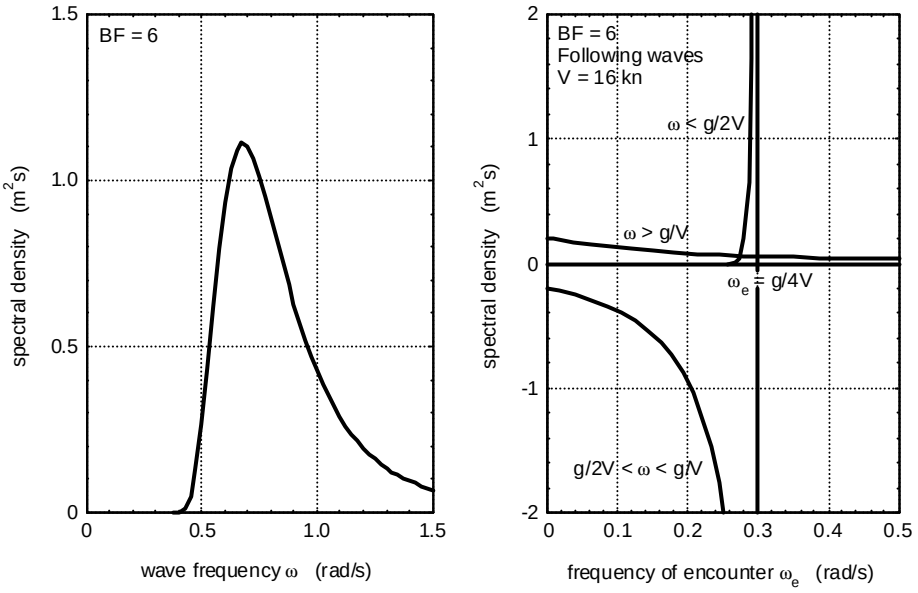

Figure 8.14: Transformed Wave Spectrum in Following Waves

Figure 8.14 shows how a wave spectrum is distorted when it is transformed in terms of encounter frequency in following waves. This type of distortion takes place whenever the waves have a velocity component in the same sense as the ship speed - whenever the waves approach from any direction aft of "beam seas". This spectrum will be hard to work with! When waves are approaching from any direction forward of "beam seas" encounter frequencies only become higher than the absolute frequencies; no special problems are encountered - see figure 8.15.
This is all used as is described below.

8.5.2 Response Spectra

The response spectrum of a motion (or response, r) on the basis of encounter frequency, ω_e, can be found from the transfer function of the motion and the wave spectrum by:

$$\boxed{S_r(\omega_e) = \left|\frac{r_a}{\zeta_a}(\omega_e)\right|^2 \cdot S_\zeta(\omega_e)} \tag{8.78}$$

The moments of the response spectrum are given by:

$$\boxed{m_{nr} = \int_0^\infty \omega_e^n \cdot S_r(\omega_e) \cdot d\omega_e} \qquad \text{with: } n = 0, 1, 2, ... \tag{8.79}$$

This computation causes no difficulty when $S_{\zeta\zeta}(\omega_e)$ is not well behaved - as in following seas. This problem can be avoided if the necessary moments are computed as follows, instead of using equation 8.79:

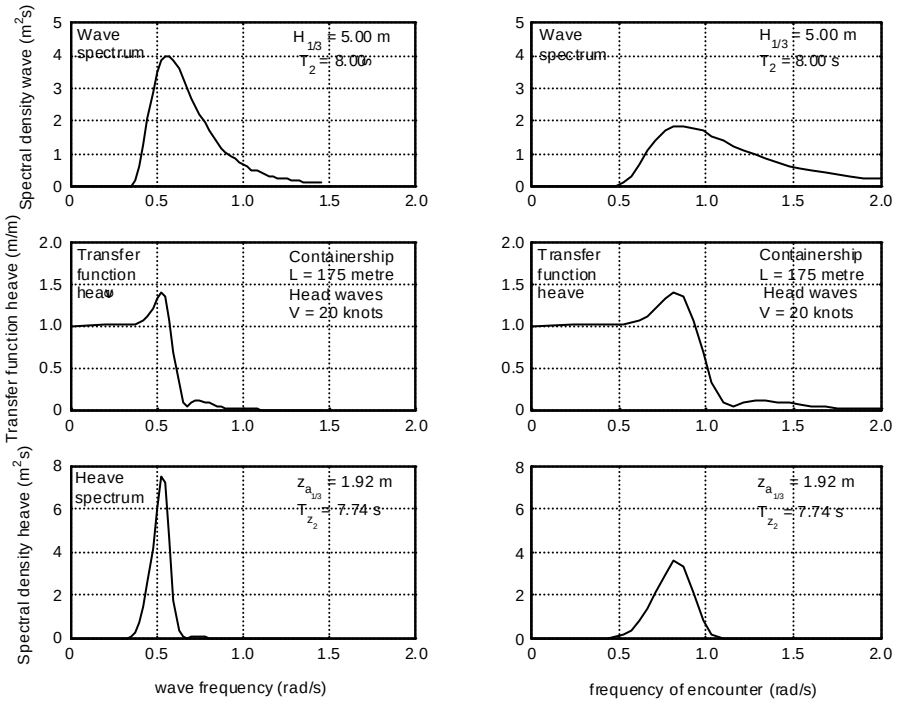

Figure 8.15: Heave Spectra in the Wave and Encounter Frequency Domains

$$
\begin{aligned}
m_{0r} &= \int_0^\infty S_r(\omega_e)\cdot d\omega_e \qquad = \int_0^\infty S_r(\omega)\cdot d\omega \\
m_{1r} &= \int_0^\infty \omega_e\cdot S_r(\omega_e)\cdot d\omega_e = \int_0^\infty \omega_e\cdot S_r(\omega)\cdot d\omega \\
m_{2r} &= \int_0^\infty \omega_e^2\cdot S_r(\omega_e)\cdot d\omega_e = \int_0^\infty \omega_e^2\cdot S_r(\omega)\cdot d\omega
\end{aligned}
\tag{8.80}
$$

This avoids integrations of $S_r(\omega_e)$ or $S_\zeta(\omega_e)$ over ω_e.
Note that a negative spectral value in figure 8.14 does not imply a negative energy; both $S_\zeta(\omega_e)$ and $d\omega_e$ are negative and the energy is their product: the area $S_\zeta(\omega_e)\cdot d\omega_e$ (which is positive).
The significant amplitude can be calculated from the spectral density function of a response. The significant amplitude is defined to be the mean value of the highest one-third part of the highest response amplitudes, or equivalently:

$$
\boxed{r_{a_{1/3}} = 2\sqrt{m_{0r}} = 2\cdot RMS}
\tag{8.81}
$$

A mean period can be found from the centroid of the spectrum (T_{1r}) or from the radius of gyration of the spectrum (zero-upcrossing period, T_{2r}):

$$
\boxed{T_{1r} = 2\pi\cdot\frac{m_{0r}}{m_{1r}}} \qquad \text{and} \qquad \boxed{T_{2r} = 2\pi\cdot\sqrt{\frac{m_{0r}}{m_{2r}}}}
\tag{8.82}
$$

Because of the linearity, which results in a linear relationship between the motion amplitude and the regular wave amplitude, and the (ideal) wave spectrum defined by $S_{\zeta\zeta}(\omega) = H_{1/3}^2 \cdot f(\omega, T)$, the calculated significant response amplitude values in irregular waves are often presented as:

$$\frac{r_{a_{1/3}}}{H_{1/3}} \quad \text{versus:} \quad T \ (= T_1, T_2 \text{ or } T_p)$$

in which $H_{1/3}$ is the significant wave height, T ($= T_1$, T_2 or T_p) are mean wave periods and $f(\omega, T)$ is a function of ω and T only.
Spectra of response velocities and accelerations are found by a multiplication of the RAO of the displacement with ω_e and ω_e^2, respectively. Because the squares of the RAO are used to define the response spectra, the spectral moments can be written as:

$$\begin{aligned} m_{0\dot{r}} &= m_{2r} \qquad \text{and} \qquad m_{0\ddot{r}} = m_{2\dot{r}} = m_{4r} \\ m_{1\dot{r}} &= m_{3r} \qquad \text{and} \qquad m_{1\ddot{r}} = m_{3\dot{r}} = m_{5r} \\ m_{2\dot{r}} &= m_{4r} \qquad \text{and} \qquad m_{2\ddot{r}} = m_{4\dot{r}} = m_{6r} \end{aligned} \tag{8.83}$$

8.5.3 First Order Motions

Figure 8.16 shows an example of the striking influence of the average wave period on a response spectrum. This response is the heave motion of a 175 meter container ship, sailing with a speed of 20 knots in head waves with a significant wave height of 5.0 meters.

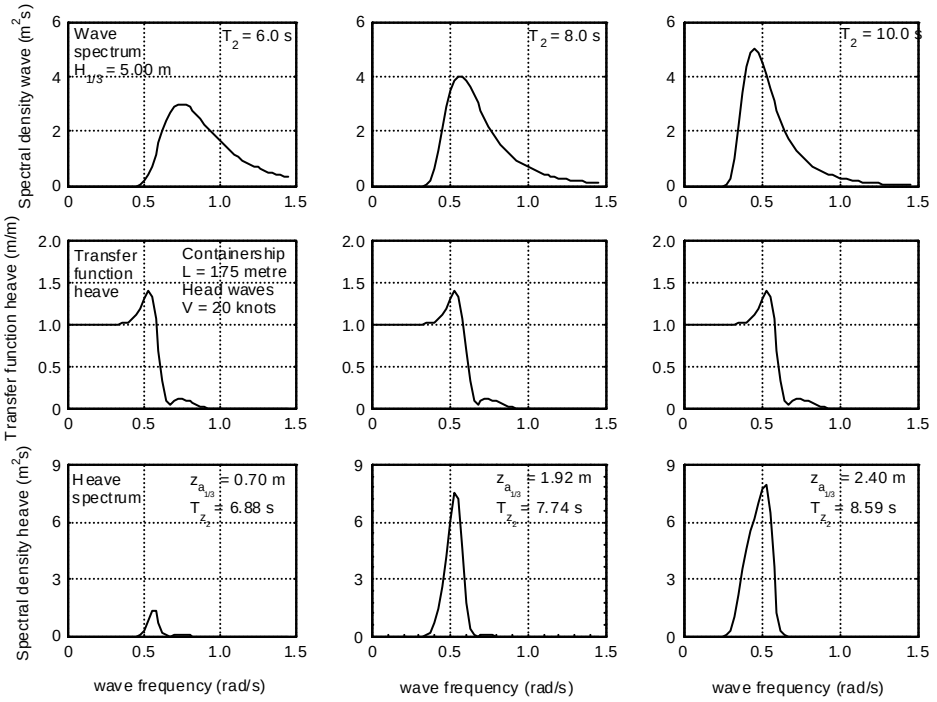

Figure 8.16: Effect of Wave Period on Heave

For the wave spectrum with an average period of 6.0 seconds, the transfer function has very low values in the wave frequency range. The response spectrum becomes small; only

small motions result. As the average wave period gets larger (to the right in figure 8.16), the response increases dramatically.

A similar effect will be obtained for a larger range of average wave periods if the transfer function of the motion shifts to the low frequency region. A low natural frequency is required to obtain this. This principle has been used when designing semi-submersibles, which have a large volume under water and a very small spring term for heave (small water plane area). However, such a shape does not make much of a wave when it oscillates; it has little potential damping. This results in large (sometimes very large) *RAO*'s at the natural frequency. As long as there is (almost) no wave energy at this frequency, the response spectrum will remain small.

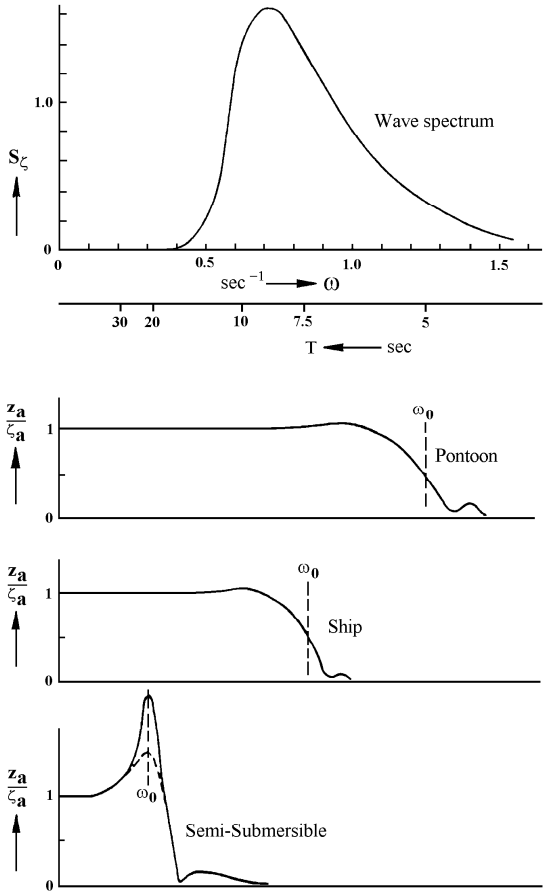

Figure 8.17: Effect of Natural Period on Heave Motions

Figure 8.17 shows a wave spectrum with sketches of *RAO*'s for heave of three different types of floating structures at zero forward speed:

- The **pontoon** has a relatively high natural frequency and as a result of this significant *RAO* values over a large part of the normal wave frequency range. Almost all wave energy will be transferred into heave motions, which results in a large motion spectrum.
  An extreme example is the **wave buoy**, which has (ideally) an *RAO* of 1.0 over the whole frequency range. Then the response spectrum becomes identical to the wave

spectrum, which is of course the aim of this measuring tool. It should follow the water surface like a sea gull!

- The **ship**, with a lower natural frequency, transfers a smaller but still considerable part of the wave energy into heave motions.
- The **semi-submersible** however, with a very low natural frequency (large mass and small intersection with the water line), transfers only a very small part of the wave energy; very low first order heave motions will appear; it remains essentially stable in the waves.

One can conclude that the natural frequency is a very important phenomenon which dictates (to a significant extent) the behavior of the structure in waves. Whenever possible, the natural frequency should be shifted out of the wave frequency region.
The fact that the resonant frequency of a motion does not necessarily coincide with the natural frequency has been explained earlier in this chapter. A clear example of this is given by [Hooft, 1970], as shown in figure 8.18, for a semi-submersible platform with different dimensions of the under water geometry. This geometry has been configured in such a way that the responses are minimal at the natural frequency.

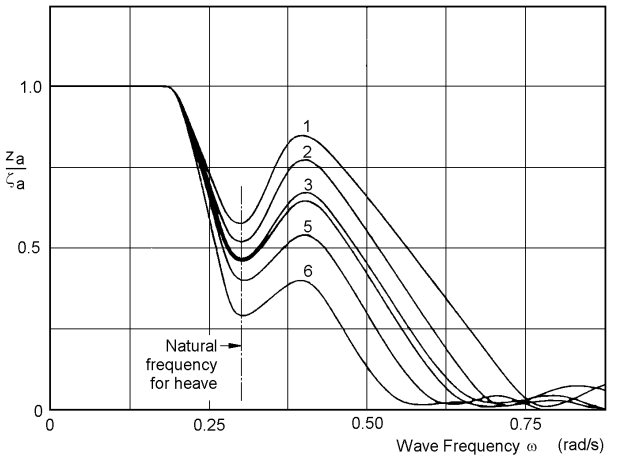

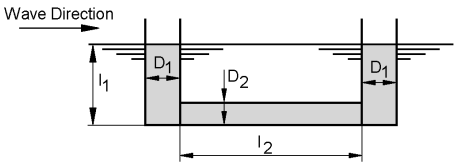

Platform	Dimensions (m)			
	D_1	l_1	D_2	l_2
1	11.11	16.52	10.06	111.10
2	11.11	20.71	8.91	133.50
3	11.11	25.82	8.02	155.80
4	25.00	31.61	17.33	150.00
5	25.00	38.12	15.30	175.00
6	25.00	55.06	11.62	225.00

[Source: Hooft, 1970]

Figure 8.18: Heave Responses of Semi-Submersible Platforms in Waves

8.5.4 Probability of Exceeding

The probability density function of the maximum and minimum values, in case of a spectrum with a frequency range which is not too wide, is given by the Rayleigh distribution - see chapter 5:

$$\boxed{f(r_a) = \frac{r_a}{m_{0r}} \cdot \exp\left\{\frac{-r_a^2}{2m_{0r}}\right\}} \tag{8.84}$$

This implies that the probability of exceeding a threshold value a by the response amplitude r_a becomes:

$$P\{r_a > a\} = \int_a^\infty \frac{r_a}{m_{0r}} \cdot \exp\left\{\frac{-r_a^2}{2m_{0r}}\right\} \cdot dr_a \tag{8.85}$$

Thus:

$$\boxed{P\{r_a > a\} = \exp\left\{\frac{-a^2}{2m_{0r}}\right\}}$$

The average number of times per hour that this happens follows from:

$$\boxed{N_{hour} = \frac{3600}{T_{2r}} \cdot P\{r_a > a\}} \tag{8.86}$$

Note that the zero-crossing period, T_{2r}, is used here, because this period determines the number of cycles per hour.

8.6 Liquids in Tanks

When a double bottom tank, a cargo tank or any other space in a rolling vessel contains a fluid with a free surface, gravity waves will appear at this surface. These gravity waves will cause additional roll exciting moments from within the vessel. In theory this is true for pitch as well, but the generally relatively large longitudinal metacentric height makes the ship less sensitive to this.
Consider a rectangular tank with a length l and a breadth b, which has been filled until a level h with a (non-viscous) fluid. The bottom of the tank is s meters above the center of rotation (center of gravity, G) of the vessel. Figure 8.19 shows a 2-D sketch of this tank with the axis system and notations.

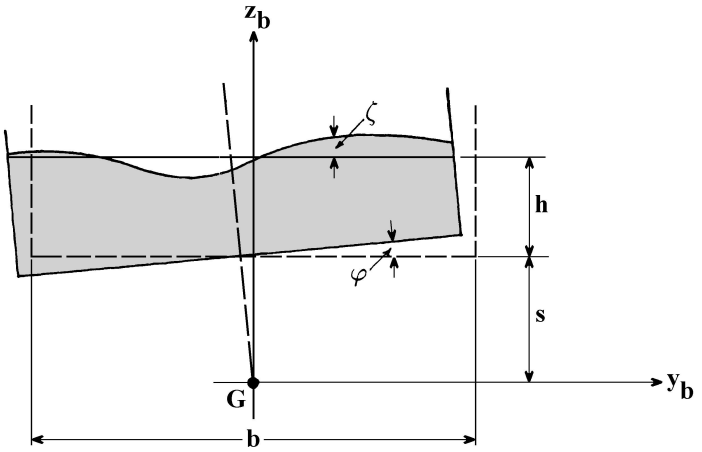

Figure 8.19: Definitions of a Rolling Tank

The natural frequency of the surface waves in a rolling tank appears when the wave length, λ, equals twice the breadth, b, so: $\lambda = 2b$.
With the wave number and the dispersion relation:

$$k = \frac{2\pi}{\lambda} \quad \text{and} \quad \omega = \sqrt{kg\tanh(kh)} \tag{8.87}$$

it follows for the natural frequency of surface waves in the tank:

$$\boxed{\omega_0 = \sqrt{\frac{\pi g}{b} \tanh\left(\frac{\pi h}{b}\right)}} \tag{8.88}$$

At small liquid depths ($h/b <\approx 0.1$), these resonant frequencies can be associated with high wave amplitudes. Under these circumstances a hydraulic jump or bore is formed, which travels periodically back and forth between the walls of the tank. This hydraulic jump can be a strongly non-linear phenomenon. Extensive 2-D model experiments on the behavior of the fluid in these so-called **free surface tanks** was carried out in the sixties by [Bosch and Vugts, 1966]. The experimental results of their study are nowadays still used to design a very simple anti-rolling device which works also at zero forward speed: the free-surface anti-roll tank. Apart from this experimental research, a fundamental theory, based on gas-dynamics for the shock wave in a gas flow under similar resonance circumstances, was developed in the sixties by [Verhagen and van Wijngaarden, 1965]. They used two different approaches: one for low and high frequencies and another one for frequencies near to the natural frequency of the tank. Recently, their approaches to describe the linear(ized) motions of the fluid have been implemented in a ship motions computer code. A very good agreement between theory and experiments was found, see [Journée, 1997].

At larger water depths ($h/b >\approx 0.1$), the behavior of the fluid tends to be more linear. Linear potential theory with the pulsating source method of [Frank, 1967], as described before for strip theory, can be used as well to describe the motions and resulting counteracting moments of fluids in a tank.
First, the study of [Bosch and Vugts, 1966] on the effect of a free-surface tanks with a low water depth on roll motions will be summarized. Then, an application of the potential theory of [Frank, 1967] for the estimation of counteracting roll moments of fluids in a liquid cargo tank and its effect on roll motions is given and the results are discussed.

8.6.1 Anti-Roll Tanks

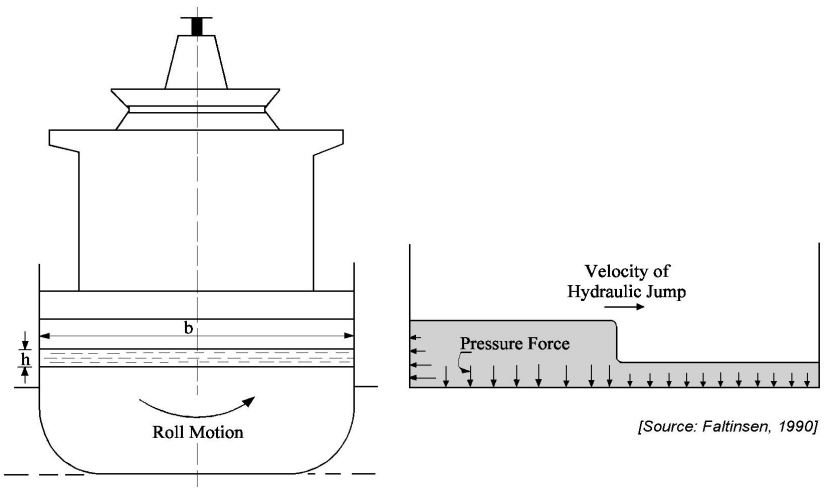

Figure 8.20: Passive Anti-Roll Stabilizer and Hydraulic Jump

A passive free-surface tank can be a very good tool to reduce roll motions, especially at low speeds where anti-roll fins are not effective. This tank has a breadth equal to the ship's breadth and its length is about 1.5 to 2.5 meter, depending on the size of the ship. The roll damping, caused by a passive free-surface tank, is essentially based on the existence of a hydraulic jump or bore in the tank, as shown in figure 8.20. [Bosch and Vugts, 1966] have described the physical behavior of passive free-surface tanks, used as an anti-roll device. They assembled extensive quantitative information on the counteracting moments caused by the water transfer in the tank. Using their notation, the roll motions and the exciting moments of an oscillating rectangular free-surface tank, are defined by:

$$\begin{aligned} \varphi &= \varphi_a \cos(\omega t) \\ K_t &= K_{t_a} \cos(\omega t + \varepsilon_{t\varphi}) \end{aligned} \tag{8.89}$$

In a practical frequency range, [Bosch and Vugts, 1966] have presented experimental data on the roll moment amplitudes, K_{t_a}, and the phase shifts of these moments with respect to roll, ε_t, for three roll amplitudes ($\varphi_a = 0.033, 0.067, 0.100$ rad), four centers of rotations ($-0.40 \leqq s/b \leqq +0.20$) and five water depths ($0.02 \leqq h/b \leqq 0.10$). An example of the experimental data is given figure 8.21.
The external roll moment due to a free surface tank, oscillating with a frequency ω, can be written as:

$$K_t = a_{4\varphi} \cdot \ddot{\varphi} + b_{4\varphi} \cdot \dot{\varphi} + c_{4\varphi} \cdot \varphi \tag{8.90}$$

with:

$$\begin{aligned} a_{4\varphi} &= 0 \\ b_{4\varphi} &= \frac{K_{t_a}}{\omega \varphi_a} \cdot \sin \varepsilon_{t\varphi} \\ c_{4\varphi} &= \frac{K_{t_a}}{\varphi_a} \cdot \cos \varepsilon_{t\varphi} \end{aligned} \tag{8.91}$$

It is obvious that for an anti-roll free-surface tank, build in the ship, the motions of ship and tank are similar:

$$\phi_a = \varphi_a \qquad \text{and} \qquad \omega_e = \omega$$

One can express the roll motion of the ship as well as the tank moment on the ship as:

$$\begin{aligned} \phi &= \phi_a \cos(\omega_e t + \varepsilon_{\phi\zeta}) \\ K_t &= K_{t_a} \cos(\omega_e t + \varepsilon_{\phi\zeta} + \varepsilon_{t\varphi}) \end{aligned} \tag{8.92}$$

Then, an additional exciting moment has to be added to the right hand side of the equations of motion for roll:

$$\boxed{X_{tank_4} = a_{44_{tank}} \cdot \ddot{\phi} + b_{44_{tank}} \cdot \dot{\phi} + c_{44_{tank}} \cdot \phi} \tag{8.93}$$

with:

$$a_{44_{tank}} = 0 \tag{8.94}$$

$$b_{44_{tank}} = \frac{K_{t_a}}{\omega_e \phi_a} \cdot \sin \varepsilon_{t\varphi} \tag{8.95}$$

$$c_{44_{tank}} = \frac{K_{t_a}}{\phi_a} \cdot \cos \varepsilon_{t\varphi}$$

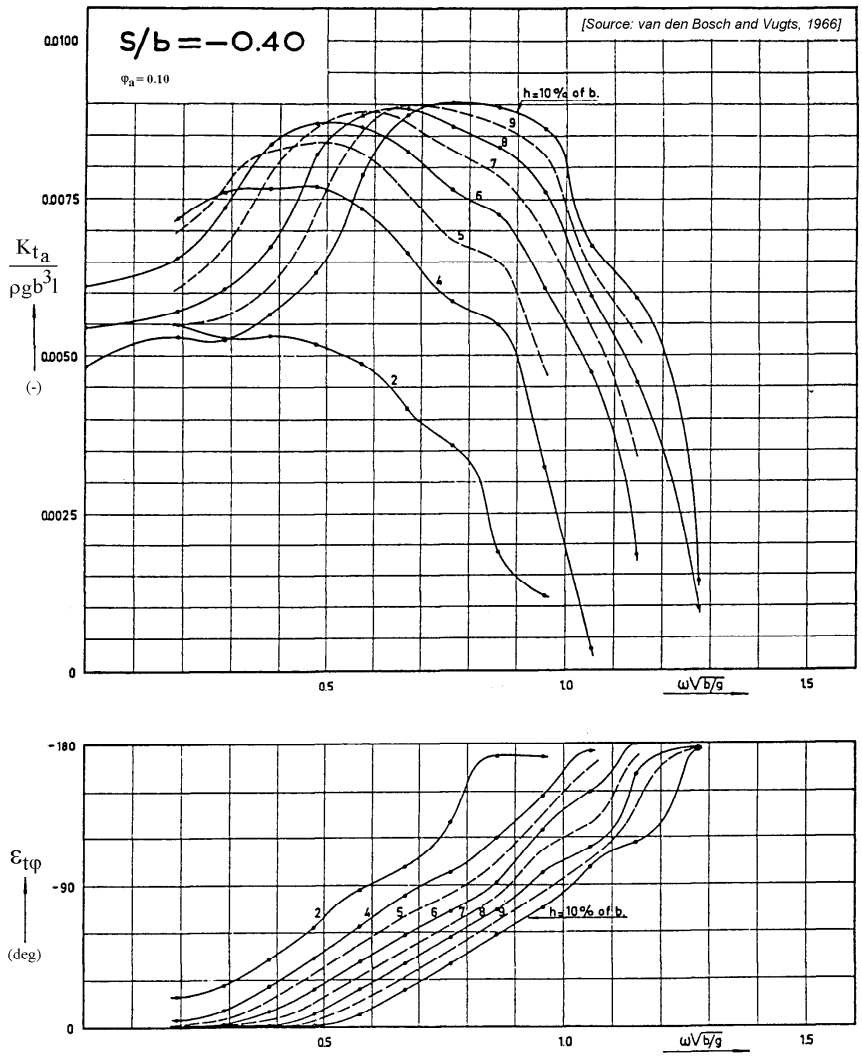

Figure 8.21: Experimental Data on Anti-Roll Free Surface Tanks

This holds that the anti-roll coefficients $a_{44_{tank}}$, $b_{44_{tank}}$ and $c_{44_{tank}}$ have to be subtracted from the coefficients a_{44}, b_{44} and c_{44} in the left hand side of the equations of motion for roll.

Figure 8.22 shows the significant reduction of the roll transfer functions for a trawler with a free surface tank.

8.6.2 Tank Loads

[Frank, 1967] used a cylinder, whose cross section is a simply connected region, which is fully or partly immersed horizontally in a previously undisturbed fluid of infinite depth for the calculation of the 2-D potential mass and damping of ship-like cross sections, see chapter 7.

Frank's method is suitable for the computation of the potential mass and damping of symmetric 2-D shapes, in or below the surface of a fluid. This method has been incorporated in a lot of 2-D ship motions computer programs, all over the world. Starting from the

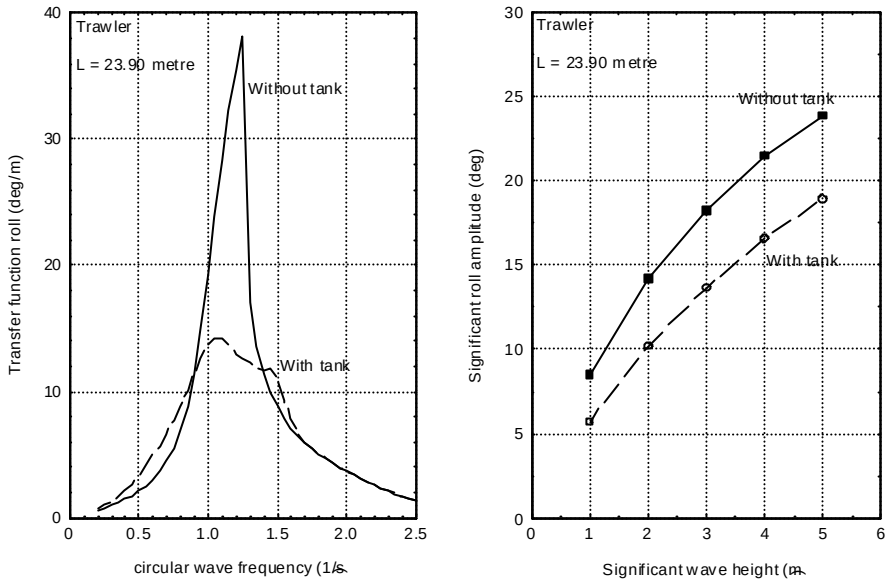

Figure 8.22: Effect of Free Surface Tanks on Roll

keel point of the cross section, the input data (the off-sets) have to be read in an upwards order. Then, the (outward) normal on the elements of the cross section will be defined to be positive in the direction of the fluid outside the cross section.
This method can be adapted easily to calculate the linear loads due to a potential flow fluid in an oscillating symmetrical tank, too. Starting from the intersection of the free surface with the tank wall, the offsets of the tank have to be read in a downwards order - in an opposite sequence as has been done for the cross section of a ship. By doing this, the (inward) normal on the elements of the cross section of the tank will be defined to be positive in the direction of the fluid in the tank. Then, the calculated potential mass and damping delivers the in-phase and out-of-phase parts of the loads due to the moving liquid in the tank. With this, the in-phase and out-of-phase parts of the additional 2-D excitation forces and moments on the ship in and about an origin at the still water fluid surface in a rectangular tank are:

$$\begin{aligned}
\text{Sway tank force, in-phase:} \quad & X_{2c} = \omega^2 M^{(2)} x_{2a} \\
\text{Sway tank force, out-of-phase:} \quad & X_{2s} = -\omega N^{(2)} x_{2a} \\
\text{Heave tank force, in-phase:} \quad & X_{3c} = \omega^2 M^{(3)} x_{3a} \\
\text{Heave tank force, out-of-phase:} \quad & X_{3s} = -\omega N^{(3)} x_{3a} \\
\text{Roll tank moment, in-phase:} \quad & X_{4c} = \omega^2 M^{(4)} x_{4a} + \rho g \left\{ bh \left(s + \frac{h}{2} \right) + \frac{b^3}{12} \right\} x_{4a} \\
\text{Roll tank moment, out-of-phase:} \quad & X_{4s} = -\omega N^{(4)} x_{4a}
\end{aligned} \tag{8.96}$$

in which $M^{(i)}$ and $N^{(i)}$ are the potential mass and damping terms obtained by Frank's method.
The roll moments above must be "translated" to moments about the ship's center of gravity. The second and third term in the in-phase roll moment expression, X_{4c}, are additional "static" terms caused by the "solid or frozen" liquid and by the emerged and immersed wedges of the "fluid or thawed" liquid; see chapter 2 on static floating stability.

This approach can be carried out easily with many existing 2-D, but also 3-D, ship motions computer programs.

Roll Moments

Forced roll oscillation experiments have been carried out with a 2-D model of a cargo tank of an LNG carrier to verify this theoretical approach. A sketch of this 1:25 model of the tank is given in figure 8.23.

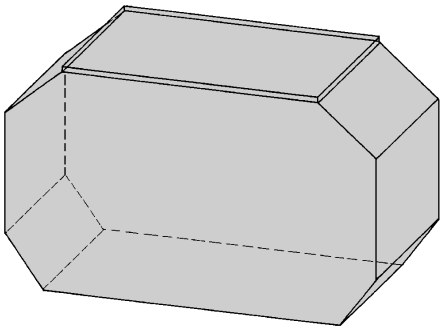

Figure 8.23: LNG Cargo Tank

The exciting roll moments have been measured for a range of oscillation frequencies and a fixed roll amplitude of 0.10 radians for several tank filling levels. Figure 8.24 shows measured and predicted in-phase and out-of-phase parts of the first harmonic of the roll moments of a 45 per cent filled LNG tank as a function of the frequency of oscillation, see [Journée, 1997]. Except at the natural frequency of the fluid in the tank, a fairly good prediction has been found with Frank's 2-D pulsating source method as incorporated in the 2-D computer program SEAWAY. Use of the 3-D computer code DELFRAC provides a similar agreement.

Roll Motions

To investigate the effect of free surface (liquid cargo) tanks on the roll motions of a ship, three tanks as given in figure 8.23 were build in a 1:60 model of an LNG carrier and equally filled with water up to 45 % of the tank height. All other cargo tanks were assumed to be filled up to 97.5 per cent, which was simulated in the experiments by solid ballast weights and an adaptation of the ship's roll radius of gyration.
First, the three cargo tanks are supposed to be equally filled up to 45 % of the tank height with a homogeneous frozen liquid cargo with a stowage factor of 1.00 ton/m^3, simulated during the experiments by solid ballast weights. The unknown radius of gyration for roll of the model has been obtained from free decay tests and the roll motions have been calculated with strip theory program SEAWAY, using the semi-empirical method of [Ikeda et al., 1978] to obtain the linearized viscous roll damping coefficients.
Then, the cargo is "allowed to melt". The ship's roll radius of gyration caused by its own mass has been obtained from the radius of gyration of the ship with the frozen liquid cargo and a theoretical correction for thawing this cargo. The exciting roll moments due to the liquid cargo have been obtained with Frank's method. Now, the roll motions have been calculated, including the effect of the fluid motions in the three tanks.

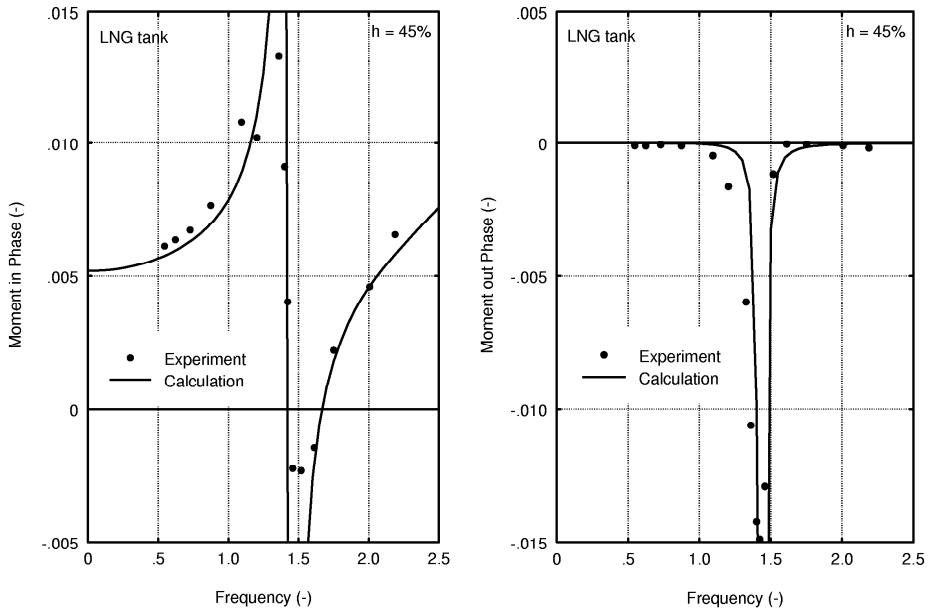

Figure 8.24: Loads Caused by an LNG Cargo Tank

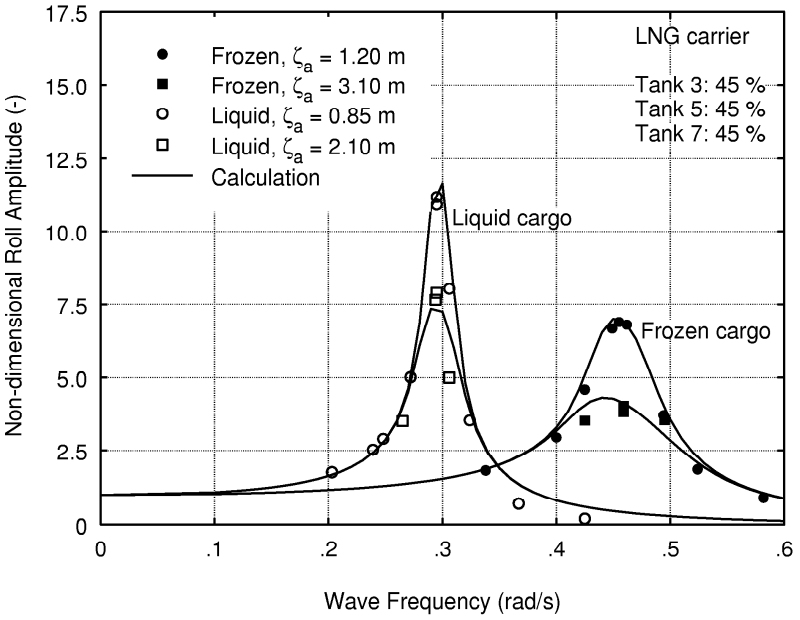

Figure 8.25: Roll an LNG Carrier

Except for some overestimation at higher frequencies, figure 8.25 shows a very good agreement between the predicted and the measured response amplitude operators for roll. However, it must be noted that the natural roll frequency of the ship is about half the lowest natural frequency of the fluid in the three cargo tanks. When these frequencies are closer to each other, non-linear effects caused by the bore or the hydraulic jump at the surface of the fluid in the tanks will play a much more important role.

8.7 Internal Loads

Attention so far has focussed on the external loads on and response of a floating structure caused by the surrounding sea and even liquids stored in tanks on board. This section goes a step further to study the resulting internal reaction forces and moments within the ship structure which is treated here as a single member for which the shear forces as well as bending moments on transverse planes are to be determined.
Obviously additional data on the ship will be needed in order to carry out these computations; the required information includes:

- $m'(x_b)$: mass or weight distribution along the ship's length
- $z'_m(x_b)$: distribution along the ship's length of the vertical location of the center of gravity
- $k'_{xx}(x_b)$: distribution along the ship's length of the mass radius of gyration

Figure 8.26 shows the mass distribution, $m'(x_b)$, as well as the mass of the displacement distribution, $\rho A_x(x_b)$, of a cruise ship. Indeed, one often finds that the ship's weight exceeds its buoyancy toward the bow and the stern; this is compensated by an excess of buoyancy amidships.

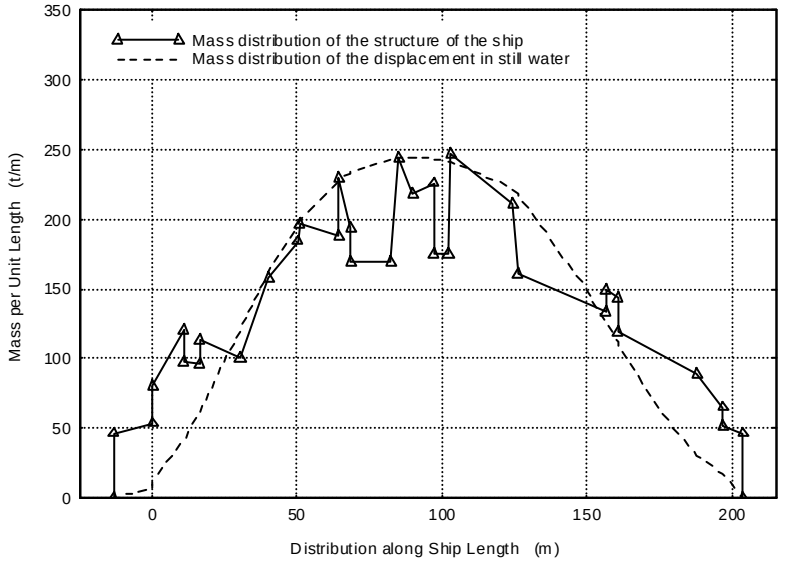

Figure 8.26: Mass Distributions of a Cruise Ship

The total mass of the ship, m, is found by an integration of the masses per unit length,

$m'(x_b)$:

$$m = \int_{stern}^{bow} m'(x_b) \cdot dx_b \tag{8.97}$$

It is obvious that this integrated mass should be equal to the mass of displacement, calculated from the underwater hull form:

$$m = \rho \int_{stern}^{bow} A_x(x_b) \cdot dx_b = \rho\nabla \tag{8.98}$$

The longitudinal position of the center of gravity, x_G, is found from the mass and the distribution of the masses over the length:

$$x_G = \frac{1}{m} \int_{stern}^{bow} m'(x_b) \cdot x_b \cdot dx_b \tag{8.99}$$

The ship's center of buoyancy, x_B, must be at the same longitudinal position (no external trimming moment), so that :

$$x_G = x_B \tag{8.100}$$

The transverse radius of inertia, k_{xx}, is found from the mass and the distribution of the radii of gyration of the masses, $k'_{xx}(x_b)$, over the length:

$$k_{xx}^2 = \frac{1}{m} \int_{stern}^{bow} m'(x_b) \cdot k'^2_{xx}(x_b) \cdot dx_b \tag{8.101}$$

For a relatively slender body, the longitudinal radius of gyration of the mass, k_{yy} and k_{zz}, are found from the mass and the distribution of the masses over the length:

$$k_{yy}^2 = k_{zz}^2 = \frac{1}{m} \int_{stern}^{bow} m'(x_b) \cdot x_b^2 \cdot dx_b \tag{8.102}$$

The position in height of the center of gravity, z_G, is found from the mass and the distribution of the heights of the centers of gravity, $z'_m(x_b)$, over the length:

$$z_G = \frac{1}{m} \int_{stern}^{bow} m'(x_b) \cdot z'_m(x_b) \cdot dx_b \tag{8.103}$$

It is obvious that this value should be zero for an axes system with the origin in the center of gravity, G.

8.7.1 Basic Approach

The ship will be made schematic as a single beam along its longitudinal axis in order to determine its the internal loads on each of its transverse cross sections. These internal loads can come from:

- axial normal force parallel to the x_b axis,
- vertical or horizontal shear in a plane parallel to the (y_b, z_b) plane,
- torsion about an axis parallel to the x_b axis,
- bending about axes parallel to the y_b or z_b axes.

Unlike most more conventional beams, generally all of this beam's properties will be functions of position along its length. The moment of inertia of its area for example will be smaller near the bow and stern of most ships.

The axes system (of which the hydrodynamic sign convention differs from that commonly used in structural engineering) and the internal load definitions are given in figure 8.27.

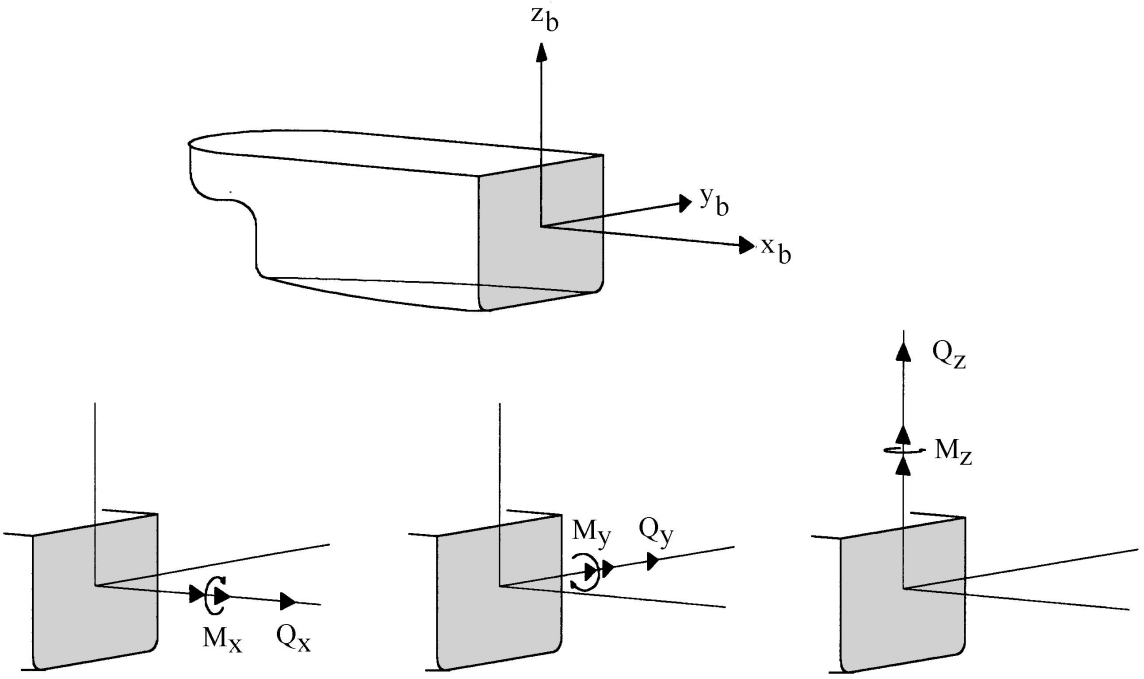

Figure 8.27: Axis System and Internal Load Definitions

Consider a section of the ship with a length dx_b, as illustrated in figure 8.28, to calculate the shear forces and the bending and torsional moments.

When the ship slice is subjected by a load distribution $q(x_b)$, this implies for the slice:

$$q(x_b) \cdot dx_b = -dQ(x_b) \qquad \text{so:} \qquad \boxed{\frac{dQ(x_b)}{dx_b} = -q(x_b)}$$

$$Q(x_b) \cdot dx_b = +dM(x_b) \qquad \text{so:} \qquad \boxed{\frac{dM(x_b)}{dx_b} = +Q(x_b)} \tag{8.104}$$

in which $Q(x_b)$ is the shear force and $M(x_b)$ is the bending moment.

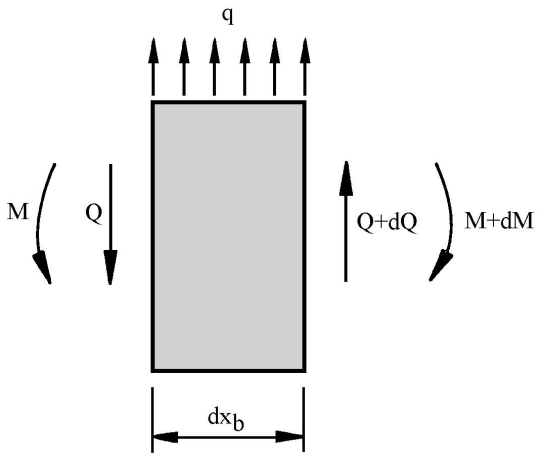

Figure 8.28: Loads on a Cross Section

The shear force and the bending moment in a cross section at $x_b = x_1$ follow from an integration of these sectional loads from the stern of the ship to this cross section. Indeed, both Q and M must be zero at the ends of the ship.
The shear force, $Q(x_1)$, and the bending moment, $M(x_1)$, in a cross section at $x_b = x_1$ can be expressed in the load distribution, $q(x_b)$, by the following integrals:

$$Q(x_1) = -\int_{stern}^{x_1} q(x_b) \cdot dx_b \tag{8.105}$$

$$\begin{aligned} M(x_1) &= -\int_{stern}^{x_1} q(x_b) \cdot (x_1 - x_b) \cdot dx_b \\ &= +\int_{stern}^{x_1} q(x_b) \cdot x_b \cdot dx_b - x_1 \cdot \int_{stern}^{x_1} q(x_b) \cdot dx_b \\ &= +\int_{stern}^{x_1} q(x_b) \cdot x_b \cdot dx_b + Q(x_1) \cdot x_1 \end{aligned} \tag{8.106}$$

For the torsional moment, an approach similar to that given for the shear force can be used.

8.7.2 Static Equilibrium

Static conditions are used first to make a number of concepts more clear. The "ship as a beam" is subjected to two distributed vertical loads: one from the weight of the ship and one from its buoyancy. While overall equilibrium of the ship requires that the total (integrated) buoyant force be equal to the total (integrated) weight of the floating body, their distributions need not be exactly the same so that a net load on any transverse section can be defined.

Consider the forces acting on a section of the ship with a length dx_b. The vertical forces on a transverse 'slice' of a ship in still water are given by:

$$(m' \cdot dx_b) \cdot (-g) = q_z(x_b) \cdot dx_b \tag{8.107}$$

in which:

$$\boxed{q_z(x_b) = \{\rho \cdot A_x(x_b) - m'(x_b)\} \cdot g} \tag{8.108}$$

where A_x is the cross sectional area.
With equations 8.105 and 8.106, the vertical shear force, $Q_z(x_1)$, and the bending moment, $M_y(x_1)$, in still water in a cross section can be obtained from the vertical load, $q_x(x_b)$, by the following integrals:

$$\boxed{Q_z(x_1) = -\int_{stern}^{x_1} q_z(x_b) \cdot dx_b}$$

$$\boxed{M_y(x_1) = +\int_{stern}^{x_1} q_z(x_b) \cdot x_b \cdot dx_b + Q_z(x_1) \cdot x_1} \tag{8.109}$$

Figure 8.29 shows an example of a calculated still water bending moment, M_y, curve of a cruise ship with a weight and buoyancy distribution as given in figure 8.26.

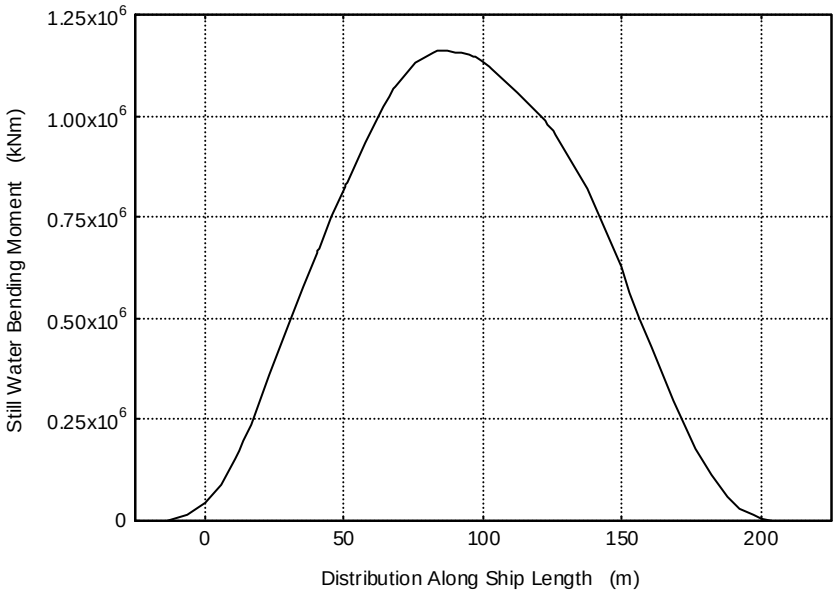

Figure 8.29: Distribution of Still Water Bending Moments of a Cruise Ship

The generally positive moment here is common in ships. As used here, a positive moment implies that the bow and stern of the ship tend to bend down. This if often called **hogging**; the opposite tendency is called **sagging**.
Still water bending moments can become significant. A well-known example of some years ago is the supertanker Energy Concentration moored in Europoort. It suffered the consequences of completely emptying the amidships cargo tanks while the fore and aft tanks

remained completely filled. In this case the ship hogged so much that the lower part of the hull failed in compression and 'folded'; luckily the tanks affected were empty so that a major oil spill was averted.

Figure 8.30: Damaged Supertanker Energy Concentration

Static shear forces as well as bending moments must also be kept in mind when moving a heavy offshore structure on to a transport barge - or when launching a heavy tower offshore, too, for that matter. Nothing in the offshore industry as spectacular as the fate of the above tanker is known to the authors, however. The important lesson from these examples is that even when the ship (as a whole) is in static equilibrium, it may at the same time be experiencing some very significant internal loads.
As long as the center of gravity of each transverse 'slice' of the ship lies on its midline plane of symmetry, there will be no torsional moment (about the x-axis) generated in the ship. On the other hand, a barge carrying two heavy loads - one forward and to port with the other on the starboard side aft - would have a significant internal torsional moment about its longitudinal axis. Such a loading would disrupt the dynamic behavior of the ship as well, reason enough to leave this topic for others.
The bending moment about the z-axis will always be zero for a free-floating ship in still water.

8.7.3 Quasi-Static Equilibrium

A quasi-static situation exists when none of the dynamic excitations involve accelerations. This means that they change so slowly that the object can be considered to respond statically to the external loads. Quasi-static horizontal loads can be exerted on a moored floating structure by currents and wind, especially when the heading of the ship is not optimal.

The ship is now a beam (when seen from above) which has a location-dependent distributed load and concentrated reaction forces (similar to the supports of a conventional beam) at the mooring line attachment points. Otherwise, the analysis is much like that for the static vertical load case handled above. In general the ends of the ship are still 'free' so that both the horizontal crosswise shear, Q_y, and moment, M_z, will be zero at each end of the ship.

There is more to this that has not yet been considered, however! In general the horizontal forces from the anchor lines, the transverse wind loads and the transverse current loads will not all act at the same elevation; the various forces will act at different elevations in the (x, z) plane. This has two consequences.

As a whole, the floating body will generally come to a static roll angle so that any imbalance of the externally caused external moments will be held in equilibrium by a static roll moment. A good example of this is how a sailboat with the wind on the beam will heel as a result of the wind load in one direction on the sails and the lateral hydrodynamic resistance of the hull working in the other direction; see figure 8.31.

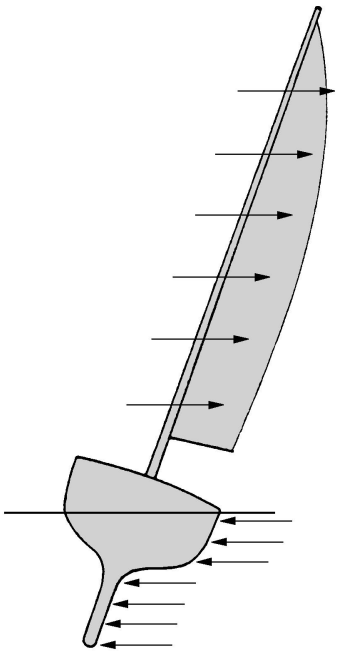

Figure 8.31: Lateral Forces on a Sailboat

Even though this static roll moment will bring the sailboat (in this example) into overall equilibrium, internal torsional moments will generally still exist. Indeed, with most sailboats, the entire moment from the sail is transferred to the hull at the cross-section where the mast is located. This moment can be distributed to the rest of the hull only via torsional moments about the ship's x-axis.

Quasi-static axial forces can be present in a ship which is sailing (not necessarily a sailboat now), too. The force driving the ship forward (from the propeller) is transferred via its shaft to a thrust bearing where this load is transferred to the hull. The hull forward of this location is obviously 'pushed' through the water; there will obviously be a compressive normal stress in the ship sections forward of the thrust bearing. By the same reasoning, all ship sections aft of the thrust bearing will be under a slight tension as the after body of the ship is pulled through the water.

A more striking example of this would be a tugboat (see figure 8.32) pulling a barge or even a gravity platform being moved to its offshore location. In this case both the towing force transferred to the ship via its towing bollard and the propulsion force at its thrust bearing are point loads in the axial force diagram. Since the towing bollard is generally forward of the thrust bearing, the ship sections between these locations will be under compression.

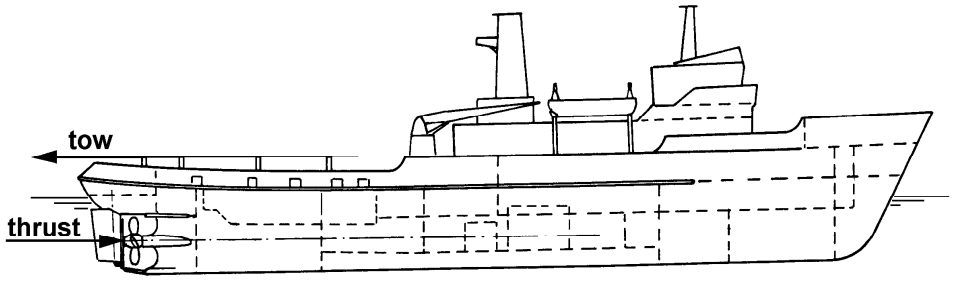

Figure 8.32: Concentration of Axial Forces on a Tug

When viewed from the side, these two forces are not colinear; indeed they deliver a couple about the y-axis; this will be compensated by a small positive (bow up) trim of the tug.

Large square-rigged sailing ships suffered at times from the opposite problem. The driving force from their sails was sometimes centered high in the masts, the ship's hydrodynamic resistance was below the water line. The generated couple now forced the bow down so that it was deeper than normal in the water (this is often referred to as rooting). This increases wave resistance which only reinforces the problem. Admiral Beaufort obviously was practicing good seamanship when he recommended that the highest sails be taken in first as the wind increased; see chapter 5.

8.7.4 Dynamic Equilibrium

The dynamics will be investigated using the principle of **dynamic equilibrium**, using Newton's second law. The dynamic forces and moments should of course be combined with its static component - equation 8.109 - in order to calculate the maximum shear force and bending moment components at each section.

A lot of load components contribute to dynamic forces and moments in a hull; the motion components as well as the direct hydromechanical and wave exciting forces and moments contribute directly and sometimes in more than one way. Shear forces and bending moments are local loads and non-linearities can play a significant role. This is one of the reasons why the strip theory does not predict them always very accurate; deviations up to about 25 percent are possible.

Anchor line forces become dynamic as well, now, making the computation even more complex in terms of bookkeeping. Indeed, since mooring line tensions will generally depend upon the instantaneous position of their attachment point, they can even introduce a coupling between vertical motions on the one hand, and roll motions and dynamic torsional moments on the other. These aspects have not been taken into account here.

Lateral Dynamic Loads

Consider the horizontal forces acting on a section of the ship with a length dx_b. According to Newton's second law, the harmonic lateral dynamic load per unit length on a transverse 'slice' of the ship is given by:

$$\begin{aligned} q_y(x_b) &= +X'_{hy}(x_b) + X'_{wy}(x_b) \\ &\quad +\rho g A_x(x_b) \cdot \phi \\ &\quad -m'(x_b) \cdot \left\{ \ddot{y} + x_b \cdot \ddot{\psi} - z'_m \cdot \ddot{\phi} + g \cdot \phi \right\} \end{aligned} \tag{8.110}$$

where $A_x(x_b)$ is the sectional area, $X'_{hy}(x_b)$ and $X'_{wy}(x_b)$ are the sectional hydromechanical and wave forces for sway and $m'g\phi$ is the lateral mass-force component due to the definition of the lateral loads in the ship-bound axes system, respectively.
With equations 8.105 and 8.106, the harmonic lateral shear force, $Q_y(x_1)$, and the bending moment, $M_z(x_1)$, in waves in cross section x_1 can be obtained from the horizontal load, $q_y(x_b)$, by the following integrals:

$$\boxed{Q_y(x_1) = Q_{y_a} \cos(\omega_e t + \varepsilon_{Q_z\zeta}) = -\int_{stern}^{x_1} q_y(x_b) \cdot dx_b}$$

$$\boxed{M_z(x_1) = M_{z_a} \cos(\omega_e t + \varepsilon_{M_z\zeta}) = -\int_{stern}^{x_1} q_y(x_b) \cdot x_b \cdot dx_b - Q_y(x_1) \cdot x_1} \tag{8.111}$$

Vertical Dynamic Loads

Consider the vertical forces acting on a section of the ship with a length dx_b. According to Newton's second law, the harmonic longitudinal and vertical dynamic forces per unit length on a transverse 'slice' of the ship are given by:

$$\begin{aligned} q_x(x_b) &= +X'_{hx}(x_b) + X'_{wx}(x_b) - m'(x_b) \cdot \left\{ \ddot{x} - \overline{bG}(x_b) \cdot \ddot{\theta} \right\} \\ q_z(x_b) &= +X'_{hz}(x_b) + X'_{wz}(x_b) - m'(x_b) \cdot \left\{ \ddot{z} - x_b \cdot \ddot{\theta} \right\} \end{aligned} \tag{8.112}$$

where $\overline{bG}(x_b)$ is the distance of the centroid of the cross section to the x_b axis and $X'_{hx}(x_b), X'_{hz}(x_b)$ and $X'_{wx}(x_b), X'_{wz}(x_b)$ are the sectional hydromechanical and wave forces for surge and heave, respectively.
With equations 8.105 and 8.106, the harmonic vertical shear force, $Q_z(x_1)$, and the bending moment, $M_y(x_1)$, in waves in cross section x_1 can be obtained from the longitudinal and vertical loads, $q_x(x_b)$ and $q_z(x_b)$, by the following integrals:

$$\boxed{Q_z(x_1) = Q_{z_a} \cos(\omega_e t + \varepsilon_{Q_z\zeta}) = -\int_{stern}^{x_1} q_z(x_b) \cdot dx_b}$$

$$\boxed{M_y(x_1) = M_{y_a} \cos(\omega_e t + \varepsilon_{M_y\zeta}) = +\int_{stern}^{x_1} q_x(x_b) \cdot \overline{bG}(x_b) \cdot dx_b}$$

$$+ \int_{stern}^{x_1} q_z(x_b) \cdot x_b \cdot dx_b \; + Q_z(x_1) \cdot x_1 \tag{8.113}$$

Figure 8.33 shows a comparison between measured and calculated distribution of the vertical wave bending moment amplitudes over the length of the ship

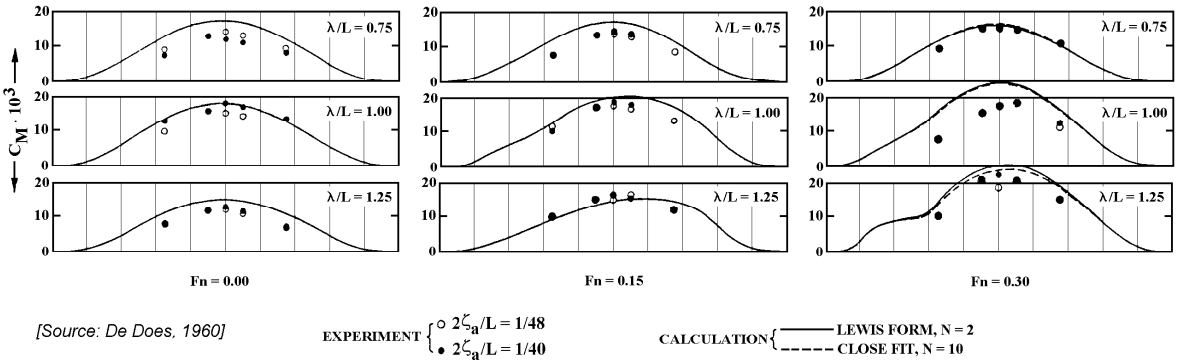

Figure 8.33: Distribution of Vertical Bending Moment Amplitudes

Torsional Dynamic Loads

Consider the moments acting on a section of the ship with a length dx_b. According to Newton's second law, the harmonic torsional dynamic moment per unit length on a transverse 'slice' of the ship about a longitudinal axis at a distance z_1 above the ship's center of gravity is given by:

$$\begin{aligned} q_\phi(x_b, z_1) \;\; = \;\; & +X'_{h\phi}(x_b) + X'_{w\phi}(x_b) \\ & +z_1 \cdot q_y(x_b) - m'(x_b) \cdot \left\{ k'^2_{xx} \cdot \ddot{\phi} - z'_m \cdot (\ddot{y} + x_b \cdot \ddot{\psi} + g \cdot \phi) \right\} \end{aligned} \tag{8.114}$$

where $X'_{h\phi}(x_b)$ and $X'_{w\phi}(x_b)$ are the sectional hydromechanical and wave moments for roll, respectively.
With equation 8.105, the harmonic torsional moment, $M_x(x_1, z_1)$, in waves in cross section x_1 at a distance z_1 above the ship's center of gravity can be obtained from the torsional loads, $q_\phi(x_b, z_1)$, by the following integral:

$$M_x(x_1, z_1) = M_{x_a} \cos(\omega_e t + \varepsilon_{M_x \zeta}) = - \int_{stern}^{x_1} q_\phi(x_b, z_1) \cdot dx_b \tag{8.115}$$

It is important to realize, for example, that a ship sailing in quartering waves -approaching from about 45 degrees off the stern - can experience very significant dynamic torsional moments - even if it is not rolling very much. Both the wave direction (and associated relative phases along the ship's axis) and the low frequency of encounter contribute to a large transfer function value in this case.

8.7.5 Internal Loads Spectra

The internal loads spectra can be calculated in a way similar to that described earlier for other harmonic responses.

8.7.6 Fatigue Assessments

It has already been pointed out that the transfer functions for any of the above forces can be computed by carefully (and properly!) superposing the components for the already known functions for forces and ship motions. One can go even deeper into the structural engineering aspects, however as long as the system remains linear in its behavior.
Knowing all six of the load components on a ship cross-section, a marine structural engineer can - knowing a lot more details of the internal structure of the ship - convert each of these forces to associated stress components. Stress concentration factors and other details must now be taken into account along the way, of course.
These stress components can in turn be combined to determine principal stresses and even to carry out a fatigue analysis. Structural engineering and offshore hydromechanics are often very closely linked - if not married - within offshore engineering! This will show up again when sea fastening of offshore structures to transport barges is discussed in chapter 11.
Fatigue analyses depend upon two independent input data items:

- Magnitude of the (local) stress change - stress range.
- Associated number of cycles with this stress range.

This information can then be combined using the Miner-Palmgren rule to obtain an overall fatigue damage estimate. The structural analysis details of this are left to others more expert in this field, but a bit more about each of the above two items is discussed here.
The magnitude of the stress change within a ship or other large structure will be linearly related to the ambient waves. If the object has a fixed location, then wave climate data is relatively easy to obtain and work with. Even if the object is only seasonally, one can approach the wave data in a quite straight forward way - see chapter 5.
More "portable" objects - such as a major pipe laying vessel that may spend some time near Australia before going to the west coast of Africa before coming to the North sea for a while - present a formidable bookkeeping problem. If the problem to be solved involves the determination of the "remaining fatigue life" of an existing vessel, then obtaining the cumulative - location and time dependent - wave climate presents a significant problem. The pragmatic solution in a design situation, on the other hand, would be to determine fatigue life based upon continuous exposure to some defined wave climate such as that for the northern North Sea.

Global and Local Loads

Fatigue sensitive locations in a vessel are the deck, bottom and possibly the sides-shell. The loads important for fatigue can be split in global and local loads. Global loads are loads in a cross section of the hull girder and make equilibrium with the "acceleration forces" due to the motions and the pressure integration over the specific hull section; these have been determined above. Local internal loads result from pressures at specific spots on the hull inducing additional locally fluctuating stresses. The simple effect of external

pressure variations (from waves) causing local (bending) stresses in the hull plating is an example of this.
Global loads - important for fatigue - are the vertical and horizontal bending moments. An important local load is the external pressure causing cyclic bending of longitudinals between their supporting frames (webs or web/bulkhead). The local external pressure loading is mainly of interest for tankers and bulk carriers. Especially FPSO tankers operated on the North Sea are to be examined thoroughly on the fatigue strength since they are built according to the rules for trading vessels but are used differently. These vessels more often encounter head waves and are permanently on site in a harsh environment.
Fatigue in the deck structure is induced by vertical and horizontal bending of the hull girder. The bottom structure is loaded both by the vertical and horizontal bending moments and the external wave pressure. The side shell is mainly loaded by the external wave pressure and horizontal bending moment and slightly by the vertical bending moment depending on the position of the neutral axis; see figure 8.34, illustrating the global and local loads acting on a vessel.

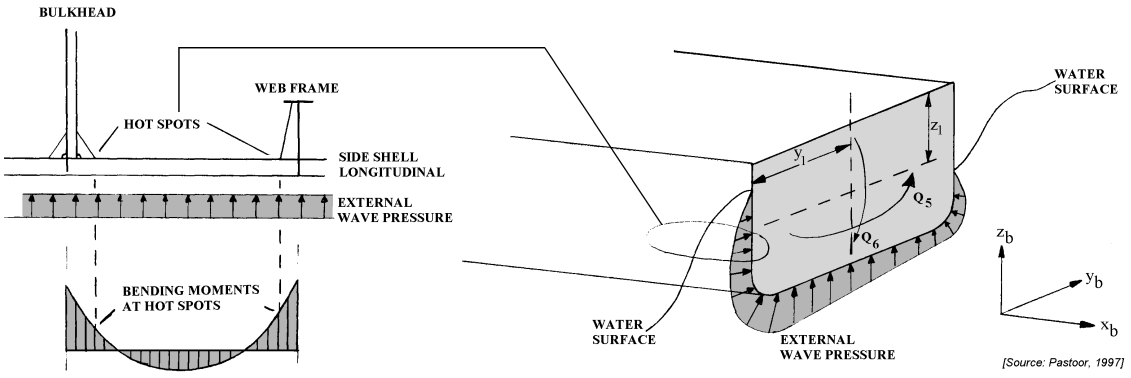

Figure 8.34: Global and Local Loads Acting on a Cross Section

Combining the horizontal and vertical wave bending moments is done by calculating one stress transfer function at the spot of interest.

$$\begin{aligned} H_{\sigma\zeta}(y_b, z_b, \omega)\cos(\omega t + \varepsilon_{\sigma\zeta}) = \frac{z_1}{I_{yy}} \quad & H_{Q_5\zeta}(y_b, z_b, \omega)\cos(\omega t + \varepsilon_{Q_5\zeta}) \\ + \frac{y_1}{I_{zz}} \quad & H_{Q_6\zeta}(y_b, z_b, \omega)\cos(\omega t + \varepsilon_{Q_6\zeta}) \end{aligned} \tag{8.116}$$

Expand the cosines into cosine products and sine products. One can determine $H_{\sigma\zeta}$ and $\varepsilon_{\sigma\zeta}$ by stating that the equation must be valid for $\omega t = 0$ and $\omega t = \pi/2$. This gives:

$$\begin{aligned} H_{\sigma\zeta}(y_b, z_b, \omega)\cos\varepsilon_{\sigma\zeta} &= \frac{z_1}{I_{yy}} H_{Q_5\zeta}(y_b, z_b, \omega)\cos\varepsilon_{Q_5\zeta} + \frac{y_1}{I_{zz}} H_{Q_6\zeta}(y_b, z_b, \omega)\cos\varepsilon_{Q_6\zeta} \\ H_{\sigma\zeta}(y_b, z_b, \omega)\sin\varepsilon_{\sigma\zeta} &= \frac{z_1}{I_{yy}} H_{Q_5\zeta}(y_b, z_b, \omega)\sin\varepsilon_{Q_5\zeta} + \frac{y_1}{I_{zz}} H_{Q_6\zeta}(y_b, z_b, \omega)\sin\varepsilon_{Q_6\zeta} \end{aligned} \tag{8.117}$$

Squaring and summing these equations results in an expressions for $H_{\sigma\zeta}$ and dividing these two equations gives an expression for $\tan\varepsilon_{\sigma\zeta}$.

The external pressure can be incorporated as well for those position which are always wet - the bottom and bilges. In this case a pressure transfer function is required along with a structural model to determine the local stress contribution - just as is needed for the global internal loads as well. Side shell loading is more complicated. Since the water surface is fluctuating the side shell is sometimes wet and sometimes dry. Hence this loading is strongly nonlinear which is difficult to account for properly. For calculation routines and ways to combine this nonlinear load with the global loads one is referred to [Cramer and et.al., 1993], [Pastoor, 1997b] and [Pastoor, 1997a].

Once the proper overall transfer functions and some form of cumulative wave scatter diagram has been determined, each of its "cells" - with its own characteristic wave height and period - can be transformed to:

- A characteristic stress variation dependent upon the waves and a whole "chain" of transfer functions.
- A number of stress variation cycles dependent upon the wave period and the number of observations associated with that wave scatter diagram cell.

Often several adjacent cells in the wave scatter diagram are combined when carrying out this transformation.
Once this procedure has been followed for all wave scatter diagram cells, one can sum up the results in order to obtain the input data for a Miner-Palmgren sum.

8.8 Added Resistance in Waves

A ship moving forward in a wave field will generate "two sets of waves": waves associated with forward speed through still water and waves associated with its vertical relative motion response to waves. Since both wave patterns dissipate energy, it is logical to conclude that a ship moving through still water will dissipate less energy than one moving through waves. The extra wave-induced loss of energy can be treated as an added propulsion resistance - see chapter 4.
Figure 8.35 shows the resistance in regular waves as a function of the time: a constant part due the calm water resistance and an oscillating part due to the motions of the ship, relative to the incoming regular waves. The time-averaged part of the increase of resistance is called: the added resistance due to waves, R_{aw}.
Two theoretical methods for the estimation of the time-averaged added resistance of a ship due to its vertical motions relative to the waves are described here:

- a **radiated wave energy method**
  introduced by [Gerritsma and Beukelman, 1972] and suitable for head to beam waves
- an **integrated pressure method**
  introduced by [Boese, 1970] and suitable for all wave directions.

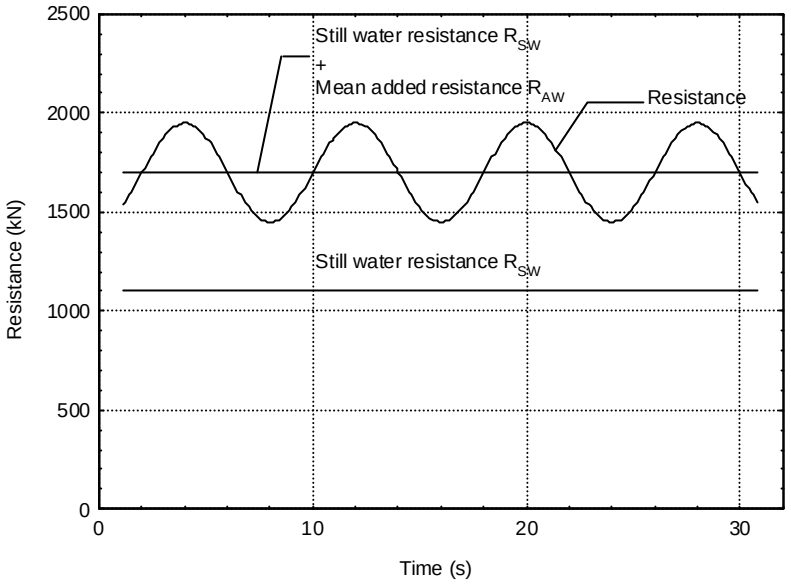

Figure 8.35: Increase of Resistance in Regular Waves

8.8.1 Radiated Energy Method

The energy relation of an oscillating body has been determined in chapter 6. Based on this relation and strip theory, the radiated wave energy during one period of oscillation of a ship in regular waves is defined by [Gerritsma and Beukelman, 1972] as:

$$\begin{aligned} P &= \int_L \left\{ \int_0^{T_e} (b'_{33} \cdot V_z^*) \cdot (V_z^* \cdot dt) \right\} \cdot dx_b \\ &= \int_0^{T_e} \int_L b'_{33} \cdot V_z^{*2} \cdot dx_b \cdot dt \end{aligned} \tag{8.118}$$

in which:

b'_{33} = hydrodynamic damping coefficient of the vertical motion of the cross section,
V_z^* = vertical average velocity of the water particles, relative to the cross sections,
T_e = period of vertical oscillation of the cross section.

The speed dependent hydrodynamic damping coefficient for the vertical motion of a cross section is defined here as shown before in equation 8.25:

$$b'_{33} = N'_{33} - V \cdot \frac{dM'_{33}}{dx_b} \tag{8.119}$$

The harmonic vertical relative velocity of a point on the ship with respect to the water particles is defined by:

$$\begin{aligned} V_z &= \dot{\zeta}'_{w_3} - \frac{D}{Dt}\{z - x_b \cdot \theta + y_b \cdot \phi\} \\ &= \dot{\zeta}'_{w_3} - \left(\dot{z} - x_b \cdot \dot{\theta} + V \cdot \theta + y_b \cdot \dot{\phi}\right) \end{aligned} \tag{8.120}$$

For a cross section of the ship, an equivalent harmonic vertical relative velocity has to be found. This equivalent relative velocity is defined by:

$$\begin{aligned} V_z^* &= \dot{\zeta}_{w_3}^* - \left(\dot{z} - x_b \cdot \dot{\theta} + V \cdot \theta\right) \\ &= V_{z_a}^* \cdot \cos(\omega_e t + \varepsilon_{V_z^*\zeta}) \end{aligned} \tag{8.121}$$

With this the radiated energy during one period of oscillation is given by:

$$P = \frac{\pi}{\omega_e} \int_L \left(N'_{33} - V \cdot \frac{dM'_{33}}{dx_b}\right) \cdot V_{z_a}^{*\,2} \cdot dx_b \tag{8.122}$$

To maintain a constant forward ship speed, this energy should be provided by the ship's propulsion plant. A mean added resistance, R_{aw}, has to be gained. The energy provided to the surrounding water is given by:

$$\begin{aligned} P &= R_{aw} \cdot \left(V - \frac{c}{\cos\mu}\right) \cdot T_e \\ &= R_{aw} \cdot \frac{2\pi}{-k\cos\mu} \end{aligned} \tag{8.123}$$

From this the transfer function of the mean added resistance according to Gerritsma and Beukelman can be found:

$$\boxed{\frac{R_{aw}}{\zeta_a^2} = \frac{-k\cos\mu}{2\omega_e} \cdot \int_L \left(N'_{33} - V \cdot \frac{dM'_{33}}{dx_b}\right) \cdot \left(\frac{V_{z_a}^*}{\zeta_a}\right)^2 \cdot dx_b} \tag{8.124}$$

This method gives good results in head to beam waves. However, this method fails in following waves. When the wave speed in following waves approaches the ship speed the frequency of encounter in the denominator tends to zero. At these low frequencies, the potential sectional mass is very high and the potential sectional damping is almost zero. The damping multiplied with the relative velocity squared in the numerator does not tend to zero, as fast as the frequency of encounter. This is caused by the presence of a natural frequency for heave and pitch at this low ω_e, so a high motion peak can be expected. This results in extreme (positive and negative) added resistances.

8.8.2 Integrated Pressure Method

[Boese, 1970] calculates the added resistance by integrating the longitudinal components of the oscillating pressures on the wetted surface of the hull. A second small contribution of the longitudinal component of the vertical hydrodynamic and wave forces has been added. The wave elevation is given by:

$$\zeta = \zeta_a \cos(\omega_e t - k x_b \cos\mu - k y_b \sin\mu) \tag{8.125}$$

The pressure in the undisturbed waves in deep water is given by:

$$p = -\rho g z + \rho g \cdot e^{kz} \zeta \tag{8.126}$$

The horizontal force on an oscillating cross section is given by:

$$f(x_b,t) = \int\limits_{-D_s+z_x}^{\zeta} p\, dz_b \qquad \text{with: } z_x = z - x_b\theta \tag{8.127}$$

As the mean added resistance during one period will be calculated, the constant term and the first harmonic term can be ignored, so:

$$\begin{aligned} f^*(x_b,t) &= -\frac{1}{2}\rho g\left\{\zeta^2 - (-D_s + z_x)^2\right\} \\ &= -\frac{1}{2}\rho g\,(\zeta - z_x)^2 \end{aligned} \tag{8.128}$$

The vertical relative motion is defined by $s = \zeta - z_x$, so:

$$f^*(x_b,t) = -\frac{1}{2}\rho g\, s^2 \tag{8.129}$$

The average horizontal force on a cross section follows from:

$$\overline{f^*}(x_b) = \int\limits_0^{T_e} f^*(x_b,t)\, dt \;=\; \frac{1}{4}\rho g\, s_a^2 \tag{8.130}$$

The added resistance due to this force is:

$$R_{aw_1} = 2\int\limits_L \overline{f^*}(x_b)\, \left(-\frac{dy_w}{dx_b}\right)\, dx_b \tag{8.131}$$

so that this part of the mean added resistance reduces to:

$$R_{aw_1} = -\frac{1}{2}\rho g \int\limits_L s_a^2\, \frac{dy_w}{dx_b}\, dx_b \tag{8.132}$$

The integrated vertical hydromechanical and wave forces in the ship bounded axis system varies not only in time but also in direction with the pitch angle. From this follows a second contribution to the mean added resistance:

$$\begin{aligned} R_{aw_2} &= \frac{-1}{T_e}\int\limits_0^{T_e} \{X_{h_3}(t) + X_{w_3}(t)\}\; \theta(t)\, dt \\ &= \frac{-1}{T_e}\int\limits_0^{T_e} \rho\nabla\; \ddot{z}(t)\; \theta(t)\; dt \end{aligned} \tag{8.133}$$

This second contribution can be written as:

$$R_{aw_2} = \frac{1}{2}\rho\nabla\; \omega_e^2\; z_a\; \theta_a\; \cos(\varepsilon_{z\zeta} - \varepsilon_{\theta\zeta}) \tag{8.134}$$

so that the transfer function of the total mean added resistance according to Boese is given by:

$$\boxed{\frac{R_{aw}}{\zeta_a^2} = \frac{1}{2}\rho g \int\limits_L \left(\frac{s_a}{\zeta_a}\right)^2\; \frac{dy_w}{dx_b}\, dx_b \;\; + \frac{1}{2}\rho\nabla\; \omega_e^2\, \frac{z_a}{\zeta_a}\, \frac{\theta_a}{\zeta_a}\; \cos(\varepsilon_{z\zeta} - \varepsilon_{\theta\zeta})} \tag{8.135}$$

8.8.3 Non-dimensional Presentation

The transfer function of the mean added resistance R_{aw}/ζ_a^2 is often presented in a non-dimensional way as:

$$\boxed{R'_{aw} = \frac{R_{aw}}{\rho g \zeta_a^2 B^2/L}} \tag{8.136}$$

in which:

$$\begin{aligned} L &= \text{length between perpendiculars} \\ B &= \text{(maximum) breadth of the waterline} \end{aligned}$$

Figure 8.36 shows a comparison of calculated and measured added resistance data of a container vessel. Because of the added resistance of a ship due to the waves is proportional to the relative motions squared, inaccuracies in the predicted motions will be amplified in resistance errors.

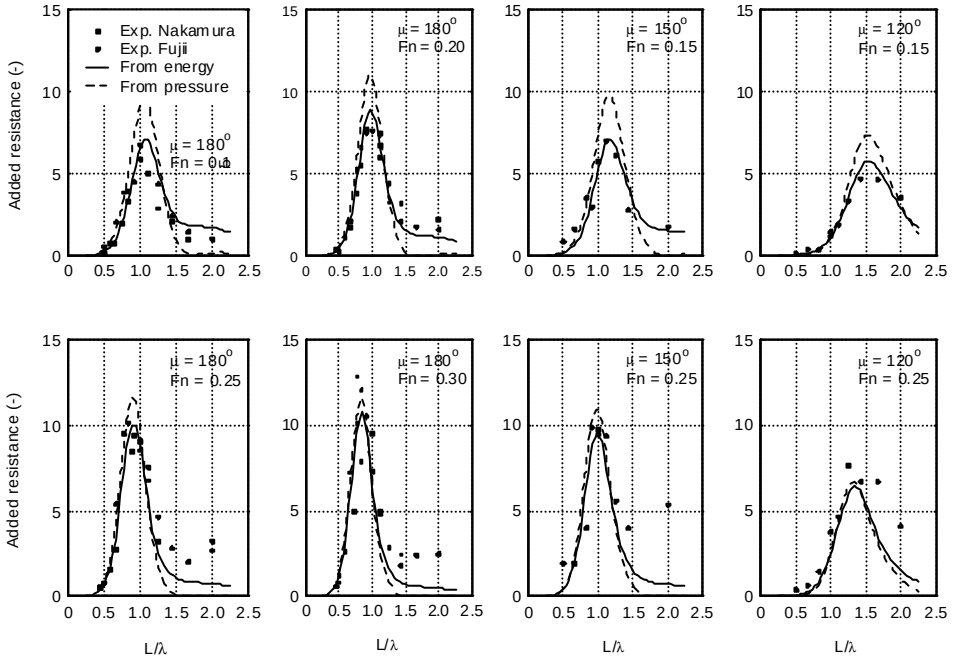

Figure 8.36: Computed and Measured Added Resistance

The deviations in the figure at low wave lengths (high frequencies) are caused by diffraction of the waves against the ship; this effect has not been taken into account. But the amount energy in irregular waves at these high frequencies is small; so generally, these deviations will not have a large influence on the added resistance in irregular waves.

8.8.4 Added Resistance in Irregular Waves

The mean added resistance in a frequency range $\Delta\omega$ can be written as:

$$R_{aw}(\omega) = 2 \cdot \left| \frac{R_{aw}}{\zeta_a^2}(\omega) \right| \cdot \frac{1}{2}\zeta_a^2 \tag{8.137}$$

$$= 2 \cdot \left| \frac{R_{aw}}{\zeta_a^2}(\omega) \right| \cdot S_\zeta(\omega) \cdot \Delta\omega \tag{8.138}$$

Then, the total mean added resistance in a seaway follows from a summation or an integration of the contributions over the whole frequency range:

$$\overline{R}_{AW} = 2 \sum_{\omega=0}^{\infty} \left| \frac{R_{aw}}{\zeta_a^2}(\omega) \right| \cdot S_\zeta(\omega) \cdot \Delta\omega \tag{8.139}$$

Thus:

$$\boxed{\overline{R}_{AW} = 2 \int_0^{\infty} \left| \frac{R_{aw}}{\zeta_a^2}(\omega) \right| \cdot S_\zeta(\omega) \cdot d\omega} \tag{8.140}$$

Because of the linear motions, which results in a linear relation between the mean added resistance and the regular wave amplitude squared, and the (ideal) wave spectrum defined by $S_\zeta(\omega) = H_{1/3}^2 \cdot f(\omega, T)$, the calculated mean added resistance values in irregular waves are often presented as:

$$\frac{\overline{R}_{AW}}{H_{1/3}^2} = 2 \int_0^{\infty} \left| \frac{R_{aw}}{\zeta_a^2}(\omega) \right| \cdot f(\omega, T) \cdot d\omega \quad \text{versus} \quad T = T_1,\, T_2 \text{ or } T_p$$

in which $H_{1/3}$ is the significant wave height, T ($= T_1$, T_2 or T_p) are mean wave periods and $f(\omega, T)$ is a function of ω and T only.

.